JAERI-M
83-044

EVALUATION REPORT ON CCTF CORE-I REFLOOD TESTS CI-6 (RUN15), CI-9 (RUN18), CI-11 (RUN20) AND CI-13 (RUN22)

—EFFECTS OF ECC WATER INJECTION RATE—

(Work done under Contract with the Government)

March 1983

Tsutomu OKUBO, Jun SUGIMOTO and Yoshio MURAO

日本原子力研究所
Japan Atomic Energy Research Institute

JAERI-Mレポートは，日本原子力研究所が不定期に公刊している研究報告書です。
入手の問合わせは，日本原子力研究所技術情報部情報資料課（〒319-11茨城県那珂郡東海村）あて，お申しこしください。なお，このほかに財団法人原子力弘済会資料センター（〒319-11 茨城県那珂郡東海村日本原子力研究所内）で複写による実費頒布をおこなっております。

JAERI-M reports are issued irregularly.
Inquiries about availability of the reports should be addressed to Information Section, Division of Technical Information, Japan Atomic Energy Research Institute, Tokai-mura, Naka-gun, Ibaraki-ken 319-11, Japan.

編集兼発行　日本原子力研究所
印　　刷　いばらき印刷㈱

JAERI-M 83-044

Evaluation Report on CCTF Core-I Reflood Tests C1-6 (RUN 15), C1-9 (RUN 18), C1-11 (RUN 20) and C1-13 (RUN 22)
—— Effects of ECC Water Injection Rate ——

Tsutomu OKUBO, Jun SUGIMOTO and Yoshio MURAO

Division of Nuclear Safety Research,
Tokai Research Establishment, JAERI

(Received February 7, 1983)

The present report describes the effects of the Emergency Core Cooling (ECC) water injection rate on the reflooding phenomena observed in the Cylindrical Core Test Facility (CCTF). The evaluation is based on the data of Tests C1-5, C1-6, C1-9, C1-11 and C1-13 of the CCTF Core-I test series. In these tests, the injection rates of an accumulator system (Acc) and a low pressure coolant injection system (LPCI) and the injection duration of the Acc were parametrically varied from Test C1-5 (base case test).

The higher ECC water injection rate caused the downcomer water head and core flooding rate to be higher resulting in the better core cooling. However, there was little effect of the LPCI injection rate on the core cooling once the downcomer water head reached the maximum level. Although the effects of the Acc injection rate and duration on the primary system thermo-hydrodynamic behavior and the core cooling behavior were dominant in an early period of the transient, they also significantly influenced the core cooling behavior through the whole transient. The similar trends of the effect of Acc injection rate on the core cooling behavior were observed in the CCTF and the FLECHT-SET Phase A experiments.

Keywords: Reflood, LOCA, PWR, ECCS, Water Injection Rate Safety Evaluation, Cylindrical Core Test Facility, Reactor Safety

---

The work was performed under contracts with the Atomic Energy Bureau of Science and Technology Agency of Japan.

JAERI－M 83 －044

大型再冠水円筒第一次炉心試験C1－6（RUN 15），C1－9（RUN 18），C1－11（RUN 20）およびC1－13（RUN 22）評価報告書
—非常用炉心冷却水注入水量の影響—

東海研究所安全工学部安全工学第2研究室
大久保　努・杉本　純・村尾　良夫

（1983年2月7日受理）

本報告書では，円筒炉心第一次炉心試験で観測された非常用炉心冷却水注入水量の再冠水現象に及ぼす影響について報告する。解析は，円筒炉心試験C1－5，C1－6，C1－9，C1－11およびC1－13の結果に基づいている。これらのパラメータ効果試験においては蓄圧注水系の流量および注水継続時間，および低圧注水系流量を基準試験C1－5に対して変化させた。

ECC注水量を増加させるとダウンカマ水頭や炉心入口流量が増加し，良好な炉心冷却が得られた。しかしダウンカマ液位がオーバーフローレベルに達した後は低圧注水系流量の増加が炉心冷却に与える効果はほとんど見られなくなった。蓄圧注水系の流量及び継続時間のシステム及び炉心冷却挙動に与える影響は，再冠水開始後初期の応答に顕著に見られたが，この影響はその後の炉心冷却全体に強く作用した。円筒炉心試験装置と米国FLECHT－SET実験との間で，蓄圧注水系流量の炉心冷却に与える影響について同様の傾向が観測された。

本報告書は，電源開発促進対策特別会計法に基づき，科学技術庁からの受託によって行った研究の成果である。

Contents

目　　次

List of Tables

List of Figures

1. Introduction

The Cylindrical Core Test Facility (CCTF) has been designed to demonstrate the emergency core cooling (ECC) behavior, to verify the best-estimate analysis codes and to supply the information for the improved thermo-hydrodynamic models during the reflood phase of a loss-of-coolant accident (LOCA) in a pressurized water reactor (PWR).

Twenty-seven tests have been conducted in the CCTF Core-I series to study the parametric effects on the reflood phenomena. The present report describes the effects of the ECC water injection rate on the reflood phenomena observed in CCTF. The data of Tests C1-5, C1-6, C1-9, C1-11 and C1-13 are evaluated in this report.

Test C1-5 is the base case of the CCTF Core-I test series. The specific parameters of the Tests C1-6, C1-9, C1-11 and C1-13 are the high Low Pressure Coolant Injection System (LPCI) injection rate, the low LPCI injection rate, the low Accumulator System (Acc) injection rate and the short Acc injection duration, respectively.

The ECC injection rates of the base case test were determined based on the reference injection curve which is the basis for the injection rates of the FLECHT-SET Phase A experiment[1]. The Acc injection rate, which varies from 378 to 287 m^3/h in the reference curve, was conservatively set to 280 m^3/h (0.078 m^3/s) in the base case test of the CCTF. The LPCI injection rate was set to 3/4 of the reference value.

The ECC water injection rates used in the licensing evaluation model calculation are generally higher than those of the base case test of the CCTF. However, the Acc water injection rate at the reflood initiation can not be specified uniquely because it depends on the conditions before the reflooding transient. Therefore, the parametric tests were performed to investigate the general effects of the ECC water injection rate on the reflooding phenomena.

Futhermore, in this report, test results are compared with those of the FLECHT-SET Phase A experiments in order to examine whether the ECC water injection rate effects on the core cooling behavior differ between the different size facilities, because the CCTF is a large scale reflood test facility and is seventeen times larger.

Test C1-5 is overviewed in reference (2). The selected data of Tests C1-6, C1-9, C1-11 and C1-13 are presented in Appendices for better understanding of the test results.

2. Test Description

2.1 Test Facility

The CCTF is an experimental test facility designed to reasonably simulate the flow conditions in the primary system of a PWR during the refill and reflood phases of a LOCA. The vertical dimensions and locations of the system components are kept as close as possible to those of reference 1000 MW PWRs with four primary loops. The reference reactors are the Trojan reactor in the USA and certain aspects of the Ohi reactor in Japan. The flow area of the system components are scaled down based on the core flow area scaling ratio of 1:21.4. The bird's-eye view and overall schematic diagram of the facility are shown in Figs. 2.1 and 2.2, respectively. The scaled dimensions of the components are given in Table 2.1.

The pressure vessel is a cylindrical type with the downcomer, the upper and lower plenums, and the core as shown in Fig. 2.3. The core consists of thirty-two 8×8 electrically heated rod bundles arranged in a cylindrical array. Each bundle simulates 15×15 array fuel assemblies including the unheated rods. The cross section of the pressure vessel and the configuration of the rods in the core are shown in Figs. 2.4 and 2.5, respectively.

The heated length and the outer diameter of the heater rods are 3.66 m and 10.7 mm, respectively. The heating element is a herical nichrome coil with a 17 step chopped cosine axial power profile as shown in Fig. 2.6 The locations of the temperature measurement in the core are also shown in the figure.

The primary loop consists of three intact loops and a broken loop. Each loop consists of hot leg and cold leg pipings, a steam generator simulator with active secondary side, and a pump simulator. A 200% cold leg break is simulated for the broken cold leg. The broken cold leg is connected to two containment tanks, The inner diameter of the piping is scaled down in proportion to the core flow area scaling. The length of each piping section is almost the same as the corresponding section of the reference PWR. ECCS consists of an Acc and a LPCI. The injection points are located at each cold leg and at the lower plenum. The primary loop arrangement is shown in Figs. 2.7 and 2.8.

Approximately 1500 channels of data are recorded on a magnetic disk or a magnetic tape, which include temperatures, pressures, differential

pressures, liquid levels and mass flow rates. Measurement locations in the pressure vessel and the primary system are shown in Figs. 2.9 through 2.12. The definitions of the data analyzed in the next chapter are given in Fig. 2.13.

2.2 Test Procedure

The test procedure was as follows: After establishing the initial conditions of the test, the electric power for preheaters was turned off and the lower plenum was filled with saturated water to a specified level (usually 0.9m). When the water level in the lower plenum reached the specified level and the other initial conditions of the test stabilized, the electric power was applied to the heater rods in the core and the data recording was started. When a specified initial clad temperature of the heater rods was reached, direct injection of the Acc water into the lower plenum was initiated. The specified initial clad temperature for the initiation of coolant injection was predetermined by the interpolation between the initial clad temperature and the clad temperature assumed for the bottom of the core recovery (BOCREC) time. The decay of the power input to the heater rods was scheduled to begin at the BOCREC time. The specified power decay was obtained by normalizing the dacay curve of the ANS standard × 1.2 + ^{238}U capture decay at 30 seconds after scram.

At a predetermined time, the injection port was switched from the lower plenum to the three (four in Test C1-9) intact cold leg ECC ports. At a specified time after the initiation of Acc injection, the valves in Acc line and LPCI circulation line were closed and the valve in LPCI injection line was opened. These action transferred the ECC water injection from Acc mode to LPCI mode.

The generated steam and the entrained water flowed through broken and intact loops to the containment tanks. The steam was then vented to the atmosphere to maintain the pressure in the containment tanks constant.

When all thermocouples on the surface of heater rods quenched and indicated temperatures close to the saturation temperature, the power supply to the heater rods was turned off. After that, the ECC water injection was terminated and then data recording was ended last terminating the test.

2.3 Test conditions

The test conditions are summarized in Table 2.2. Except for the ECC water injection rate, all the conditions ware set as closely as possible in those five tests. The injection rate of the Acc and the LPCI for the base case test (Test C1-5) were 0.072 m^3/s and 0.0083 m^3/s, respectively. The Acc injection duration was 14 s. These values were determined based on the reference injection curve of the FLECHT-SET Phase A experiment [1], as mentioned in Introduction.

In Test C1-6 (denoted as high LPCI injection rate test in the following), the LPCI injection rate was doubled. In Test C1-9 (low LPCI injection rate test), the LPCI injection rate into the intact loops was halved. The Acc injection rate in Test C1-11 (low Acc injection rate test) was reduced by 13% compared to that in the base case test. The Acc injection duration was shortened by 3 s in Test C1-13 (short Acc injection duration test). The detailed test conditions are given in Tables 2.3 through 2.7 for each test.

In the low LPCI injection rate test (Test C1-9), the ECC water was injected into the broken cold leg as well as the three intact cold legs. Out of 0.011 m^3/s of the total LPCI injection rate, 0.0064 m^3/s was injected into the broken loop and 0.0047 m^3/s was injected into the intact loops, due to the differences of the pressure at the injection ports.

The chronology of events of those tests are presented in Tables 2.8 through 2.12.

Table 2.1 Scaled Dimensions of CCTF Component

COMPONENT		PWR	JAERI	RATIO
PRESSURE VESSEL				
VESSEL INSIDE DIAMETER	(mm)	4394 (173")	1084	
VESSEL THICKNESS	(mm)	216 (8 1/2")	90	
CORE BARREL OUTSIDE DIAMETER	(mm)	3974	961	
CORE BARREL INSIDE DIAMETER	(mm)	3760	929	
THERMAL SHIELD OUTSIDE DIAMETER	(mm)	4170		
THERMAL SHIELD INSIDE DIAMETER	(mm)	4030		
DOWNCOMER LENGTH	(mm)	4849	4849	1/1
DOWNCOMER GAP	(mm)	114.3	61.5	
DOWNCOMER FLOW AREA	(m^2)	4.23	0.197	1/21.44
LOWER PLENUM VOLUME	(m^3)	29.6	1.38	1/21.44
UPPER PLENUM VOLUME	(m^3)	43.6	2.04	1/21.44
FUEL (HEATER ROD) ASSEMBLY				
NUMBER OF BUNDLES	(—)	193	32	
ROD ARRAY	(—)	15 × 15	8 × 8	
ROD HEATED LENGTH	(mm)	3660	3660	1/1
ROD PITCH	(mm)	14.3	14.3	1/1
FUEL ROD OUTSIDE DIAMETER	(mm)	10.72	10.7	1/1
THIMBLE TUBE DLAMETER	(mm)	13.87	13.8	1/1
INSTRUMENT TUBE DIAMETER	(mm)	13.87	13.8	1/1
NUMBER OF HEATER RODS	(—)	39372	1824	1/21.58
NUMBER OF NON-HEATED RODS	(—)	4053	224	1/18.09
CORE FLOW AREA	(m^2)	5.29	0.25	1/21.2
CORE FLUID VOLUME	(m^3)	17.95	0.915	1/19.6
PRIMARY LOOP				
HOT LEG INSIDE DIAMETER	(mm)	736.6 (29")	155.2	1/4.75
HOT LEG FLOW AREA	(m^2)	0.426	0.019	1/22.54
HOT LEG LENGTH	(mm)	3940	3940	1/1
PUMP SUCTION INSIDE DIAMETER	(mm)	787.4 (31")	155.2	1/5.07
PUMP SUCTION FLOW AREA	(m^2)	0.487	0.019	1/25.77
PUMP SUCTION LENGTH	(mm)	7950	7950	1/1

Table 2.1 (cont'd)

COMPONENT		PWR	JAERI	RATIO
COLD LEG INSIDE DIAMETER	(mm)	698.5 (27.5")	155.2	1/4.50
COLD LEG FLOW AREA	(m^2)	0.383	0.019	1/20.26
COLD LEG LENGTH	(mm)	5600	5600	1/1
STEAM GENERATOR SIMULATOR				
NUMBER OF TUBES	(—)	3388	158	1/21.44
TUBE LENGTH (AVERAGE)	(m)	20.5	15.2	1/1.35
TUBE OUTSIDE DIAMETER	(mm)	22.225 (0.875")	25.4	
TUBE INSIDE DIAMETER	(mm)	19.7 (0.05")	19.6	1/1
TUBE WALL THICKNESS	(mm)	1.27	2.9	
HEAT TRANSFER AREA	(m^2)	4784 (51500 ft^2)	192	1/24.92
TUBE FLOW AREA	(m^2)	1.03	0.048	1/21.44
INLET PLENUM VOLUME	(m^3)	4.25	0.198	1/21.44
OUTLET PLENUM VOLUME	(m^3)	4.25	0.198	1/21.44
PRIMARY SIDE VOLUME	(m^3)	30.50 (1077 ft^3)	1.2	1/25.41
SECONDARY SIDE VOLUME	(m^3)	157.33 (5556 ft^3)	2.5	1/62.93
CONTAINMENT TANK - I	(m^3)		30	
CONTAINMENT TANK - II	(m^3)		50	
STORAGE TANK	(m^3)		25	
ACC. TANK	(m^3)		5	
SATURATED WATER TANK	(m^3)		3.5	
ELEVATION				
BOTTOM OF HEATED REGION IN CORE	(mm)	0	0	
TOP OF HEATED REGION IN CORE	(mm)	3660	3660	0
TOP OF DOWNCOMER	(mm)	4849	4849	0
BOTTOM OF DOWNCOMER	(mm)	0	0	0
CENTERLINE OF COLD LEG	(mm)	5198	4927	- 271
BOTTOM OF COLD LEG (INSIDE)	(mm)	4849	4849	0
CENTERLINE OF LOOP SEAL LOWER END	(mm)	2056	2047	- 9
BOTTOM OF LOOP SEAL LOWER END	(mm)	1662	1959	+ 297

Table 2.1 (cont'd)

COMPONENT		PWR	JAERI	RATIO
CENTER OF HOT LEG	(mm)	5198	4927	- 271
BOTTOM OF HOT LEG (INSIDE)	(mm)	4830	4849	+ 19
BOTTOM OF UPPER CORE PLATE	(mm)	3957	3957	0
TOP OF LOWER CORE PLATE	(mm)	- 108	- 50	+ 58
BOTTOM OF TUBE SHEET OF STEAM GENERATOR SIMULATOR	(mm)	7308	7307	- 1
LOWER END OF STEAM GENERATOR SIMULATOR PLENUM	(mm)	5713	5712	- 1
TOP OF TUBES OF STEAM GENERATOR SIMULATOR (avg)	(mm)	17952.7	14820	

Table 2.2 Summary of Test Conditions

Parameters: Test No.	Parameters: Test names	Acc injection rate ($\times 10^{-2}$ m^3/s)	Acc duration (sec)	LPCI injection rate ($\times 10^{-2}$ m^3/s)
C1-5	Base case	7.72	14	0.83
C1-6	High LPCI injection rate	7.75	13	1.72
C1-9	Low LPCI injection rate	7.86	13	0.47
C1-11	Low Acc injection rate	6.72	11	0.83
C1-13	Short Acc injection duration	7.69	10	0.83

System pressure : 0.2 (MPa)
Average linear power : 1.4 (kW/m)
ECC water temperature : 313 (K)

Table 2.3 Test Conditions for Test C1-5

	Estimated	Measured
Power		
Total (MW) :	9.41	9.36
Linear (KW/m) :	1.4	1.40
Radial Power Distribution :	1.06:1.0:0.82	1.07:1.0:0.82
Decay Type : ANS x 1.2 + Actinide (30 sec after Scram)		
Pressure (kg/cm^2a)		
System :	2.0	2.02
Steam Generator Secondary :	52	50
Temperature (°C)		
Downcomer Wall :	198	182
Primary Piping Wall :	119	120
Steam Generator Secondary :	265	262
Peak Clad at ECC Initiation :	502	502
Peak Clad at BOCREC :	600	615
Lower Plenum Filled Liquid :	119	114
ECC Liquid :	35	39
Water Level (m)		
Lower Plenum :	0.9	0.87
Steam Generator Secondary :	7.4	7.3
Injection Rate (m^3/hr)		
Accumlator :	251	278
LPCI :	30	30.2

Table 2.4 Test Conditions for Test C1-6

	Estimated	Measured
Power		
Total (MW) :	9.41	9.37
Linear (KW/m) :	1.4	1.4
Radial Power Distribution :	1.06:1.0:0.82	1.07:1.0:0.82
Decay Type : ANS x 1.2 + Actinide (30 sec after Scram)		
Pressure (kg/cm^2a)		
System :	2.0	2.03
Steam Generator Secondary :	52	50
Temperature (°C)		
Downcomer Wall :	198	179
Primary Piping Wall :	119	119
Steam Generator Secondary :	265	263
Peak Clad at ECC Initiation :	502	502
Peak Clad at BOCREC :	600	599
Lower Plenum Filled Liquid :	119	114
ECC Liquid :	35	37
Water Level (m)		
Lower Plenum :	0.9	0.88
Steam Generator Secondary :	7.4	7.2
Injection Rate (m^3/hr)		
Accumlator :	251	279
LPCI :	60	61.5

Table 2.5 Test Conditions for Test C1-9

	Estimated	Measured
Power		
Total (MW) :	9.41	9.39
Linear (KW/m) :	1.4	1.4
Radial Power Distribution :	1.06:1.0:0.82	1.07:1.0:0.82
Decay Type : ANS x 1.2 + Actinide (30 sec after Scram)		
Pressure (kg/cm^2a)		
System :	2.0	2.03
Steam Generator Secondary :	52	53.5
Temperature (°C)		
Downcomer Wall :	198	180
Primary Piping Wall :	119	119
Steam Generator Secondary :	265	267
Peak Clad at ECC Initiation :	502	530
Peak Clad at BOCREC :	600	607
Lower Plenum Filled Liquid :	119	110
ECC Liquid :	35	37.5
Water Level (m)		
Lower Plenum :	0.9	0.86
Steam Generator Secondary :	7.4	7.4
Injection Rate (m^3/hr)		
Accumlator :	251	283
LPCI :	40	40.4

Table 2.6 Test Conditions for Test C1-11

	Estimated	Measured
Power		
Total (MW) :	9.41	9.40
Linear (KW/m) :	1.4	1.4
Radial Power Distribution :	1.06:1.0:0.82	1.07:1.0:0.82
Decay Type : ANS x 1.2 + Actinide (30 sec after Scram)		
Pressure (kg/cm^2a)		
System :	2.0	2.05
Steam Generator Secondary :	52	51
Temperature (°C)		
Downcomer Wall :	198	178
Primary Piping Wall :	119	120
Steam Generator Secondary :	265	266
Peak Clad at ECC Initiation :	502	525
Peak Clad at BOCREC :	600	610
Lower Plenum Filled Liquid :	119	111
ECC Liquid :	35	39
Water Level (m)		
Lower Plenum :	0.9	0.88
Steam Generator Secondary :	7.4	7.3
Injection Rate (m^3/hr)		
Accumlator :	251	242
LPCI :	30	30.1

Table 2.7 Test Conditions for Test C1-13

	Estimated	Measured
Power		
Total (MW) :	9.41	9.40
Linear (KW/m) :	1.4	1.4
Radial Power Distribution :	1.06:1.0:0.82	1.07:1.0:0.82
Decay Type : ANS x 1.2 + Actinide (30 sec after Scram)		
Pressure (kg/cm^2a)		
System :	2.0	2.04
Steam Generator Secondary :	52	52
Temperature (°C)		
Downcomer Wall :	198	176
Primary Piping Wall :	119	119
Steam Generator Secondary :	265	265
Peak Clad at ECC Initiation :	502	524
Peak Clad at BOCREC :	600	601
Lower Plenum Filled Liquid :	119	114
ECC Liquid :	35	40
Water Level (m)		
Lower Plenum :	0.9	0.86
Steam Generator Secondary :	7.4	7.5
Injection Rate (m^3/hr)		
Accumlator :	251	277
LPCI :	30	30.3
Injection duration Time (s)		
Accumlator :	21	21

Table 2.8 Chronology of Events for Test C1-5

EVENT	TIME (sec)
Test C1-5 initiated (Heater rods power on) (Data recording initiated)	0.0
Accumulator injection initiated	52.5
Power decay initiated (Bottom of core recovery)	63
Accumulator injection switched from lower plenum to cold leg	67
Accumulator injection ended and LPCI injection initiated	77
All heater rods quenched	598
Power off	648
LPCI injection ended	738
Test ended (Data recording ended)	1068

Table 2.9 Chronology of Events for Test C1-6

EVENT	TIME (sec)
Test Initiated (Heater Rods Power on) (Data Recording Initiated)	0.0
Accumulator Injection Initiated	52.5
Power Decay Initiated (Bottom of Core Recovery)	63.0(64.0)
Accumulator Injection Switched from Lower Plenum to Cold Leg	67
Accumulator Injection Ended and LPCI Injection Initiated	77
All Heater Rods Quenched	595.5
Power Off	650
LPCI Injection Ended	770
Test Ended (Data Recording Ended)	1070

Table 2.10 Chronology of Events for Test C1-9

EVENT	TIME (sec)
Test Initiated (Heater Rods Power on) (Data Recording Initiated)	0.0
Accumulator Injection Initiated	54
Power Decay Initiated (Bottom of Core Recovery)	64.5(64.0)
Accumulator Injection Switched from Lower Plenum to Cold Leg	70
Accumulator Injection Ended and LPCI Injection Initiated	77
All Heater Rods Quenched	693.5
Power Off	768
LPCI Injection Ended	873
Test Ended (Data Recording Ended)	1071

Table 2.11 Chronology of Events for Test C1-11

EVENT	TIME (sec)
Test Initiated (Heater Rods Power on) (Data Recording Initiated)	0.0
Accumulator Injection Initiated	55
Power Decay Initiated (Bottom of Core Recovery)	66.0(67.5)
Accumulator Injection Switched from Lower Plenum to Cold Leg	72.5
Accumulator Injection Ended and LPCI Injection Initiated	78.5
All Heater Rods Quenched	598
Power Off	648
LPCI Injection Ended	948
Test Ended (Data Recording Ended)	1074

Table 2.12 Chronology of Events for Test C1-13

EVENT	TIME (sec)
Test Initiated (Heater Rods Power on) (Data Recording Initiated)	0
Accumulator Injection Initiated	53.5
Power Decay Initiated (Bottom of Core Recovery)	64.5
Accumulator Injection Switched from Lower Plenum to Cold Leg	70
Accumulator Injection Ended and LPCI Injection Initiated	74.5
All Heater Rods Quenched	603
Power Off	678
LPCI Injection Ended	858
Test Ended (Data Recording Ended)	1068

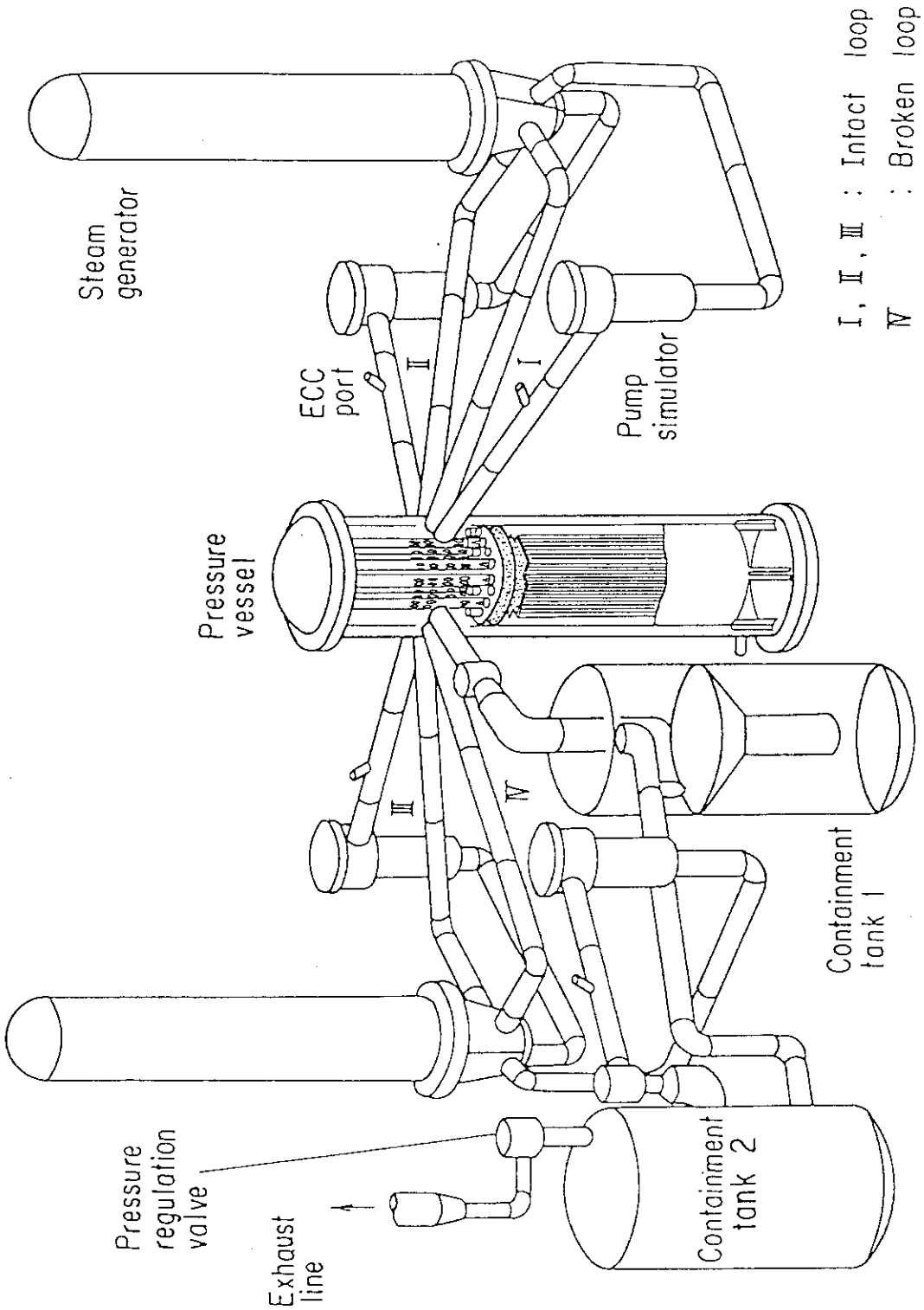

Fig. 2.1 Bird's-eye view of CCTF

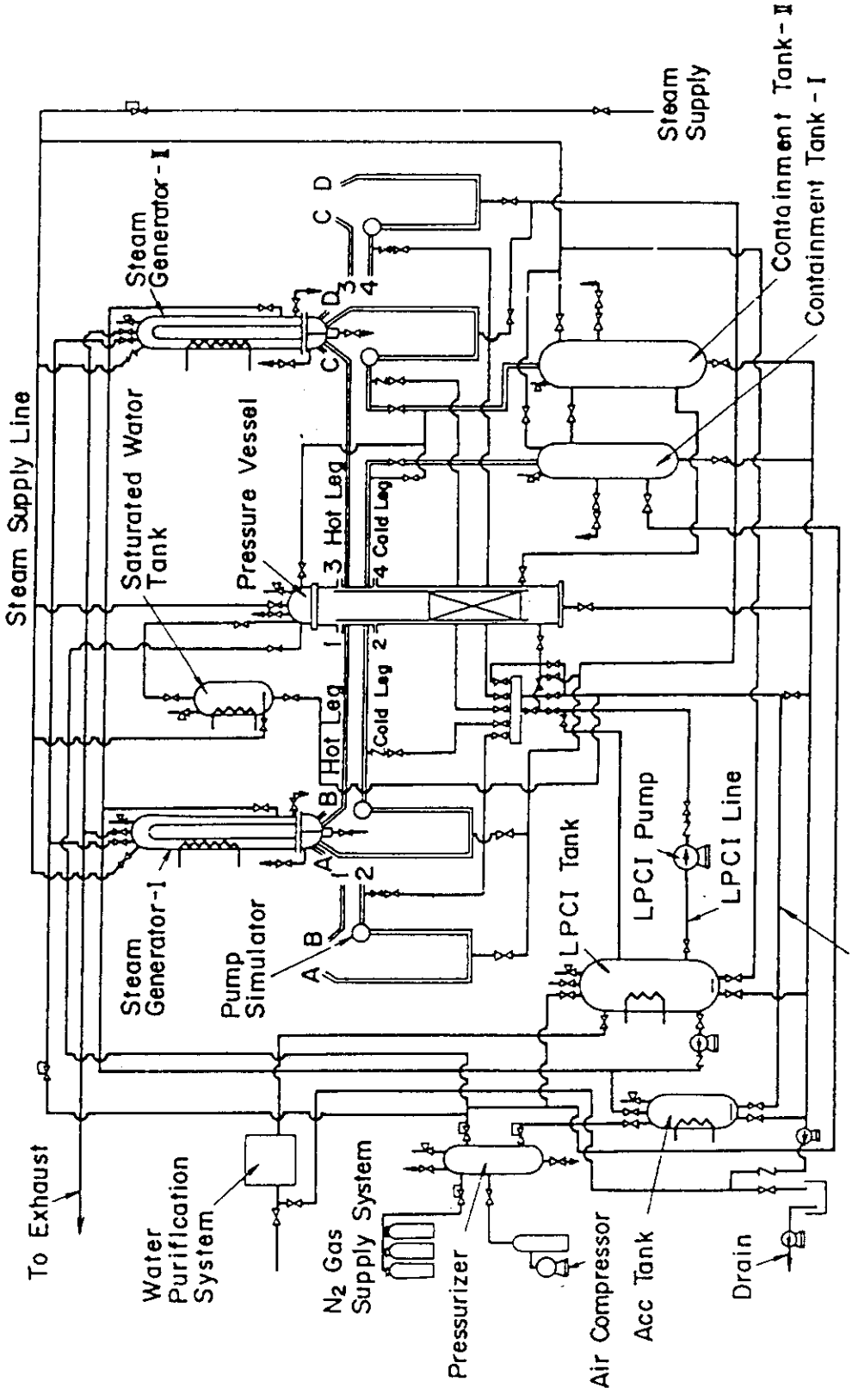

Fig. 2.2 Schematic diagram of CCTF

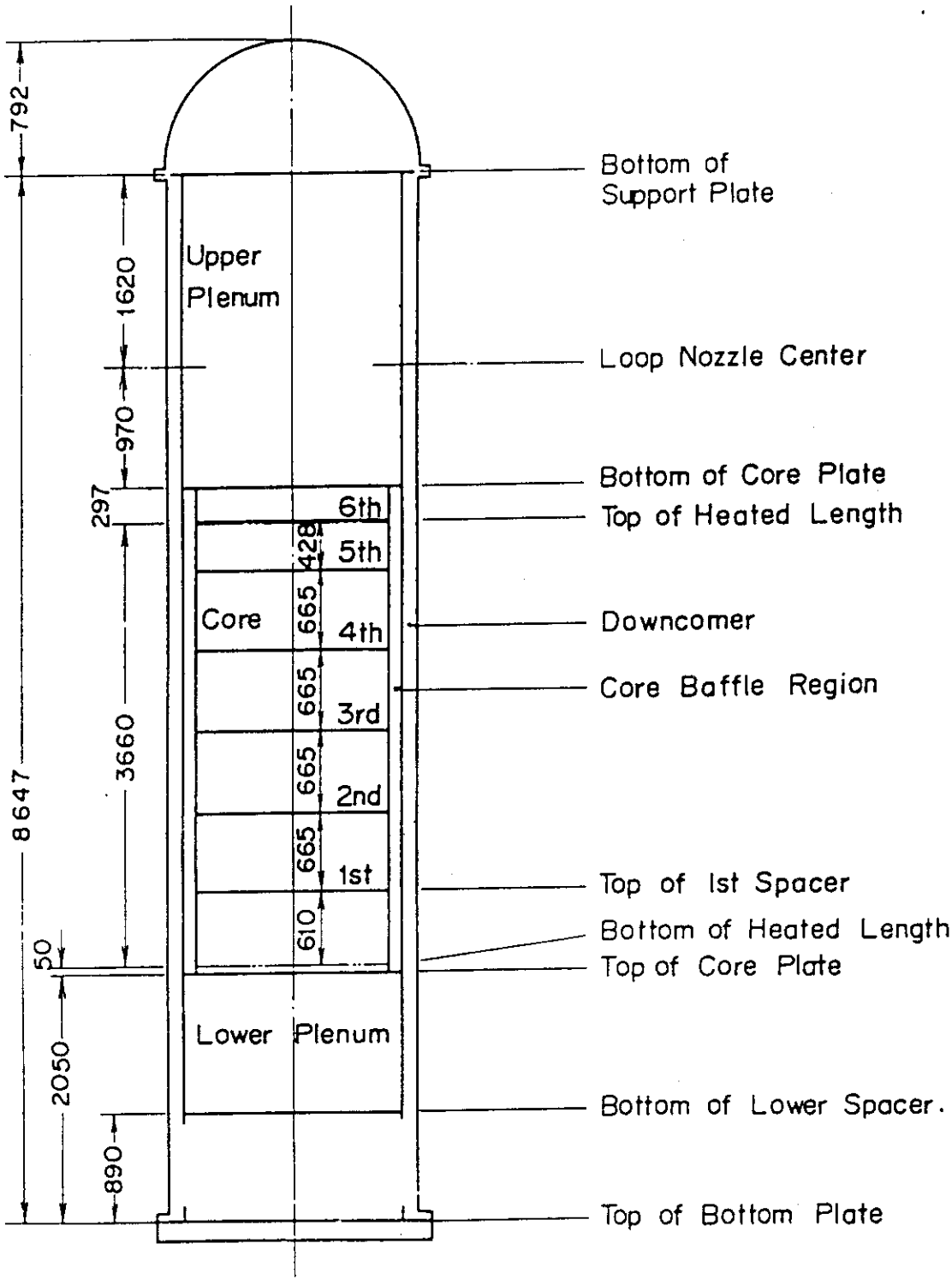

Fig. 2.3 Dimensions of pressure vessel

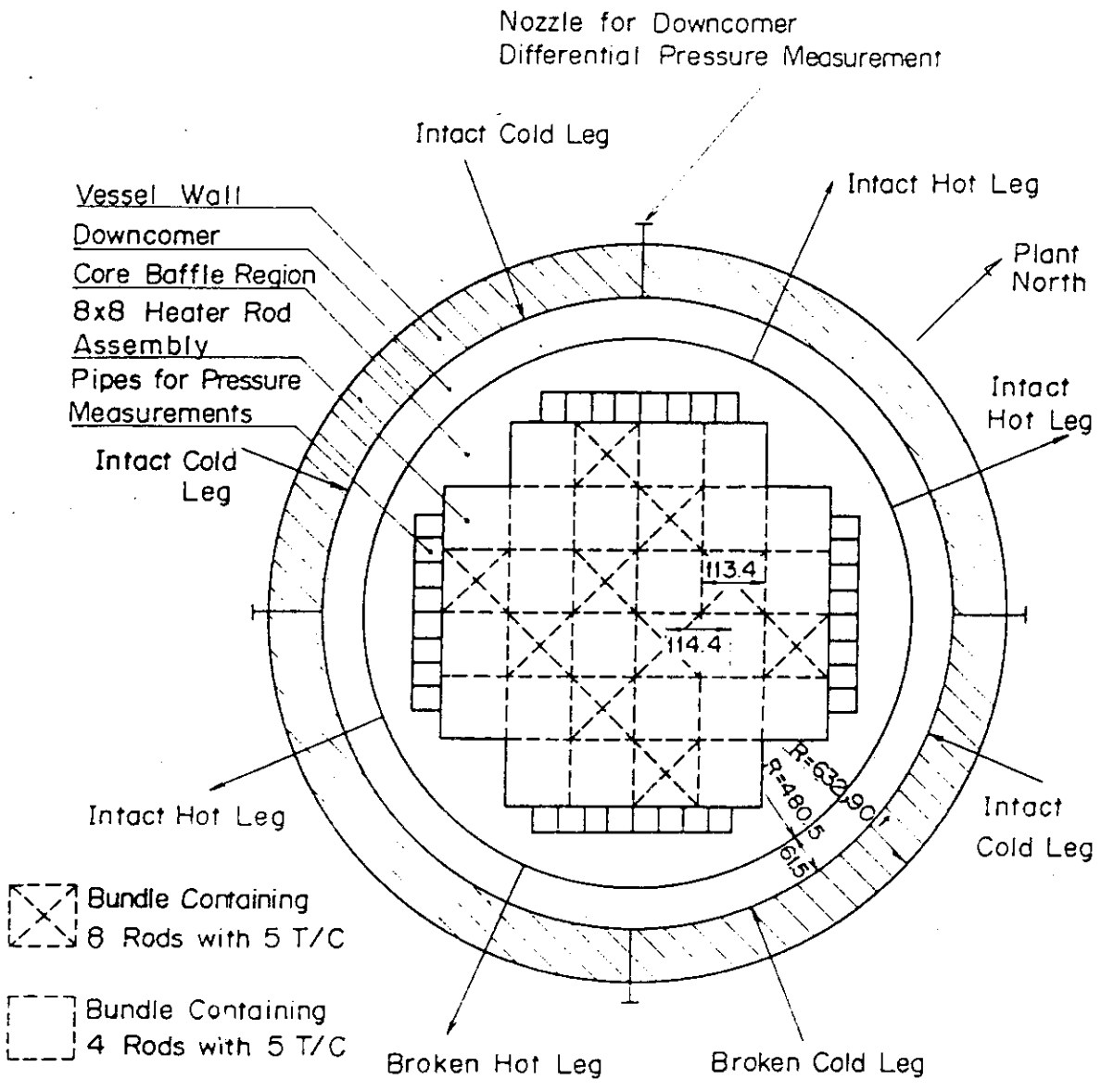

Fig. 2.4 Cross section of pressure vessel

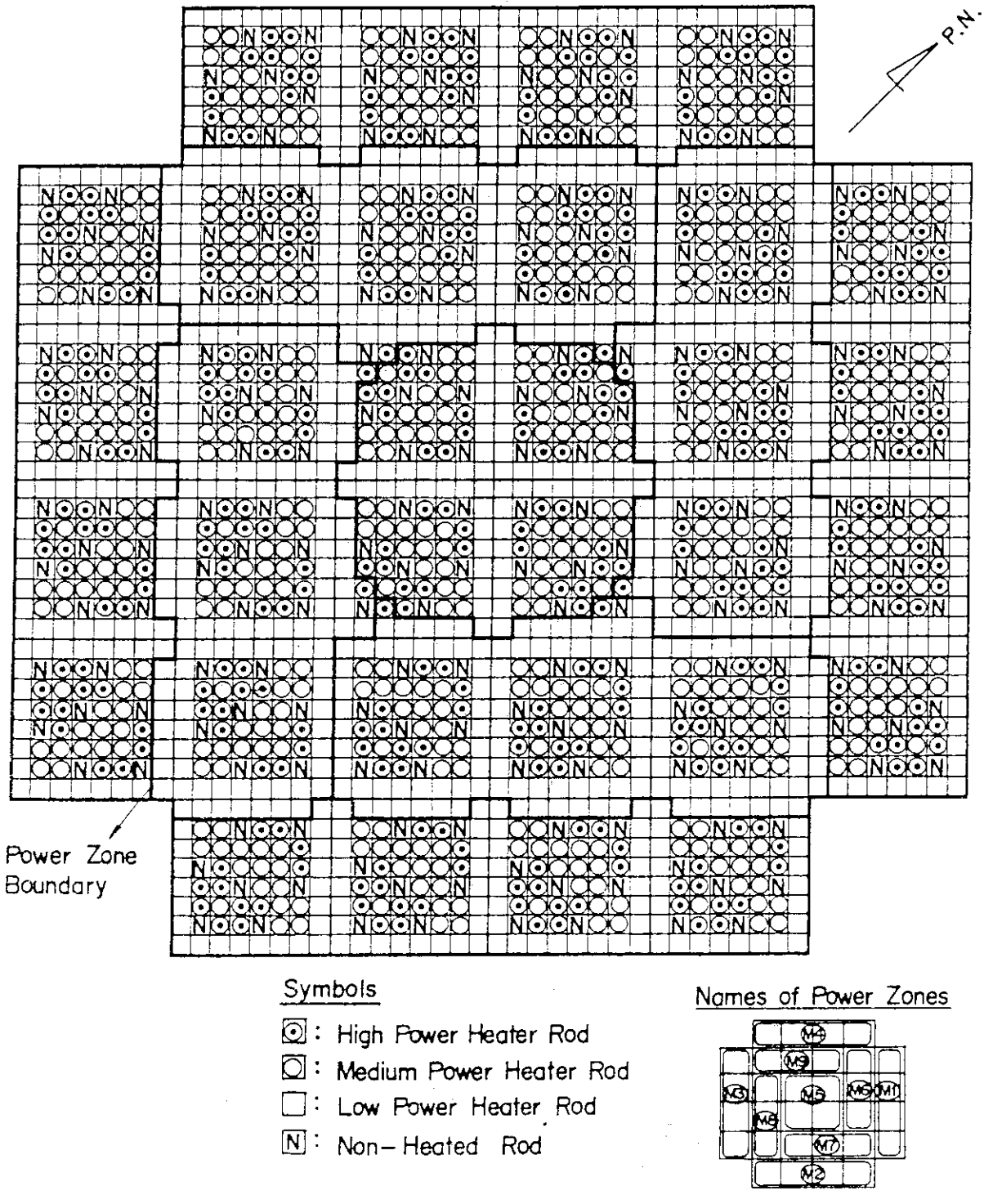

Fig. 2.5 Configuration of rods in core

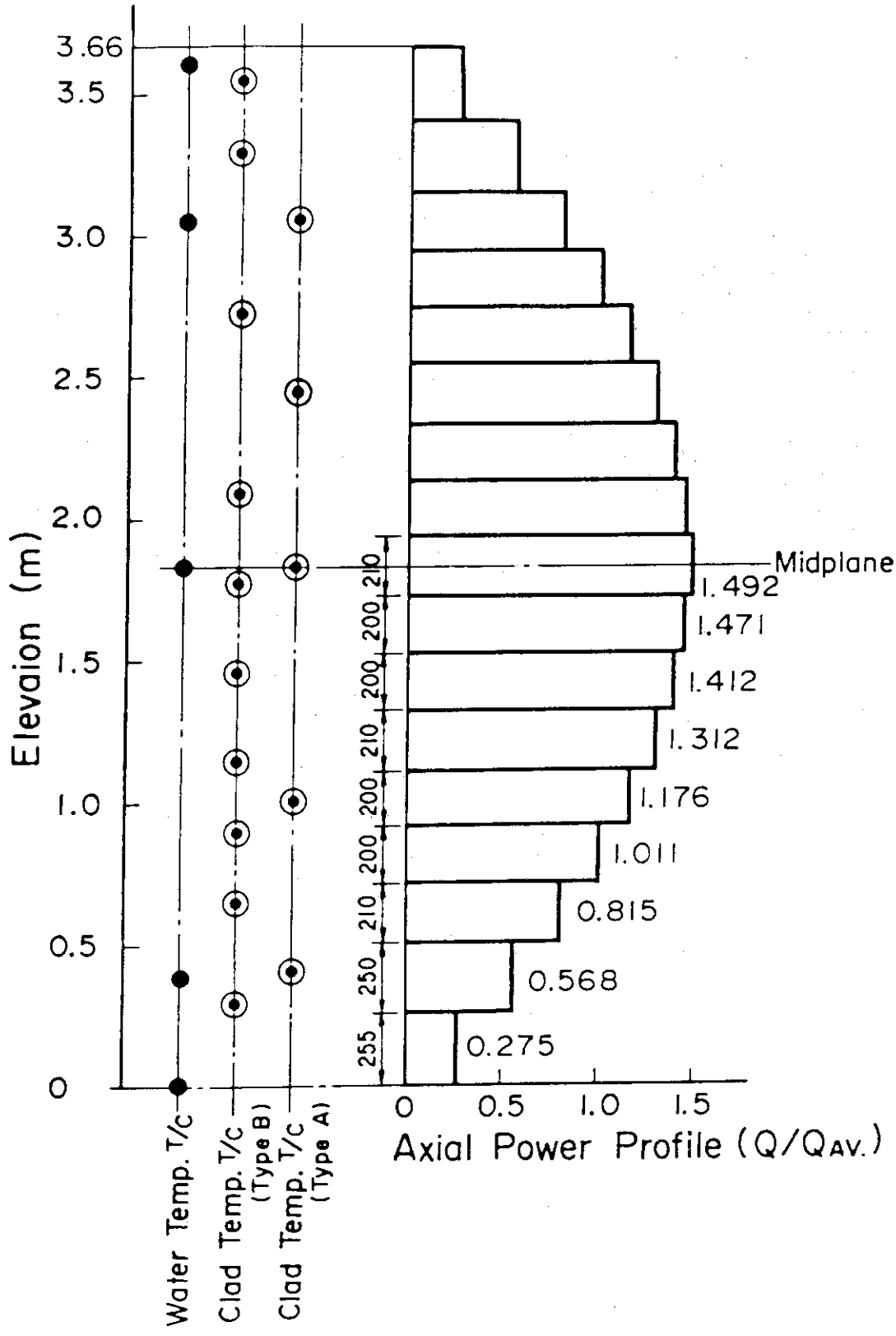

Fig. 2.6 Power profile and thermocouple elevations of heater rods

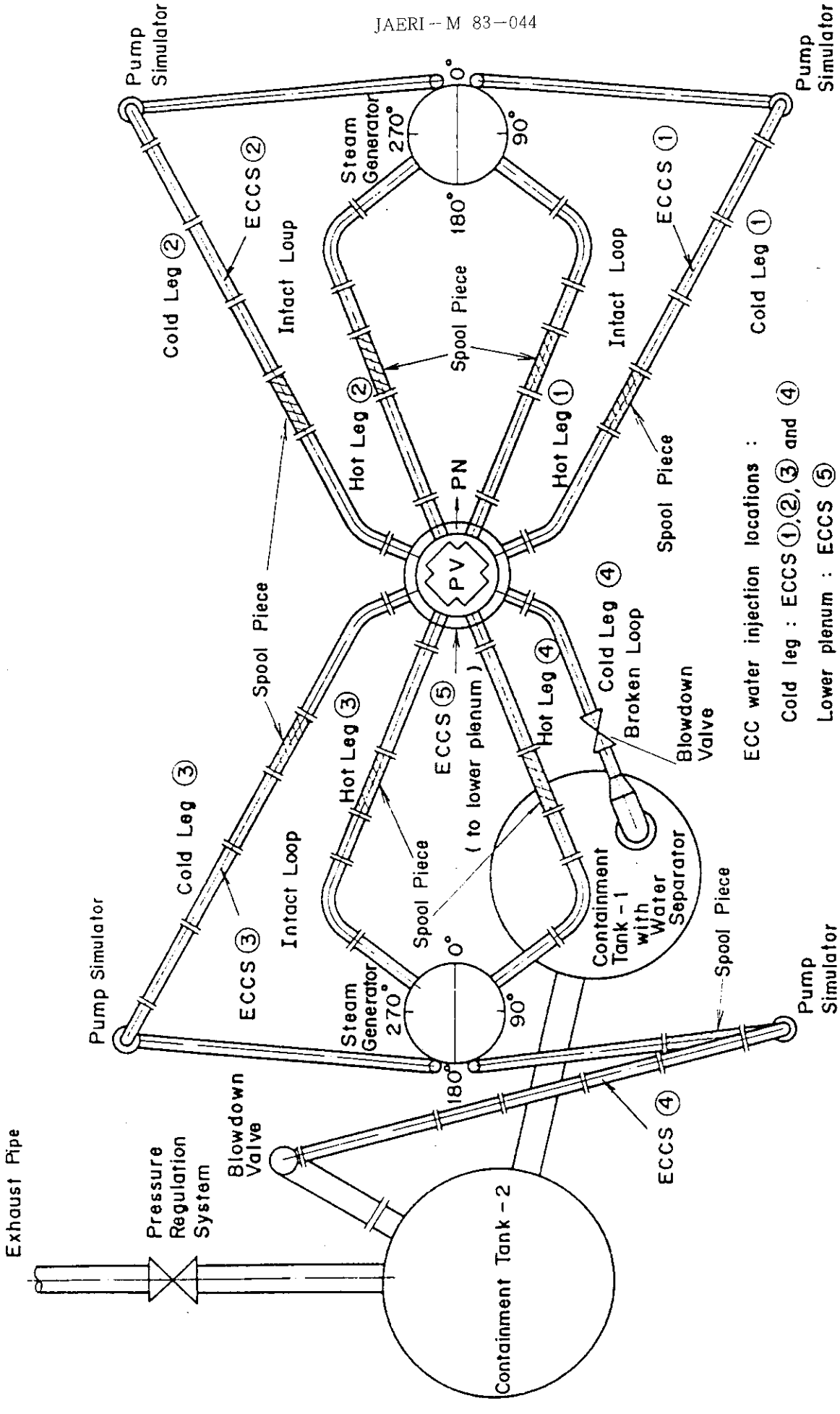

Fig. 2.7 Primary loop piping

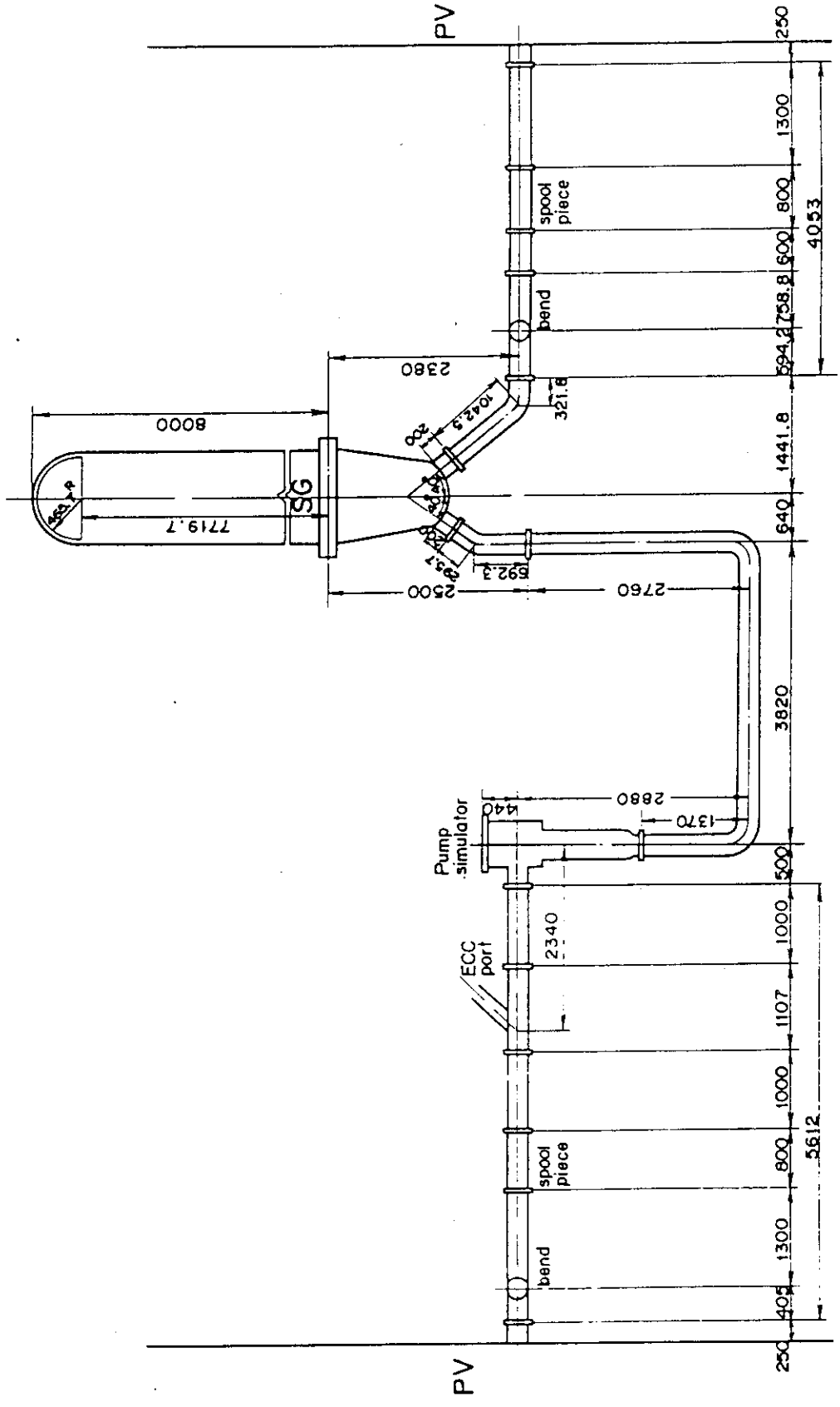

Fig. 2.8 Primary loop

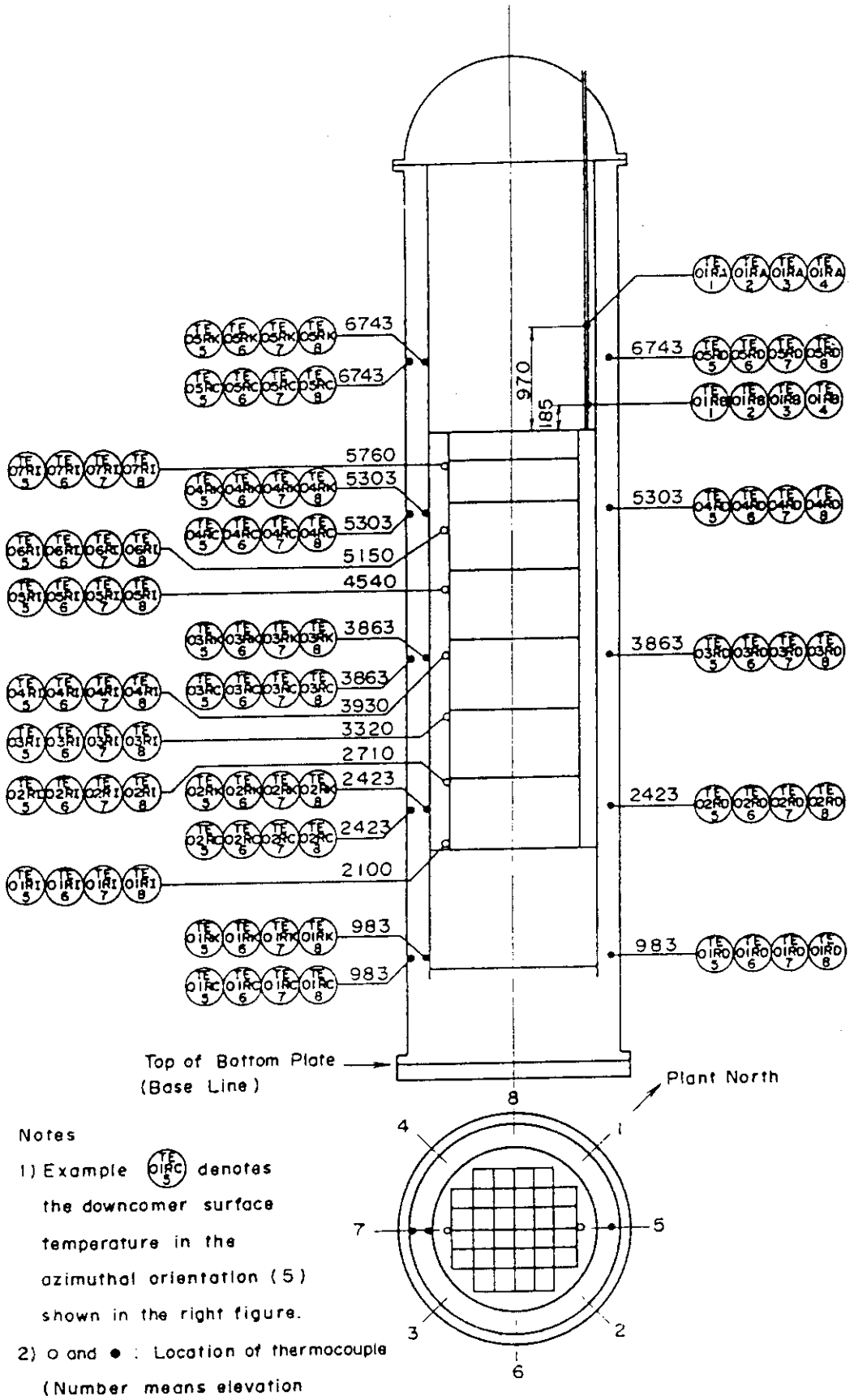

Fig. 2.9 Thermocouple locations in pressure vessel

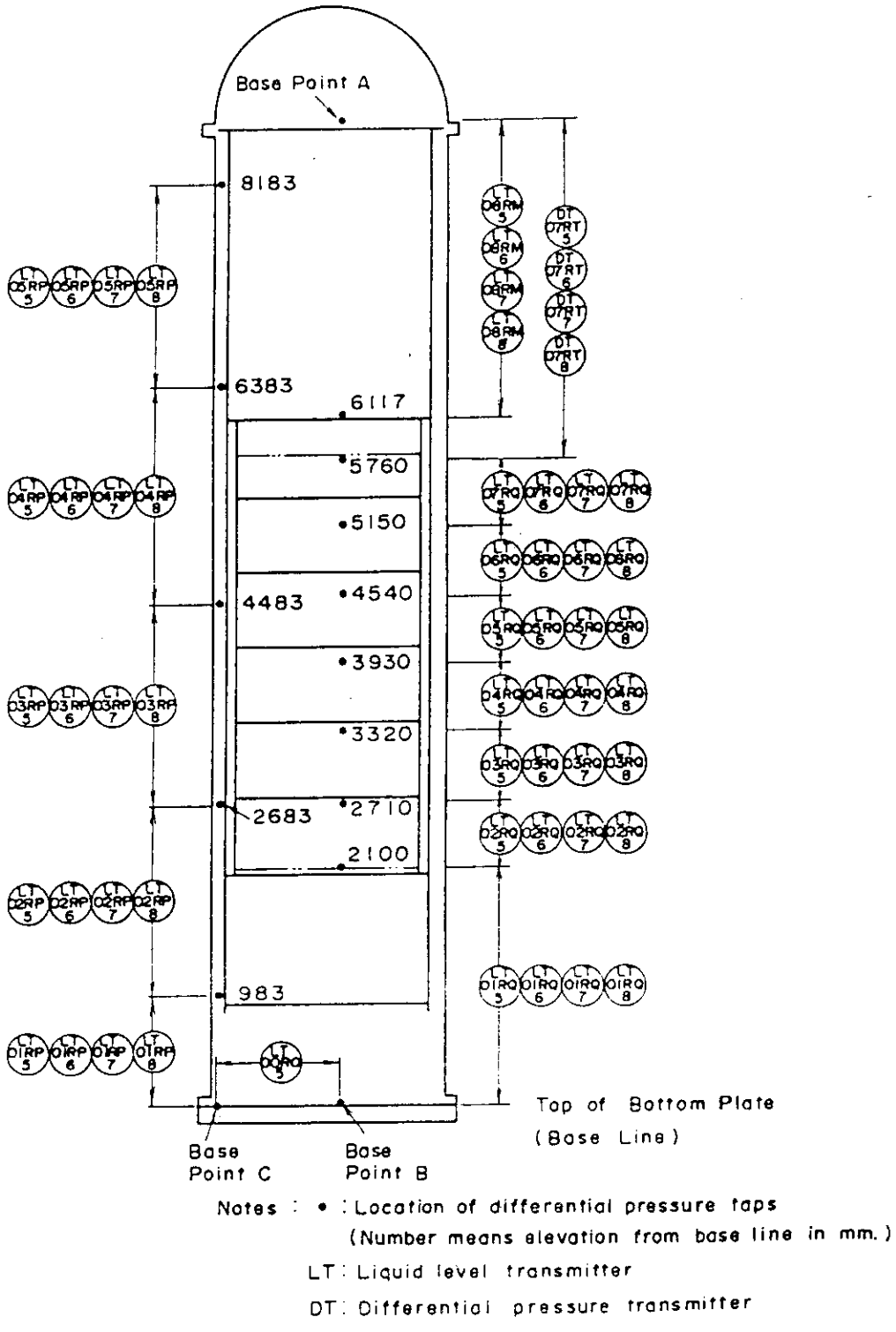

Fig. 2.10 Pressure, differential pressure and liquid level instrumentation locations in pressure vessel

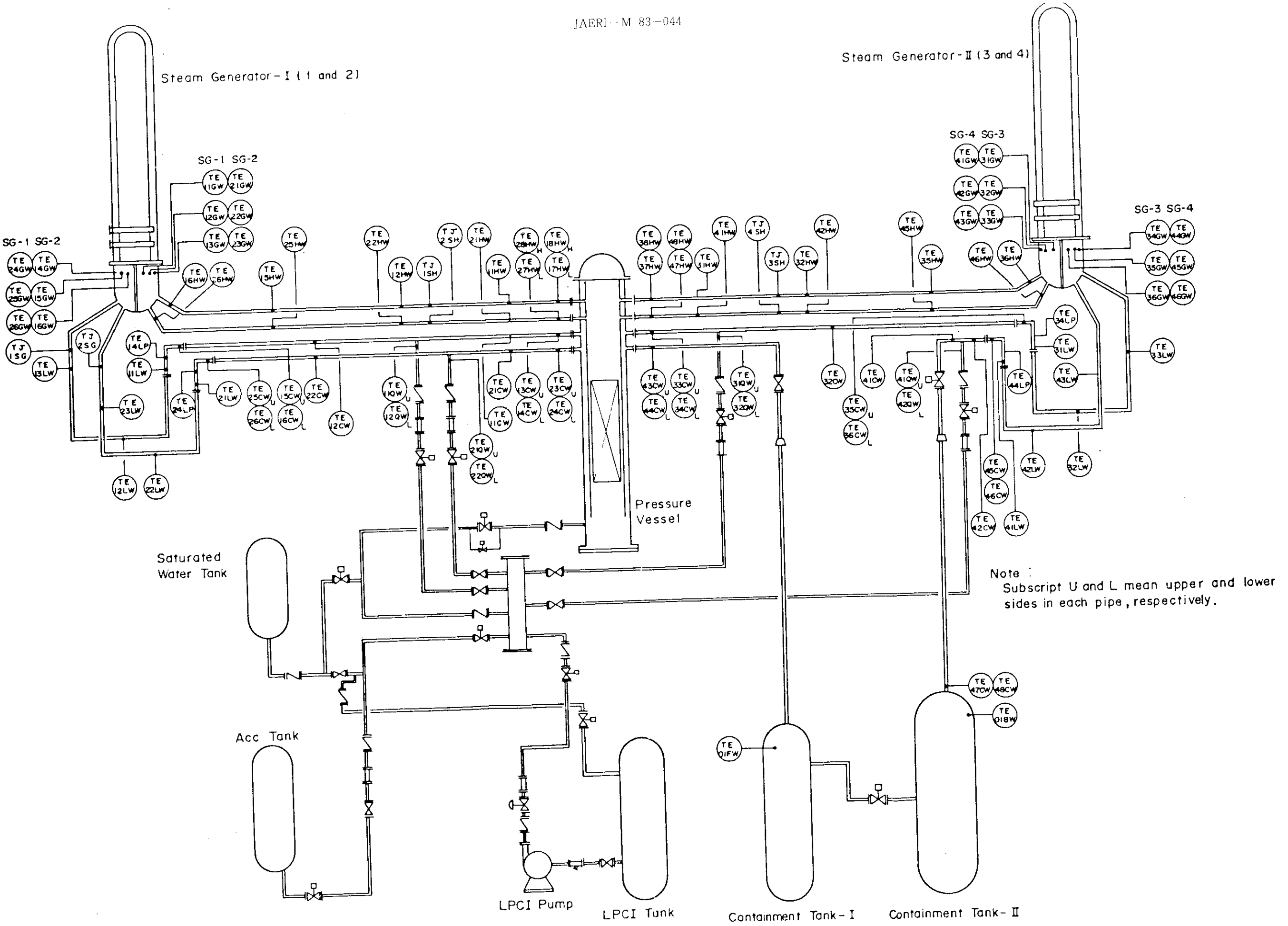

Fig. 2.11 Thermocouple locations in primary loop

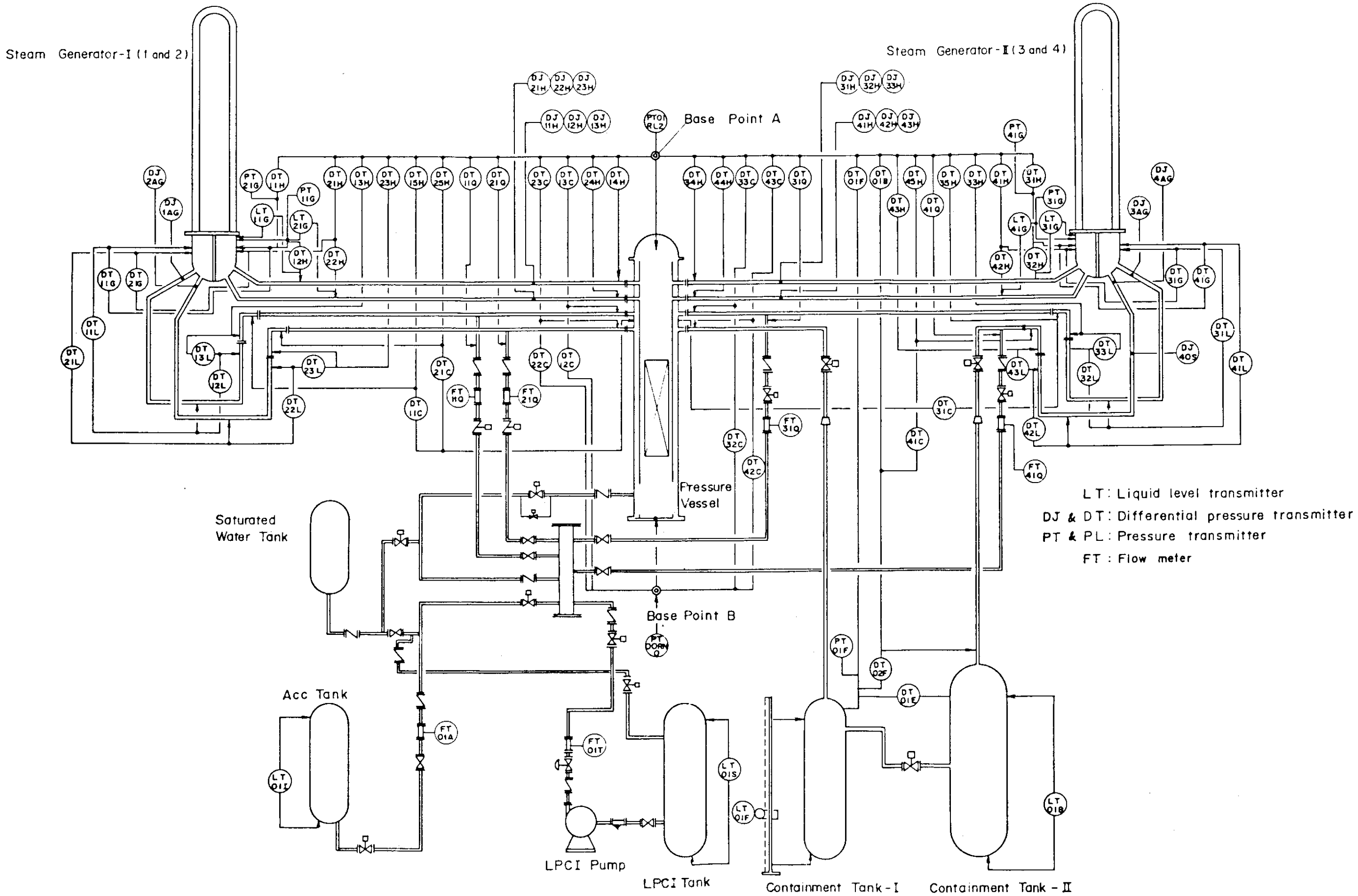

Fig. 2.12 Pressure, differential pressure and liquid level instrumentation locations in primary loop

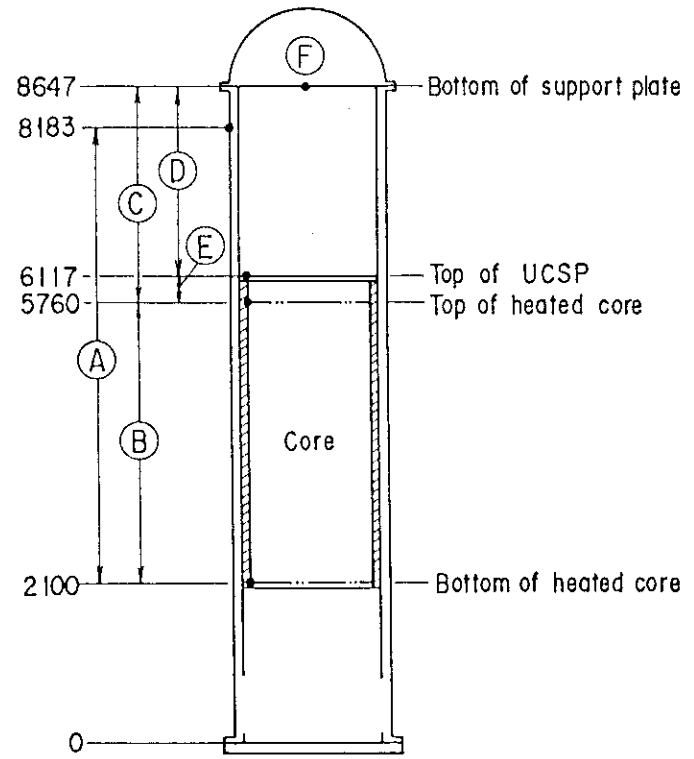

Unit : mm

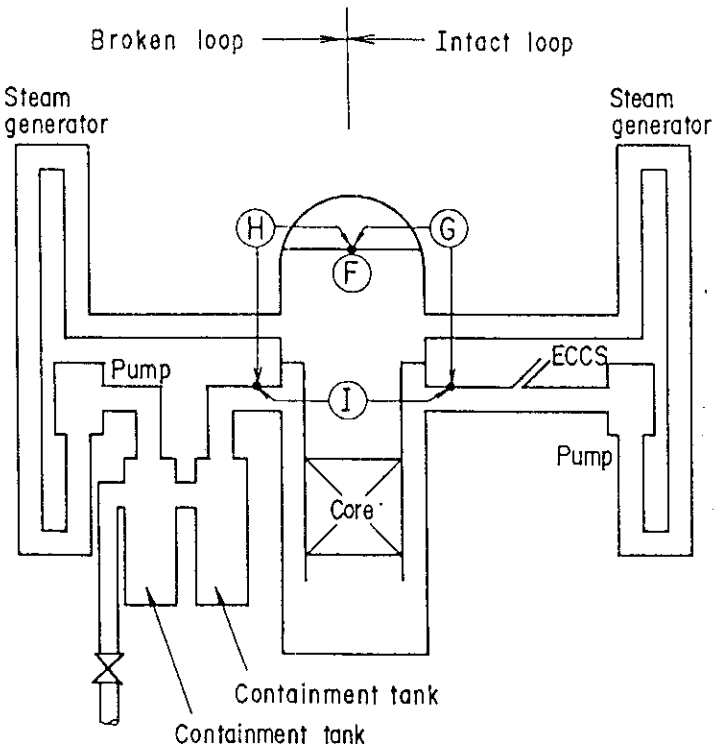

A : Downcomer differential pressure
B : Core differential pressure
C : Upper plenum differential pressure
D : Differential pressure above UCSP
E : Differential pressure in end box region
F : Upper plenum pressure
G : Intact loop differential pressure
H : Broken loop differential pressure
I : Differential pressure across boroken cold leg nozzle

Fig. 2.13 Definitions of pressure and differential pressures

3. Results and Discussion

3.1 Primary System Thermo-hydrodynamic Behavior

In this section, the thermo-hydrodynamic behavior observed in the primary system is analyzed. Since the overall thermo-hydrodynamic behavior in the CCTF system is presented in reference(2), an emphasis is placed upon the core flooding rate, the system pressure and the core inlet subcooling in this report. This is because they are the key factors to determine the core cooling and also they vary from test to test corresponding to the difference in the ECC water injection rate. Previous studies[1),(3)] have shown that each factor mentioned above results in a better core cooling when it gets larger.

In the following, the primary system behavior is investigated separately for the Acc injection rate and duration effects tests, *i.e.* the base case, the low Acc injection and the short Acc injection duration tests, and the LPCI injection rate effects tests, *i.e.* the base case, the high LPCI injection rate and the low LPCI injection rate tests. The former is presented in Section 3.1.1 and the latter is in Section 3.1.2. The effects of the broken cold leg injection are described in Section 3.1.3.

3.1.1 Effects of Acc Injection Rate and Duration

The differential pressures in the downcomer, core, intact loop and upper plenum for the Acc injection rate and duration effects tests are shown in Fig. 3.1. The definitions of these data are given in Fig. 2.13. Figure 3.1 summarize the data for the momentum balance in the system. As described later, the core flooding rate is determined by the momentum balance in the system.

In an early period, the downcomer differential pressures for the low Acc injection rate and the short Acc injection duration tests are lower than for the base case test. This is because the amounts of Acc water injected in these two tests were less than in the base case test. The downcomer differential pressures for those two tests, however, approach gradually that for the base case test and become almost identical by 150 s. The differential pressure for the low Acc injection rate test is nearly identical to that for the short Acc injection duration test except for the first 10 s. This is because the amount of ECC water injected during the Acc period for both tests were nearly the same.

Those amounts were about 75 percent of that for the base case test. During the first 10 s, the downcomer differential pressure is much lower in the low Acc injection rate test. This is due to its lower Acc injection rate.

The core, intact loop and upper plenum differential pressures follow the same trend as the downcomer differential pressures, as shown in Fig. 3.1. That is, the differential pressures for the base case test are higher than those for the other two tests in an early period, and in those two tests the differential pressures are similar. By 150 s, the differential pressures for all three tests become identical. During the first 10 s, the intact loop differential pressure for the low Acc injection rate test is nearly zero. This seems to be caused by the delay of the steam generation due to the higher water subcooling at the core inlet (Fig. 3.8) as well as the condensation of the steam in the upper plenum due to the slightly subcooled water observed to exist there by chance.

The core flooding rates are shown in Fig. 3.2. They are evaluated based on the mass balance calculation. Namely, the core flooding rate $\dot{m}_F$ was obtained using the following equation[2]:

$$\dot{m}_F = \dot{m}_C + \dot{m}_U + \dot{m}_L \ , \qquad (1)$$

where, the symbols $\dot{m}_C$ and $\dot{m}_U$ are the water accumulation rates in the core and in the upper plenum including the end box area, respectively. The symbol $\dot{m}_L$ is the total mass flow rate in all primary loops and is evaluated from the differential pressure data across the orifices in the pump simulators.

Figure 3.2 indicates that the core flooding rate for the base case test is the highest before 25 s but they become almost identical after that time. The core flooding rate for the low Acc injection rate test is smaller than for the other two tests during the first 5 s. This is corresponding to its lower Acc injection rate and downcomer differential pressure mentioned above. The core flooding rate for the short Acc injection duration test is almost identical to that for the base case test during the first 7 s. After 7 s, the core flooding rate for the short Acc injection duration test is almost identical to that for the low Acc injection rate test. The time-integrations of the core flooding rates are given in Fig. 3.3. The gradients of the curves give the average core flooding rates. They are almost identical and about 5.0 kg/s for the time period after 25 s. This mass flow rate corresponds

to the flooding velocity of about 2 cm/s. This figure also shows that the value for the low Acc injection rate test is the smallest.

The core flooding rate $\dot{m}_F$ is determined based on the momentum balance in the system, that is, the balance among the dowmcomer, core, upper plenum and intact loop differential pressures as described below in a quasi-steady state:

$$\dot{m}_F^2 \propto \Delta P_D - \Delta P_C - \Delta P_U - \Delta P_I \ , \qquad (2)$$

where, the symbols ΔP_D, ΔP_C, ΔP_U and ΔP_I are the downcomer, core, upper plenum and intact loop differential pressures, respectively.

This equation means that the downcomer differential pressure acts as a driving force for the core flooding, whereas the core, upper plenum and intact loop differential pressures act as the negative feed-back for it. Once the core flooding initiates, the water starts to accumulate in the core generating the steam. The steam generated flows through the primary loops causing the pressure drop. An increase of the downcomer differential pressure by the ECC water injection causes an increase of the core flooding rate. The differential pressures in the core, upper plenum and primary loops increase with the increased core flooding rate, but they, in turn, reduce the core flooding rate as estimated from above equation. The contribution of the upper plenum differential pressure is very small compared to the others as shown in Fig. 3.1.

If the increasing rate of the downcomer differential pressure is not high, the core flooding rate tends to be self-controlled to stay at a balanced value as the result of the negative feed-back effects mentioned above. Therefore, when the downcomer differential pressure becomes nearly constant, the core flooding rate is expected to stay at a balanced value. Figures 3.2 and 3.3 support above discussion indicating that the balance is achived by 25 s in those three tests and the balanced value of the core flooding rate is about 5.0 kg/s. It should be noted that the balance was achieved by 25 s in these cases, although it was much earlier than the time of 180 s when the downcomer differential pressures become nearly constant. This suggests that the negative feed-back was fairly effective and could follow the increasing rates of the downcomer differential pressures achieving the balance with it.

The primary system effects on the core flooding rate is evaluated from the discussion above, and this can reasonably explain that the core flooding rates are identical among the Acc injection rate and duration

effects tests after 25 s as shown in Fig. 3.2.

Figure 3.4 gives the water mass flow rates bypassing through the broken cold leg nozzle. They are nearly identical. In this figure, it should be noted that the timing of initiation for bypass is much earlier than when the downcomer water reaches the overflow level. This suggests that the bypass is caused by the steam flow in the intact loops. When the steam flow rate at the ECC port becomes higher than the rate of the steam condensation with the subcooled ECC water, the bypass is expected to begin. It should be noted that the bypass causes the reduction of the available ECC water for the core flooding, and hence, the reduction of the downcomer differential pressure increasing rate, resulting in the reduction of the core flooding rates in this period.

The differential pressures across the broken cold leg nozzle are shown in Fig. 3.5. They are the differences between the broken loop differential pressures and the intact loop differential pressures (Fig. 2.13). These fairly large pressure drops are evaluated to be caused by the acceleration and friction losses of the bypassing two-phase flow, because the two-phase flow from the three intact loops get together in the downcomer and then flow into the broken cold leg nozzle being accelerated significantly. The coincidence of the trends of the data shown in Figs. 3.4 and 3.5 suggests that the flow conditions for these three tests were nearly the same. This is consistent with the similarity of the other data for these three tests.

The pressure at the top of the upper plenum are shown in Fig. 3.6. Although it has been known[3] that the difference in the primary system pressure has significant effects on the core cooling and the system thermo-hydrodynamic behavior, the pressures for those Acc injection rate and duration effects tests are nearly identical indicating no difference in pressure effects among those tests.

Figure 3.7 shows the upper plenum differential pressures. They are divided into two parts. One is the differential pressures between the tops of the heated part of the core and the upper core support plate (UCSP) including the end box region, and the other is between the tops of the UCSP and the upper plenum. From this figure, it is found that the differential pressures above UCSP start to increase after the differential pressures in the end box region become to saturate. In the end box region, the differential pressures for the low Acc injection rate and the short Acc injection duration tests increase slower than for

the base case test, and hence, the increases of the differential pressures above the UCSP are later. The increase of the upper plenum differential pressure seems to have close relation with the core flooding rate.

Figure 3.8 shows the core inlet subcoolings for the Acc injection rate and duration effects tests. The data for the low Acc injection rate and the base case tests show much larger subcooling than for the short Acc injection duration test before 80 s. There seem to be two reasons for the lower subcooling for the short Acc injection duration test. One of them is its slightly higher (about 5 K) initial structure temperature measured in the lower plenum. The other is the higher water temperature measured in the downcomer. This is probably due to the smaller amount of the subcooled Acc water injected at the cold legs in this test. Although the amounts of the subcooled Acc water injected in the low Acc injection rate test was almost identical to that in the short Acc injection duration test, the considerable difference in the core inlet subcooling was obeserved in these two tests before 80 s. The reason for this difference has not been clarified. However, one important factor seems to be the lower downcomer water temperature measured in the low Acc injection rate test during that period. This lower downcomer water temperature can be attributed to the lower heating of the Acc water by the steam condensation in the cold leg due to the lower steam flow rate in an early period for the test.

As described above, the effect of the Acc injection rate and duration on the core inlet subcooling can not be concluded from the data of those tests. However, it should be noted that the difference in the core inlet subcooling becomes small and at most 5 K after 100 s.

3.1.2 Effects of LPCI Injection Rate

Figure 3.9 shows the differential pressures in the downcomer, core, intact loop and upper plenum for the LPCI injection rate effects tests. In the high LPCI injection rate test, the downcomer is filled rapidly and the differential pressure approaches the value corresponding to the overflow level (about 45 kPa) at about 60 s. This is due to its higher LPCI injection rate. After that time, however, the downcomer differential pressure begins to decrease and becomes identical to that for the base case test at about 180 s. This decraese seems to be caused by the overflow of the downcomer water to the break through the broken cold leg nozzle (Fig. 3.12). After 180 s, the downcomer differential pressure increases

gradually to the overflow level value. In contrast, in the low LPCI injection rate test, the downcomer differential pressure becomes nearly constant at a much lower value than the overflow level value. This is because the LPCI injection rate was not enough to fill the downcomer. The core, intact loop and upper plenum differential pressures for the low LPCI injection rate test are smaller than those for the base case test, corresponding to the smaller downcomer differential pressure for the low LPCI injection rate test than for the base case test. The intact loop differential pressure for the high LPCI injection rate test is larger than for the base case test. The core and upper plenum differential pressures are also larger around 60 s in the high LPCI injection rate test than in the base case test. They are also coincident with the larger downcomer differential pressure in the high LPCI injection rate test than in the base case test. However, after 180 s, the core and upper plenum differential pressures for the high LPCI injection rate test are almost identical to those for the base case test. This is attributed to the almost identical core flooding rates in the two tests, which are shown in the next figure.

The core flooding rates are shown in Fig. 3.10. During the first 17 s, all the values are nearly identical. This is consistent with the nearly identical differential pressures shown in Fig. 3.9 in that period. After that, in the high LPCI injection rate test, the core flooding rate becomes higher than in the other two tests for about 50 s. This is corresponding to the higher increasing rate of its downcomer differential pressure shown in Fig. 3.9. After 60 s, however, the core flooding rate begins to decrease and becomes a little lower than in the base case test around 100 s. This is understood to be caused by the decrease of the downcomer differential pressure after 60 s, as shown in Fig. 3.9. After about 130 s, the core flooding rates for the high LPCI injection rate and the base case tests become identical in average. The average core flooding rates for both the tests are about 5.0 kg/s after 130 s. They were obtained from the time-integration data of the core flooding rate shown in Fig. 3.11. The gradients of the curves give the average core flooding rate.

In the low LPCI injection rate test, the core flooding rate is lower than in the other two tests after Acc injection period (14 s) as shown in Fig. 3.10. The average core flooding rate after 60 s is about 3.6 kg/s (Fig. 3.11). This lower core flooding rate is due to its lower

downcomer differential pressure resulting from the lower LPCI injection rate in the test.

From the results and discussion mentioned above, the downcomer differential pressure is found to work as an driving force for core flooding, as also observed in the Acc injection rate and duration effects tests. Before the downcomer is filled with ECC water, the larger downcomer differential pressure results in the higher core flooding rate.

The water mass flow rates bypassing through the broken cold leg nozzle are shown in Fig. 3.12. The bypass is mainly caused by the uncondensed steam flow in the intact cold legs as described in the previous sction. However, when the ECC water injection rate is high enough to completely condense the steam flowing in the cold legs, the overflow of the downcomer is expected to cause the bypass. In the high LPCI injection rate test, about 90 percent of the steam flowing in the cold legs is evaluated to be condensed at the ECC ports based on the mass and energy balance calculation. Therefore, in the high LPCI injection rate test, the bypass is expected to be caused by the overflow of the downcomer water as well as the uncondensed steam. For the high LPCI injection rate test, the bypassing water mass flow rate is significantly higher than for the base case test, and the difference between them is about 10 kg/s. This value is almost equal to the summation of the differences in the LPCI injection rates (8.9 kg/s) and the steam condensation rates (1.3 kg/s, based on the mass and energy balance calculation at the ECC ports) between these two tests. This suggests that once the downcomer is almost filled, an exessive amount of ECC water just bypasses the downcomer to the break without increasing the core flooding rate.

For the low LPCI injection rate test, the bypassing water mass flow rate is about 2 kg/s. This indicates that the bypass of ECC water occurs and is fairly large even in the case with a relatively lower downcomer differential pressure (about 30 kPa) than the overflow level value (45 kPa). This is due to the uncondensed steam flow in the cold leg.
In this test, the bypass was expected to be enhanced, because its lower LPCI injection rate resulted in the higher mass flow rate of the uncondenced steam. Therefore, in this test, the higher uncondensed steam flow as well as the lower LPCI injection rate significantly reduced the available ECC water for the core flooding resulting in the lower core flooding rate and the lower downcomer differential pressure.

As recognized from Fig. 3.12, the downcomer bypass occurs much earlier

than the time when the downcomer water reaches the overflow level in the base case test (Fig. 3.9), whereas in the high LPCI injection rate test, the bypass is not noticeable until 50 s. This is due to the higher steam condensation rate at the ECC port in the high LPCI injection rate test. This results in the higher water accumulation rate in the downcomer, causing the core flooding rate to be higher.

The differential pressures across the broken cold leg nozzle for the LPCI injection rate effects tests are shown in Fig. 3.13. The value is different from test to test, and the pressure drop for the high LPCI injection rate test is the lowest. The difference is caused by the difference in the flow conditions in the three tests. For instance, the average steam qualities in the broken cold leg have been evaluated to be 0.24, 0.04 and 0.47 based on the mass and energy balance calculation for the base case, high LPCI injection rate and low LPCI injection rate tests, respectively.

The upper plenum pressures are presented in Fig. 3.14. The pressure for the base case test becomes the highest after 200 s. This is attributed to the highest pressure drop in the broken cold leg nozzle for the base case test shown in Fig. 3.13. From the results of the pressure parametric effects tests of the CCTF Core-I series, the higher primary system pressure has been found to increase the core flooding rate. The main reason for this is found to be the increase of the steam density at the higher pressure. From Fig. 3.14, the difference in the upper plenum pressure is 15 kPa at most. This increase of the pressure is evaluated to increase the loop mass flow rate by about 6 percent keeping the loop differential pressure the same. Therefore, it is concluded to be only a little difference.

Figure 3.15 shows the upper plenum differential pressures. Although the differential pressures in the end box region are similar in all tests, the upper plenum differential pressures and thier increasing rates are different from test to test. This differences correspond to the differences in the core flooding rates shown in Fig. 3.10.

The core inlet subcoolings are shown in Fig. 3.16. The data for the base case and the high LPCI injection rate tests are nearly identical. The low LPCI injection rate test gives the larger subcooling in an early period, but the magnitude of difference becomes small gradually. A little larger subcooling during an early period in this test seems to be caused by the lower initial temperature in the lower plenum region as described in the following.

Figure 3.17 shows the core inlet fluid temperatures from the beginning of the tests. The initial fluid temperatures for the low and high LPCI injection rate tests are lower than for the base case test by 38 K and 16 K, respectively. The same magnitudes of the differences were observed in the initial temperatures on the inner surface of the core barrel and the surface of the other structures in the lower plenum region. These data suggest that the initial temperatures in the lower plenum region for the low and high LPCI injection rate tests were lower than for the base case test by 38 K and 16 K, respectively, and hence, caused the increases of the core inlet subcoolings in those two tests during an early period.

Therefore, the large differences in the core inlet subcooling observed among those tests were concluded to be caused mainly by the differences in the initial temperatures in the lower plenum region and judging from a little difference in the subcoolings after 100 s, it can be said that the effect of the LPCI injection rate on the core inlet subcooling is not large.

3.1.3 Effects of Broken Loop Injection

As mentioned in Section 2.3, the ECC water was injected into the broken cold leg as well as the intact cold legs in the low LPCI injection rate test. In the following, the effects of the broken cold leg injection is investigated.

In this test, out of the total injection rate of 0.011 m^3/s, only 0.0047 m^3/s was distributed to the three intact loops and the remainder (0.0064 m^3/s) to the broken loop. As already mentioned, the differences in the LPCI injection rate was caused by the differences in the pressure at the ECC ports, because the LPCI in the CCTF is shared with all four loops and the injection rates are determined significantly depending upon the pressures at the ECC ports. However, in an actual reactor, the injection system is normaly designed to mitigate the dependency of the injection rate on the pressures at the ECC ports. Therefore, the nonunitorm distribution of the LPCI water injection rate observed in the CCTF test is not expected to occurr in an actual reactor and is not discussed further.

Figure 3.18 shows the differential pressures between the pump exit in the broken loop and the containment tank 2. The differential pressure for the low LPCI injection rate (*i.e.* broken cold leg injection) test is about 0.7 kPa after 100 s, whereas the values for the base case and the high LPCI injection rate tests are seven to ten times larger. Since the injected LPCI water into the broken cold leg was 0.0064 m^3/s, about 80 percent of the

steam flowing there is evaluated to be condensed forming downstream a two-phase flow with a relatively low quality (about 0.03). This results in the reduction of the pressure drop described above. The reduction of the pressure drop results in the reduction of the total flow resistance of the broken loop. In order to confirm the reduction of the flow resistance, the K-factor were compared among the LPCI injection rate effects tests. The K-factor is defined as

$$K = 2\Delta P/\rho u^2 \ , \qquad (3)$$

where, ΔP is the pressure drop, and ρ and u are the density and velocity of the fluid, respectively. The evaluated K-factor for the pressure drop between the upper plenum and containment tank 2 was smaller by 10 percent in the low LPCI injection rate test than in the other tests.

The reduction of the flow resistance in the broken loop results in the increase of the mass flow rate in the broken loop. This, in turn, results in the decrease of the mass flow rate, and hence, the differential pressure in the intact loops. According to the momentum balance in the primary system, the reduction of the intact loop differential pressure causes the core flooding rate to be higher. Therefore, a decrease of the pressure drop in the broken cold leg is concluded to cause a better core cooling. Since the frictional pressure drop tends to increase corresponding to an increase of the quality of two-phase flow, it can be concluded that to inject enough ECC water to condense all the steam flowing in the broken cold leg is of advantage to the better core cooling during the reflood phase.

3.2 Core Thermo-hydrodynamic Behavior

The comparison of the rod surface temperature histories is presented in Fig. 3.19 for an average power rod (*i.e.* Z-rod in B-region, see Appendix A) at the midplane level (1.83 m). The average linear power densities of the rod were 1.4 kW/m. The temperature for the high LPCI injection rate test turnarounds earliest at 59 s and then becomes the lowest. After about 120 s, however, it becomes closer to that for the base case test gradually and quench at the same time. In contrast, the temperature in the low LPCI injection rate test turnarounds last at 131 s and becomes the highest after that. The quench time is longer by 32 s than in the base case test. In the low Acc injection rate test, on the other hand, the temperature is higher than in the base case test. The turnaround

temperature is higher by 57 K and the quench time is longer by 14 s. Also, in the short Acc injection duration test, the temperature is higher than in the base case test. Although the temperature for this test is lower than in the low Acc injection rate test until the turnaround time, they become identical each other after that and quench at the same time.

The tendencies of the rod surface temperature histories shown in Fig. 3.19 are consistently explained with those of the core flooding rates shown in Figs. 3.2 and 3.10, as described in the following. The higher core flooding rate until 60 s in the high LPCI injection rate test resulted in the earlier turnaround and the lower temperature than in the base case test, whereas the same average core flooding rates in these two tests after 130 s caused the nearly identical temperature histories after 200 s and the same quench time. In contrast, the lower core flooding rate in the low LPCI injection rate test resulted in the higher temperature history with the higher turnaround temperature and the longer quench time.

The higher temperature histories in the low Acc injection rate and the short Acc injection duration tests than in the base case test are mainly the results of the lower core flooding rates during the first 25 s. However, a little higher initial rod surface temperatures than in the base case test are also the reason for those higher temperatures to some extent, especially in the low Acc injection rate test. The differences in the initial temperatures were caused by the differences in the BOCREC time. The important point is that the difference in the core flooding rates during the first 25 s caused a considerable difference in the rod surface temperature histories.

From above-mentioned results, it can be said that the cooling during the Acc injection period influences the temperature rise significantly and determines the trend of the rod surface temperature history. That is, the better cooling during the Acc injection period results in the earlier turnaround at the lower temperature, whereas the worse cooling during that period causes the temperature to get higher resulting in the later turnaround at the higher temperature, and the difference between them are considerable.

Figure 3.20 shows the rod surface temperature histories of the same rod as in Fig. 3.19 but for the 2.44 m elevation. The tendencies are almost the same as those at the midplane level, although the worse cooling in the low LPCI injection rate test is more remarkable at this elevation.

The quench time for this test is longer than for the base case test by 78 s and the turnaround temperature is the highest.

Figure 3.21 gives the heat transfer coefficients for the average power rod at the midplane level. They are evaluated from the data of the rod surface temperature and the supplied power. From this figure and Fig. 3.19, it can be confirmed that the tendencies of the rod surface temperature histories follow those of the heat transfer coefficients. It should be noted that the heat transfer coefficient for the short Acc injection duration test is larger than for the low Acc injection rate test before 65 s. This means that the core cooling during that period was better in the short Acc injection duration test corresponding to its higher core flooding rate shown in Fig. 3.2, although the total amounts of the Acc water injected were almost the same in those two tests.

The quench envelopes for the average power rod are shown in Fig. 3.22. In the low LPCI injection rate test, the quench front moves significantly slower especially in the upper half of the core as already observed in Fig. 3.20. In the low Acc injection rate and the short Acc injection duration tests, the quench envelopes are nearly identical to each other and the differences from the base case test is found to be caused in an early period. After that, the difference is almost constant. The quench envelope for the high LPCI injection rate test is almost identical to that for the base case test.

Figure 3.23 shows the average void fractions in two sections, that is, between 1,22 m and 1.83 m and between 1.83 m and 2,44 m in the core. They are evaluated from the differential pressure measurements. It should be noted that the void fractions starts to decrease at the beginning of the reflooding even in the upper part of the core. In both the sections, much lower void fraction in the high LPCI injection rate test around 60 s is remarkable. This is attributed to its higher core flooding rate as shown in Fig. 3.10. In contrast, in the 1.83 - 2.44 m section, the void fraction for the low LPCI injection rate test is much higher than for the other tests. This is also attributed to its lower core flooding rate (Fig. 3.10). The void fraction influences the core cooling and the higher void fraction tends to result in the smaller heat transfer coefficient.

3.3 Comparison with FLECHT-SET Experiments

In the FLECHT-SET Phase A experiments[1], the effects of the Acc injection rate on the core flooding phenomena have been investigated.

The scaling ratio for the FLECHT-SET facility to an reference PWR is 1/370, whereas 1/21.4 for the CCTF. Therefore, the CCTF is 17 times larger than the FLECHT-SET facility. The purpose of this section is to investigate the scaling effects on the Acc injection rate and duration effects, that is, to investigate whether the Acc injection rate and duration effects on the core cooling differ between the different size facilities.

The FLECHT-SET Phase A experimental facility consists of a test section with a 10×10 rod bundle, a simulated primary loop and a downcomer piping. The major experimental conditions are summarized in Table 3.1 for the concerned FLECHT-SET Phase A experiments and CCTF Core-I tests. In Fig. 3.24, the ECC water injection rates for those concerned tests are compared. The injection rates in the figure are normarized by the core flow area. As an example of the results for the FLECHT-SET Acc injection rate and duration parameter effects tests, the quench envelopes are shown in Fig. 3.25.

Based on reference (1), the effects of the Acc injection rate and duration observed in the FLECHT-SET Phase A experiments are summarized in the following:

(1) The higher Acc injection rate caused the higher increasing rate of the downcomer differential pressure resulting in the higher core flooding rate.

(2) The higher core flooding rate resulted in the larger heat transfer coefficient and the faster moving of the quench front (Fig. 3.25).

(3) Although the amounts of the Acc water injected in Runs 3117 and 2605 were almost the same, the core flooding rate and the heat transfer coefficient were observed to be larger in Run 3117 (higher injection rate initially) during the initial period of the transient.

The items mentioned above were also observed in the CCTF Acc injection rate and duration effects tests, as described in the previous sections. Therefore, it can be concluded that although the sizes of the facilities are different significantly between the CCTF and the FLECHT-SET facility, the effects of the Acc injection rate and duration on the downcomer water accumulation behavior and the core cooling behavior observed in the FLECHT-SET Phase A experiments were the same as observed in the CCTF tests.

Table 3.1 Summary of Test Conditions of CCTF and FLECHT-SET Phase A

	CCTF	FLECHT-SET Phase A
System pressure (MPa)	0.20	0.14
Initial clad temperature (°C)	600	600
Average linear power (kW/m)	1.4	1.4
Peak linear power (kW/m)	2.7	2.3
ECC water temperature (°C)	40	70

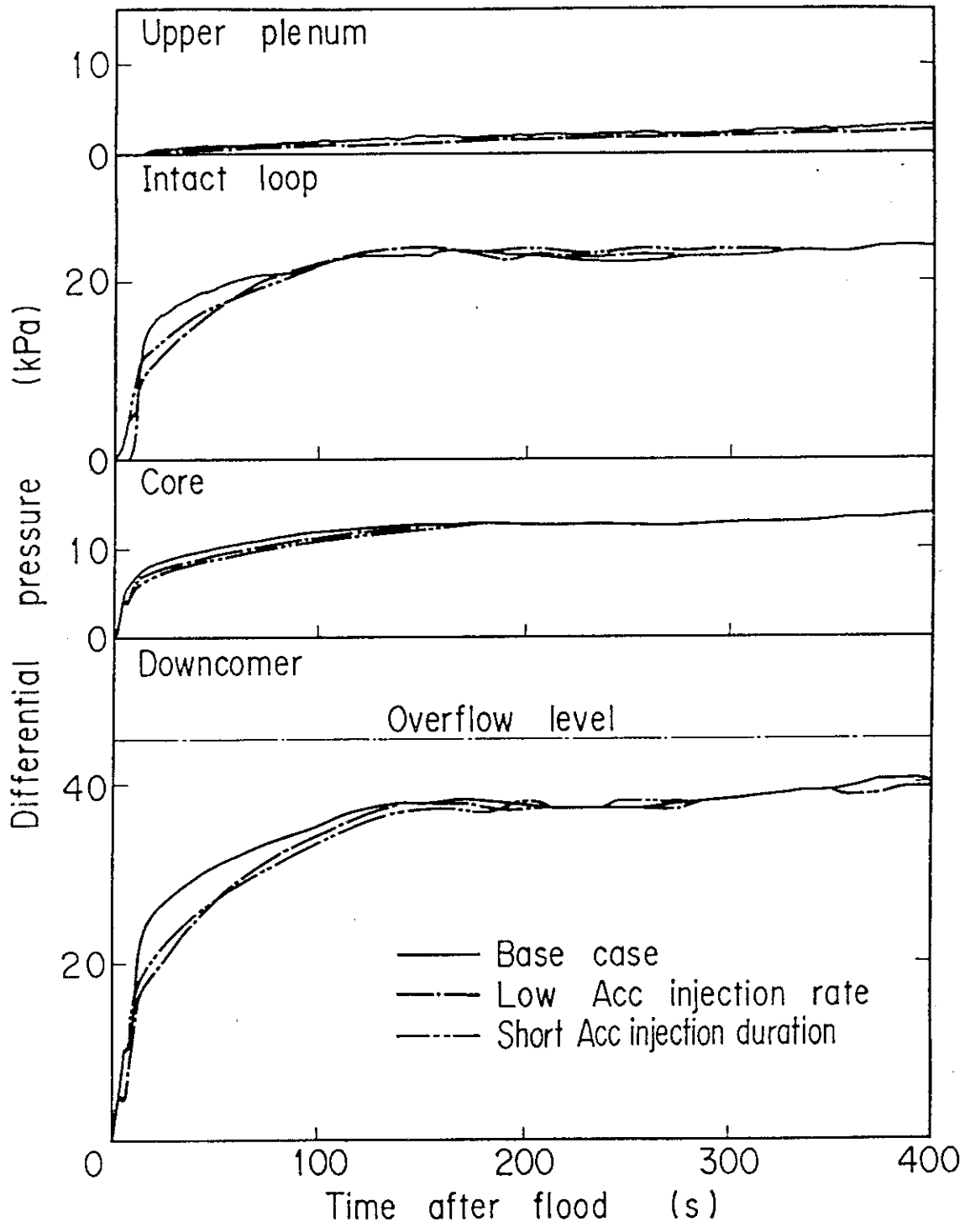

Fig. 3.1 Differential pressures in downcomer, core, intact loop and upper plenum for Acc injection rate and duration effects tests

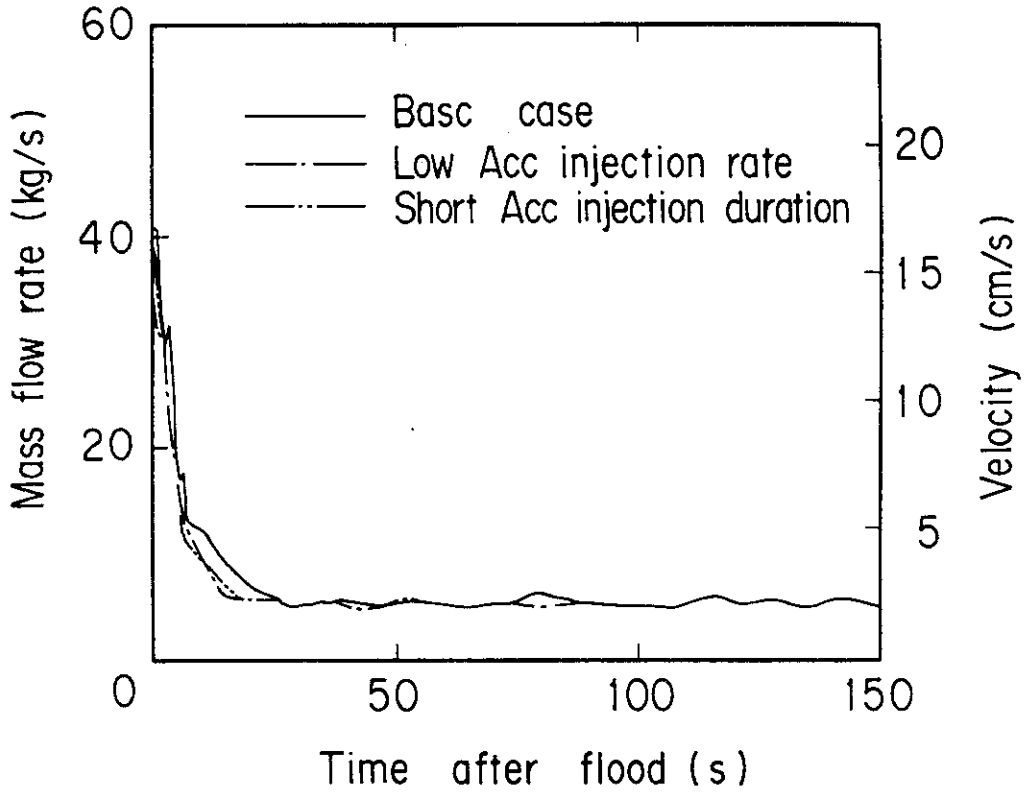

Fig. 3.2 Core flooding rates for Acc injection rate and duration effects tests

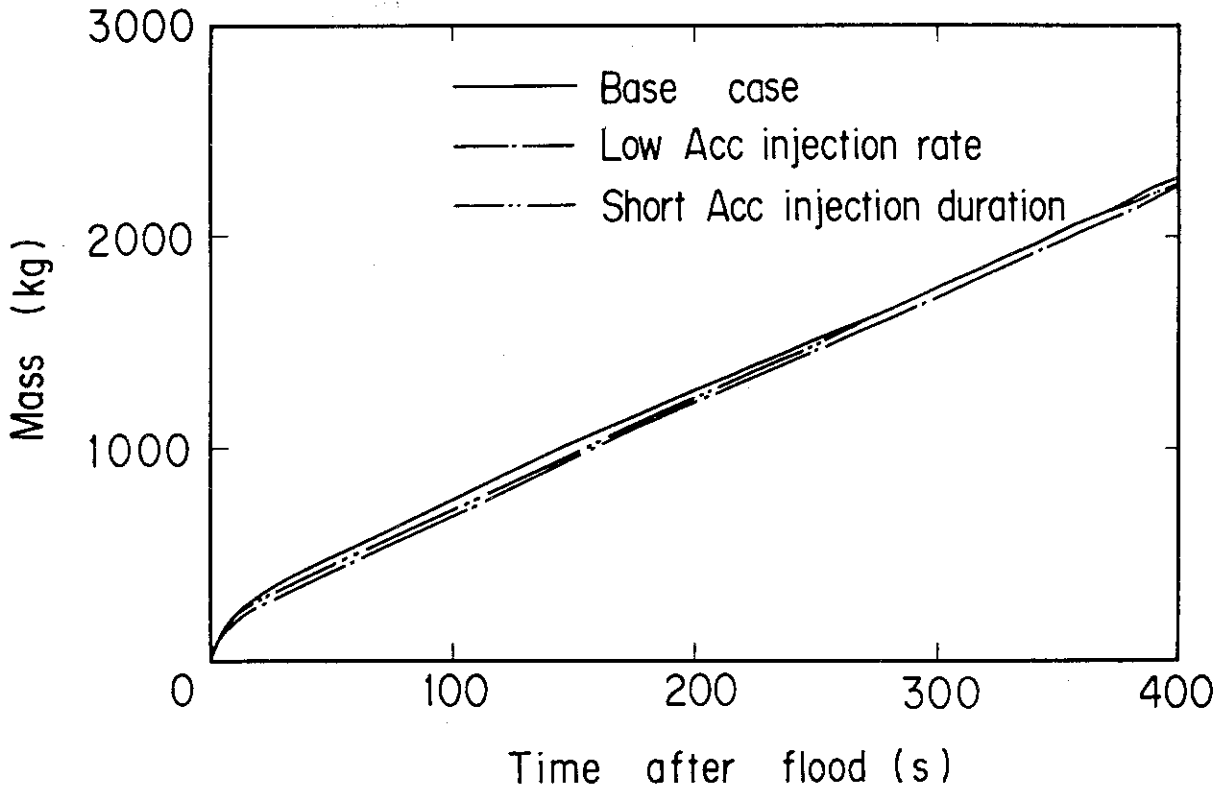

Fig. 3.3 Time-integrations of core flooding rates for Acc injection rate and duration effects tests

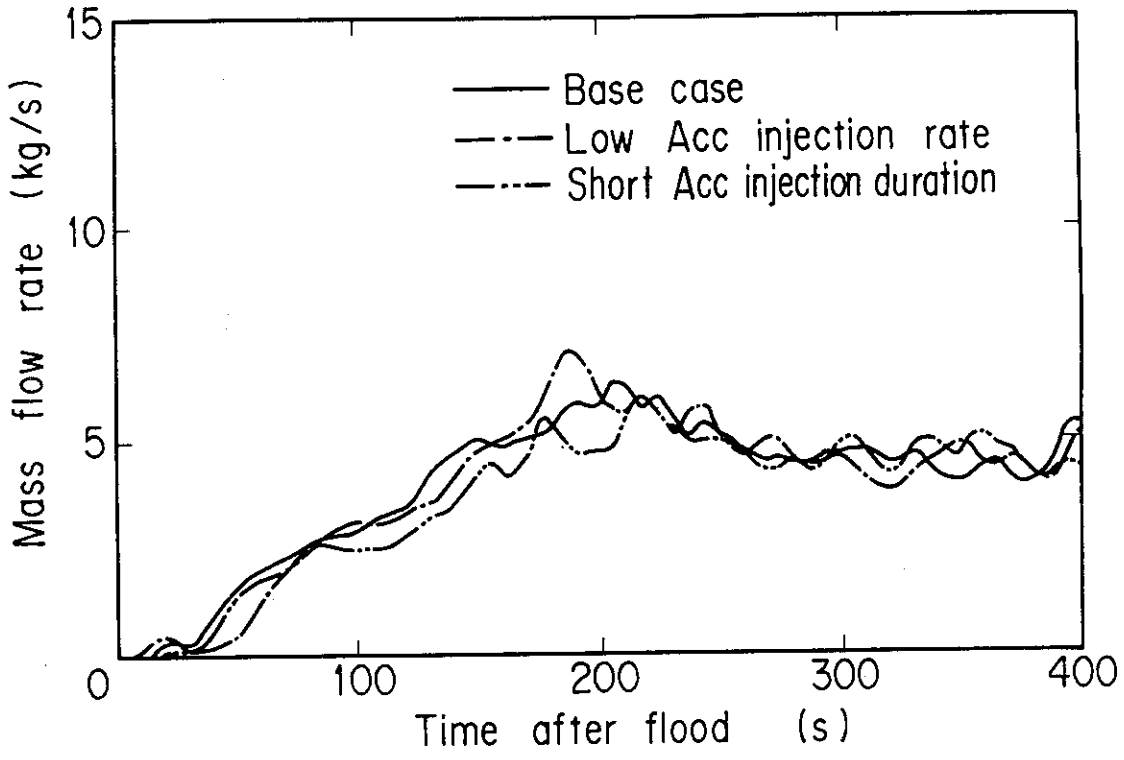

Fig. 3.4 Bypassing water mass flow rates for Acc injection rate and duration effects tests

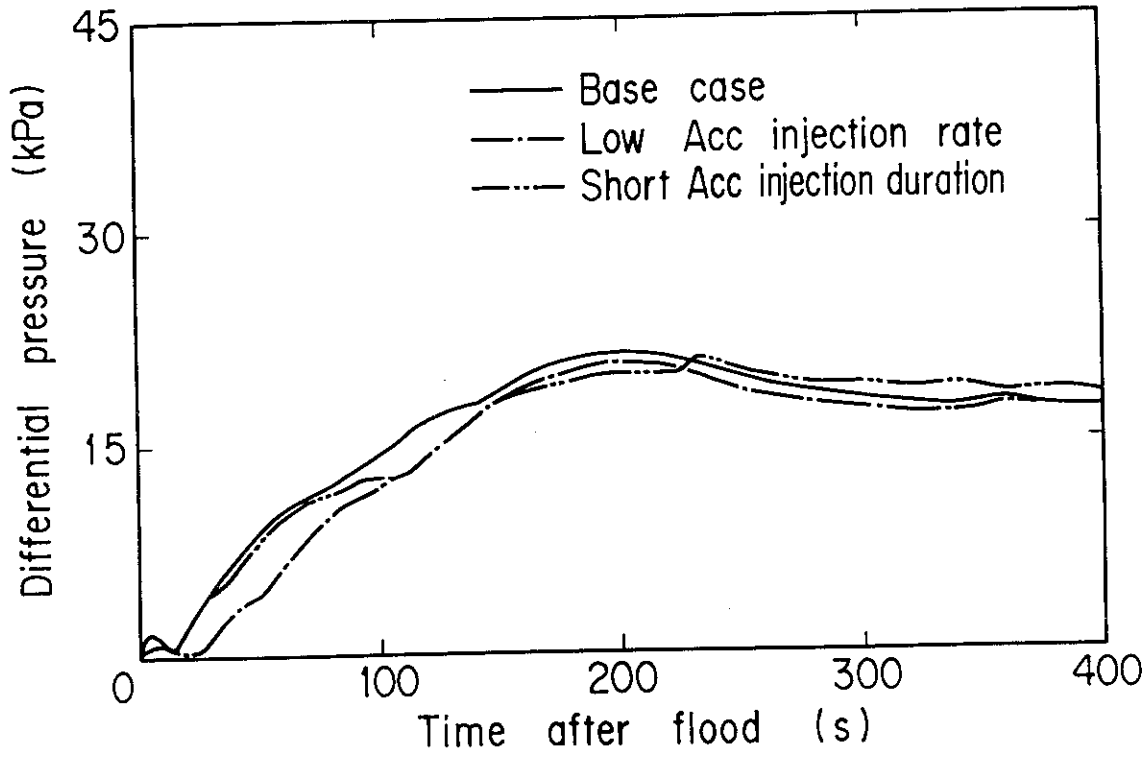

Fig. 3.5 Differential pressures across broken cold leg nozzle for Acc injection rate and duration effects tests

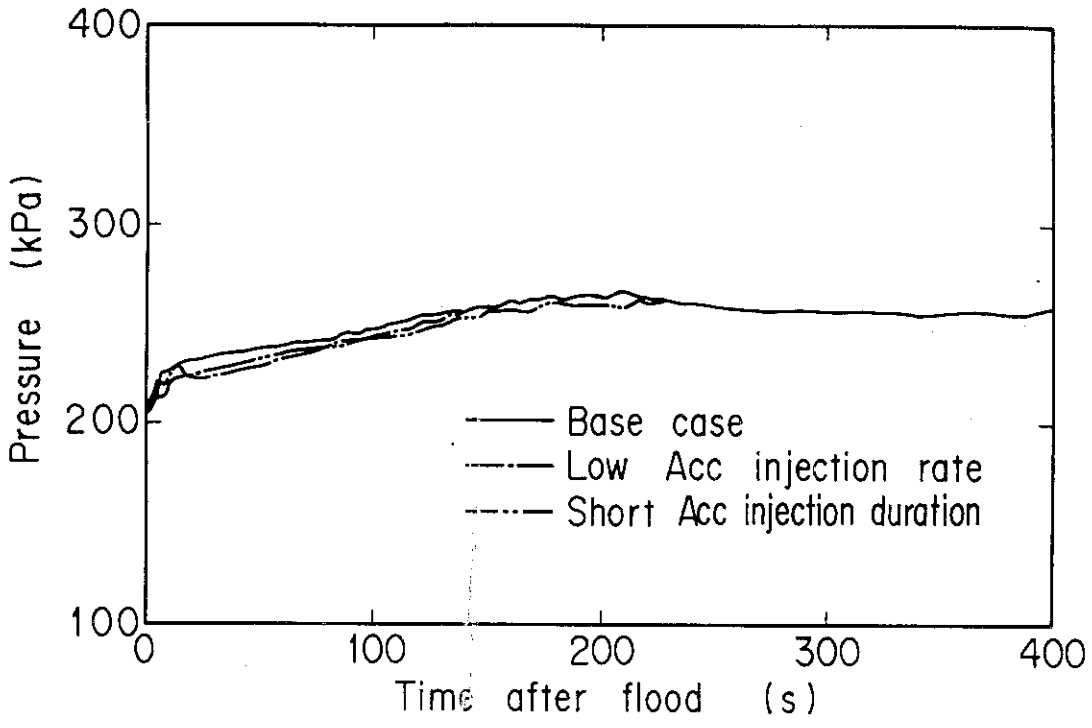

Fig. 3.6 Upper plenum pressures for Acc injection and duration effects tests

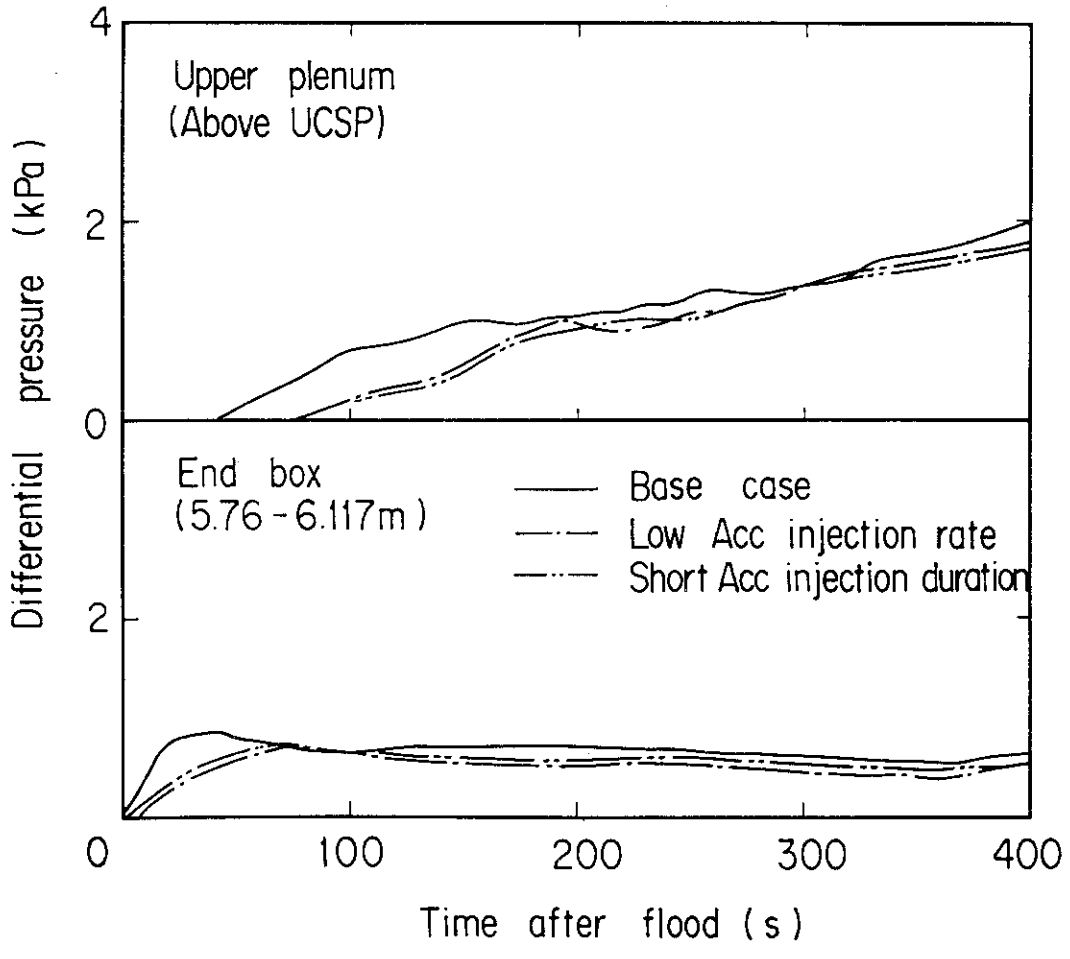

Fig. 3.7 Upper plenum differential pressures for Acc injection rate and duration effects tests

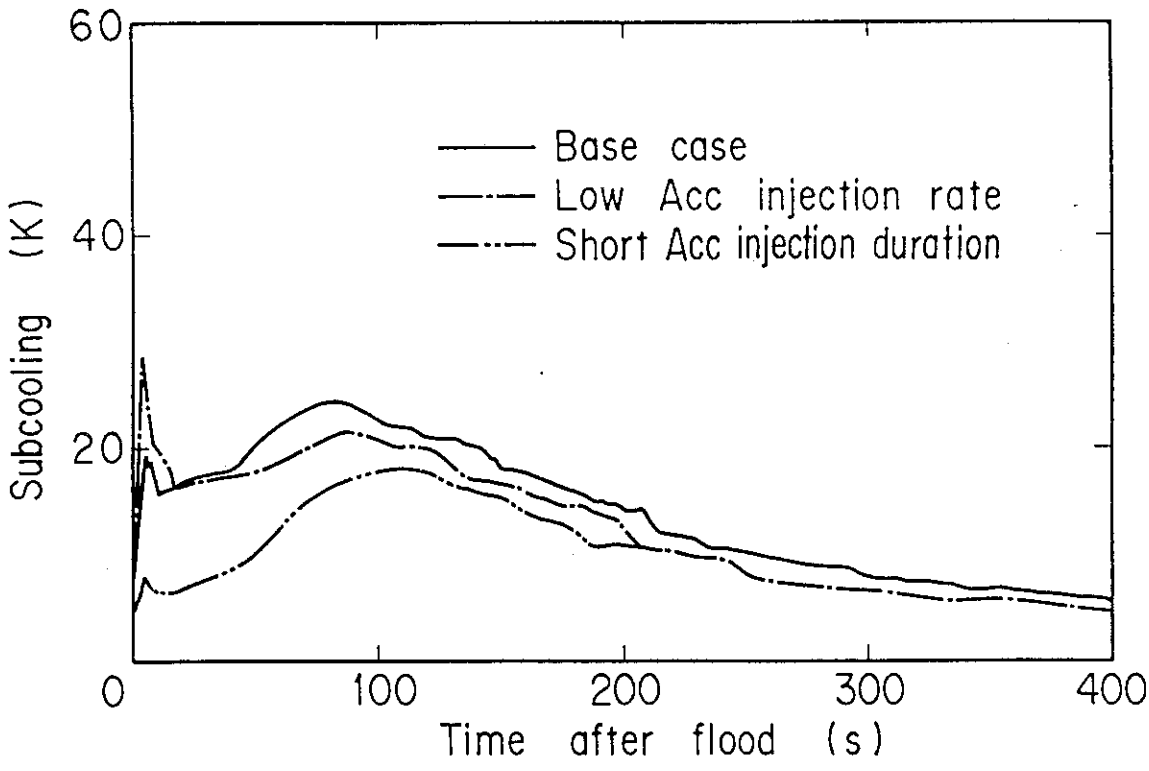

Fig. 3.8 Core inlet subcoolings for Acc injection rate and duration effects tests

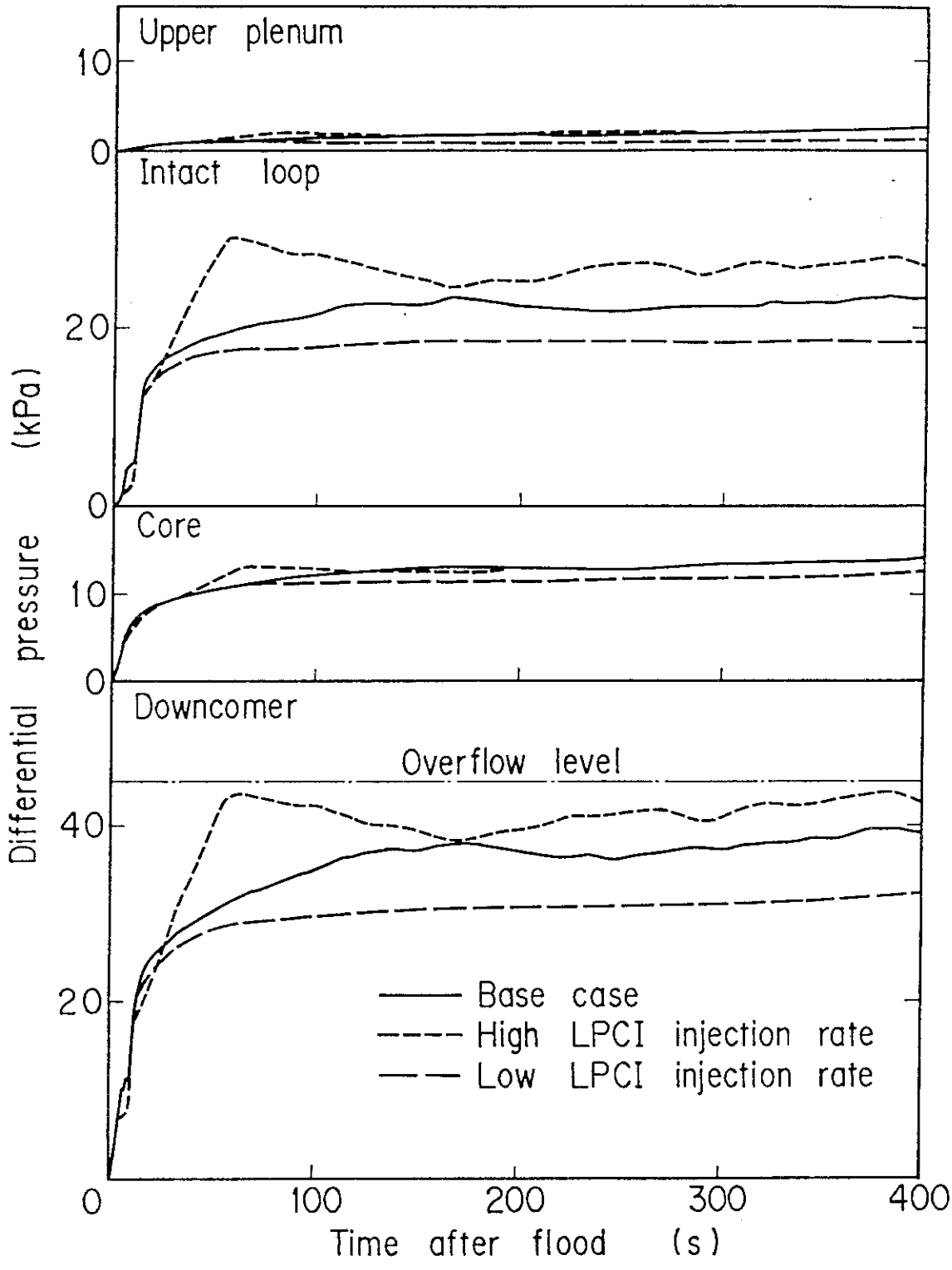

Fig. 3.9 Differential pressures in downcomer, core, intact loop and upper plenum for LPCI injection rate effects tests

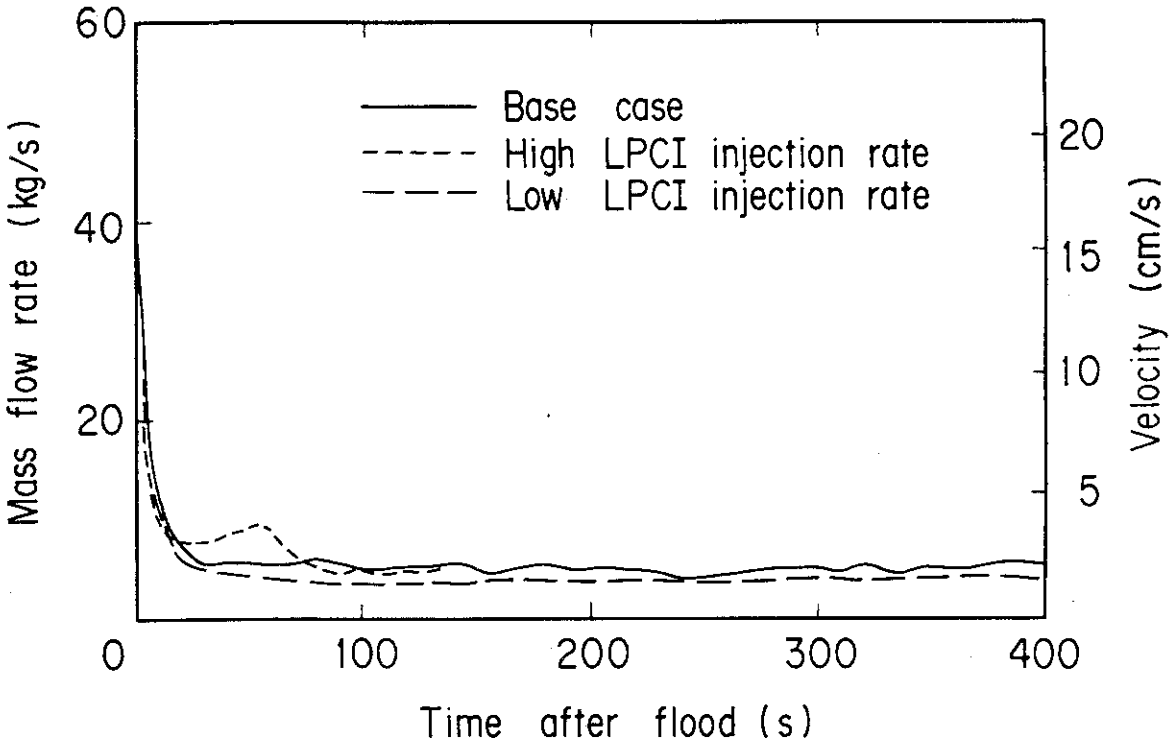

Fig. 3.10 Core flooding rates for LPCI injection rate effects tests

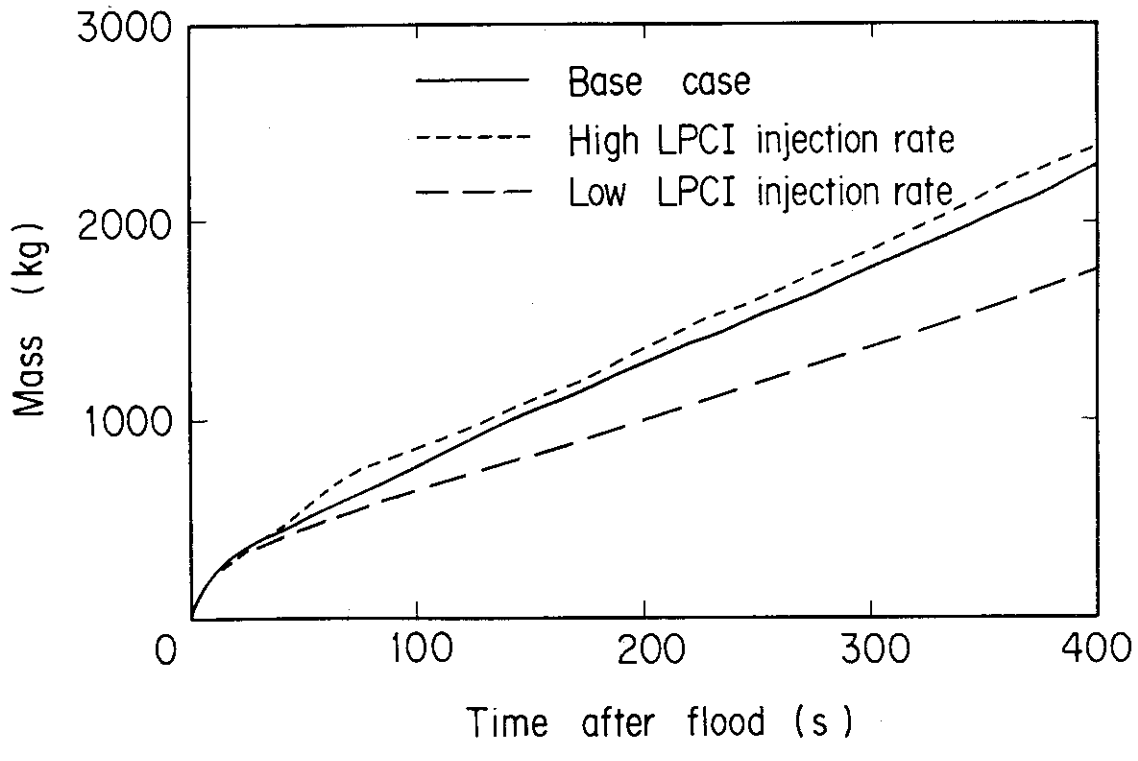

Fig. 3.11 Time-integrations of core flooding rates for LPCI injection rate effects tests

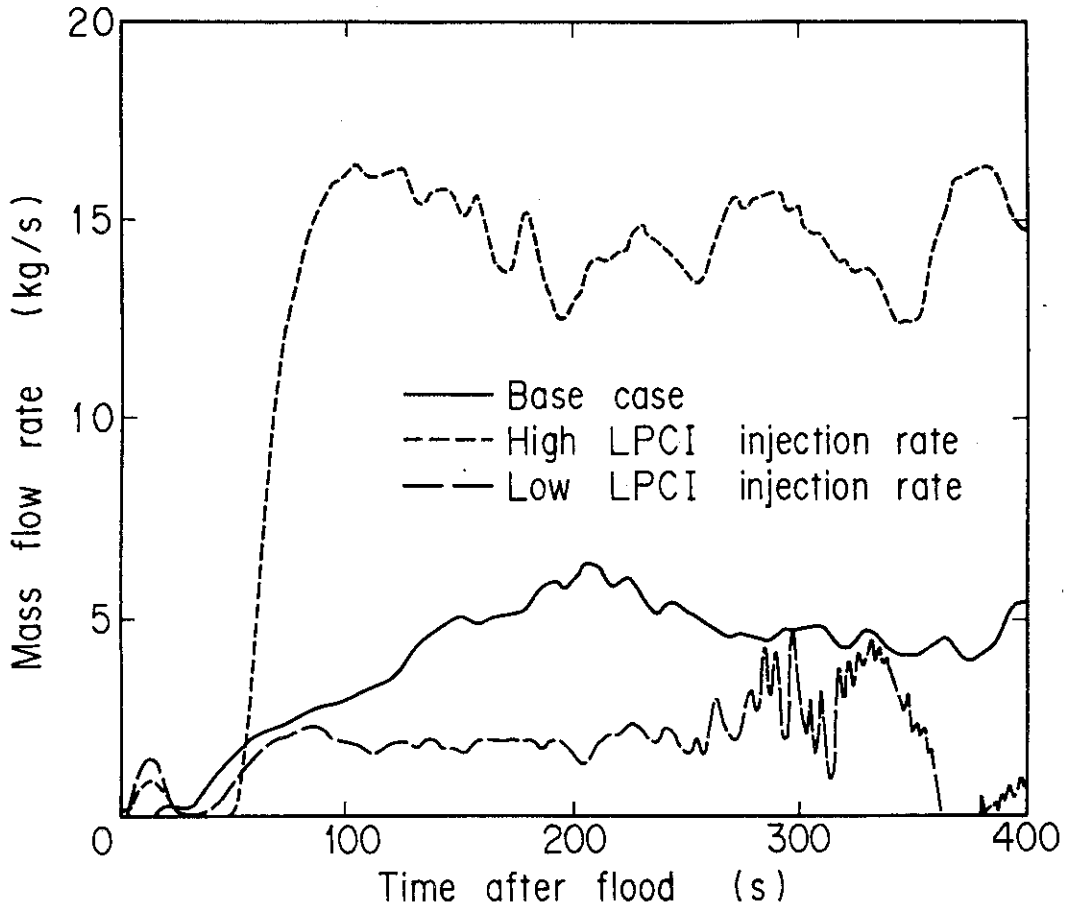

Fig. 3.12 Bypassing water mass flow rates for LPCI injection rate effects tests

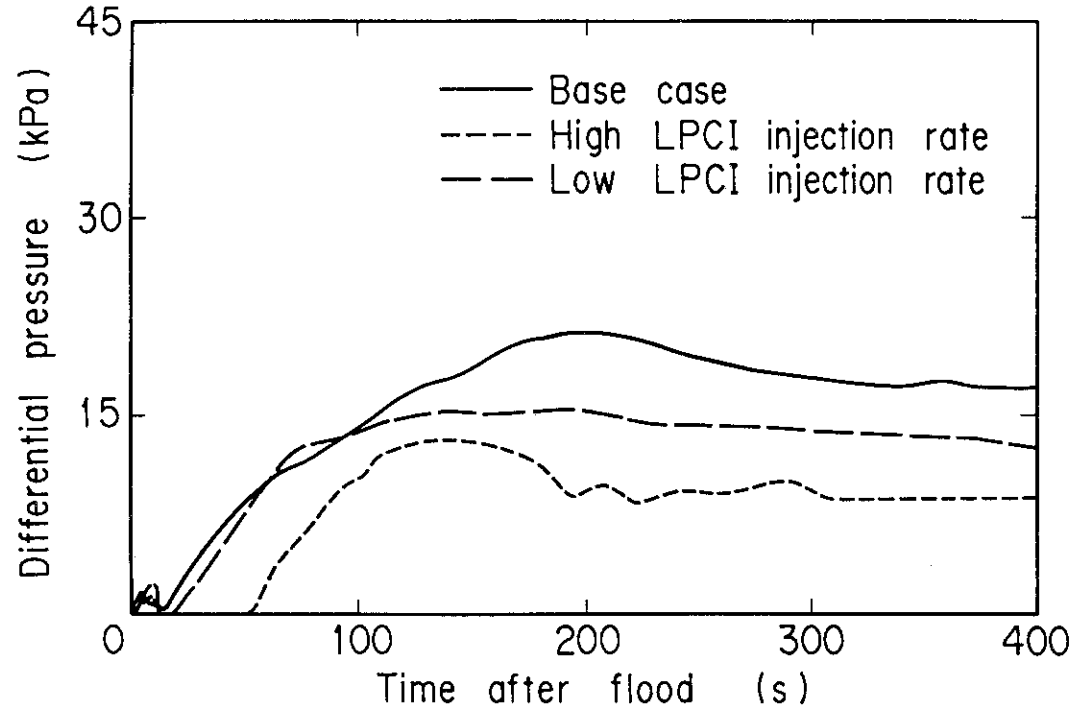

Fig. 3.13 Differential pressures across broken cold leg nozzle for LPCI injection rate effects tests

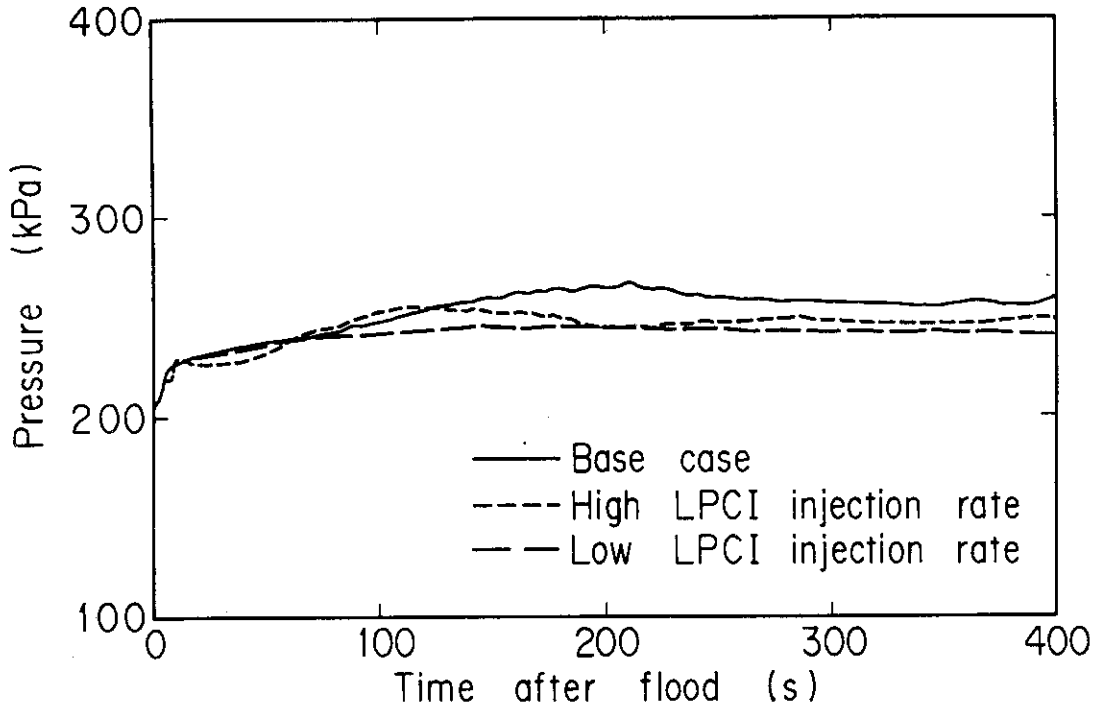

Fig. 3.14 Upper plenum pressures for LPCI injection rate effects tests

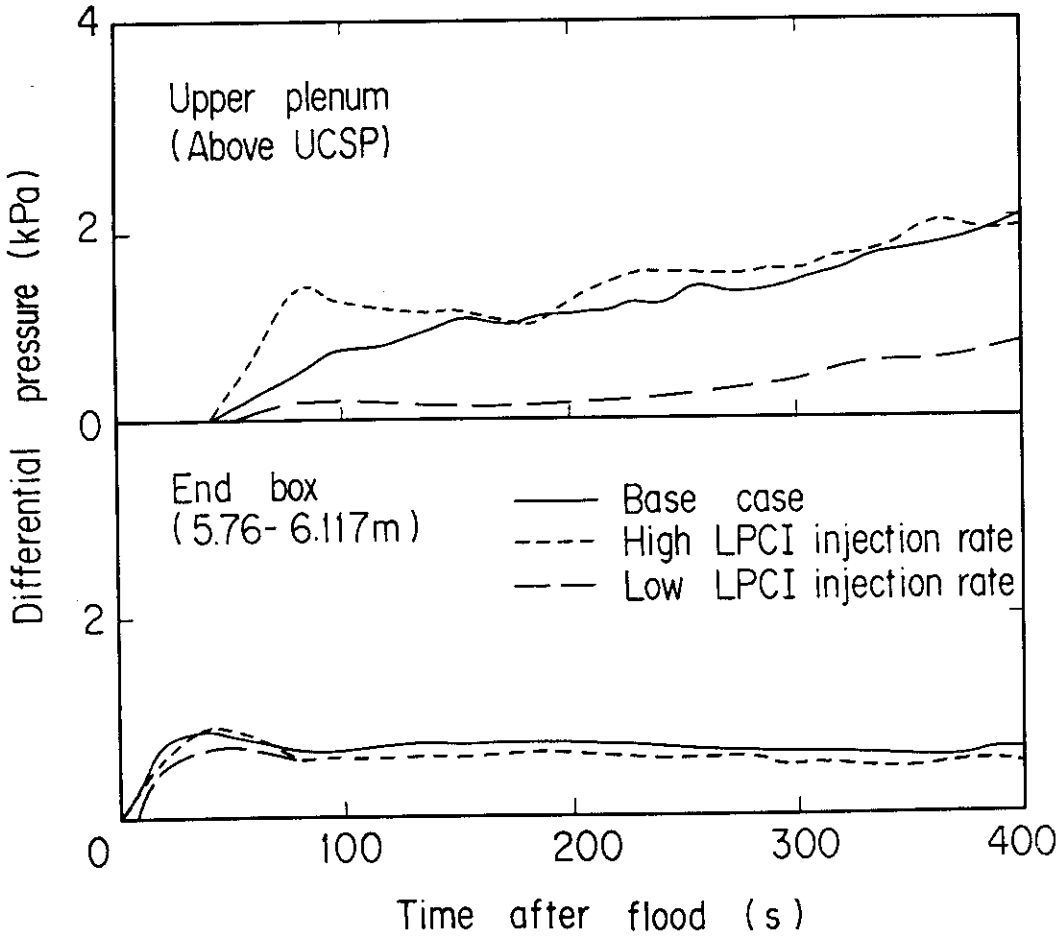

Fig. 3.15 Upper plenum differential pressures for LPCI injection rate effects tests

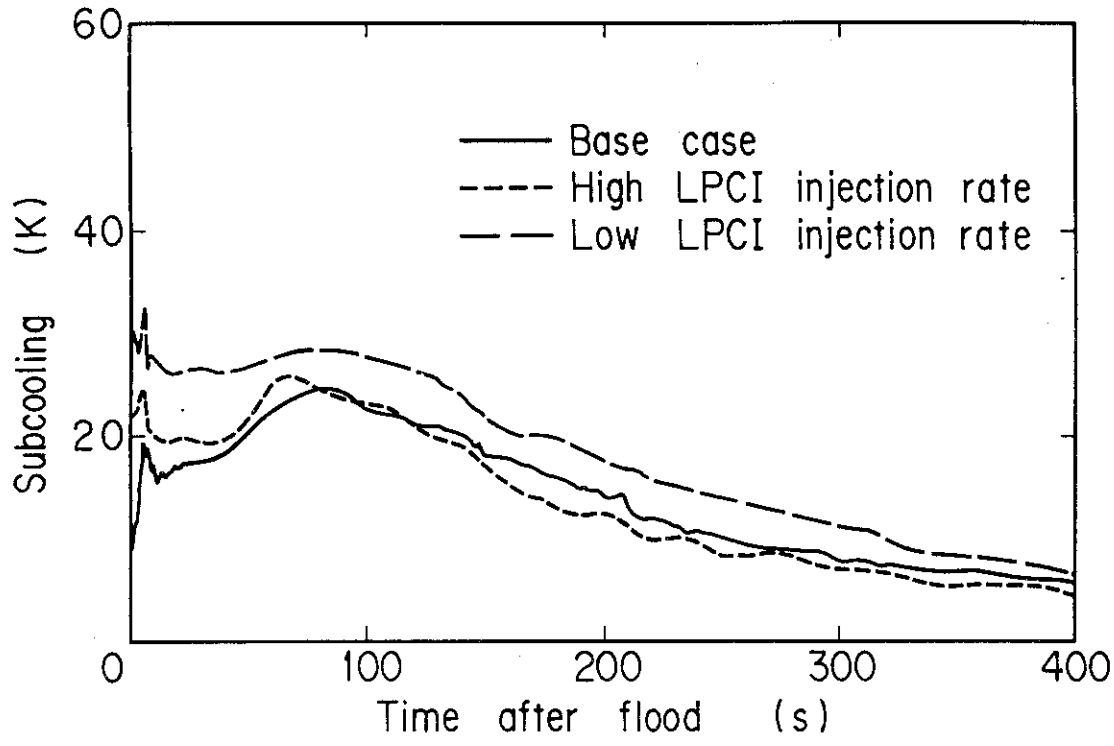

Fig. 3.16 Core inlet subcoolings for LPCI injection rate effects tests

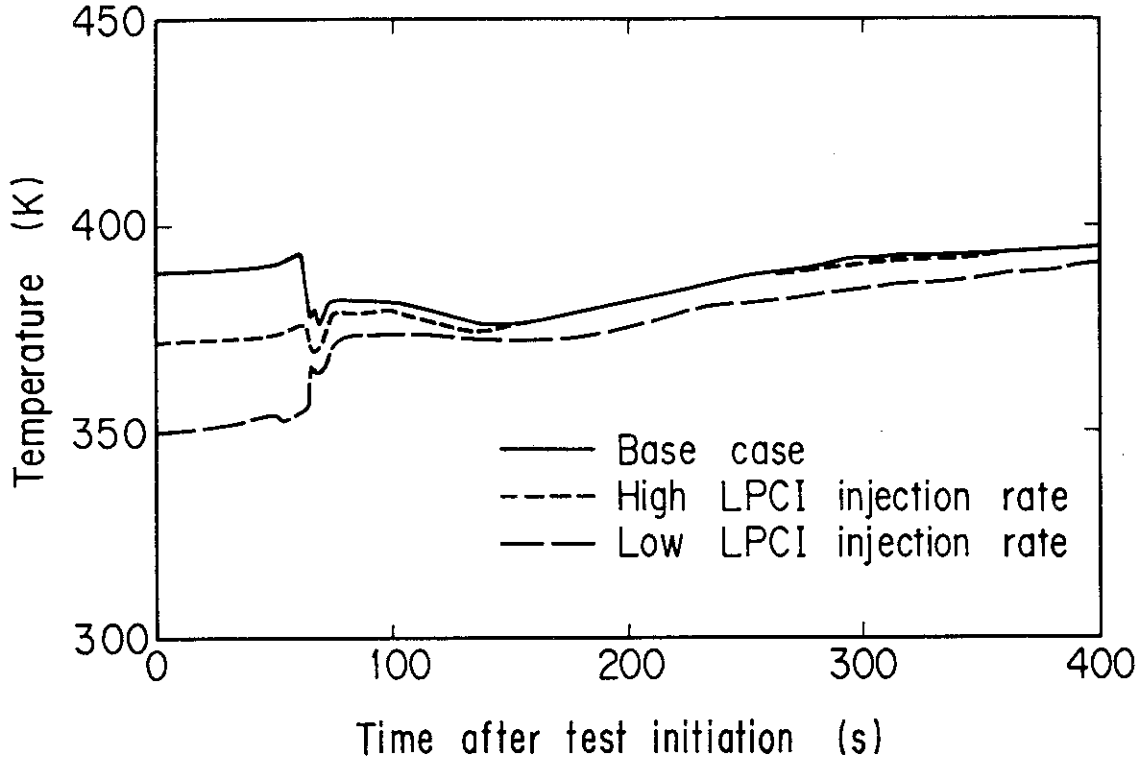

Fig. 3.17 Core inlet fluid temperature from the beginning of tests for LPCI injection rate effects tests

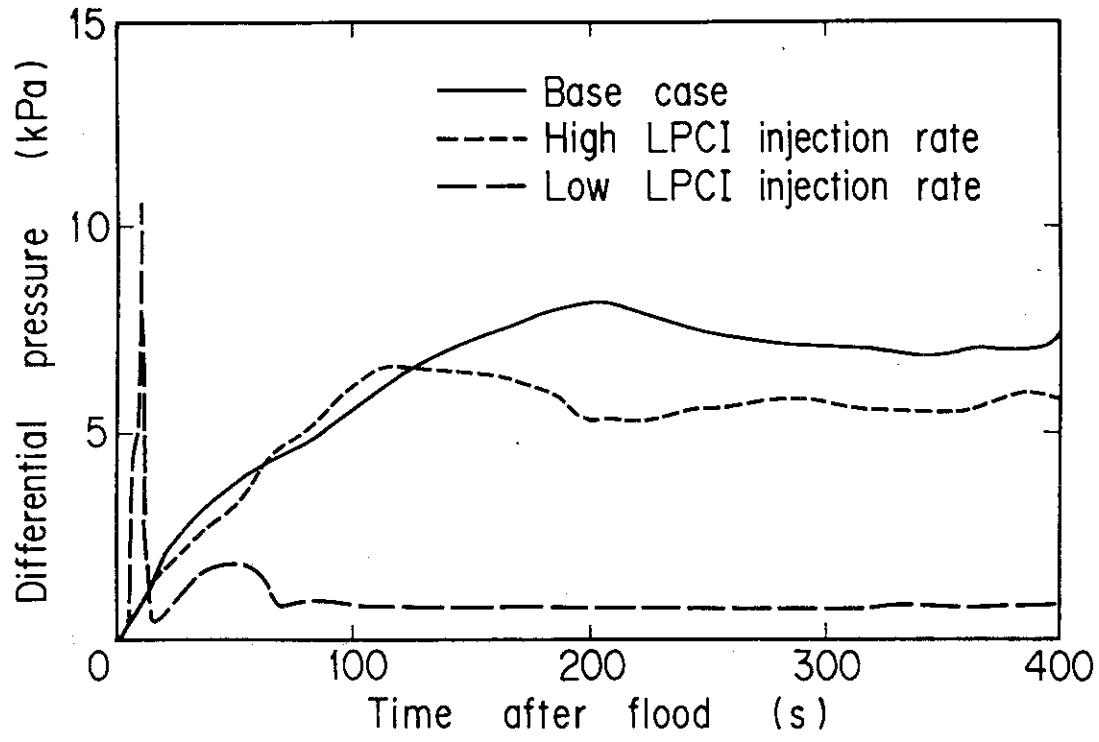

Fig. 3.18 Differential pressures between pump exit and containment tank 2 for LPCI injection rate effects tests

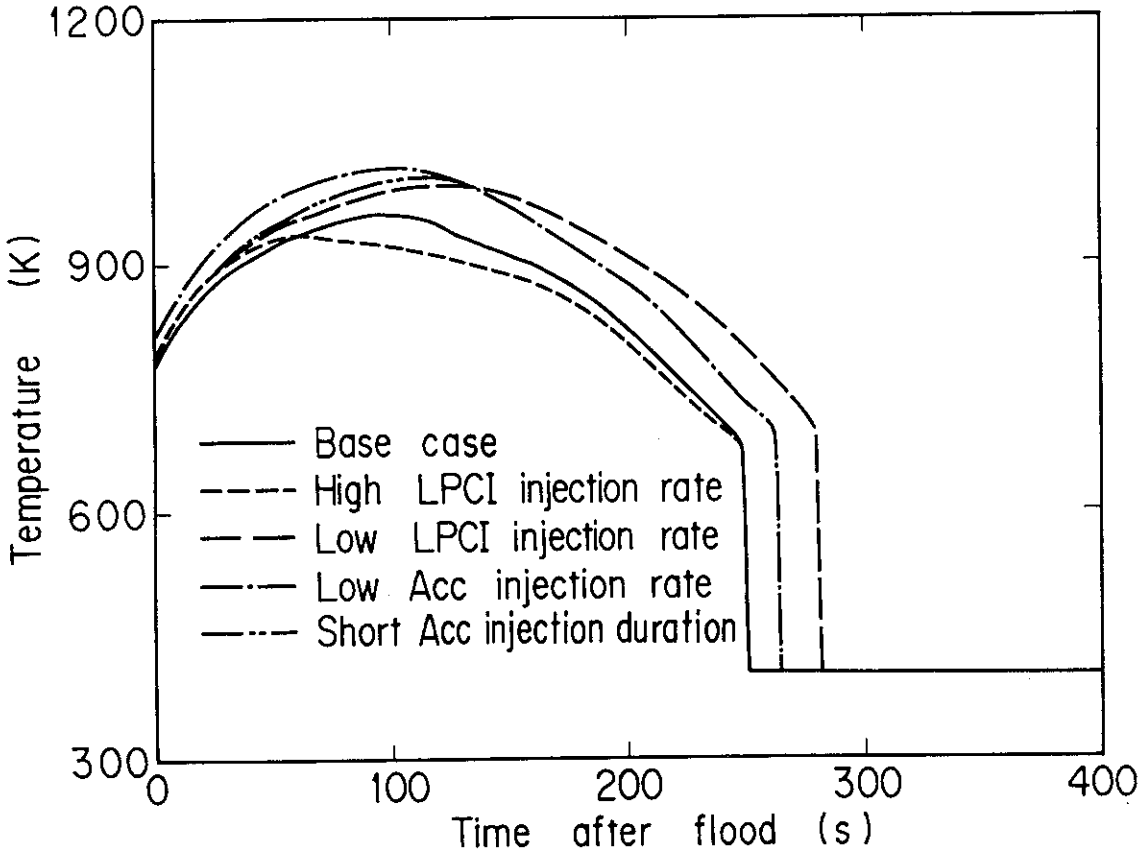

Fig. 3.19 Rod surface temperatures of average power rods at midplane level

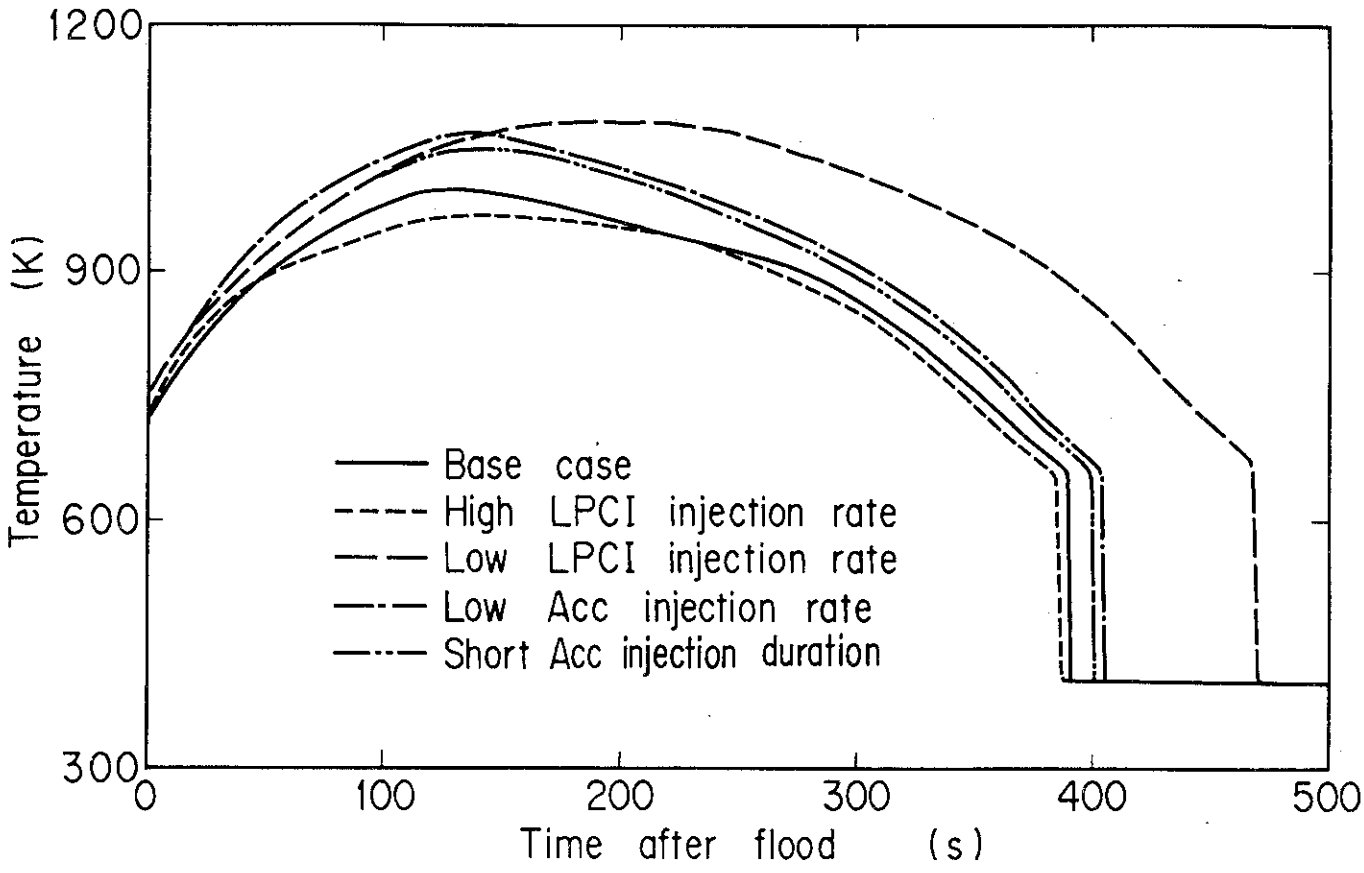

Fig. 3.20 Rod surface temperatures of average power rods at 2.44 m elevation

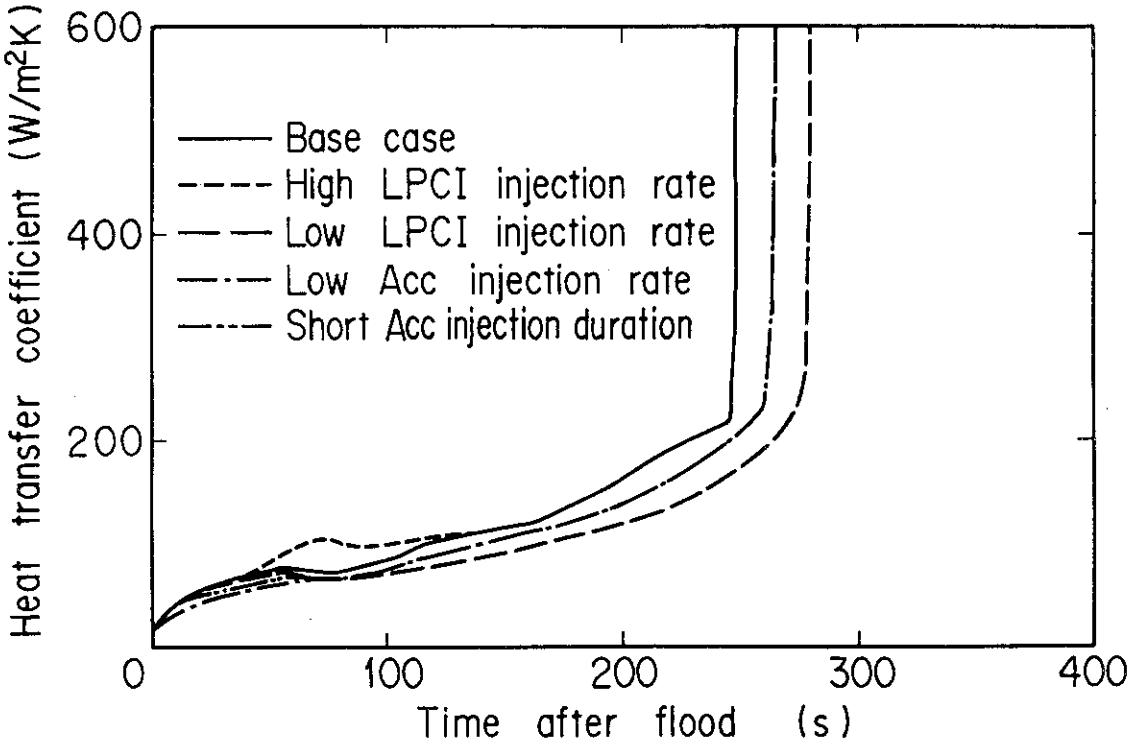

Fig. 3.21 Heat transfer coefficients for average power rods at midplane level

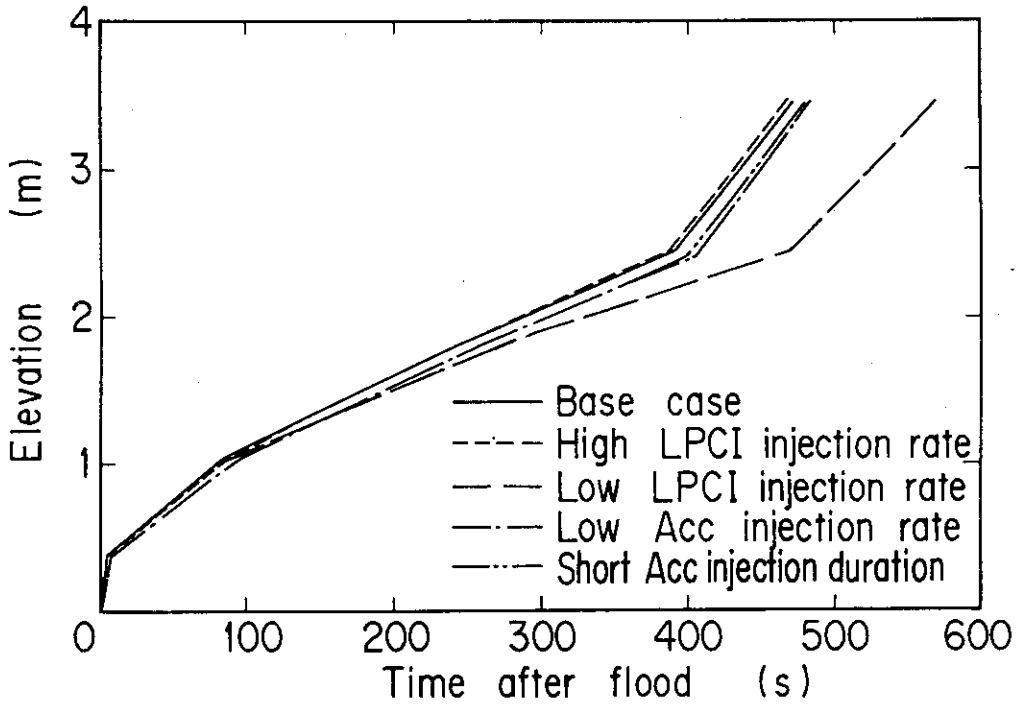

Fig. 3.22 Quench envelopes for average power rods

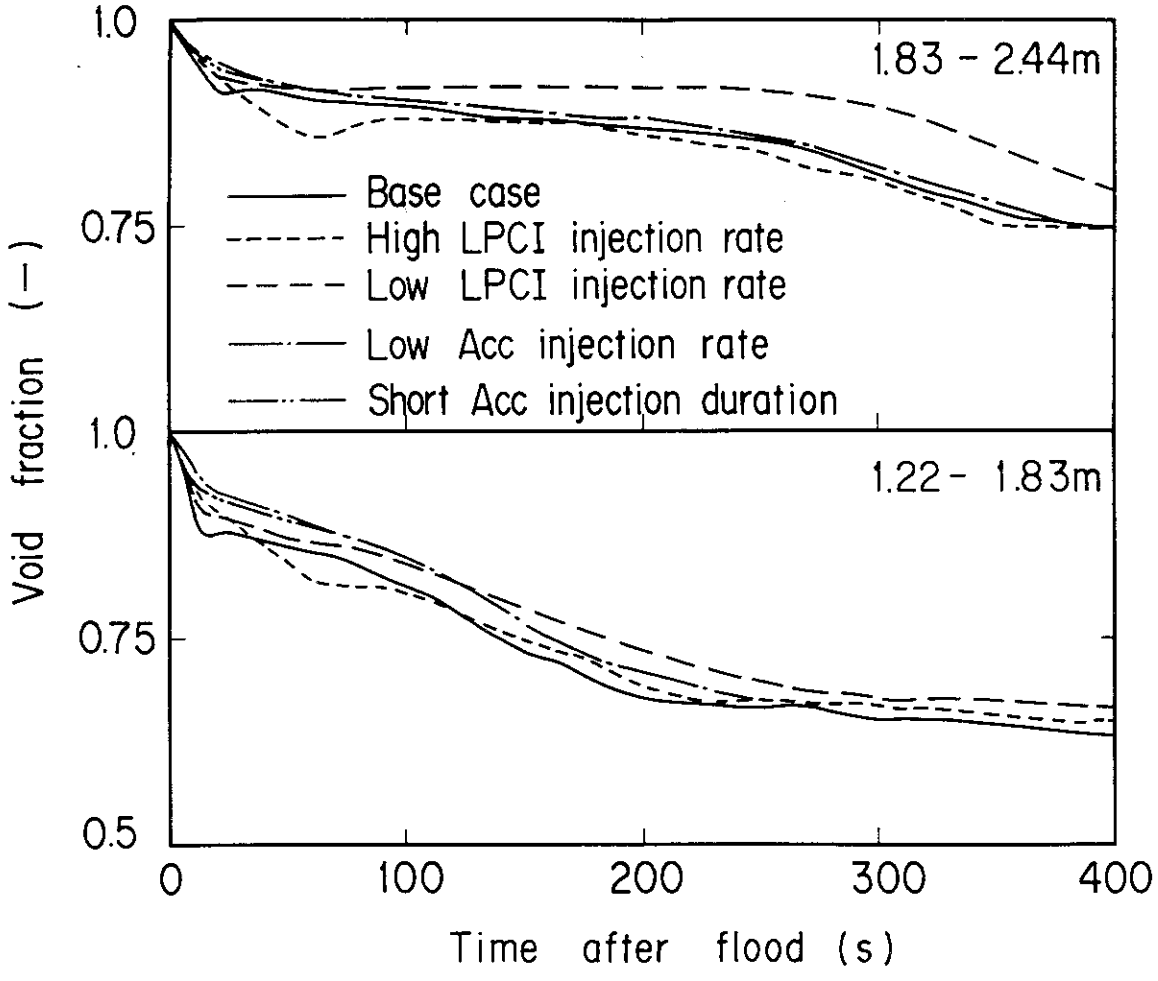

Fig. 3.23 Average void fractions in core

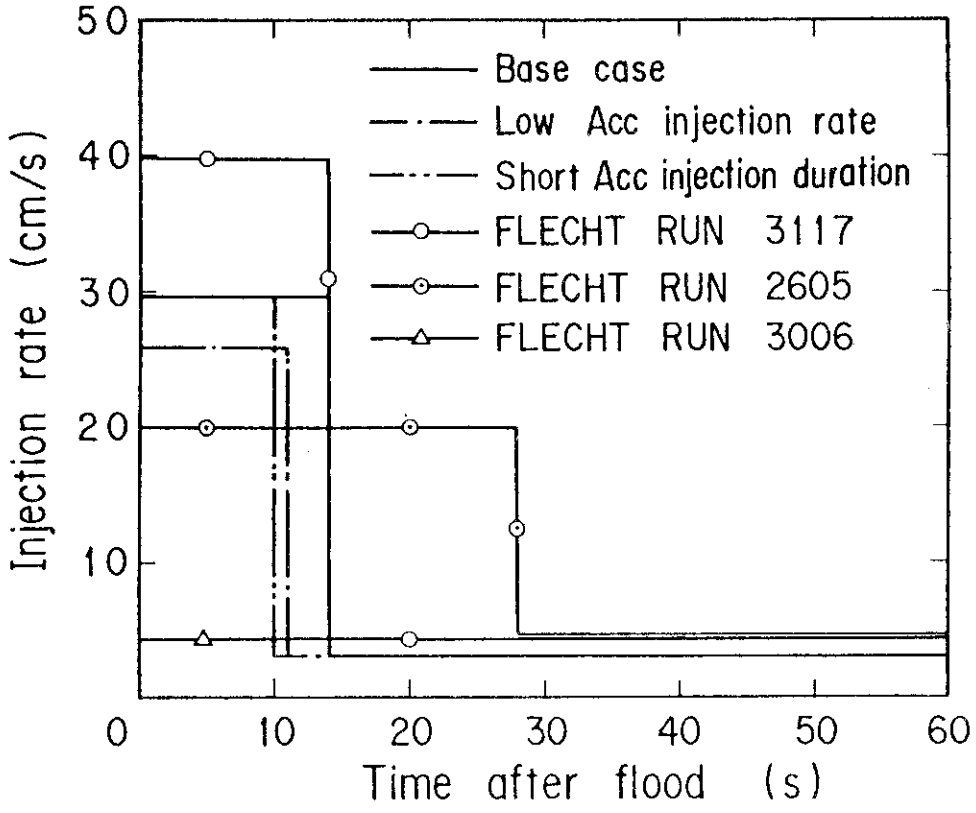

Fig. 3.24 ECC water injection rates of FLECHT-SET Phase A and CCTF Acc injection rate and duration effects tests

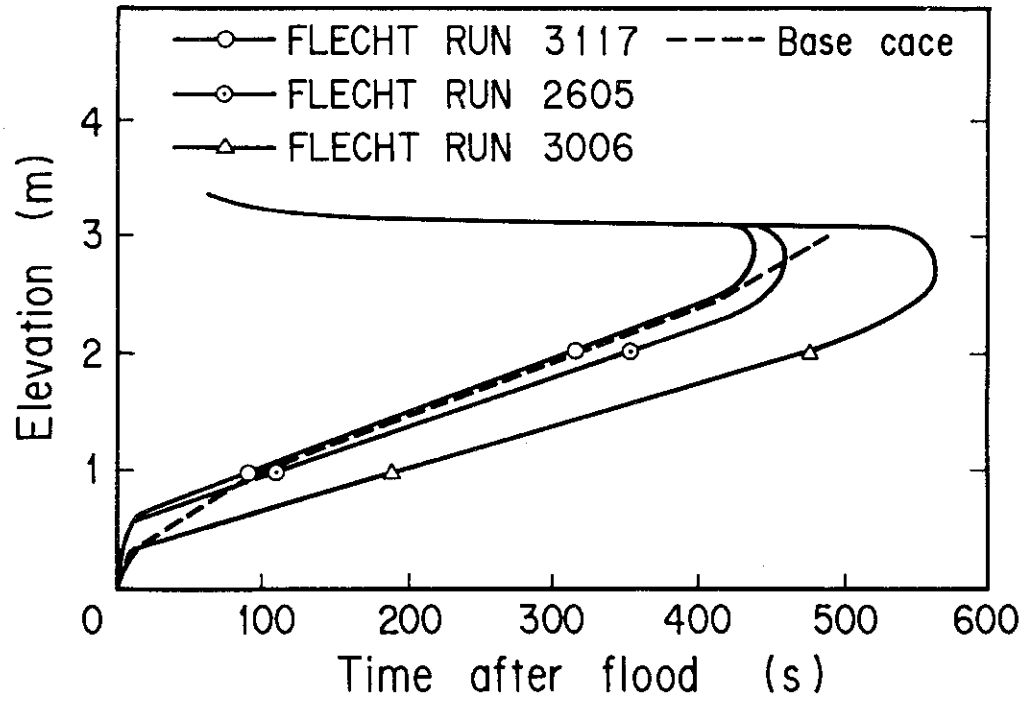

Fig. 3.25 Quench envelopes of FLECHT-SET Phase A Acc injection rate and duration effects tests (From ref. (1))

4. Conclusions

The effects of the ECC water injection rate on the reflooding phenomena were investigated with regard to the CCTF data of Tests C1-5, C1-6, C1-9, C1-11 and C1-13. The major conclusions are as follows:

(1) A strong effect of the ECC water injection rate on the core flooding was observed. Until the downcomer was almost filled, a higher ECC water injection rate caused the higher water accumulation in the downcomer and resulted in a higher core flooding rate. This is reasonable because the downcomer differential pressure was the driving force for the core reflooding. However, once the downcomer was almost filled, the higher ECC water injection rate could not increase the core flooding rate.

(2) Even until the downcomer was filled, a considerable amount of ECC water bypassed to the break. The bypass of the ECC water reduced the amont of the ECC water available for the core reflooding, resulting in the reduction of the increasing rate of the downcomer differential pressure and core flooding rate. The bypass was caused by the uncondensed steam flowing from the intact cold legs to the break. Therefore, reduction of the ECC water injection rate would cause reduction of the core flooding rate significantly, because the reduction of the ECC water injection rate causes the increase of the uncondensed steam mass flow rate, which is expected to result in the higher bypass mass flow rate, as well as the reduction of the ECC water available for the core reflooding.

(3) A higher core flooding rate resulted in better core cooling. Especially, the higher core flooding rate in the early period reduced the turnaround temperature significantly.

(4) Although the duration of the Acc injection was short (14 s at most), the effects of the Acc injection rate and duration remained on the core cooling behavior through the whole transient.

(5) The effect of the ECC water injection rate on the pressure in the vessel was weak.

(6) Differences in the core inlet subcooling were observed among those five tests. Although they were relatively large in the initial periods, they became to be within 5 K after 100 s.

(7) The ECC water injection into the broken cold leg reduced the total flow resistance of the broken loop. This effect would increase the core flooding rate.

(8) Although the sizes of the facilities are different significantly between the CCTF and the FLECHT-SET facility, the effects of the Acc injection rate and duration on the downcomer behavior and the core cooling behavior observed in the FLECHT-SET Phase A experiments were almost the same as observed in the CCTF tests as described in Section 3.3.

Acknowledgement

The authors are grateful to Dr. M. Nozawa, Director of the Nuclear Safety Research Center of JAERI, and Dr. S. Katsuragi and Dr. M. Ishikawa, Head and Deputy Head of Division of Nuclear Safety Research, respectively, for their suggestions and encouragement.

The authors are also grateful to Dr. K. Hirano, Chief of Reactor Safety Laboratory II, for his suggestions and encouragement.

They are indebted to Mr. T. Iguchi, Mr, T. Sudoh, and Dr. H. Akimoto for their valuable suggestions and discussion.

References:

(1) Blaisdell, J.A. *et al.*, 'PWR FLECHT-SET PHASE A REPORT', WCAP-8238 (1973).

(2) Murao, Y. *et al.*, 'Experimental Study of System Behavior during Reflood Phase of PWR-LOCA Using CCTF', J. Nucl. Sci. Tech. 19, 705-719 (1982).

(3) For instance, Lilly, G.P. *et al.*, 'PWR FLECHT COSINE LOW FLOODING RATE TEST SERIES EVALUATION REPORT', WCAP-8838 (1977) and Lee, N. *et al.*, 'PWR FLECHT SEASET Unblocked Bundle, Forced and Gravity Reflood Task Data Evaluation and Analysis Report', NUREG/CR-2256 (1981).

(8) Although the sizes of the facilities are different significantly between the CCTF and the FLECHT-SET facility, the effects of the Acc injection rate and duration on the downcomer behavior and the core cooling behavior observed in the FLECHT-SET Phase A experiments were almost the same as observed in the CCTF tests as described in Section 3.3.

Acknowledgement

The authors are grateful to Dr. M. Nozawa, Director of the Nuclear Safety Research Center of JAERI, and Dr. S. Katsuragi and Dr. M. Ishikawa, Head and Deputy Head of Division of Nuclear Safety Research, respectively, for their suggestions and encouragement.

The authors are also grateful to Dr. K. Hirano, Chief of Reactor Safety Laboratory II, for his suggestions and encouragement.

They are indebted to Mr. T. Iguchi, Mr. T. Sudoh, and Dr. H. Akimoto for their valuable suggestions and discussion.

References:

(1) Blaisdell, J.A. *et al.*, 'PWR FLECHT-SET PHASE A REPORT', WCAP-8238 (1973).

(2) Murao, Y. *et al.*, 'Experimental Study of System Behavior during Reflood Phase of PWR-LOCA Using CCTF', J. Nucl. Sci. Tech. 19, 705-719 (1982).

(3) For instance, Lilly, G.P. *et al.*, 'PWR FLECHT COSINE LOW FLOODING RATE TEST SERIES EVALUATION REPORT', WCAP-8838 (1977) and Lee, N. *et al.*, 'PWR FLECHT SEASET Unblocked Bundle, Forced and Gravity Reflood Task Data Evaluation and Analysis Report', NUREG/CR-2256 (1981).

Appendix A

Information for selected data

Figure list

1. Definition of Tag.ID for clad surface temperatures

Notation : TENNWAM

NN : Bundle number

WA : Power zone

WA = X1, X2 : High power (Local power factor 1.1)

WA = Y1, Y2 : Medium power (Local power factor 1.0)

WA = Z1, Z2 : Low power (Local power factor 0.95)

M : Elevation

	Elevation (m)	Axial power factor
1	0.38	0.568
2	1.015	1.176
3	1.83	1.492
4	2.44	1.312
5	3.05	0.815

2. Definition of power zone and bundle number

See Fig. A-1

3. Definition of Tag.ID for void fraction

See Fig. A-2

4. Definition of Tag.ID for average linear power of heater rod in each power unit zone

See Fig. A-3

5. Definition of carry-over rate fraction (C.R.F)

$$CRF = \frac{\dot{m}_{UP} + \dot{m}_{L}}{\dot{m}_{CR} + \dot{m}_{UP} + \dot{m}_{L}}$$

The calculated data within ±25 s are averaged:

$$(CRF)_i = \frac{1}{101} \sum_{k=i-50}^{i+50} (CRF)_k$$

where

ΔP_{UP} : Average of measured data at four orientations

ΔP_{CR} : Same as above

$$\dot{m}_{UP} = A_{up} \frac{d}{dt} (\Delta P_{UP})$$

$$\dot{m}_{CR} = A_{CR} \frac{d}{dt} (\Delta P_{CR})$$

$$\dot{m}_L = \sum_{k=1}^{4} \dot{m}_{pk}$$

$\dot{m}$: mass flow rate or mass accumulation rate

ΔP: differential pressure

suffix

UP: upper plenum

CR: core

L : loop

p : primary pump

6. Definition of Tag.ID for differential pressure through downcomer, upper plenum, core and lower plenum

See Fig. A-4

7. Definition of Tag.ID for differential pressure through intact and broken loop and broken cold leg nozzle

See Fig. A-5

8. Definition of Tag.ID for fluid temperature in inlet and outlet plenum and secondary of steam generator

See Fig. A-6

9. Evaluation of core inlet mass flow rate

The core inlet mass flow rate can be evaluated by the two ways. Namely,

$$\dot{m}_{F,u} = \dot{m}_{ECC,LP} + \dot{m}_{ECC,CL} - \dot{m}_{CT} - \dot{m}_{D} - \dot{m}_{LP} \quad (1)$$

and

$$\dot{m}_{F,d} = \dot{m}_{C} + \dot{m}_{U} + \dot{m}_{L} \quad (2)$$

where, $\dot{m}_{F,u}$ and $\dot{m}_{F,d}$ are core inlet mass flow rate evaluated from the data of the upstream side and the downstream side, respectively. $\dot{m}_{ECC,LP}$ and $\dot{m}_{ECC,CL}$ are the ECC water injection rate at the lower plenum and the cold legs, respectively. $\dot{m}_{CT}$, $\dot{m}_{D}$, $\dot{m}_{LP}$, $\dot{m}_{C}$ and $\dot{m}_{U}$ are the increasing rate of the mass in the containment tank 1, the downcomer, the lower plenum, the core and the upper plenum, respectively. $\dot{m}_{L}$ is the total mass flow rate flowing in all primary loops, and is evaluated from the differential pressure data across the orifices in the pump simulators.

As shown in Figs. B-23 and B-24, for instance, $\dot{m}_{F,u}$ is not the same as $\dot{m}_{F,d}$ and the time-integrations of them differ from each other considerably. After the investigation and discussion for a long time, it has been tentatively concluded that $\dot{m}_{F,d}$ seems to be correcter in an early period and $\dot{m}_{F,u}$ seems to be correcter during the period the core inlet mass flow rate is almost constant. Therefore, the K-factor for the pump orifice was determined to be adjusted in the evaluation of $\dot{m}_{F,d}$ so as to give the same average value as $\dot{m}_{F,u}$ during the later period. The core inlet mass flow rate evaluated with the above procedure is shown as the recommended value in Fig. B-22 for instance. It should be mentioned that the smoothing (*i.e.* avaraging) procedure is used to obtain $\dot{m}_{CT}$, $\dot{m}_{D}$, $\dot{m}_{LP}$, $\dot{m}_{C}$ and $\dot{m}_{U}$. The smoothing is less in the evaluation of the recommended value than those of $\dot{m}_{F,u}$ and $\dot{m}_{F,d}$.

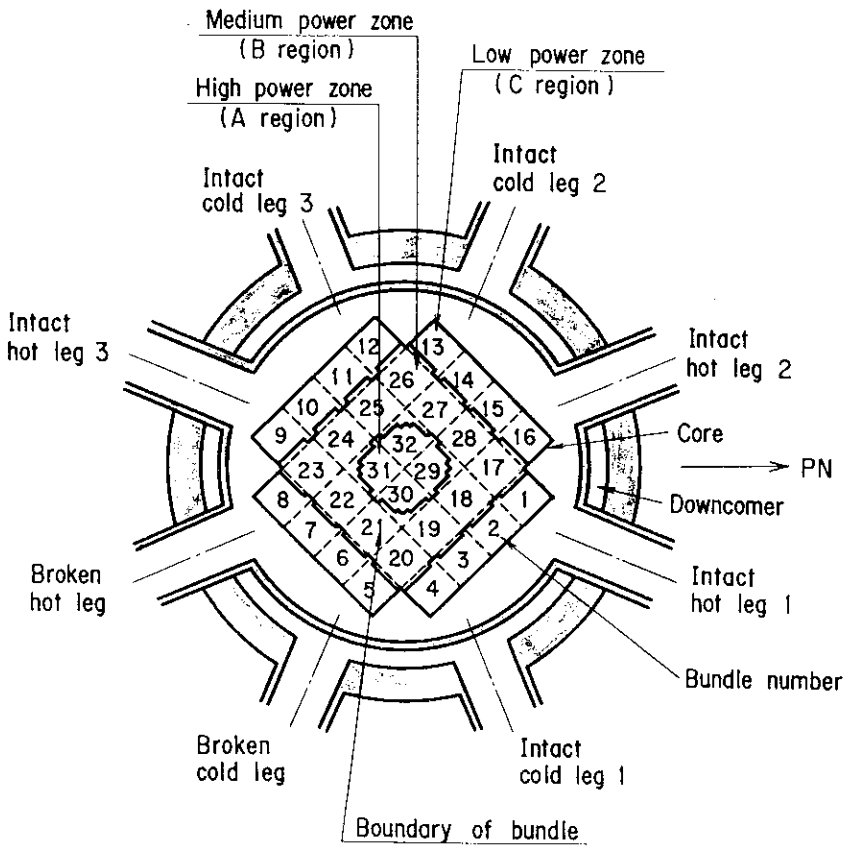

Fig.A-1 Definition of power zones and bundle numbers

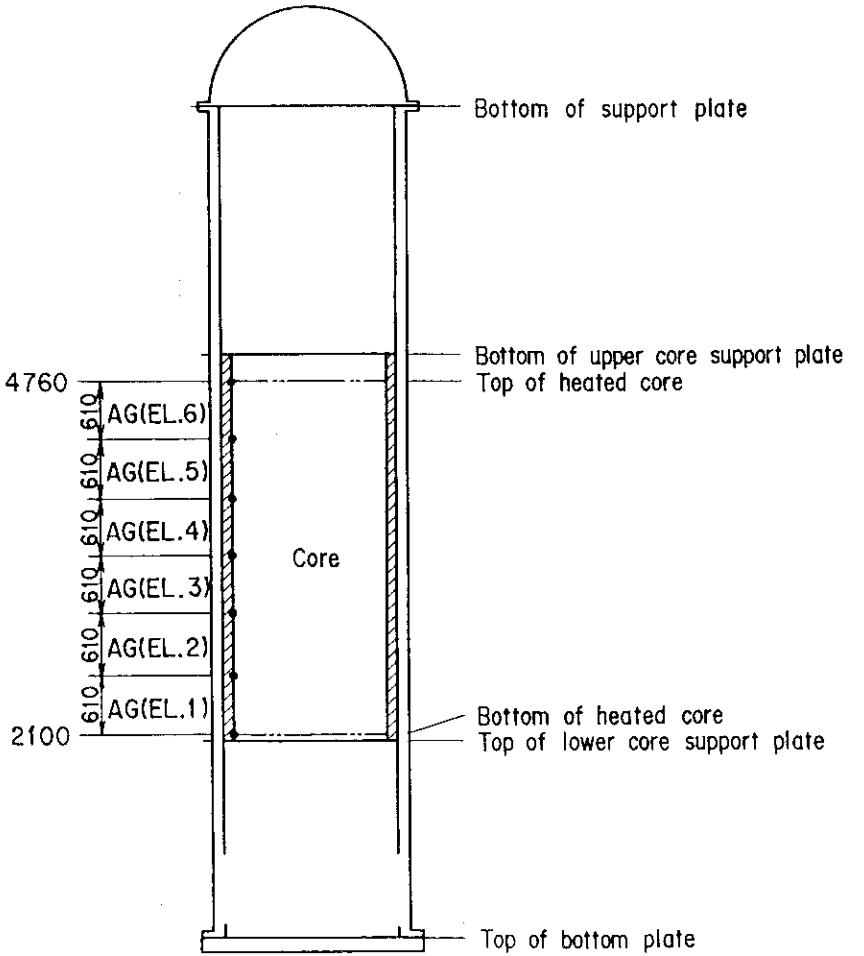

Fig.A-2 Definition of Tag.ID for void fraction (AG(EL.1) ~ AG(EL.6))

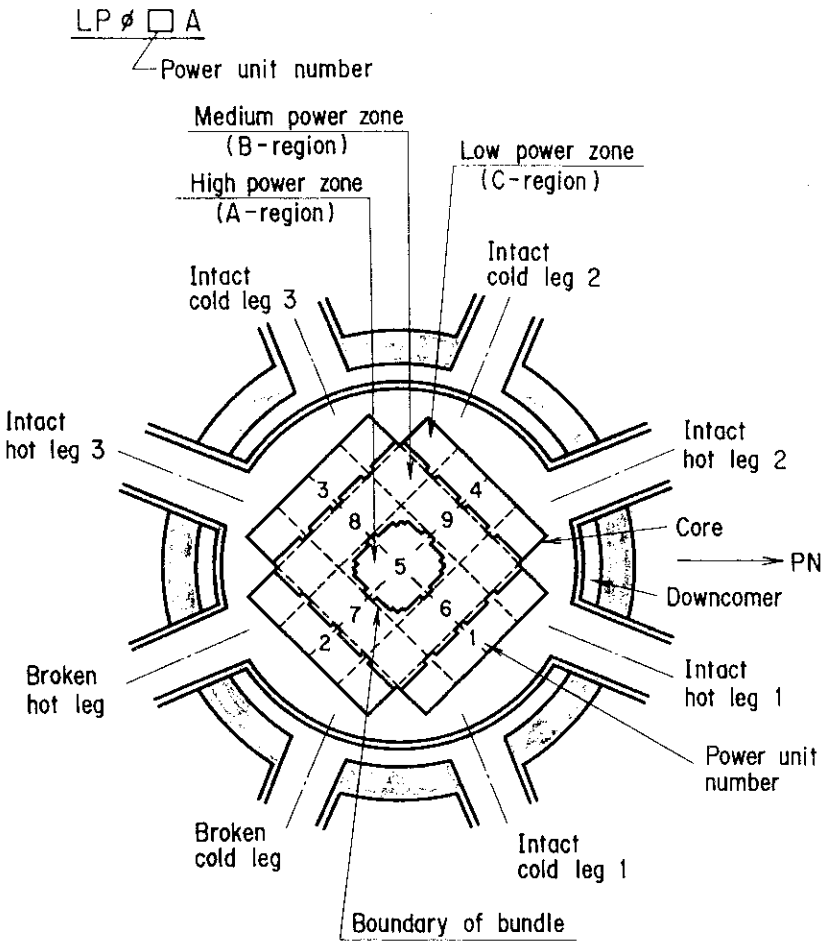

Fig. A-3 Definition of Tag. ID for average linear power of heater rod in each power unit zone (LP01A ~ LP09A)

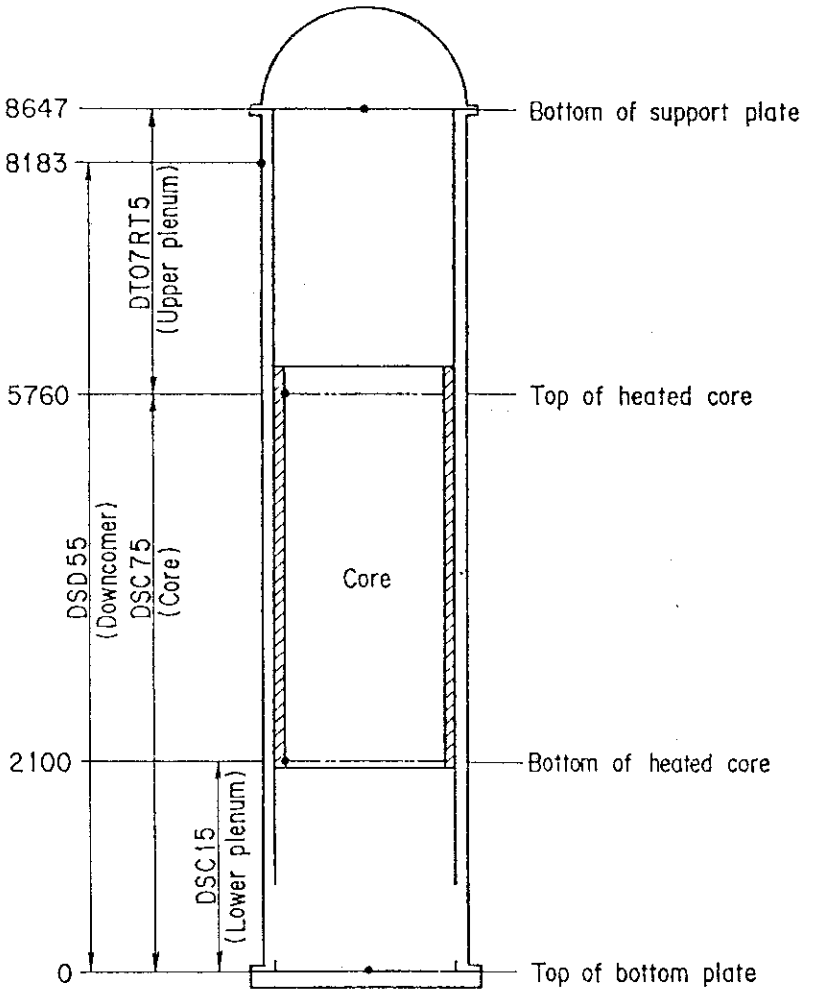

Fig. A-4 Definition of Tag. ID for differential pressure through downcomer, upper plenum, core, and lower plenum (DSD55, DTO7RT5, DSC75, DSC15)

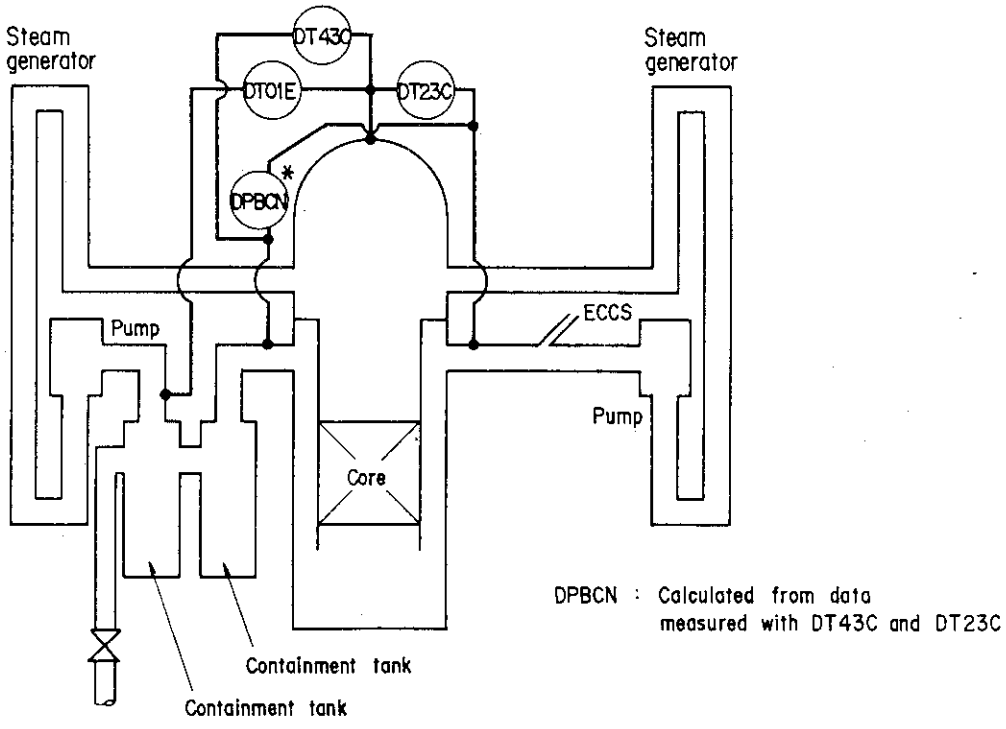

Fig. A-5 Definition of Tag. ID for differential pressure through intact and broken loop and broken cold leg nozzle (DT23C, DT01B, DPBCN)

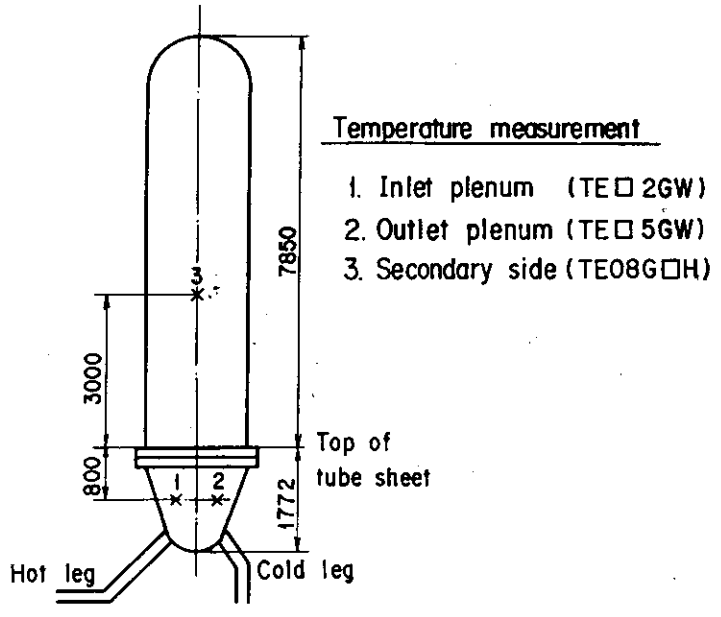

Fig. A-6 Definition of Tag. ID for fluid temperature in inlet and outlet plenum and secondary of steam generator (TE□2GW, TE□5GW, TE08G□H)

Appendix B

Selected data of CCTF Test C1-6 (Run15)

Table and Figure List

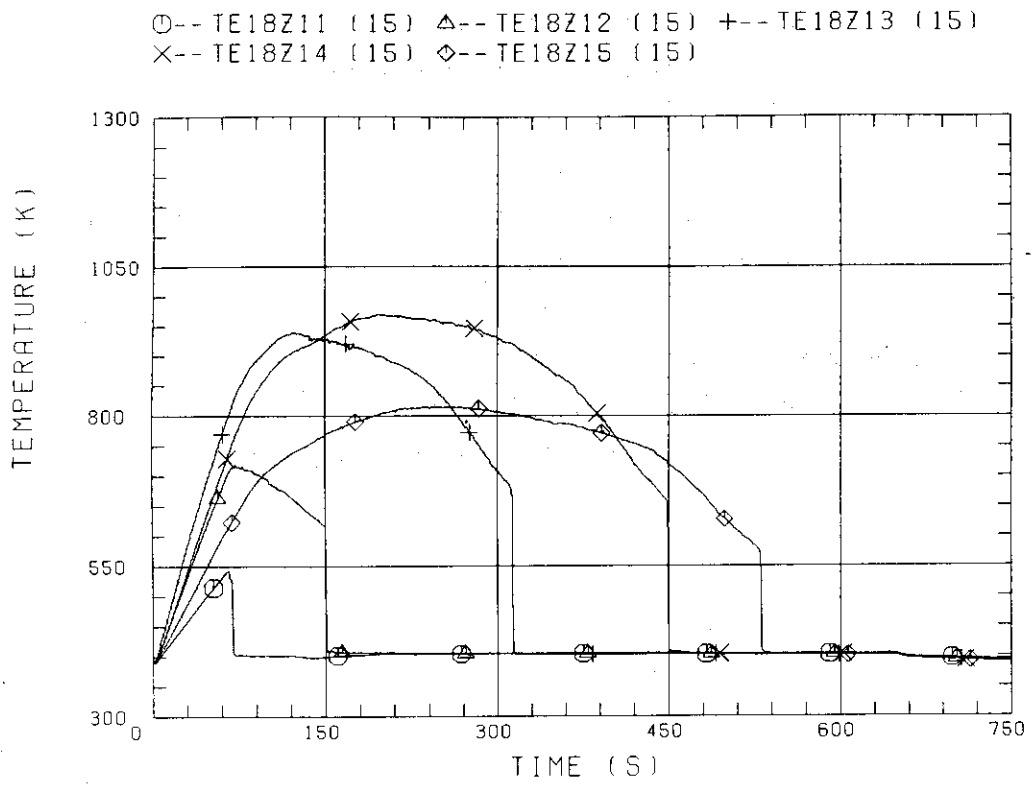

Fig. B-1 Surface temperature on low power rod (Z-rod) in medium power region (B region) (average power rod)

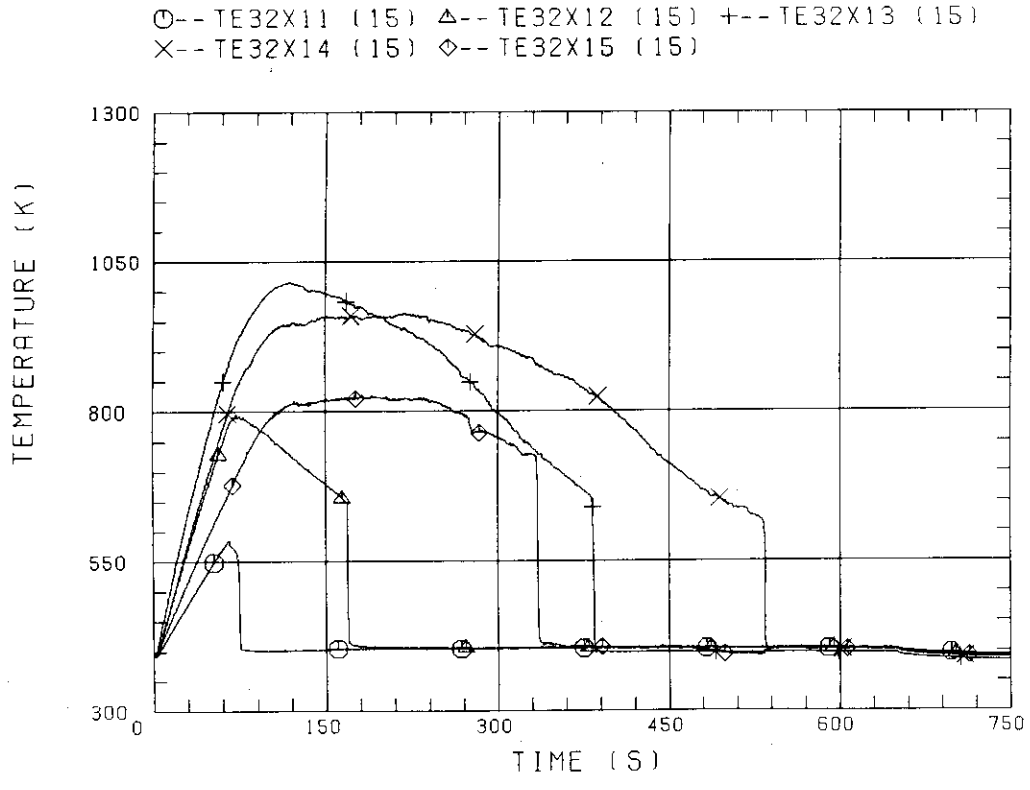

Fig. B-2 Surface temperature on high power rod (X-rod) in high power region (A region) (peak power rod)

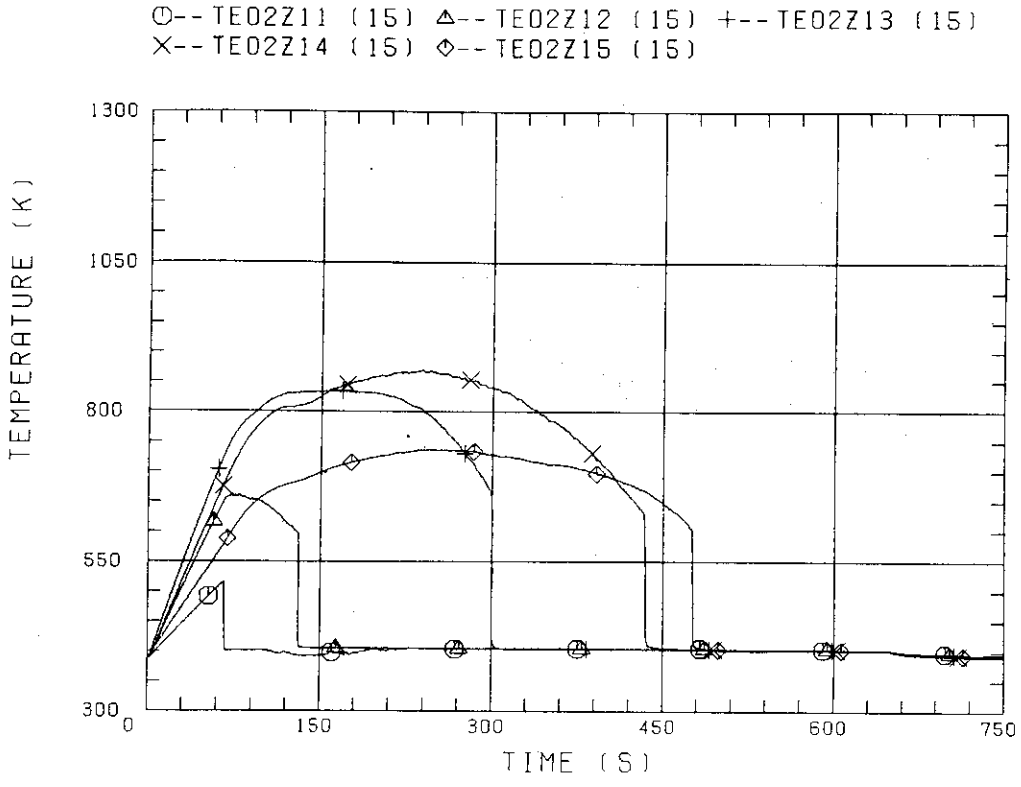

Fig. B-3 Surface temperature on low power rod (Z-rod) in low power region (C region) (lowest power rod)

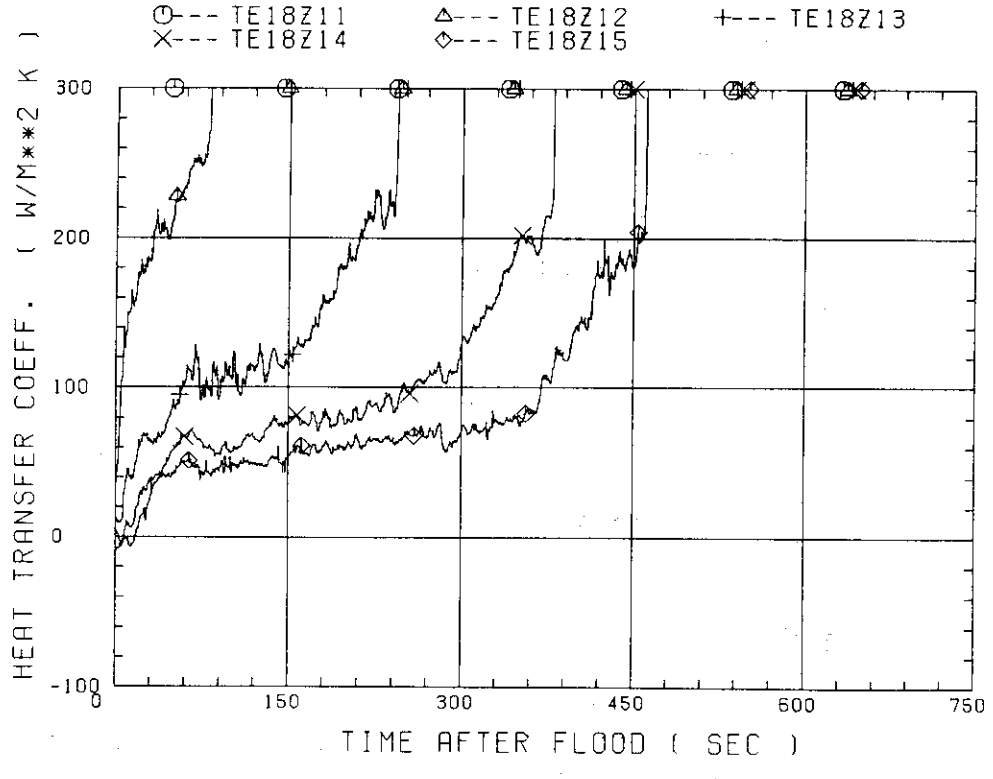

Fig. B-4 Heat transfer coefficient of low power rod (Z-rod) in medium power region (B region) (average power rod)

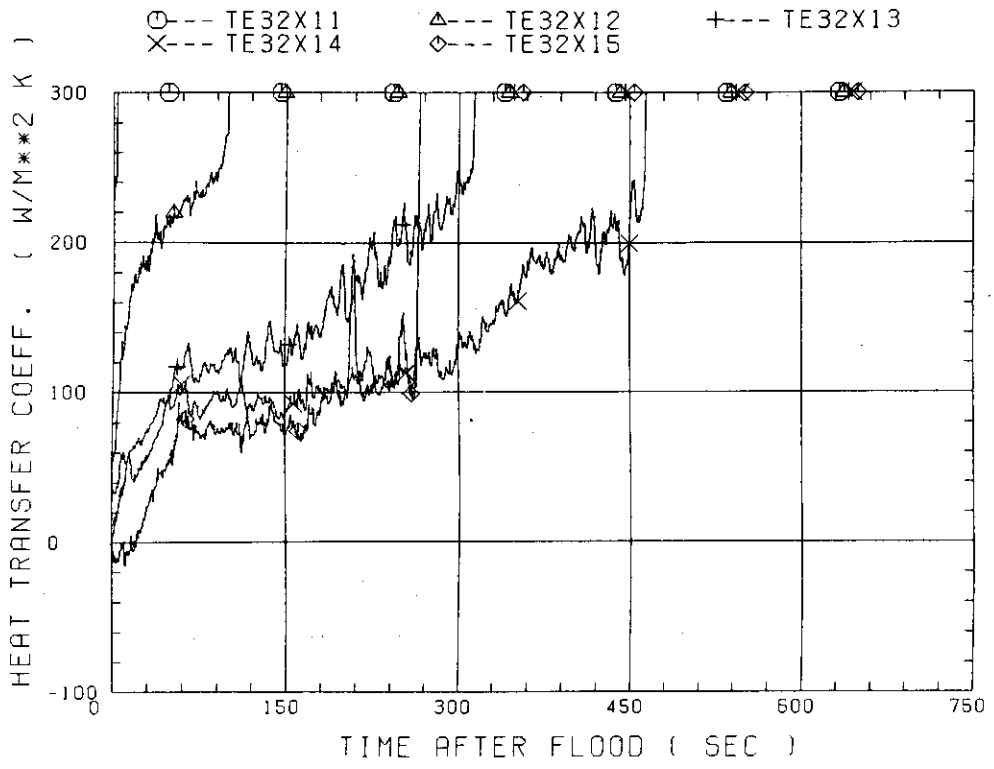

Fig. B-5 Heat transfer coefficient of high power rod (X-rod) in high power region (A region) (peak power rod)

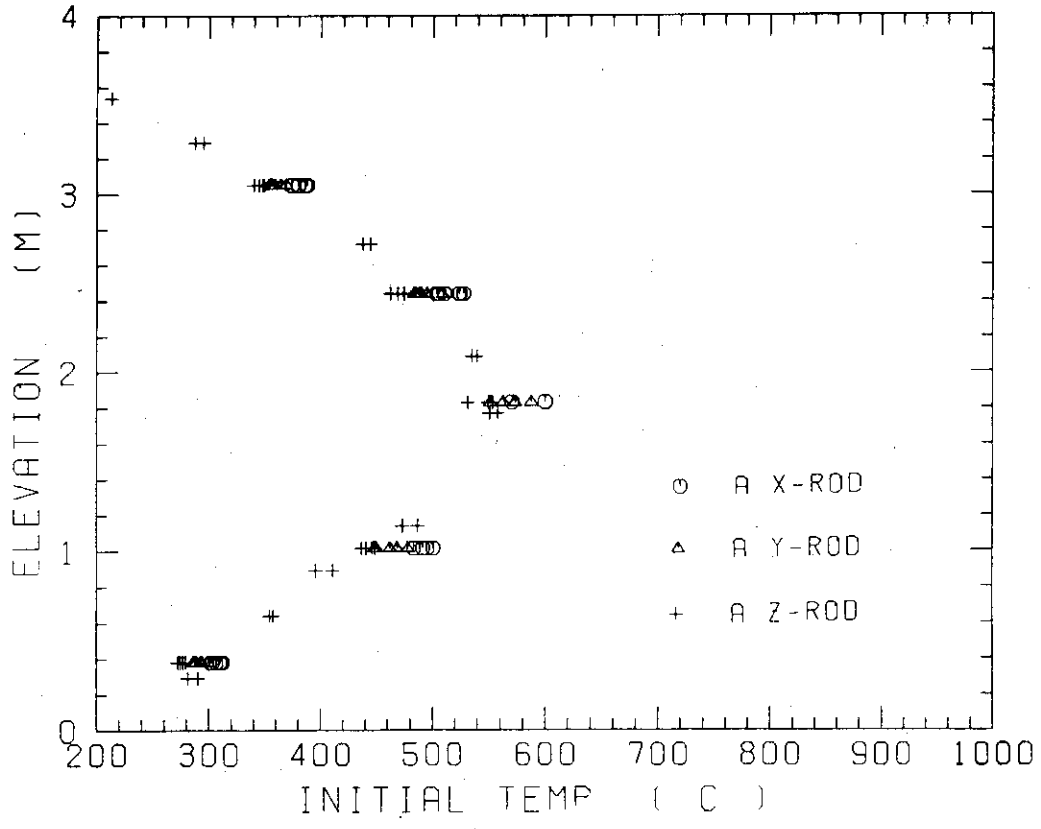

Fig. B-6 Initial rod surface temperature in high power region (A region)

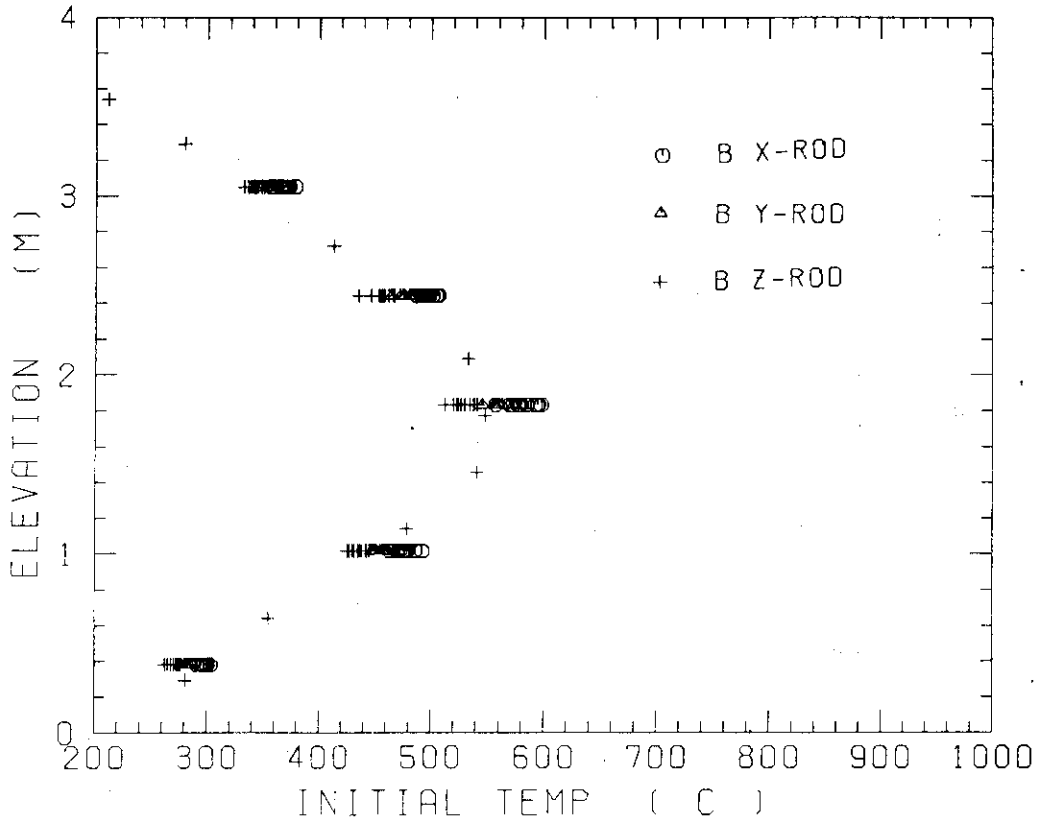

Fig. B-7 Initial rod surface temperature in medium power region (B region)

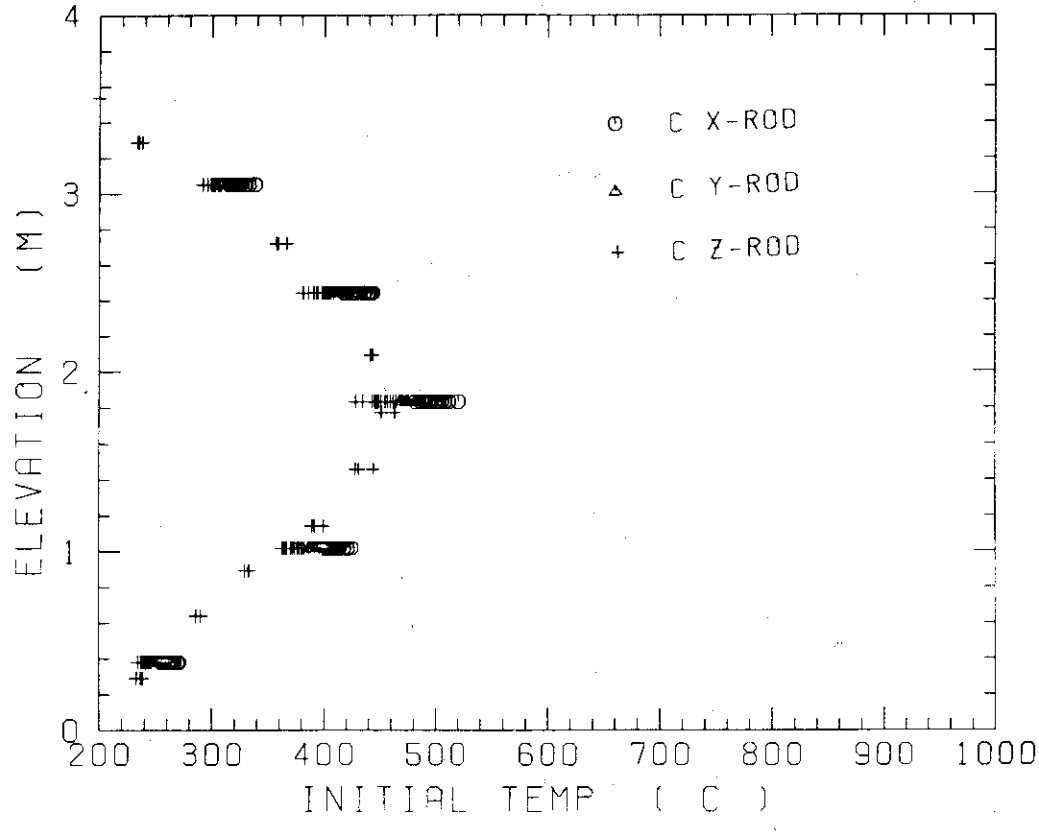

Fig. B-8 Initial rod surface temperature in low power region (C region)

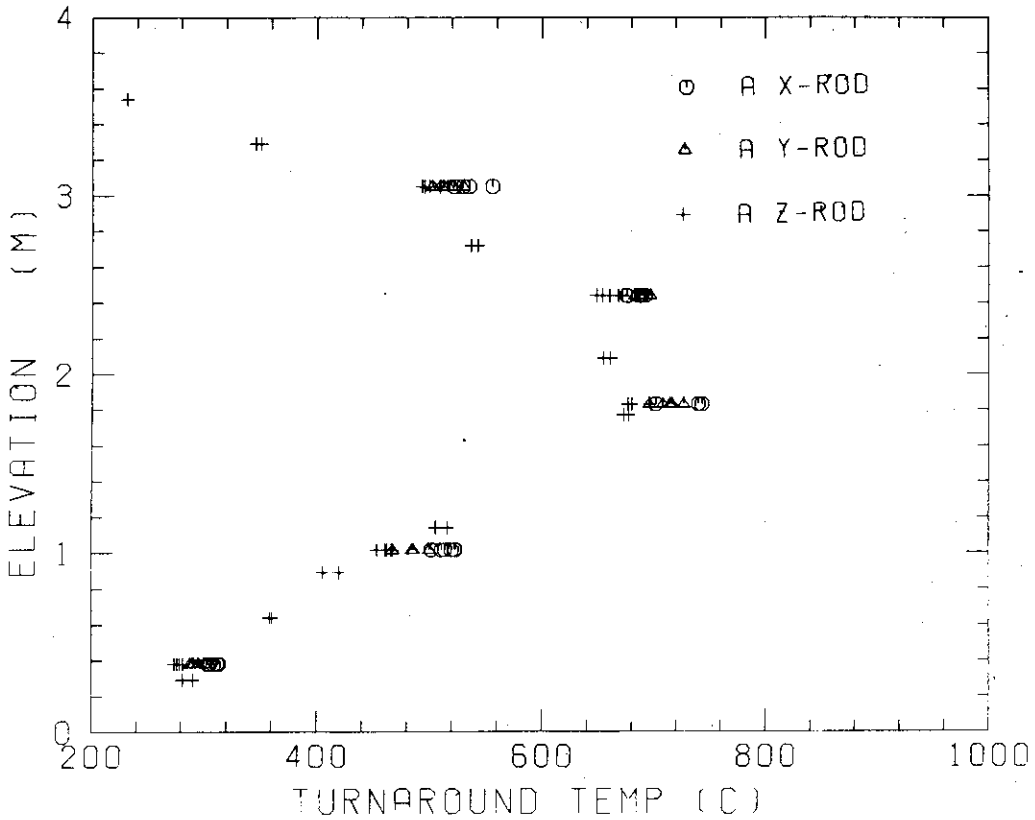

Fig. B-9 Turnaround temperature in high power region (A region)

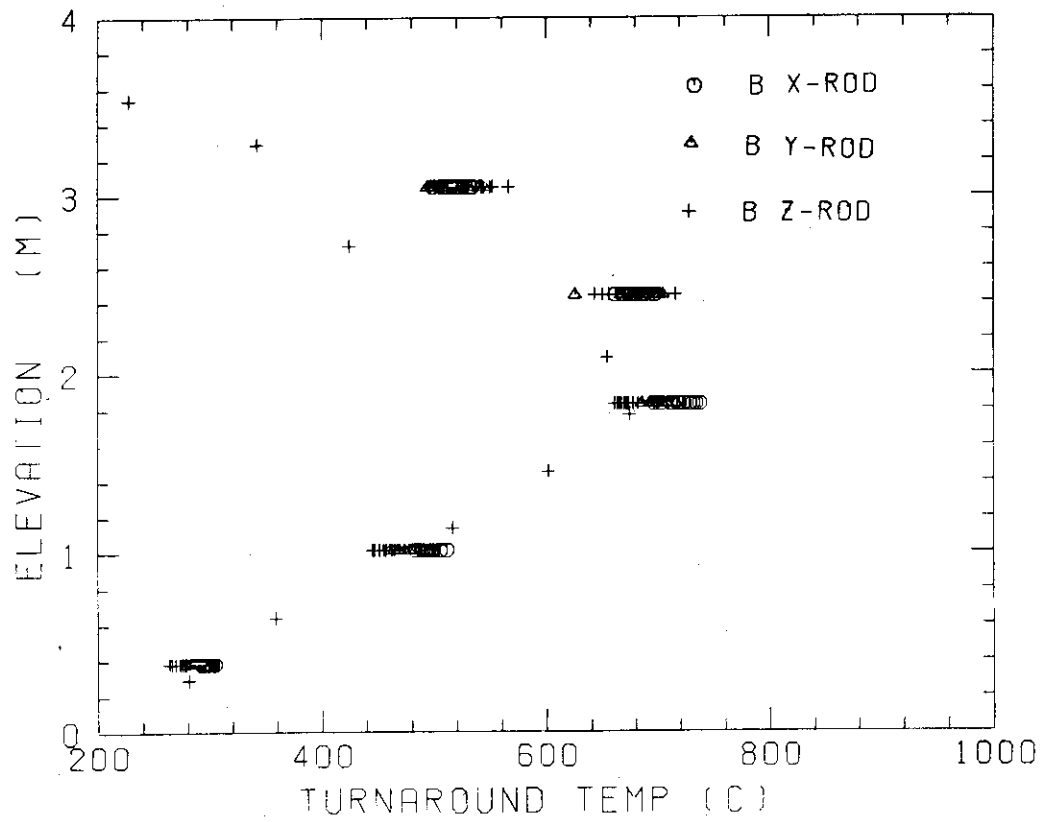

Fig. B-10 Turnaround temperature in medium power region (B region)

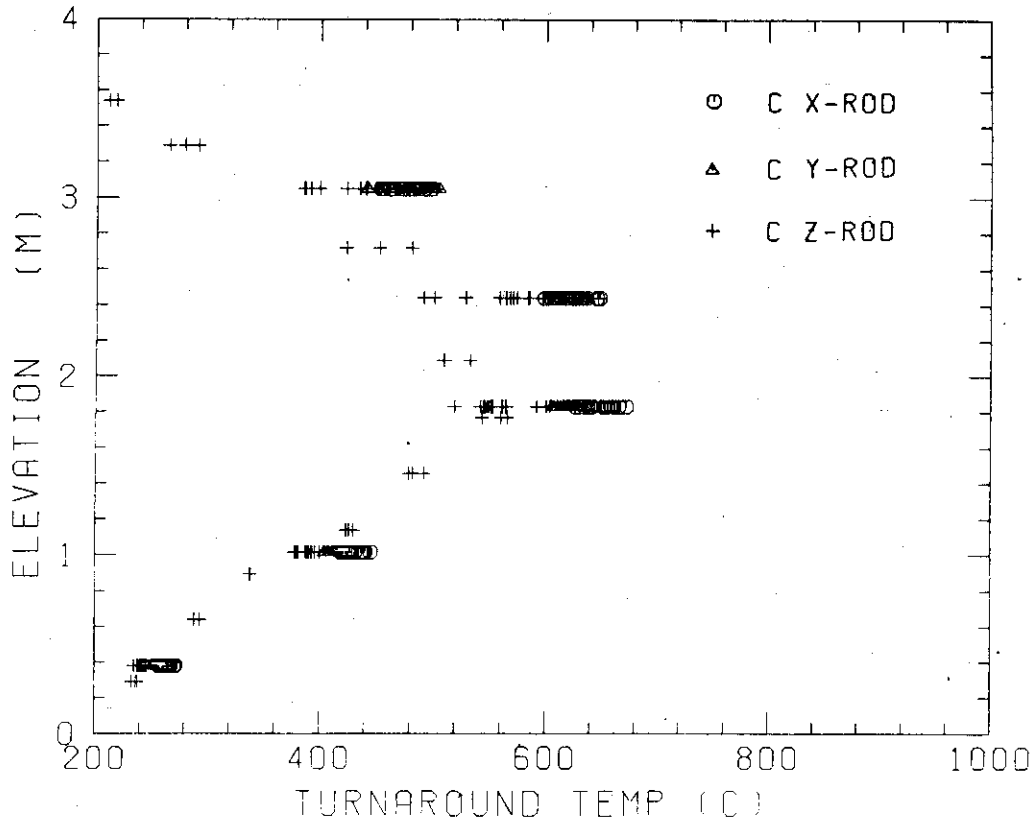

Fig. B-11 Turnaround temperature in low power region (C region)

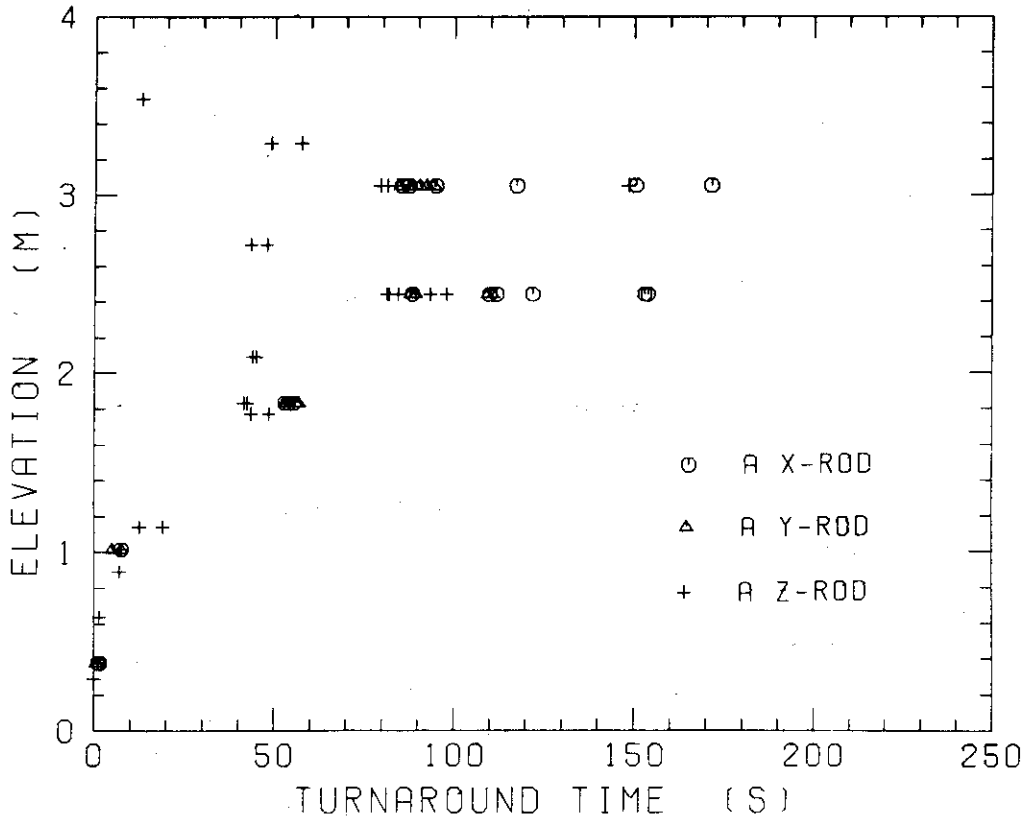

Fig. B-12 Turnaround time in high power region (A region)

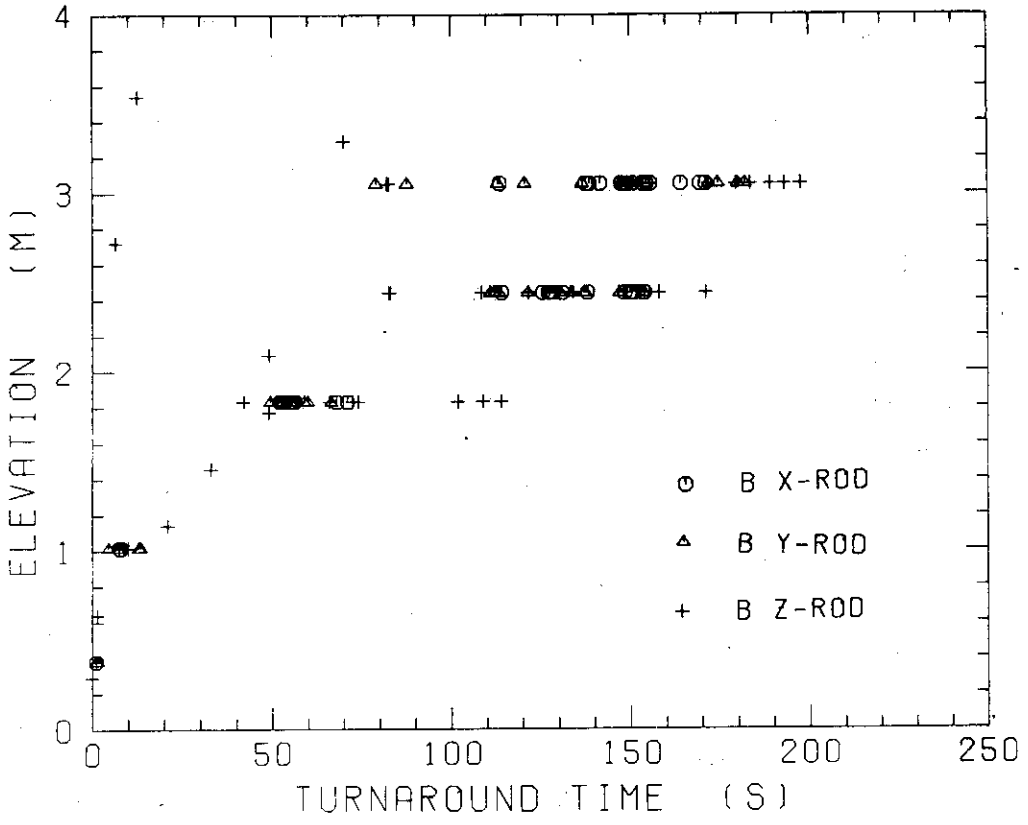

Fig. B-13 Turnaround time in medium power region (B region)

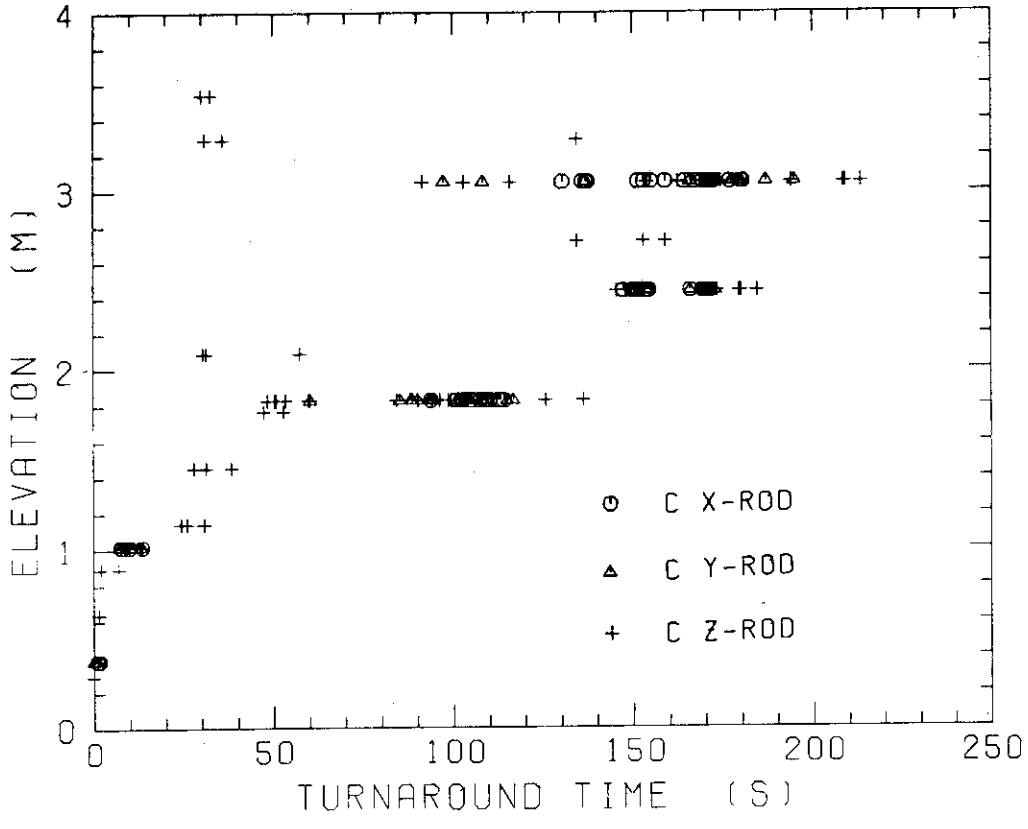

Fig. B-14 Turnaround time in low power region (C region)

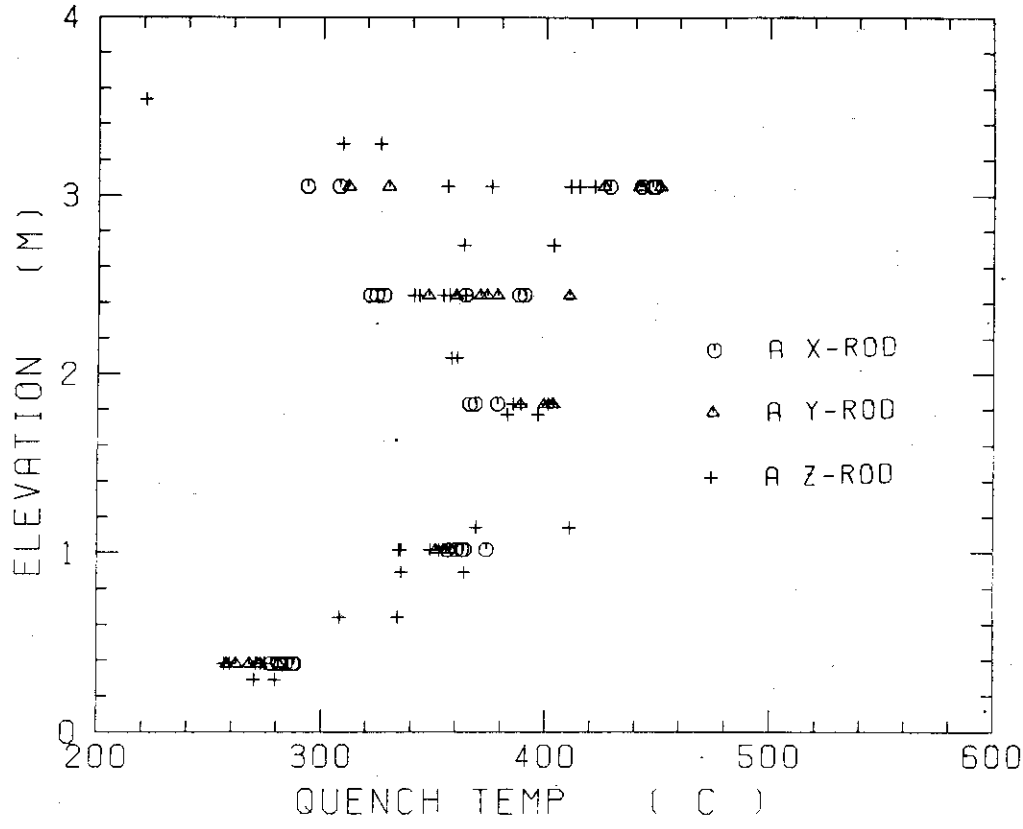

Fig. B-15 Quench temperature in high power region (A region)

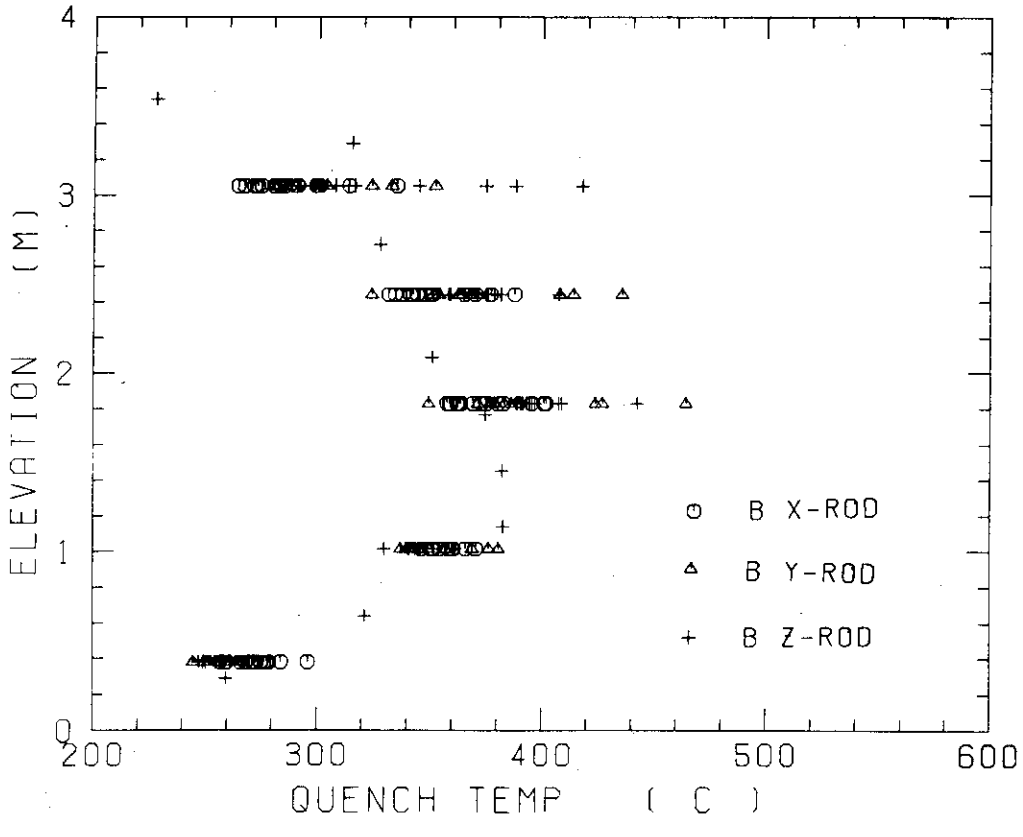

Fig. B-16 Quench temperature in medium power region (B region)

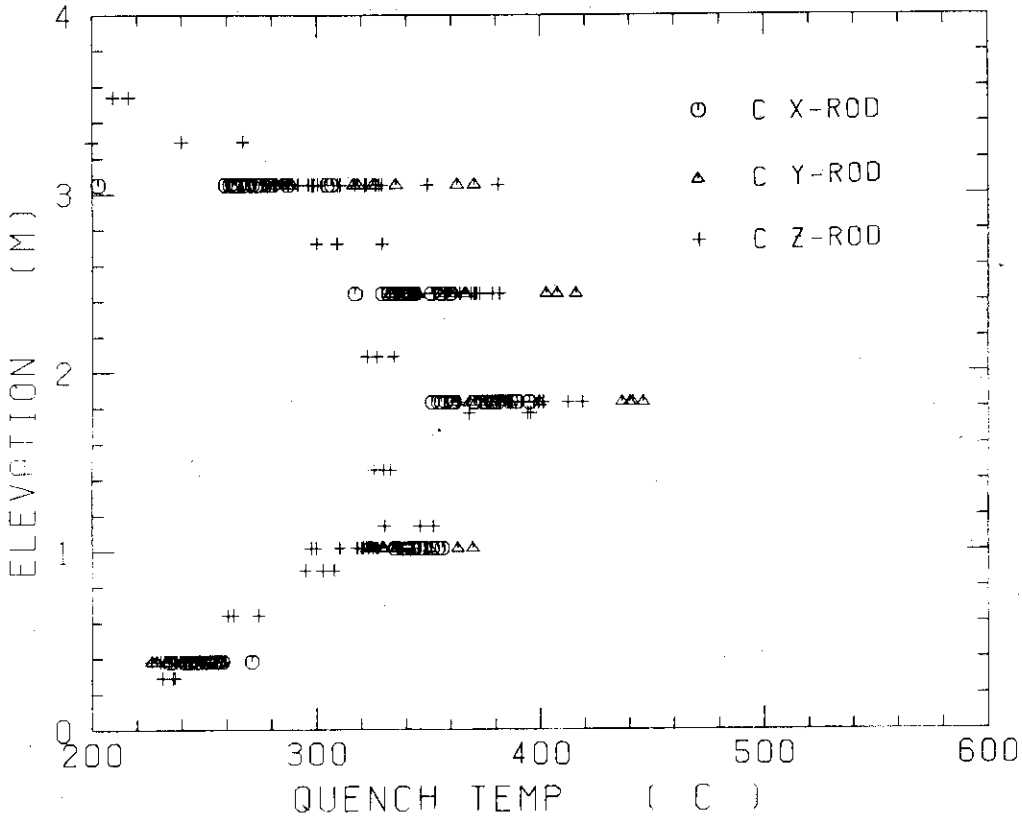

Fig. B-17 Quench temperature in low power region (C region)

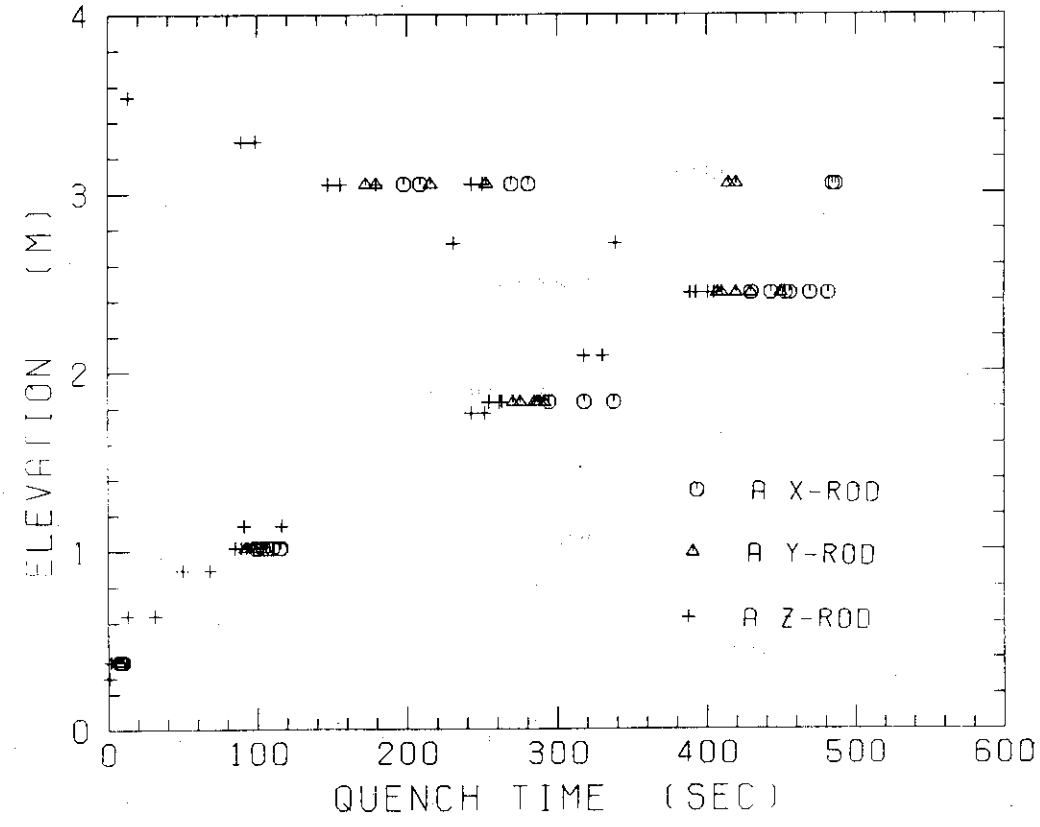

Fig. B-18 Quench time in high power region (A region)

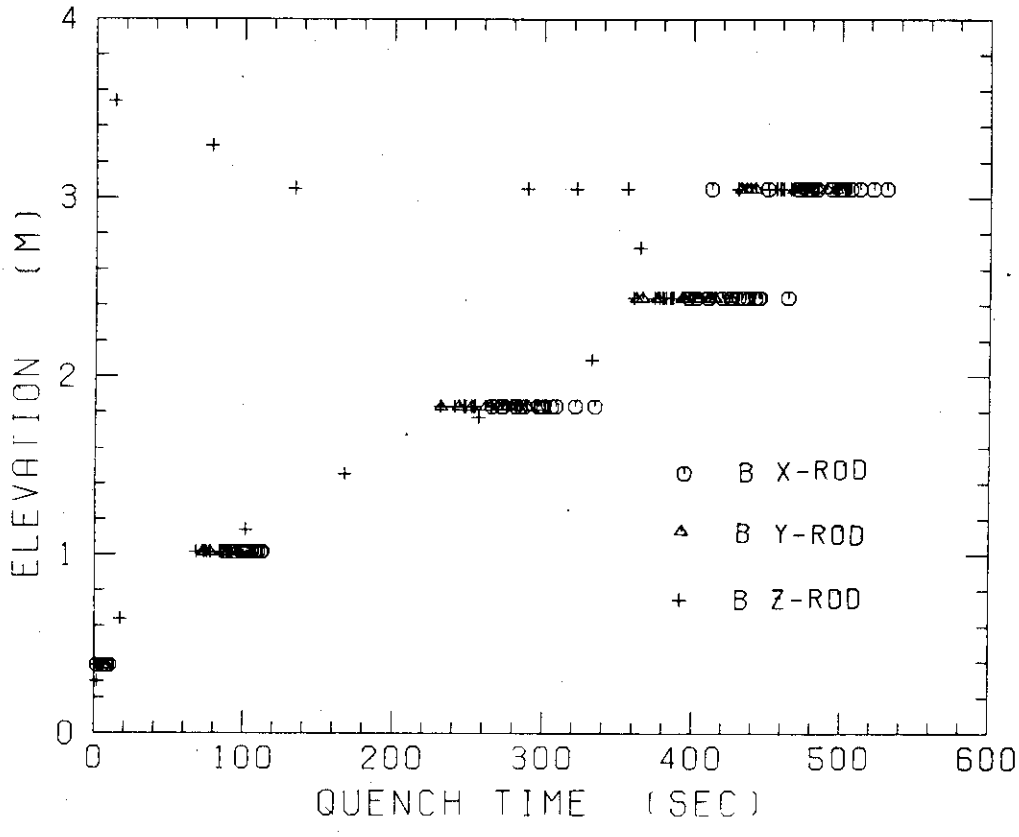

Fig. B-19 Quench time in medium power region (B region)

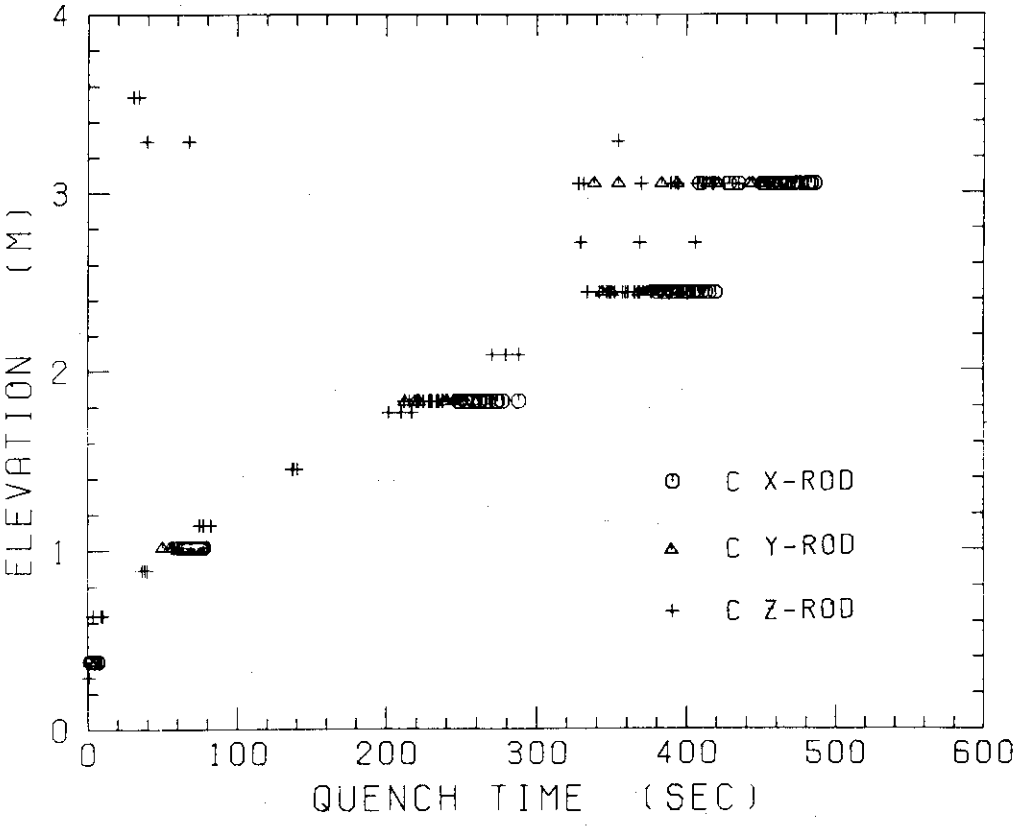

Fig. B-20 Quench time in low power region (C region)

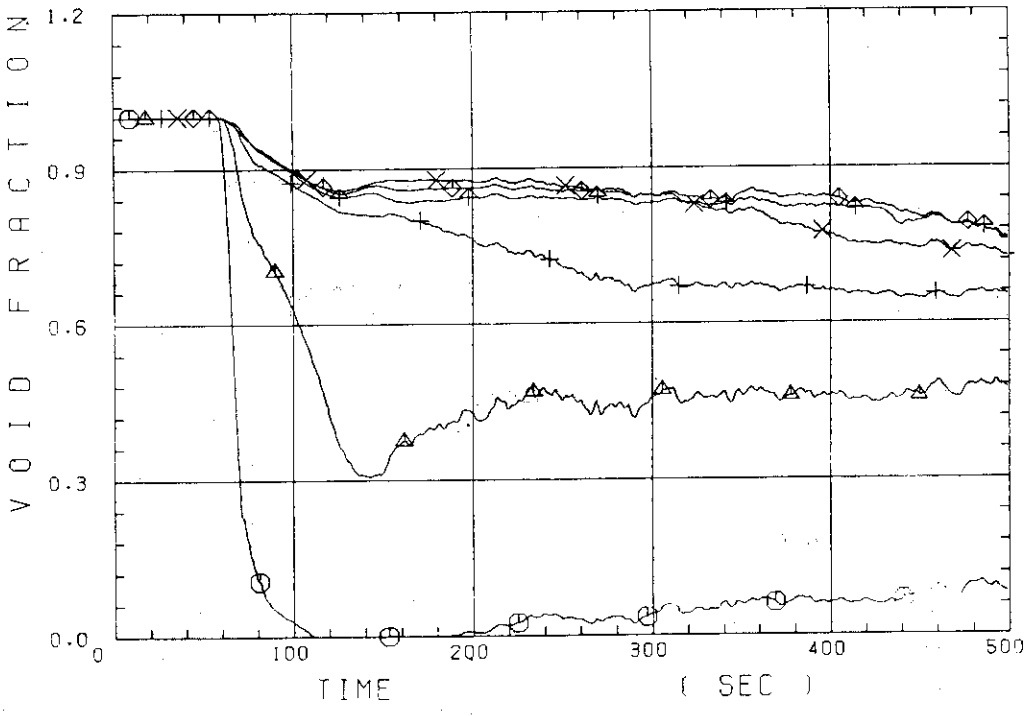

Fig. B-21 Void fraction in core

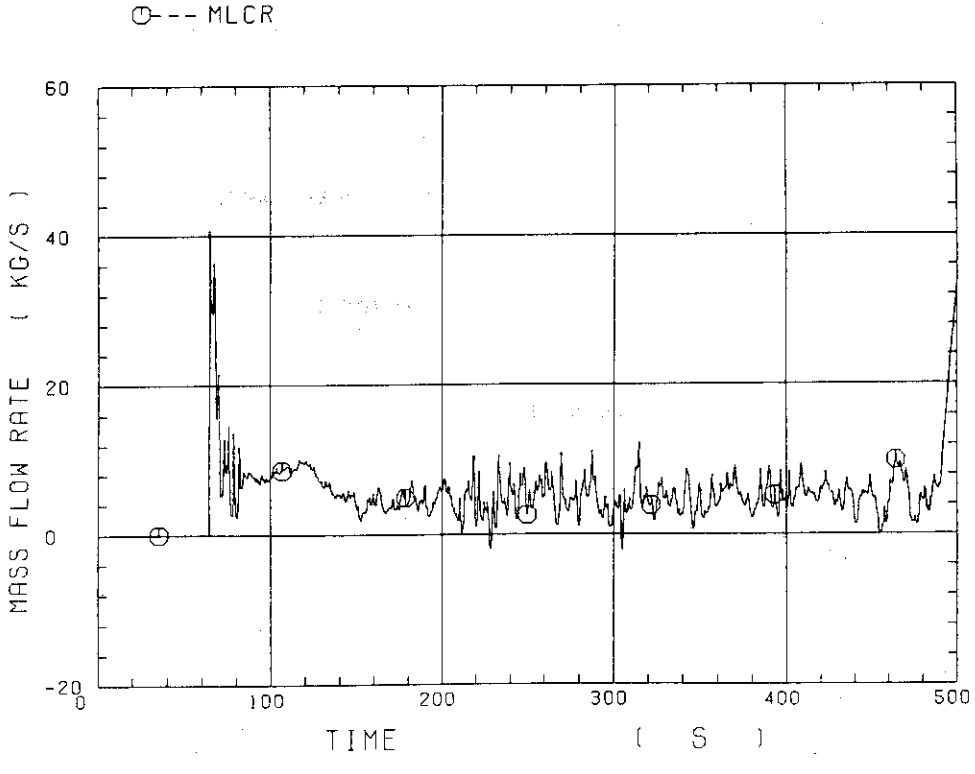

Fig. B-22 Core inlet mass flow rate (recommended value)

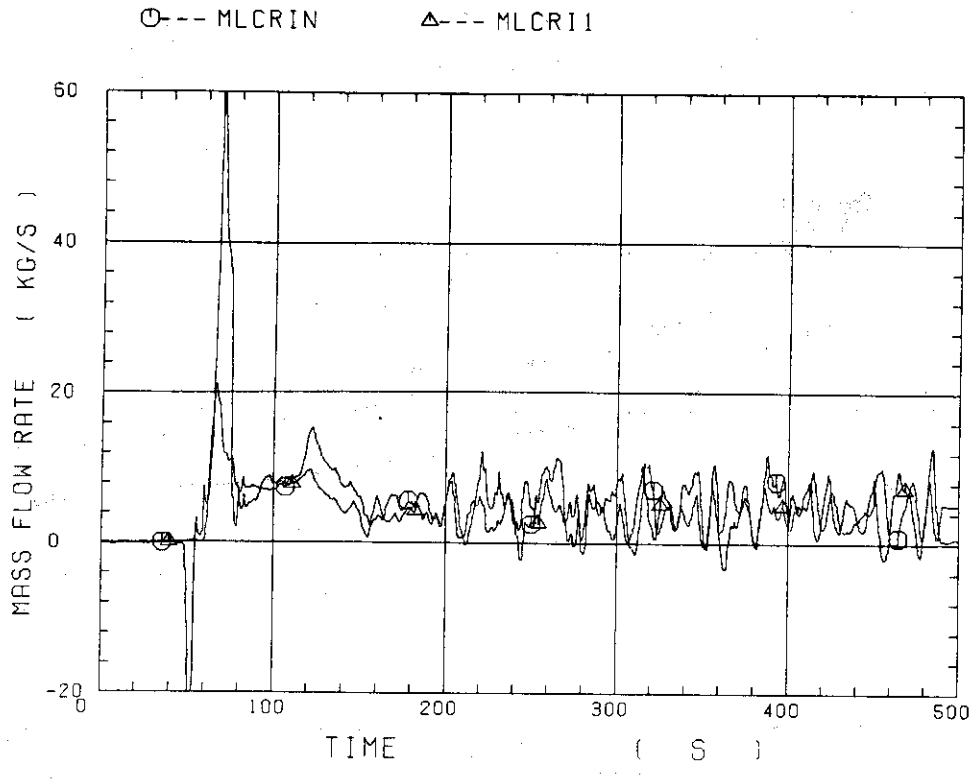

Fig. B-23 Core inlet mass flow rate

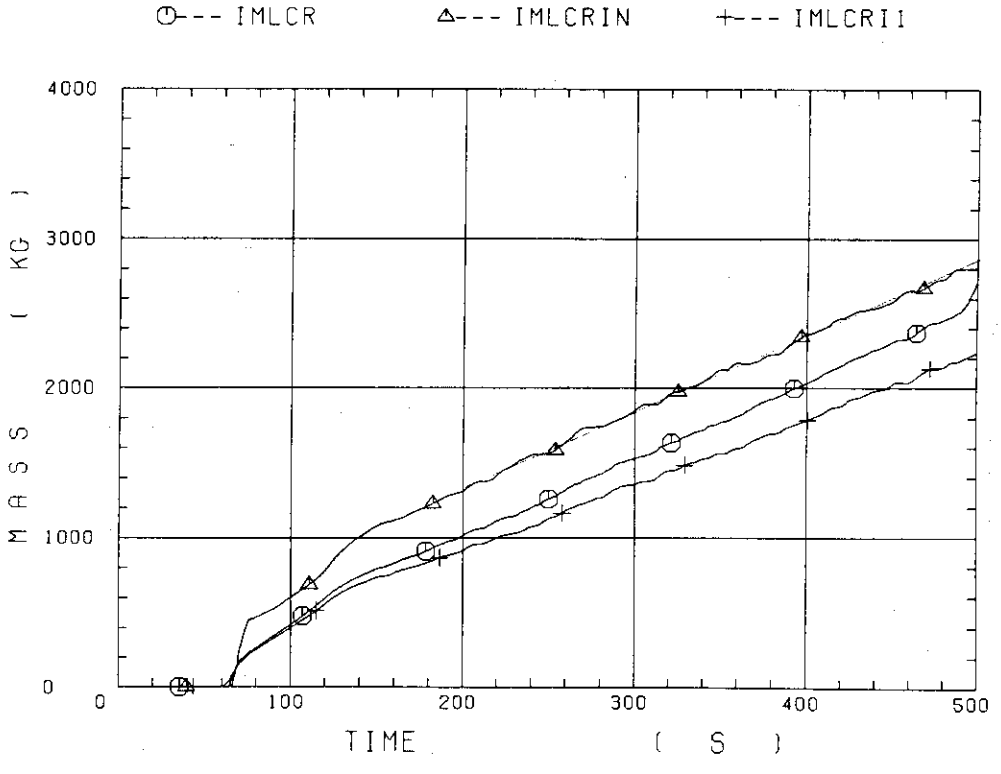

Fig. B-24 Time-integration of core inlet mass flow rate

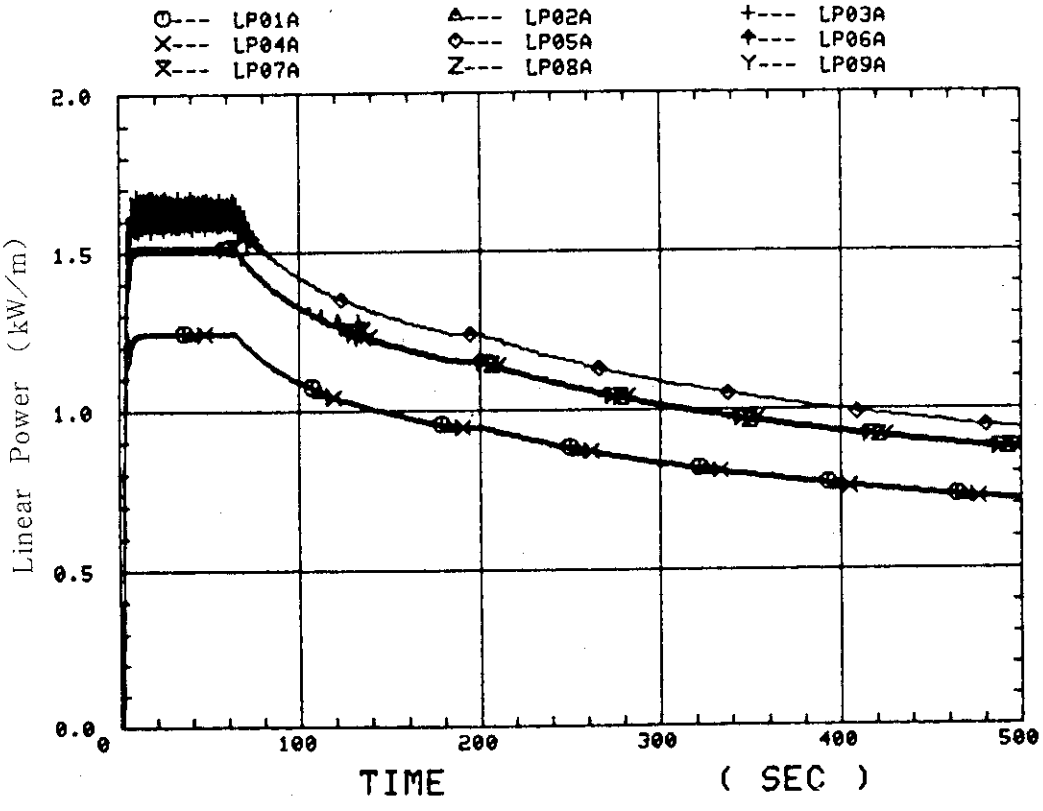

Fig. B-25 Average linear power of heater rod in each power unit zone

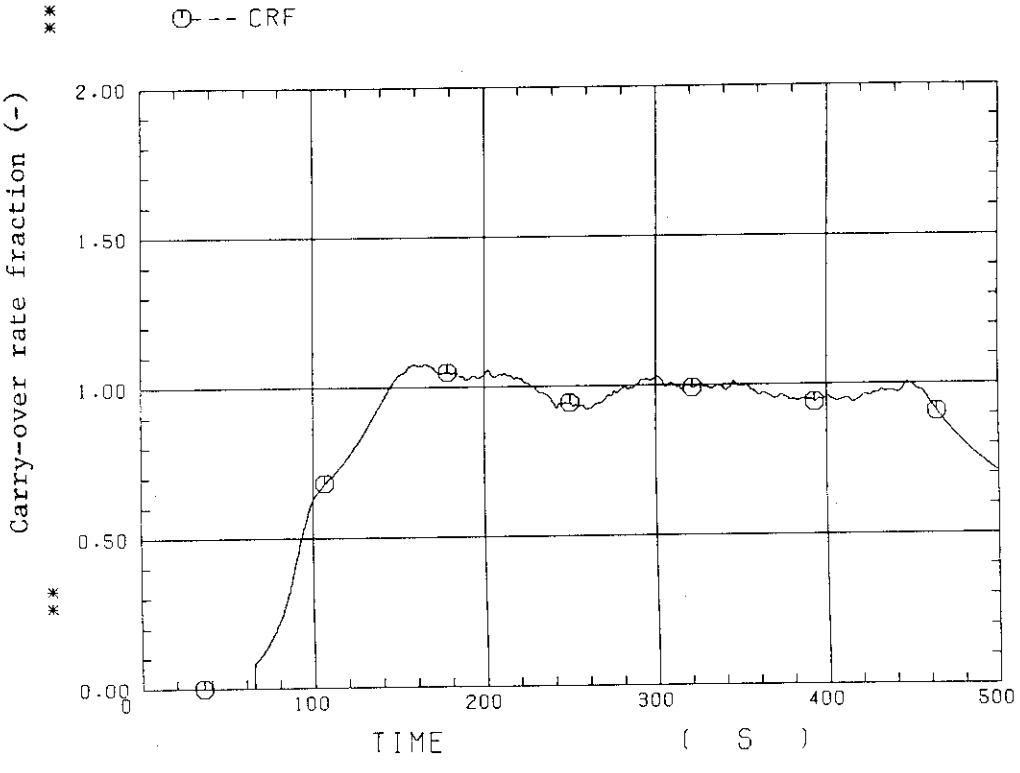

Fig. B-26 Carry-over rate fraction

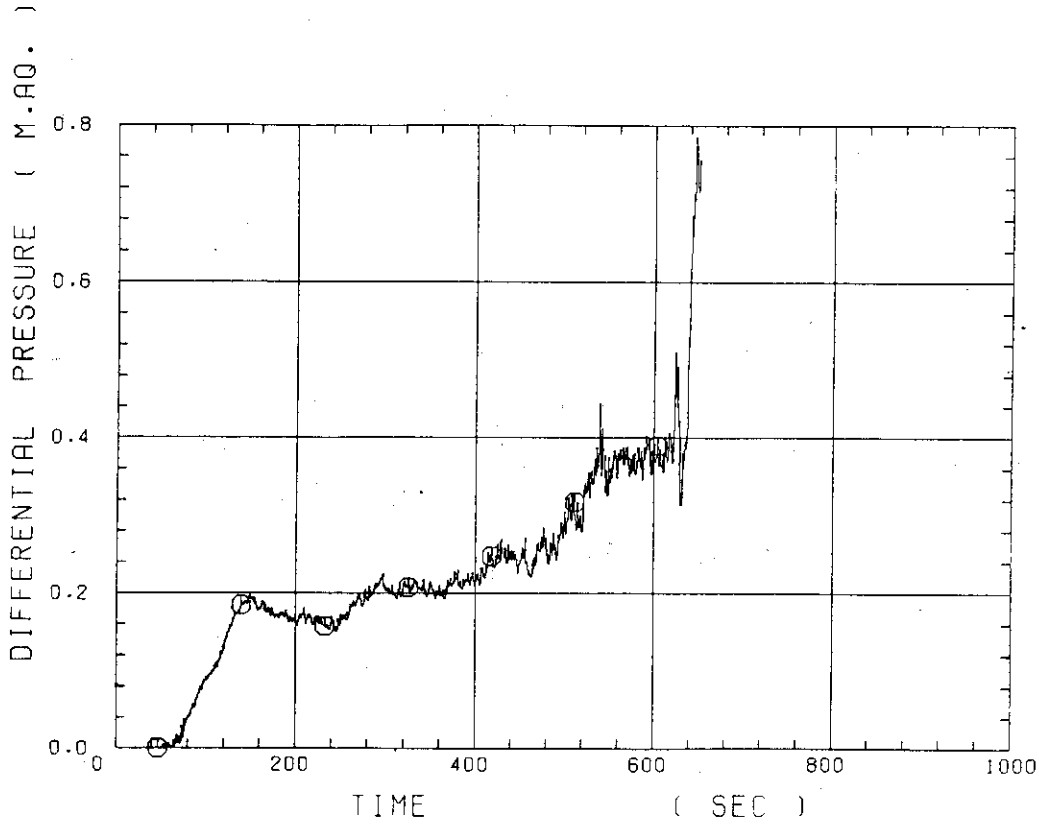

Fig. B-27 Differential pressure through upper plenum

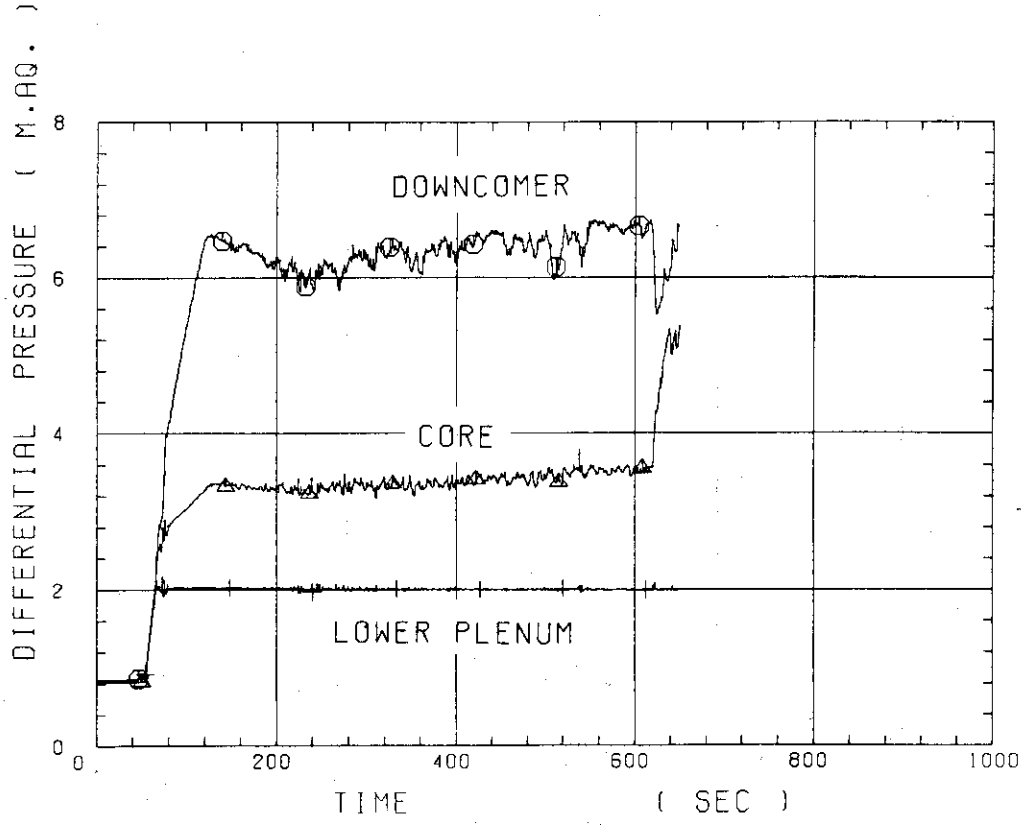

Fig. B-28 Differential pressure through downcomer, core, and lower plenum

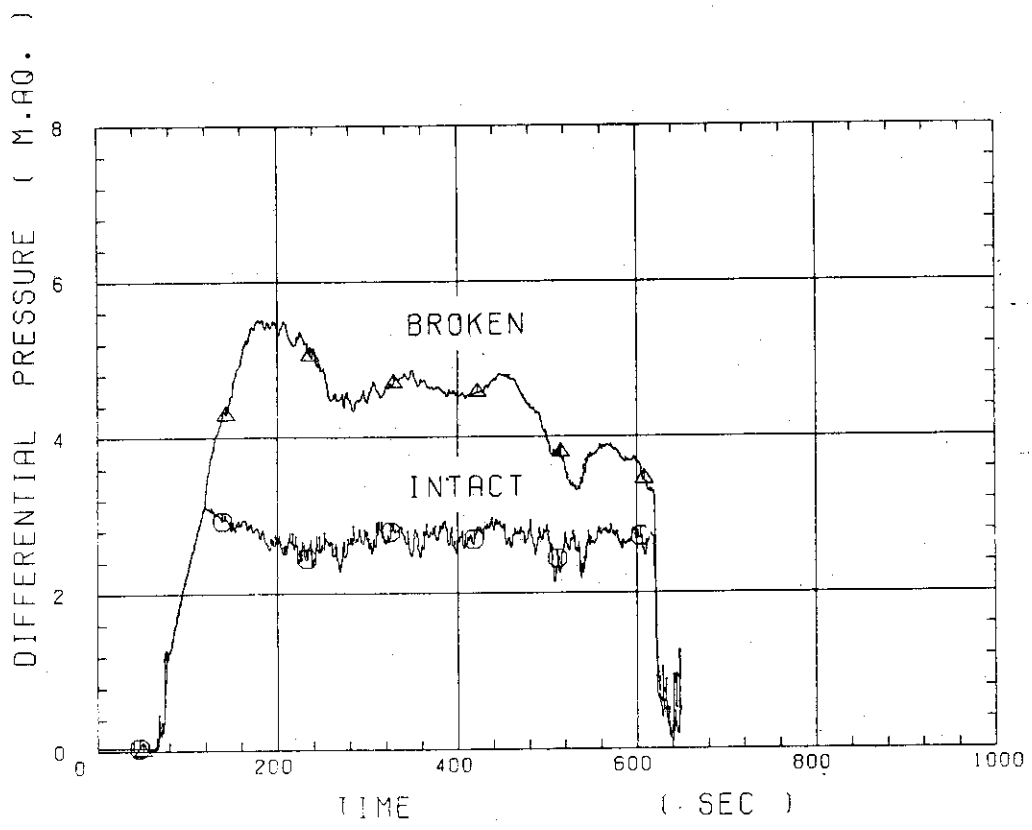

Fig. B-29 Differential pressure through intact and broken loops

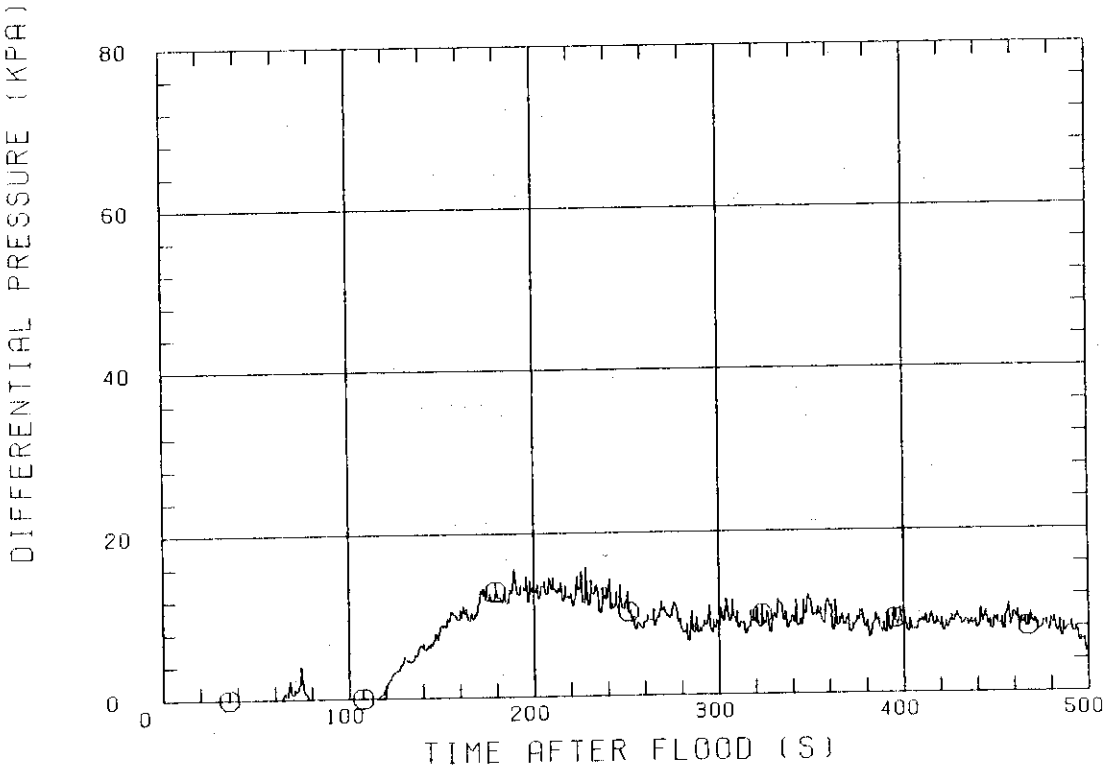

Fig. B-30 Differential pressure through broken cold leg nozzle

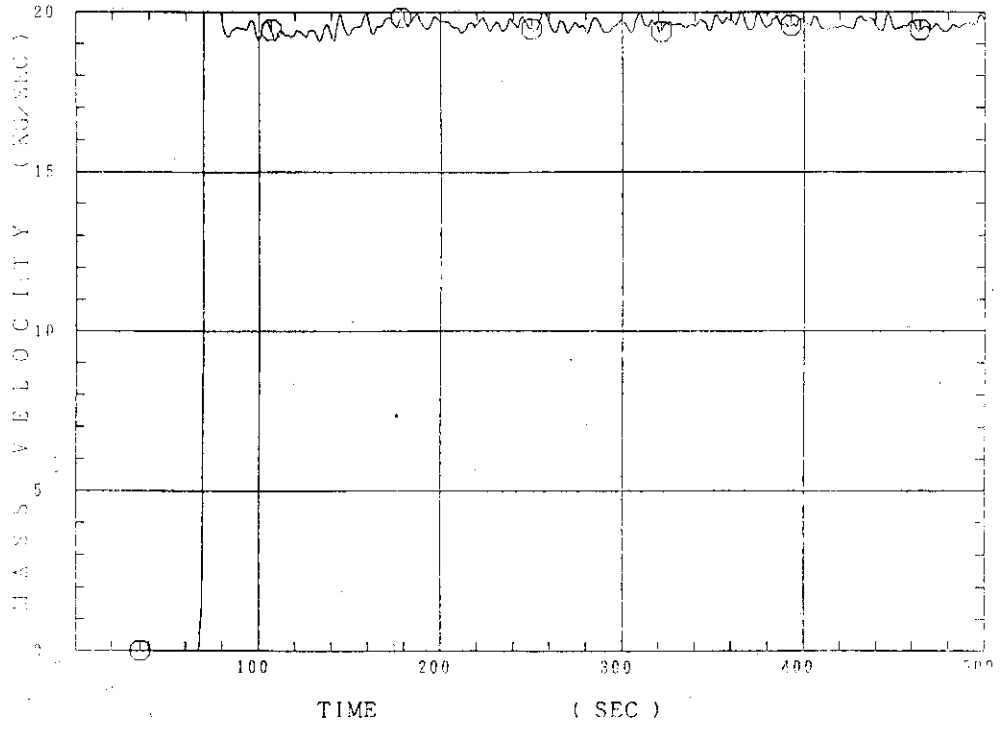

Fig. B-31 Total water mass flow rate from intact loops to downcomer

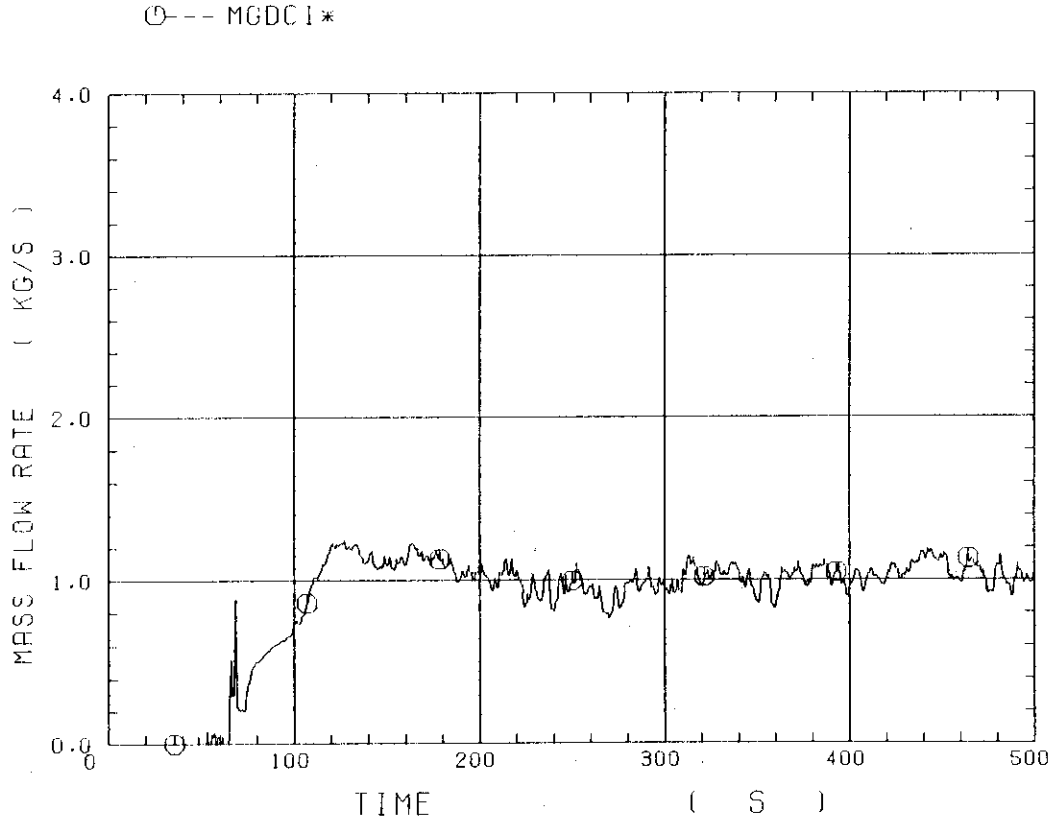

Fig. B-32 Total steam mass flow rate from intact loops to downcomer

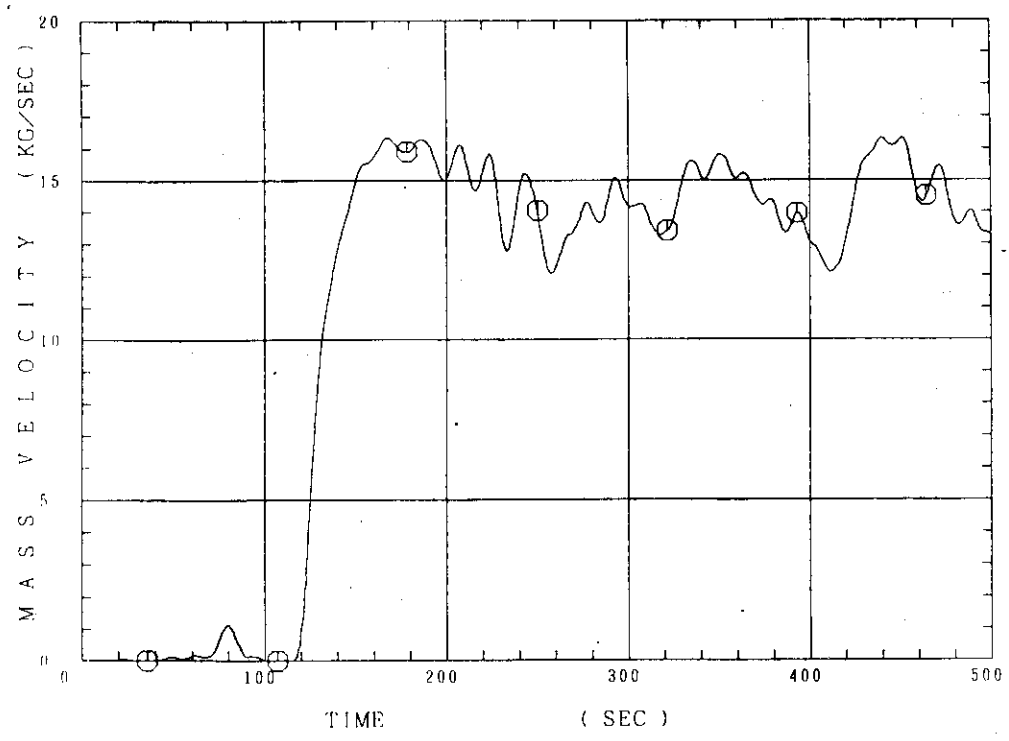

Fig. B-33 Water mass flow rate through broken cold leg nozzle

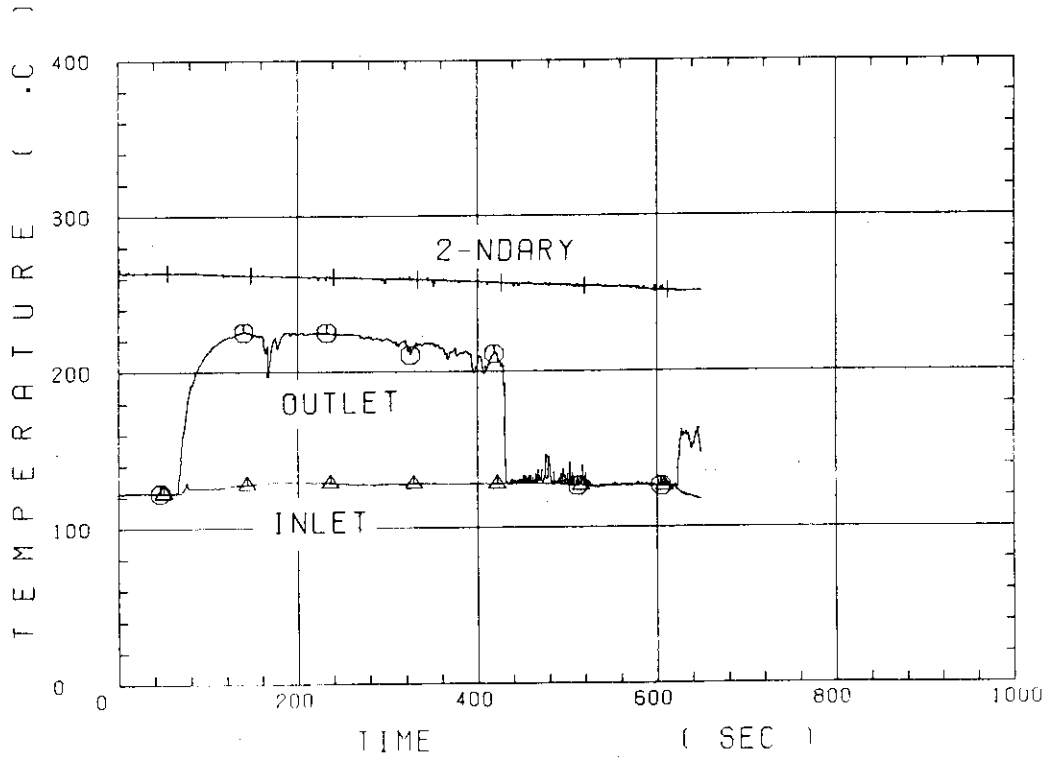

Fig. B-34 Fluid temperature in inlet plenum, outlet plenum, and secondary of steam generator 1

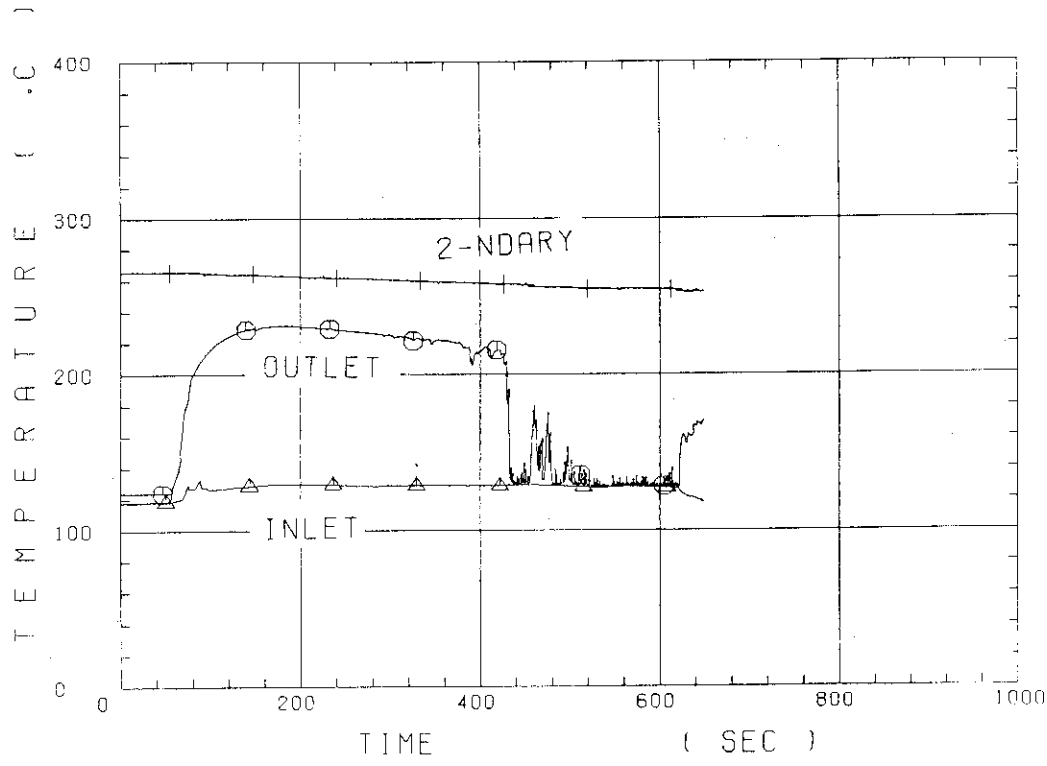

Fig. B-35 Fluid temperature in inlet plenum, outlet plenum, and secondary of steam generator 2

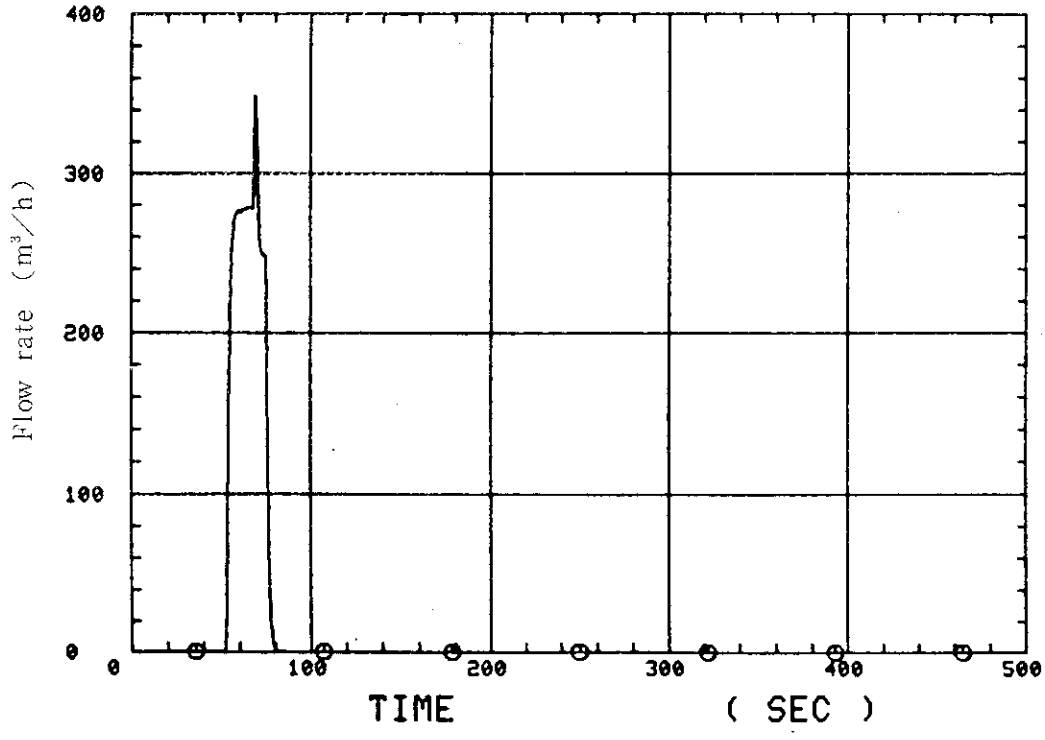

Fig. B-36 Total accumulator injection rate

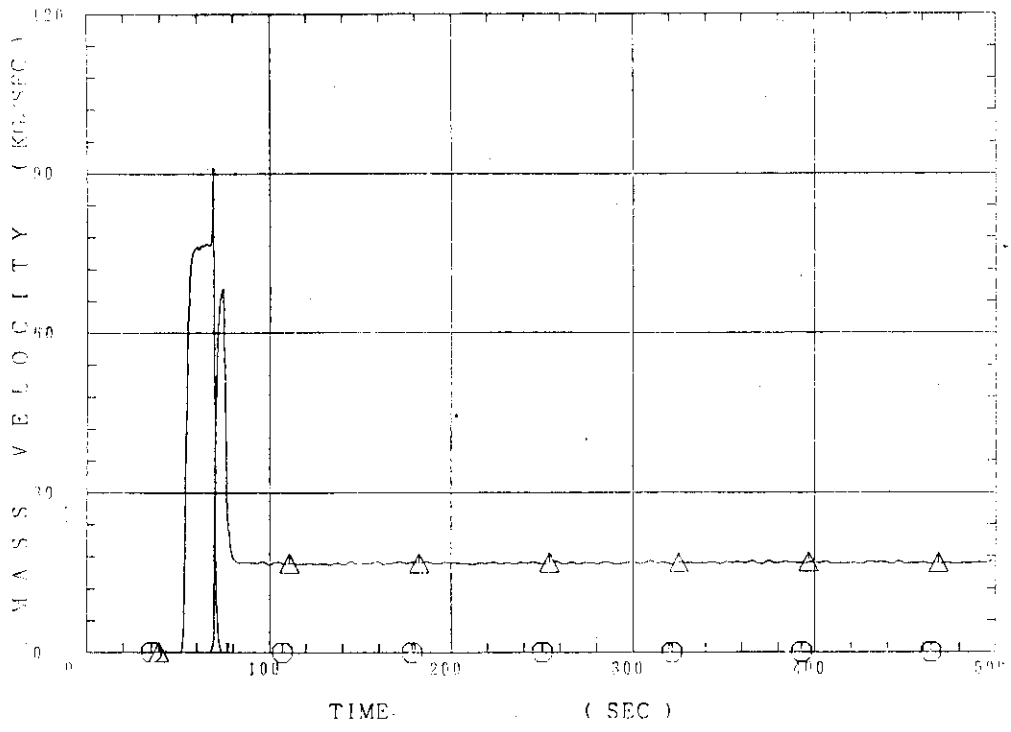

Fig. B-37 ECC water injection rates to lower plenum and to cold legs

Appendix C

Selected data of CCTF Test C1-9 (Run18)

Table and Figure List

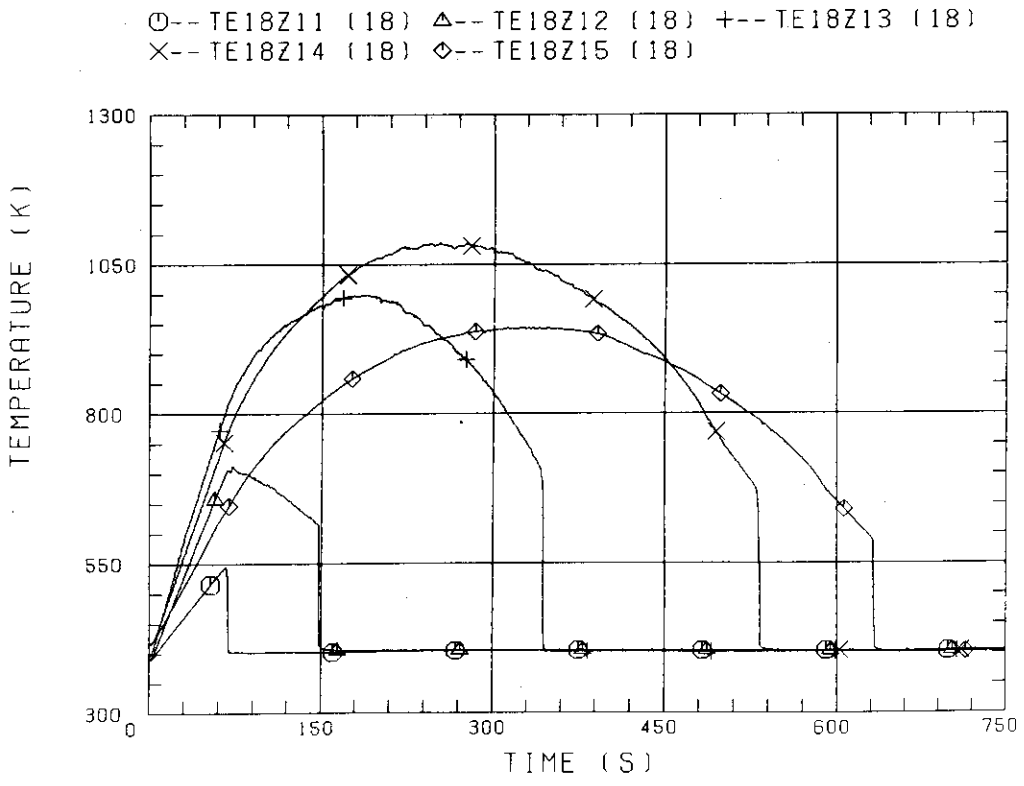

Fig. C-1 Surface temperature on low power rod (Z-rod) in medium power region (B region) (average power rod)

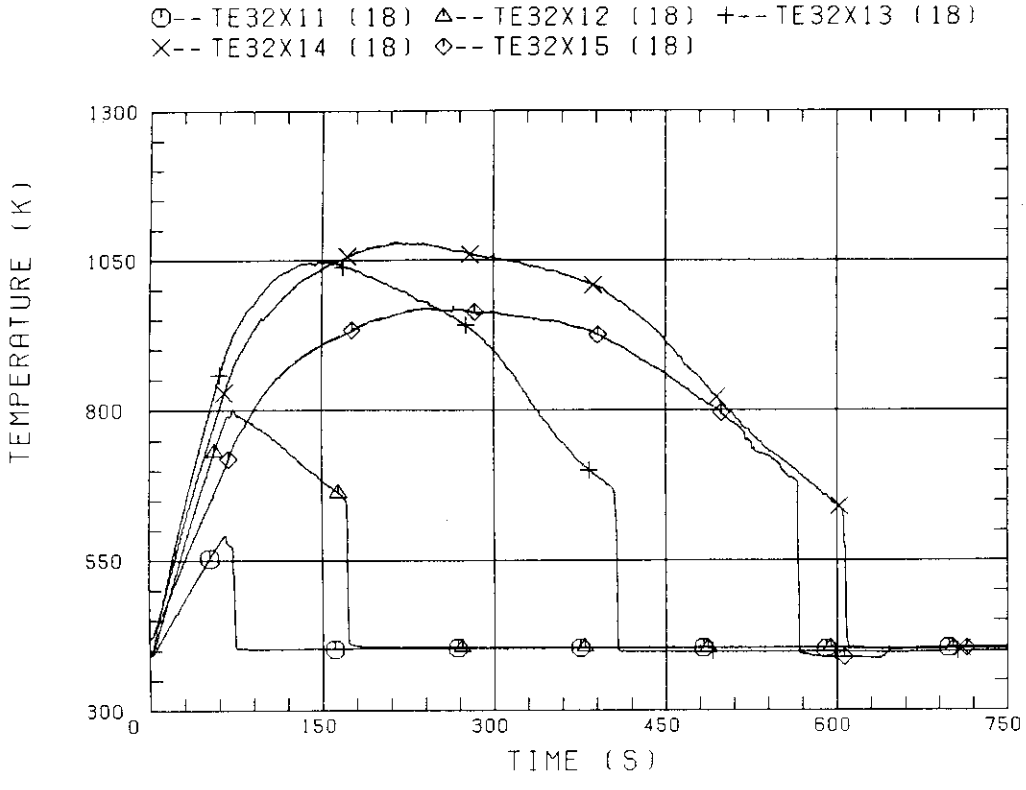

Fig. C-2 Surface temperature on high power rod (X-rod) in high power region (A region) (peak power rod)

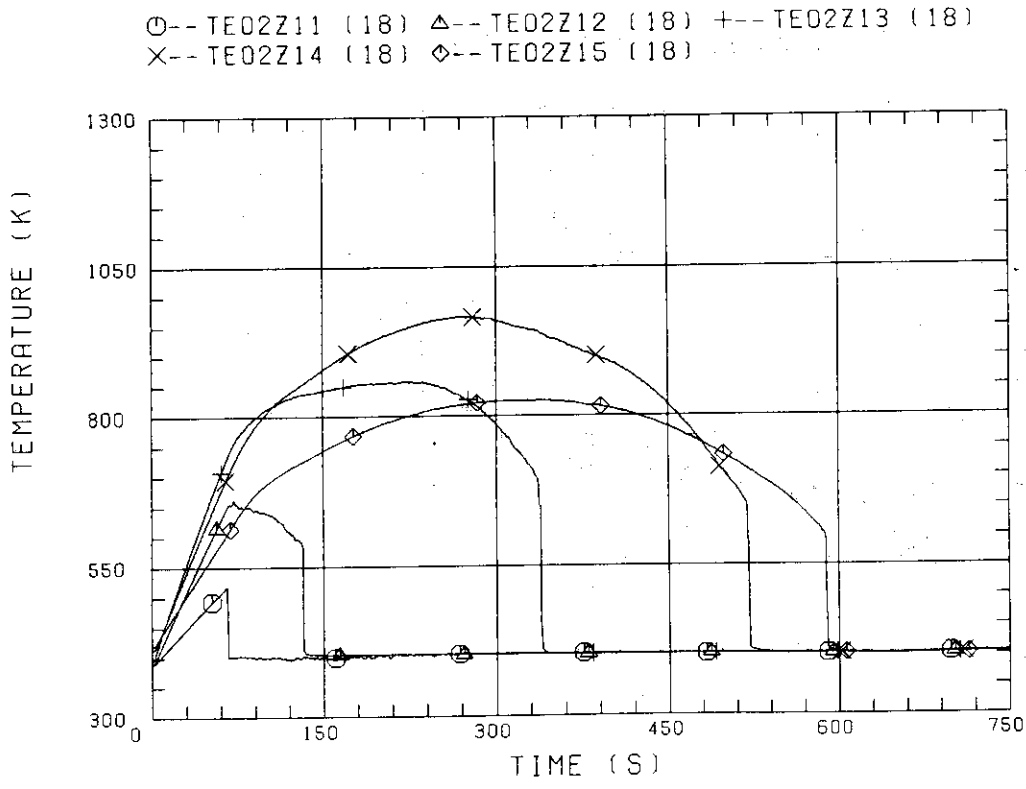

Fig. C-3 Surface temperature on low power rod (Z-rod) in low power region (C region) (lowest power rod)

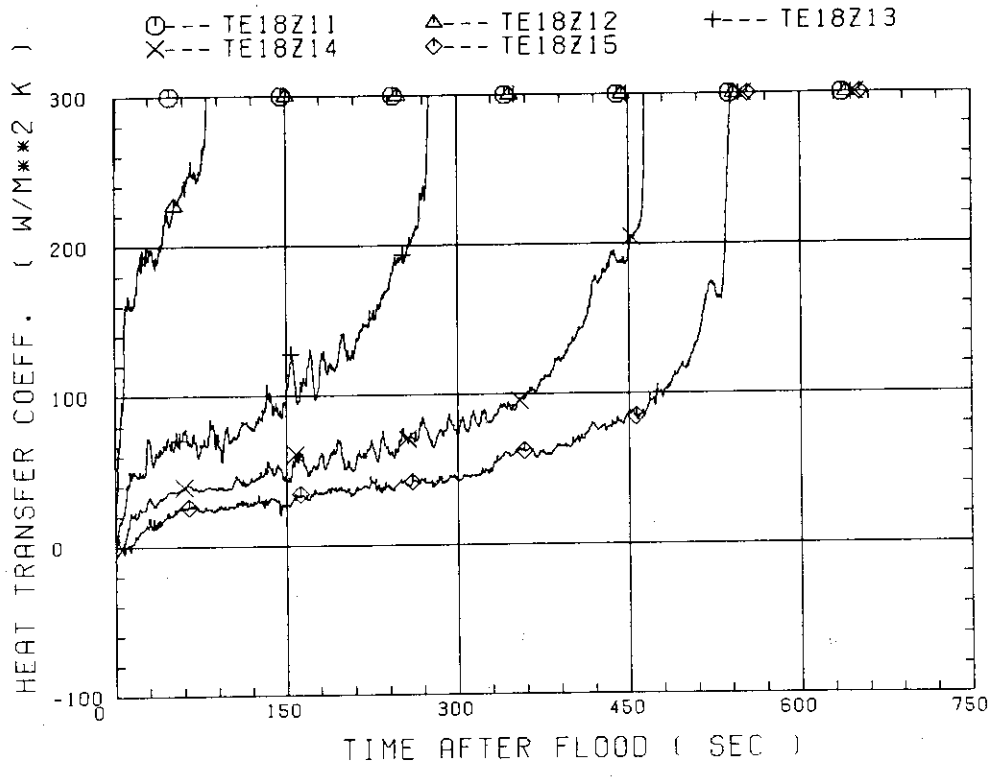

Fig. C-4 Heat transfer coefficient of low power rod (Z-rod) in medium power region (B region) (average power rod)

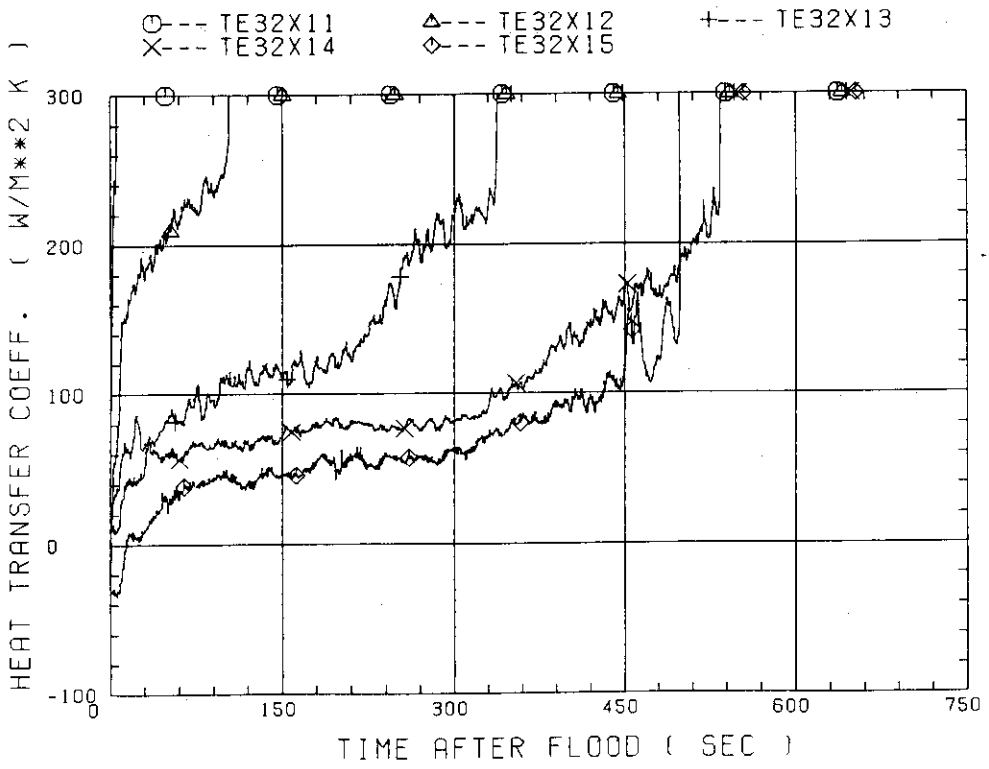

Fig. C-5 Heat transfer coefficient of high power rod (X-rod) in high power region (A region) (peak power rod)

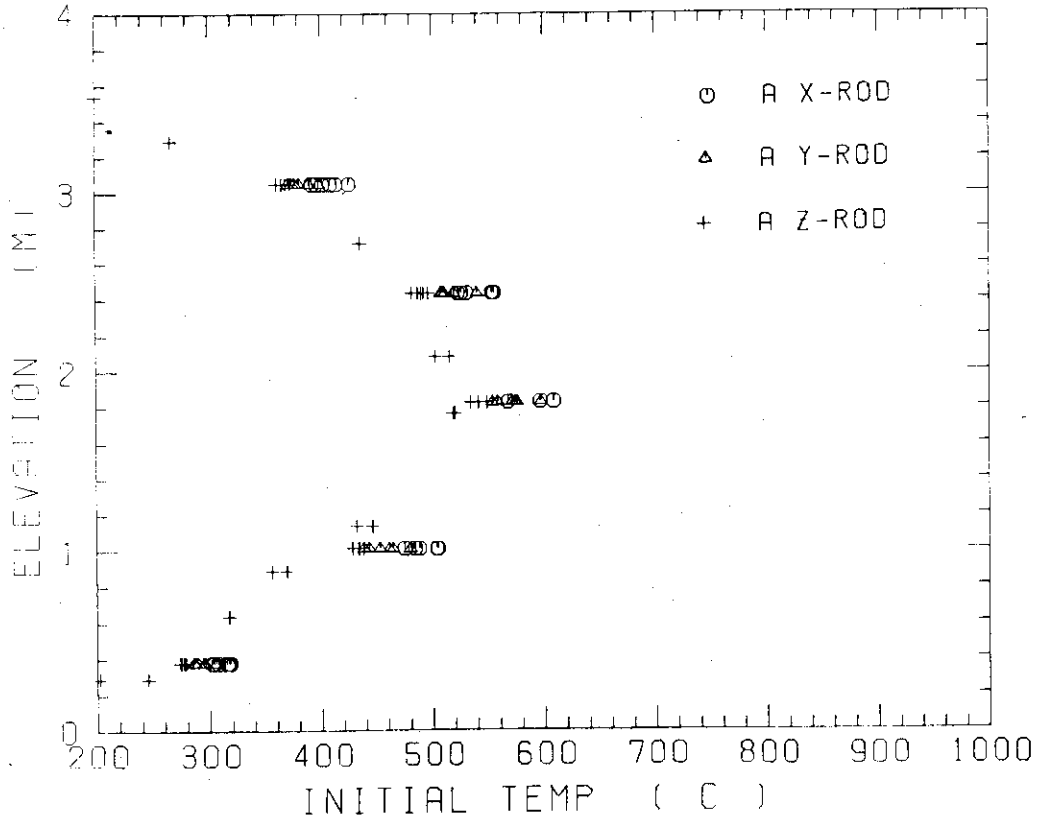

Fig. C-6 Initial rod surface temperature in high power region (A region)

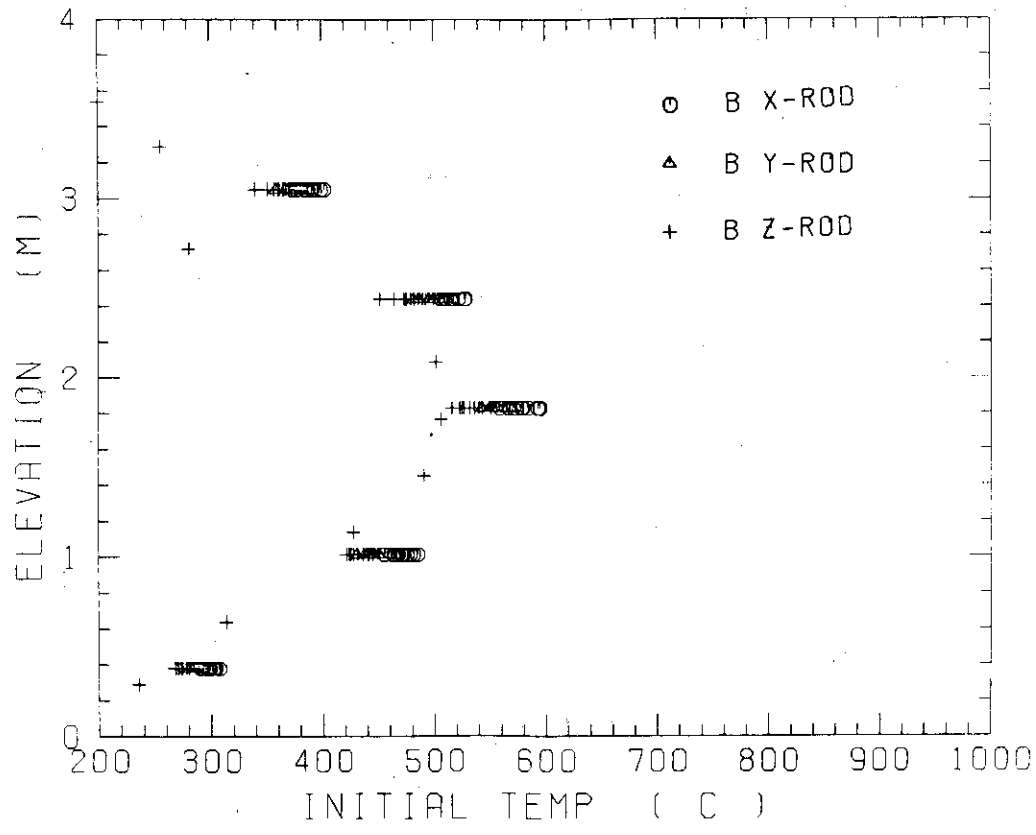

Fig. C-7 Initial rod surface temperature in medium power region (B region)

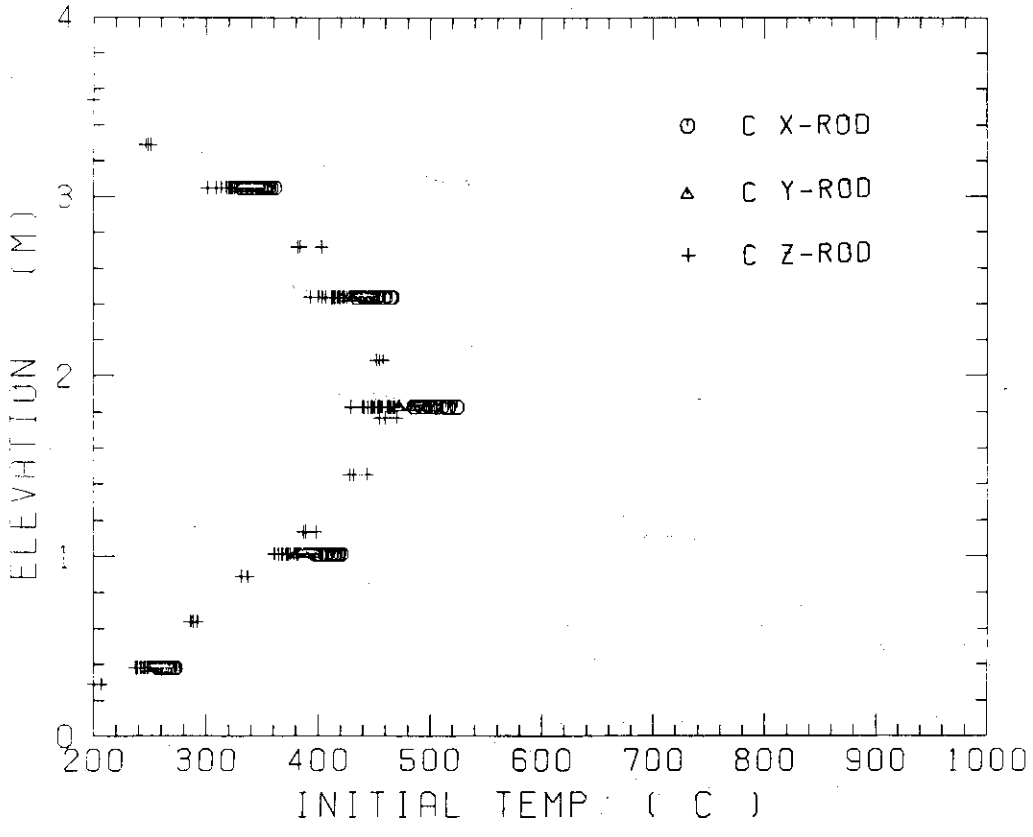

Fig. C-8 Initial rod surface temperature in low power region (C region)

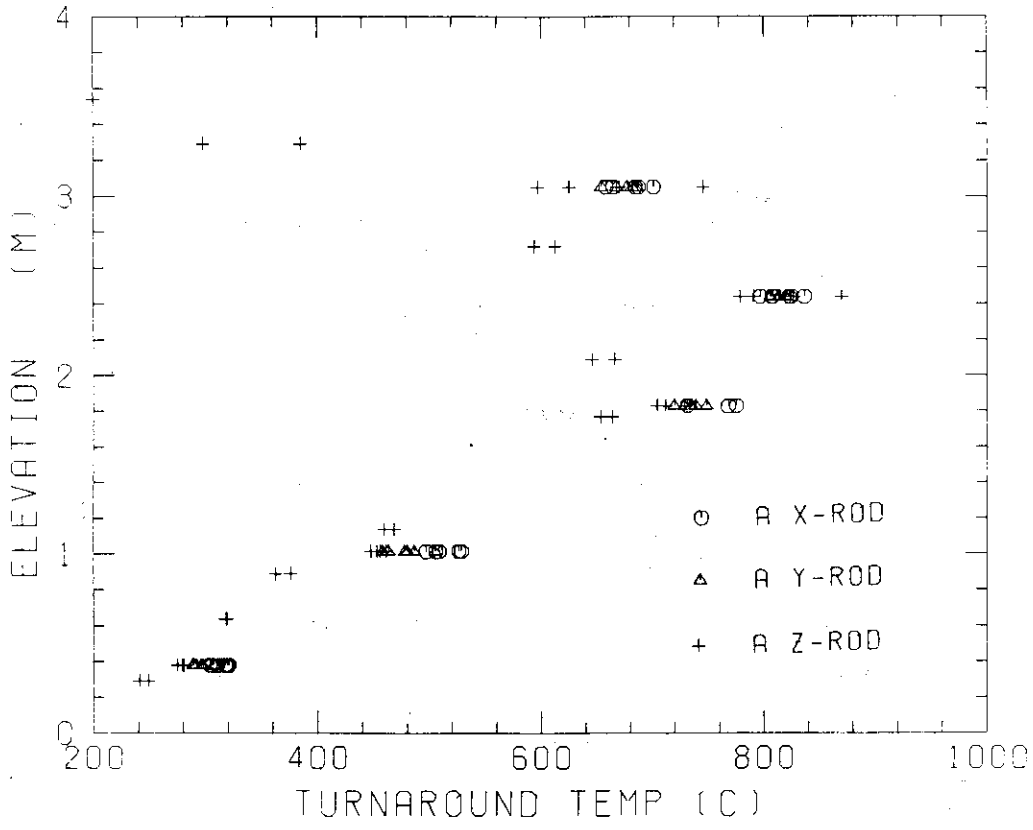

Fig. C-9 Turnaround temperature in high power region (A region)

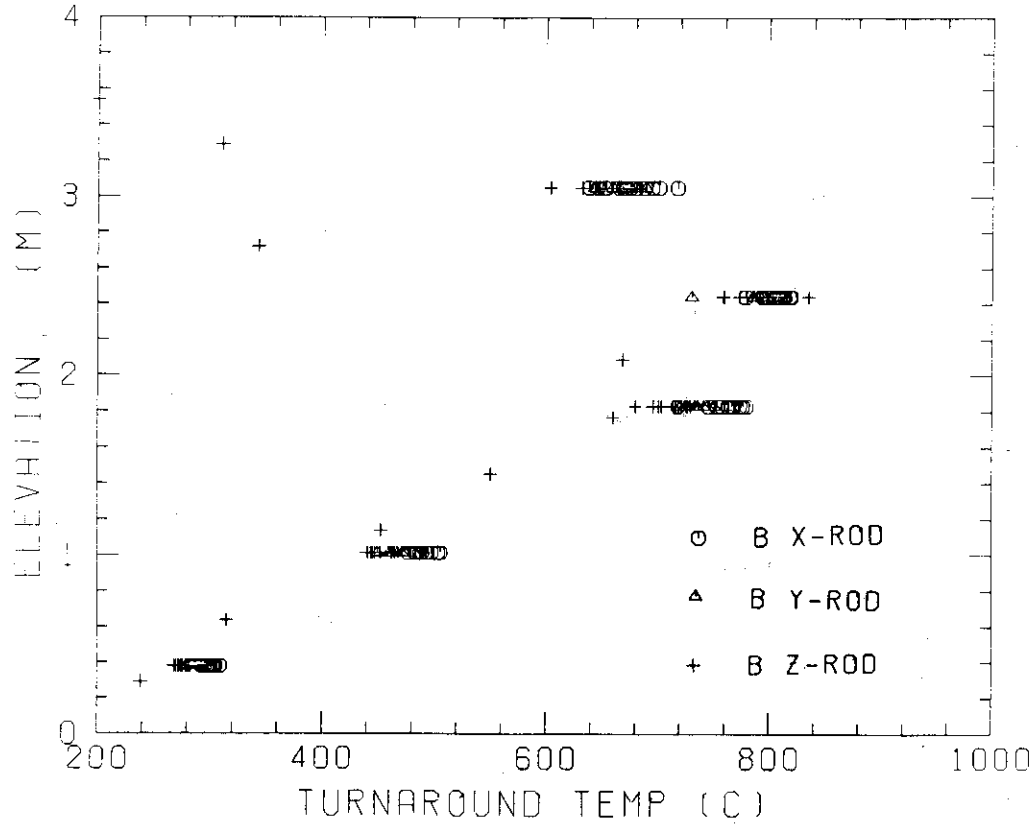

Fig. C-10 Turnaround temperature in medium power region (B region)

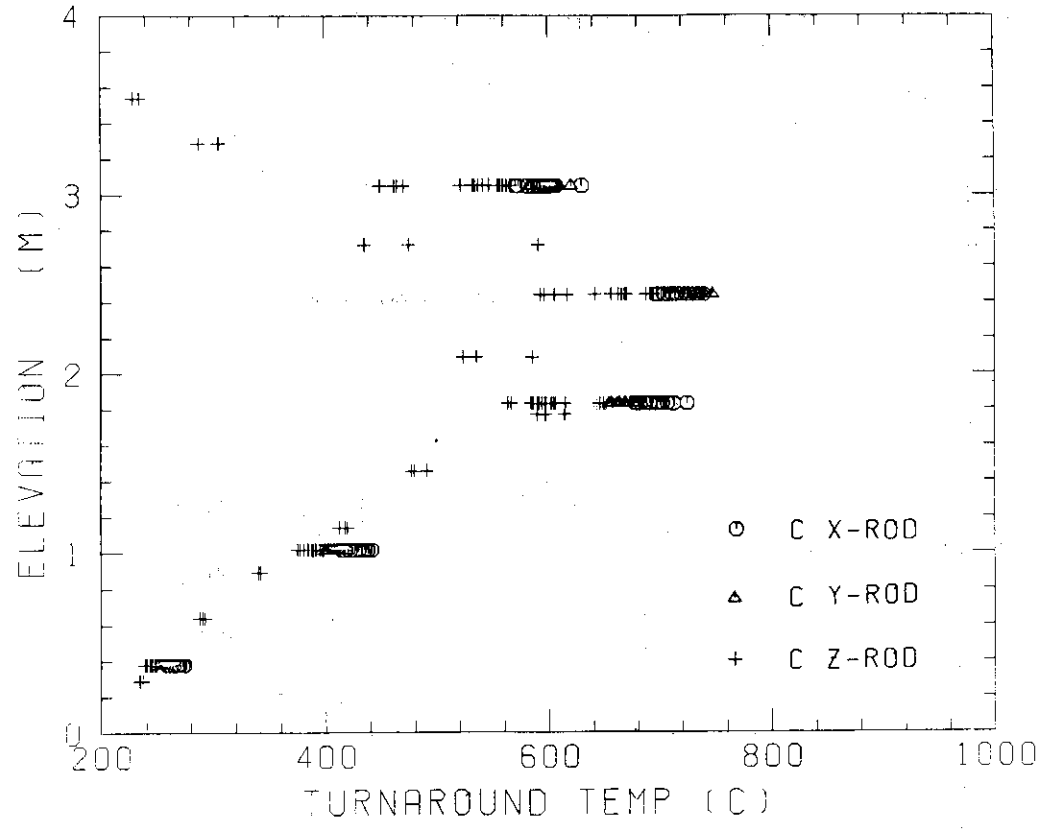

Fig. C-11 Turnaround temperature in low power region (C region)

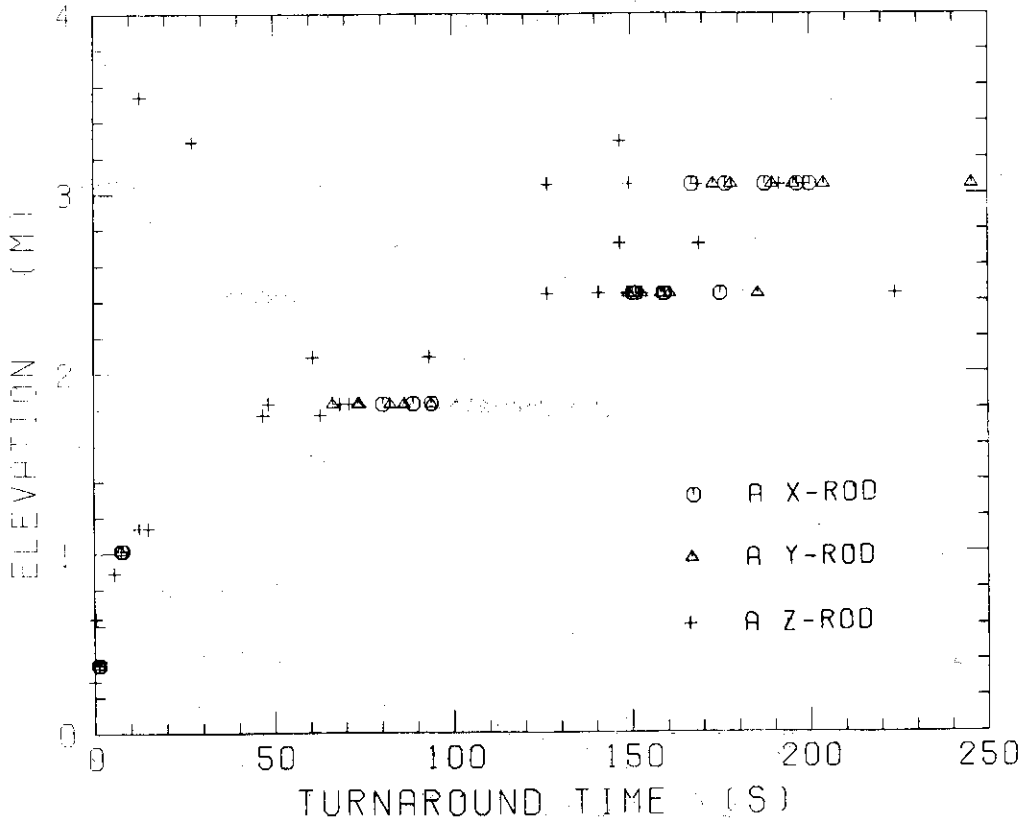

Fig. C-12 Turnaround time in high power region (A region)

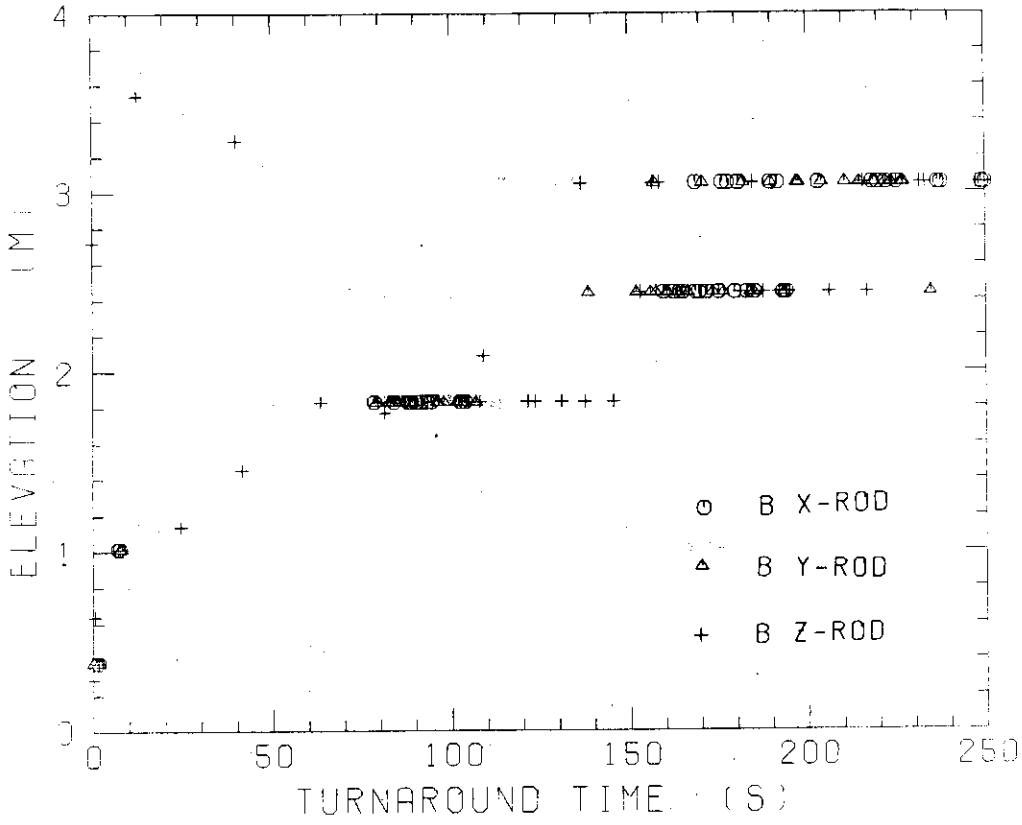

Fig. C-13 Turnaround time in medium power region (B region)

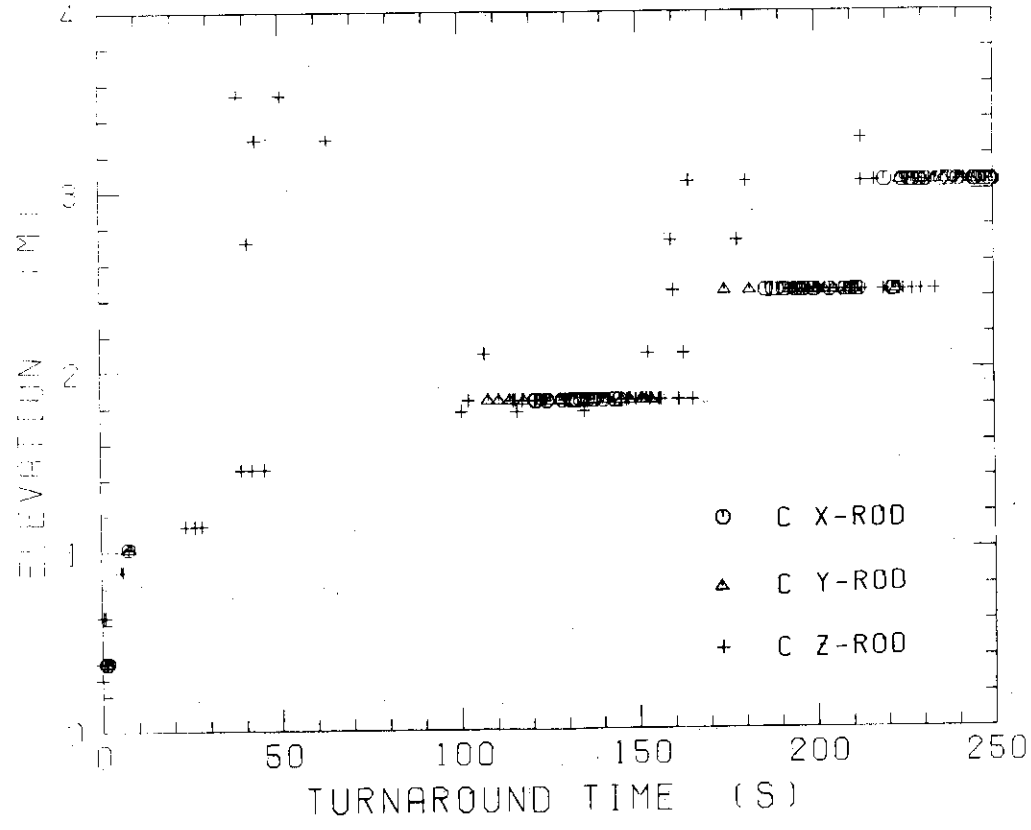

Fig. C-14 Turnaround time in low power region (C region)

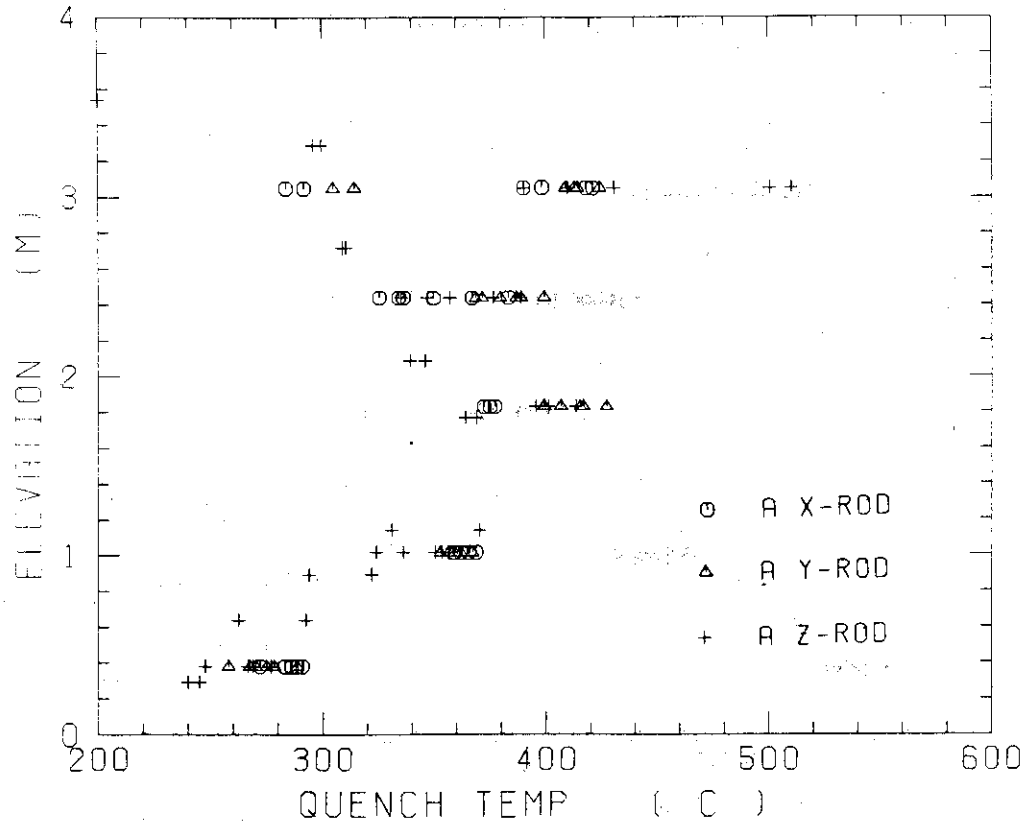

Fig. C-15 Quench temperature in high power region (A region)

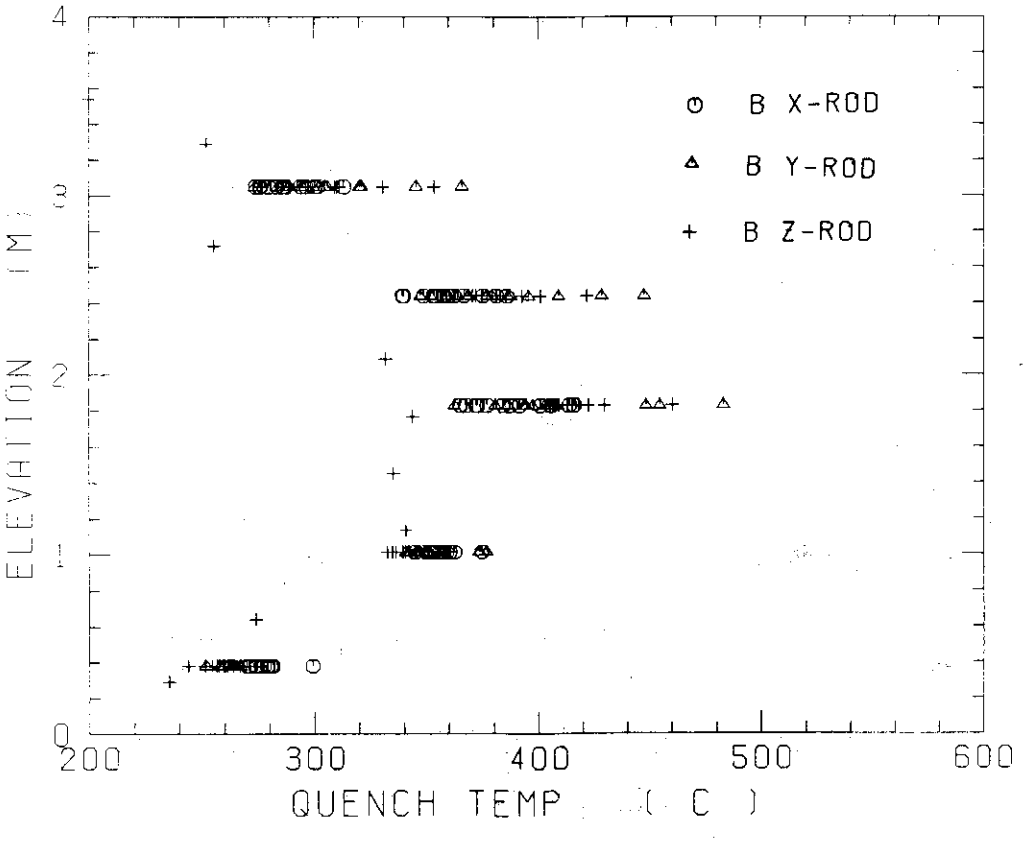

Fig. C-16 Quench temperature in medium power region (B region)

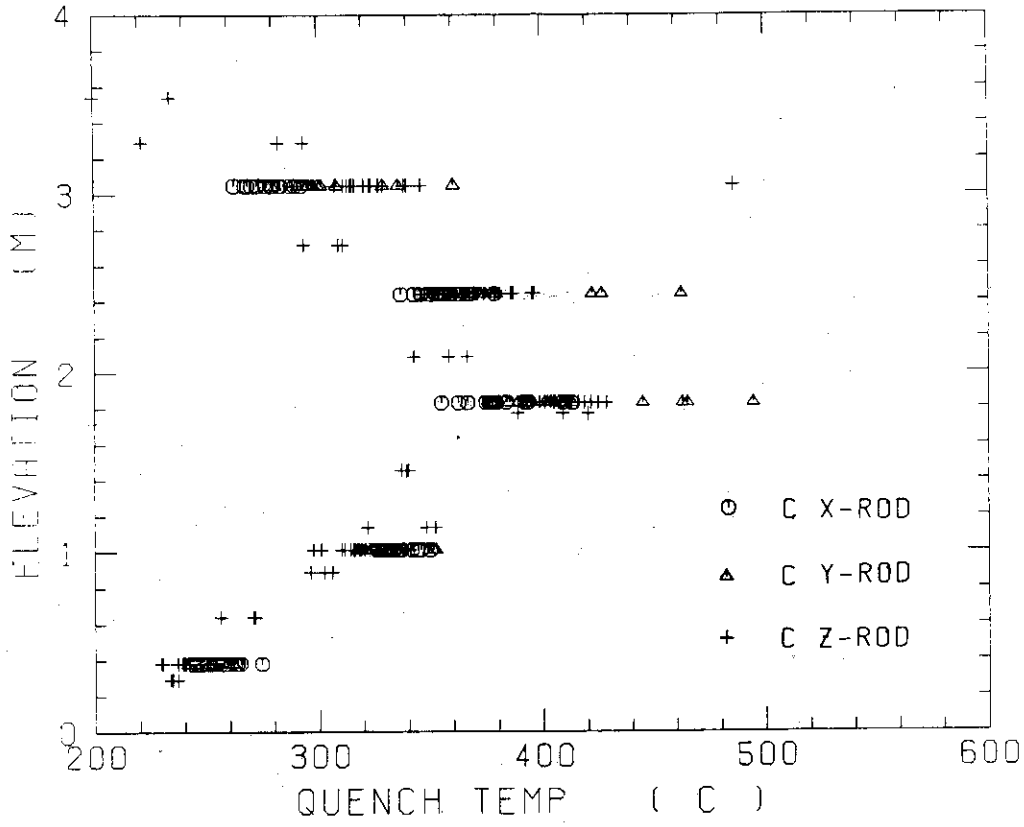

Fig. C-17 Quench temperature in low power region (C region)

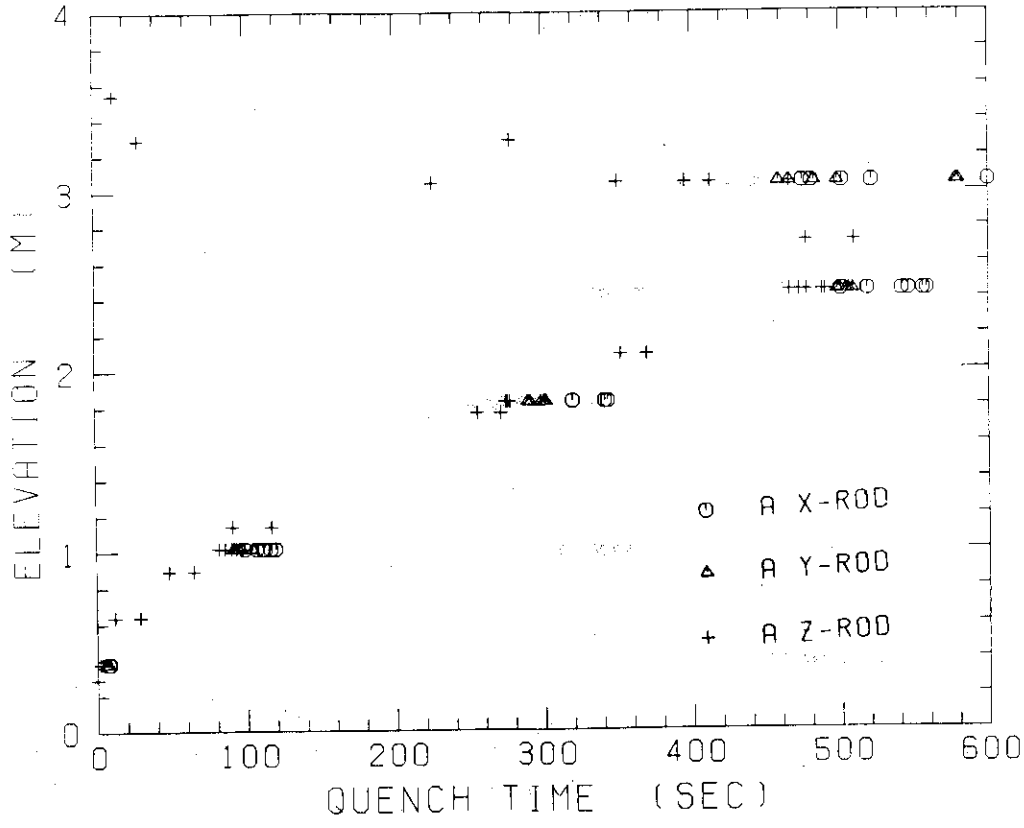

Fig. C-18 Quench time in high power region (A region)

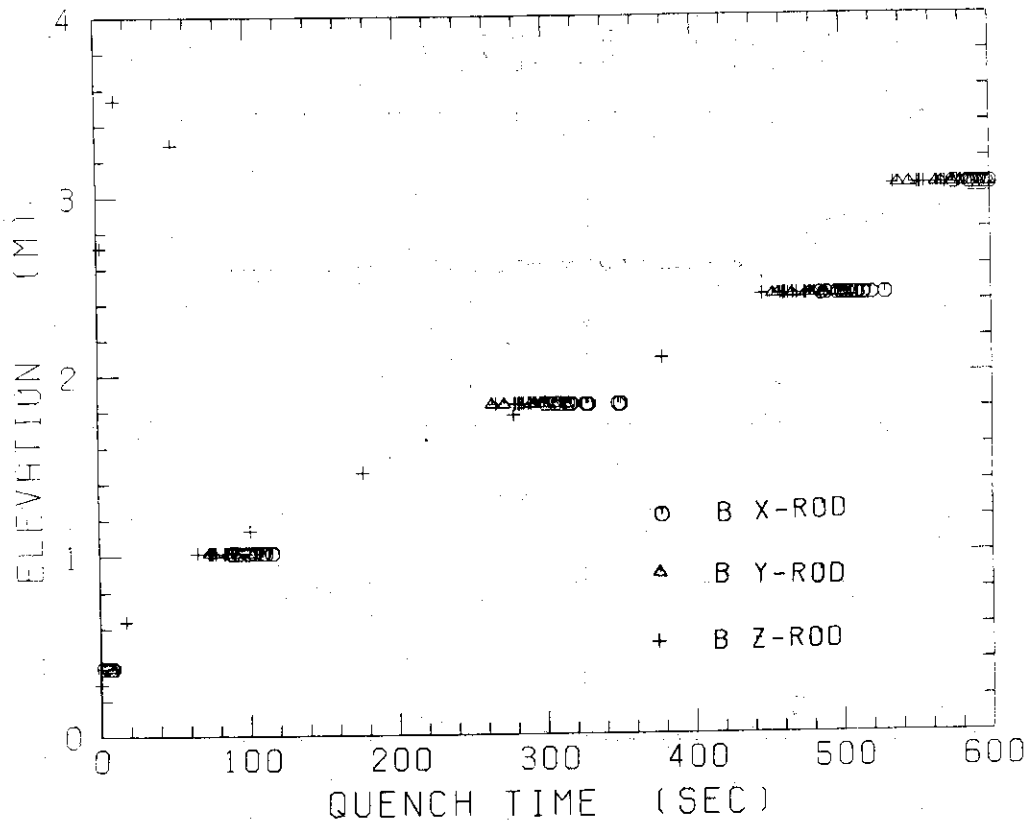

Fig. C-19 Quench time in medium power region (B region)

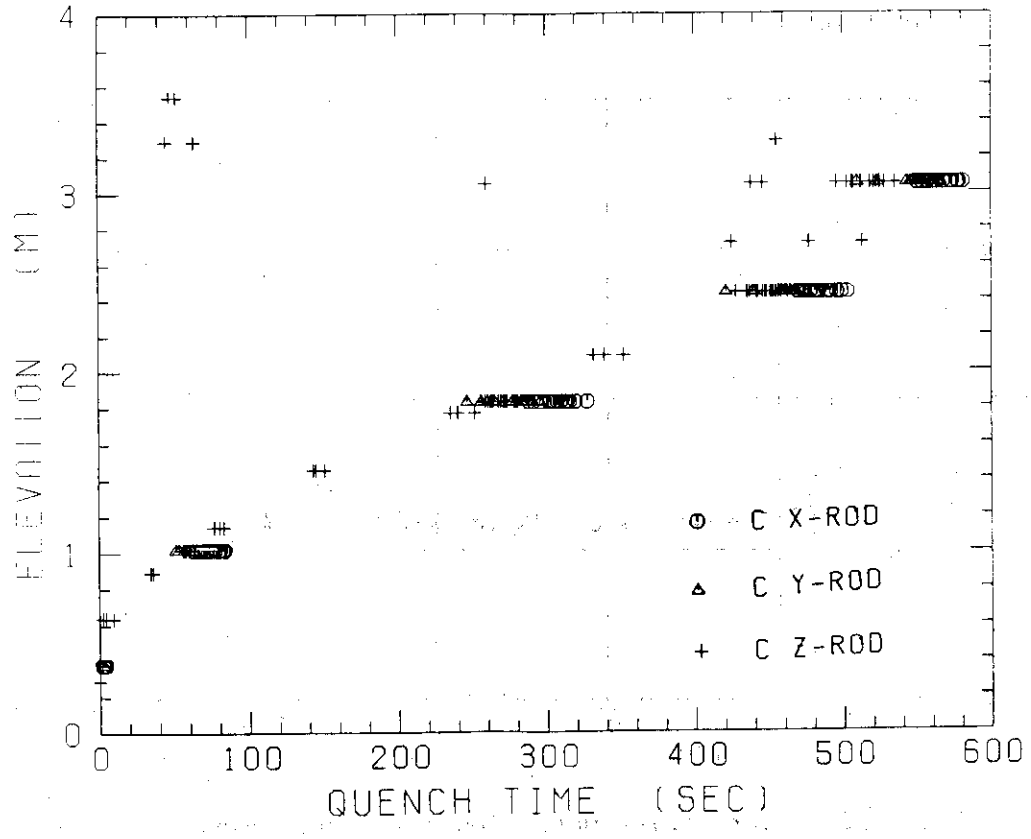

Fig. C-20 Quench time in low power region (C region)

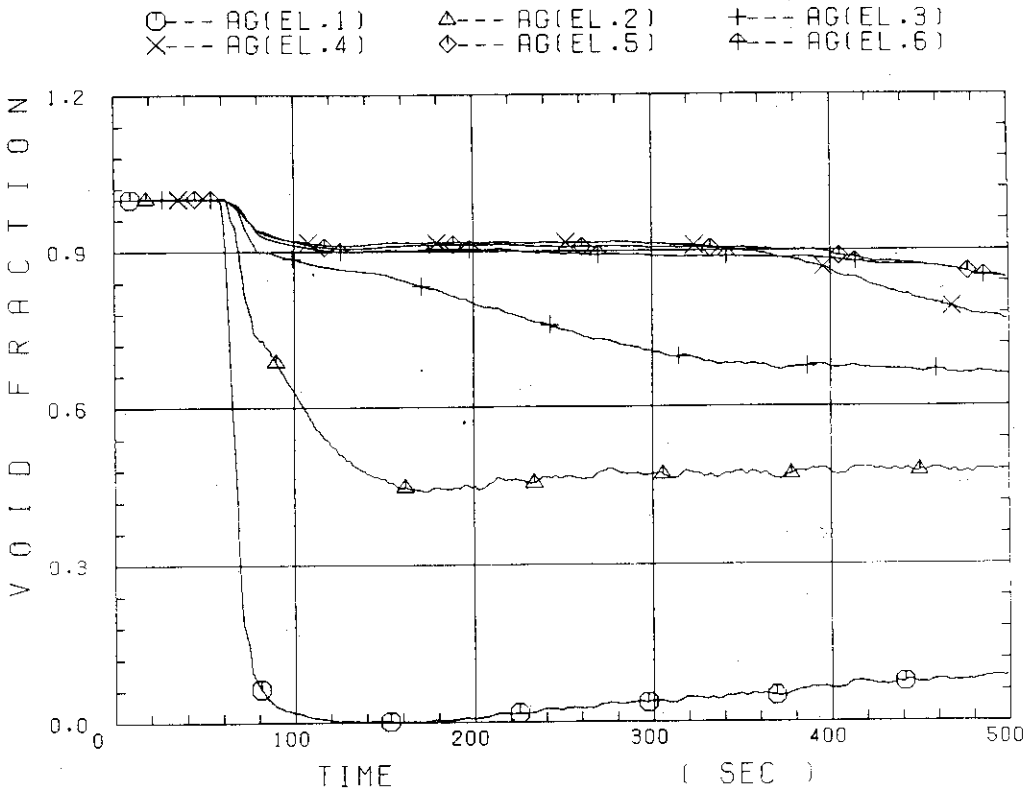

Fig. C-21 Void fraction in core

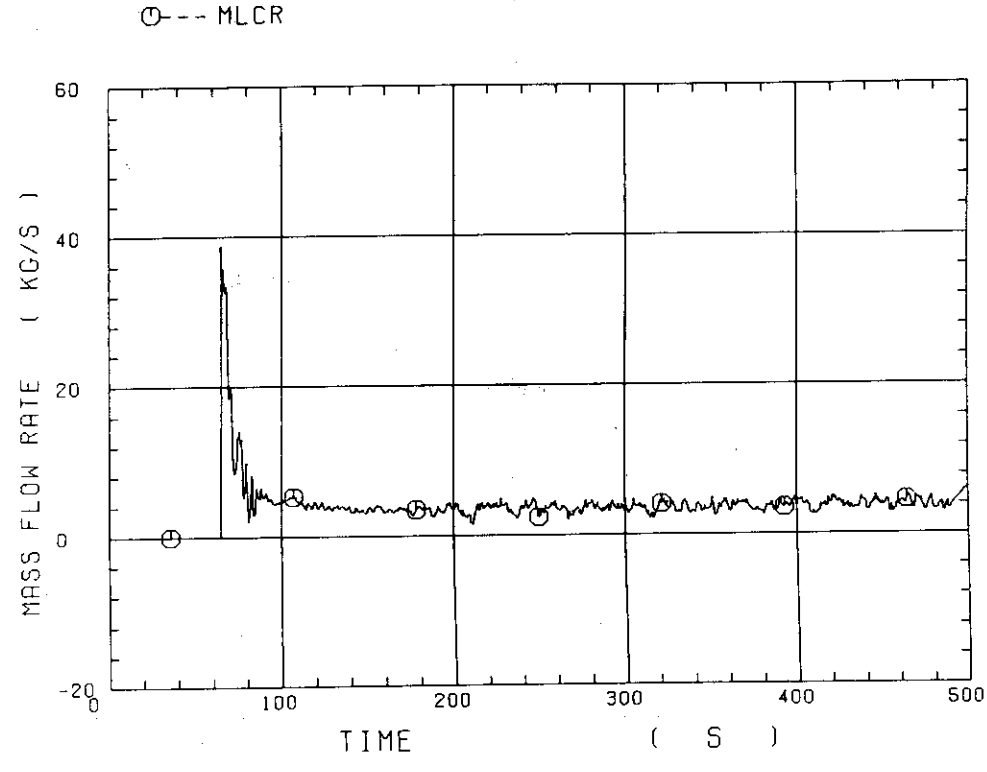

Fig. C-22 Core inlet mass flow rate (recommended value)

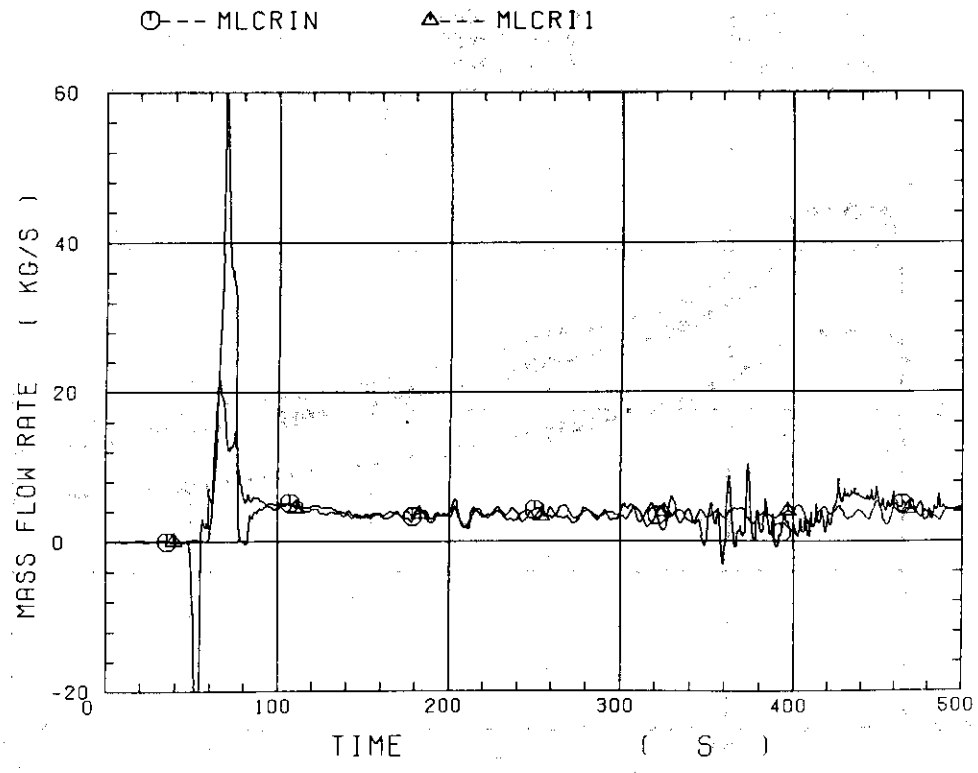

Fig. C-23 Core inlet mass flow rate

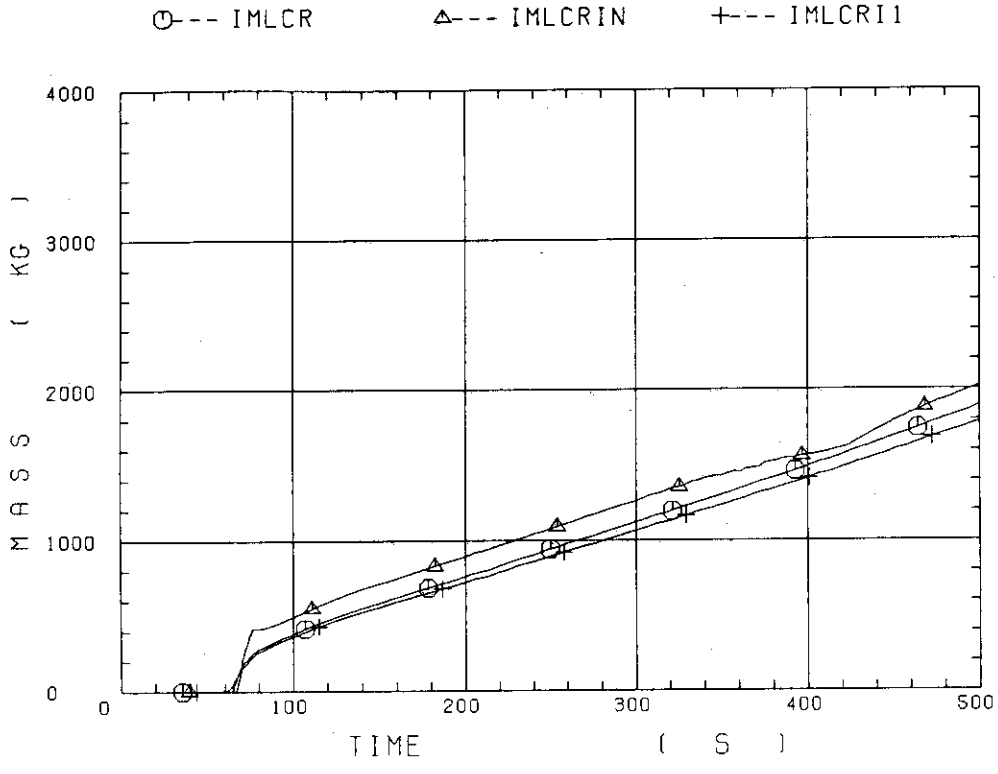

Fig. C-24 Time-integration of core inlet mass flow rate

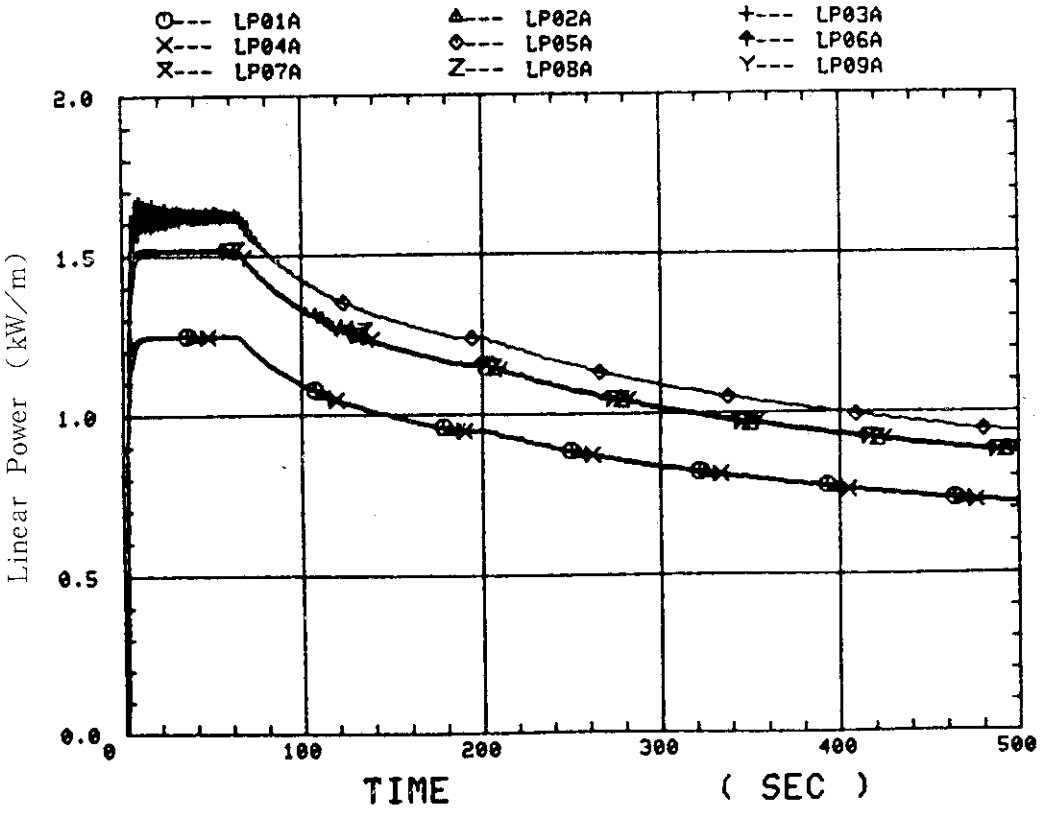

Fig. C-25 Average linear power of heater rod in each power unit zone

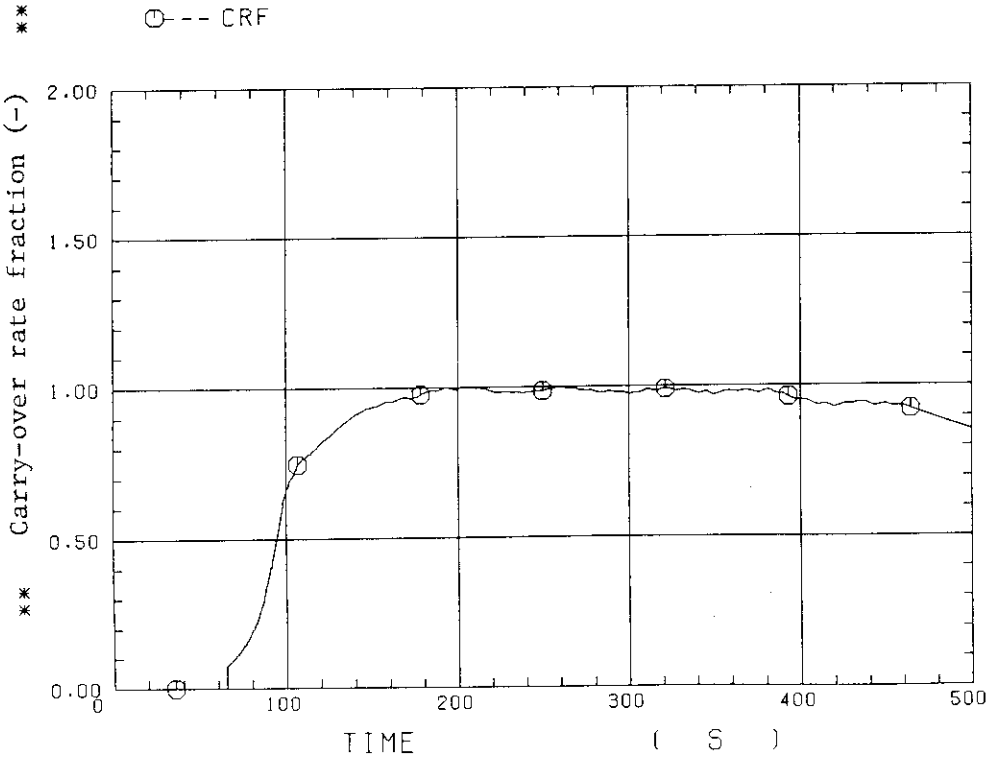

Fig. C-26 Carry-over rate fraction

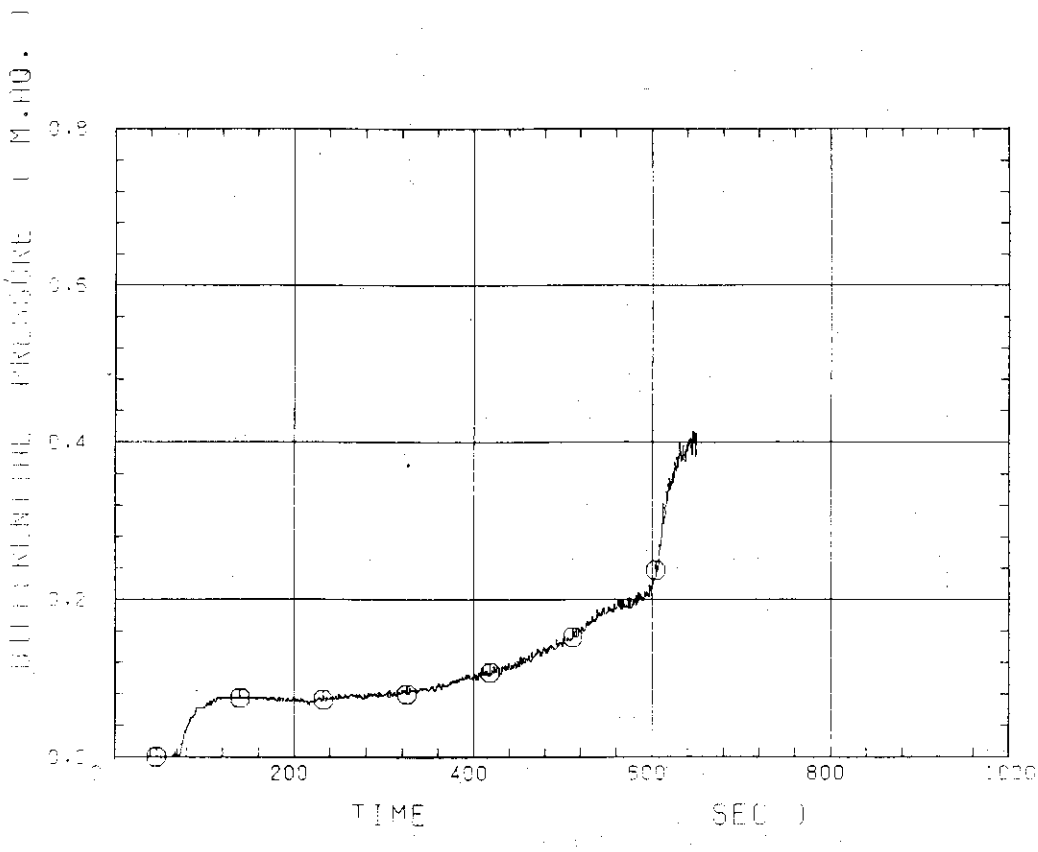

Fig. C-27 Differential pressure through upper plenum

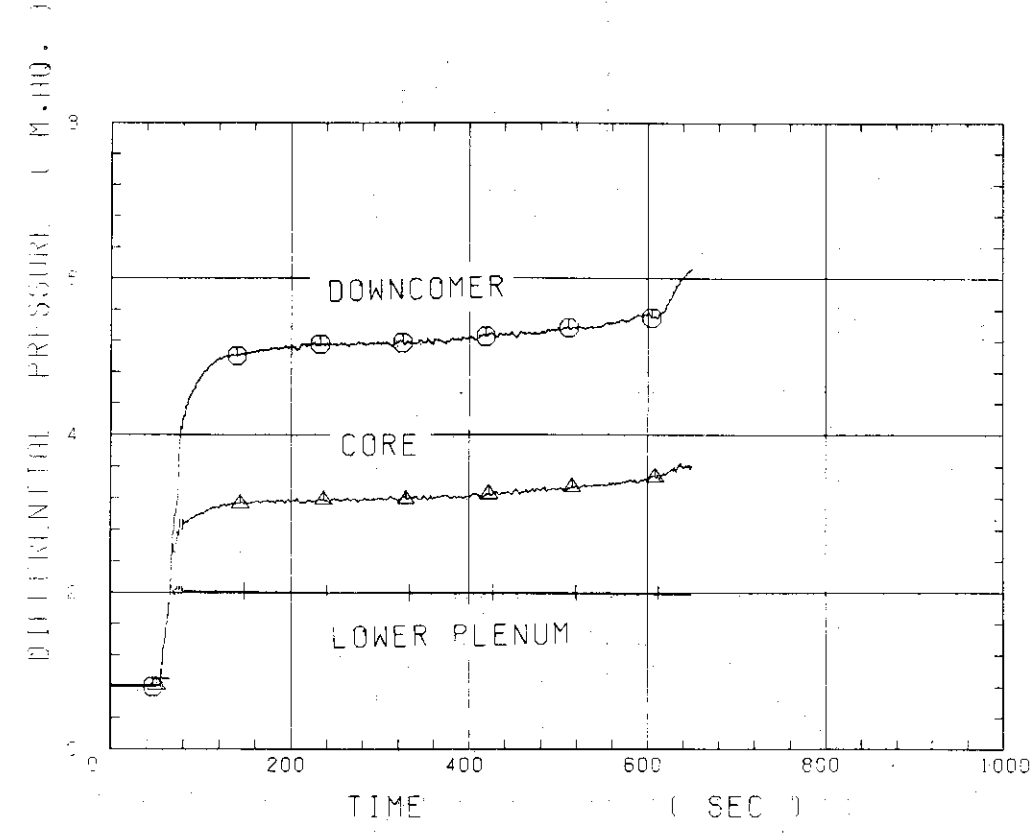

Fig. C-28 Differential pressure through downcomer, core, and lower plenum

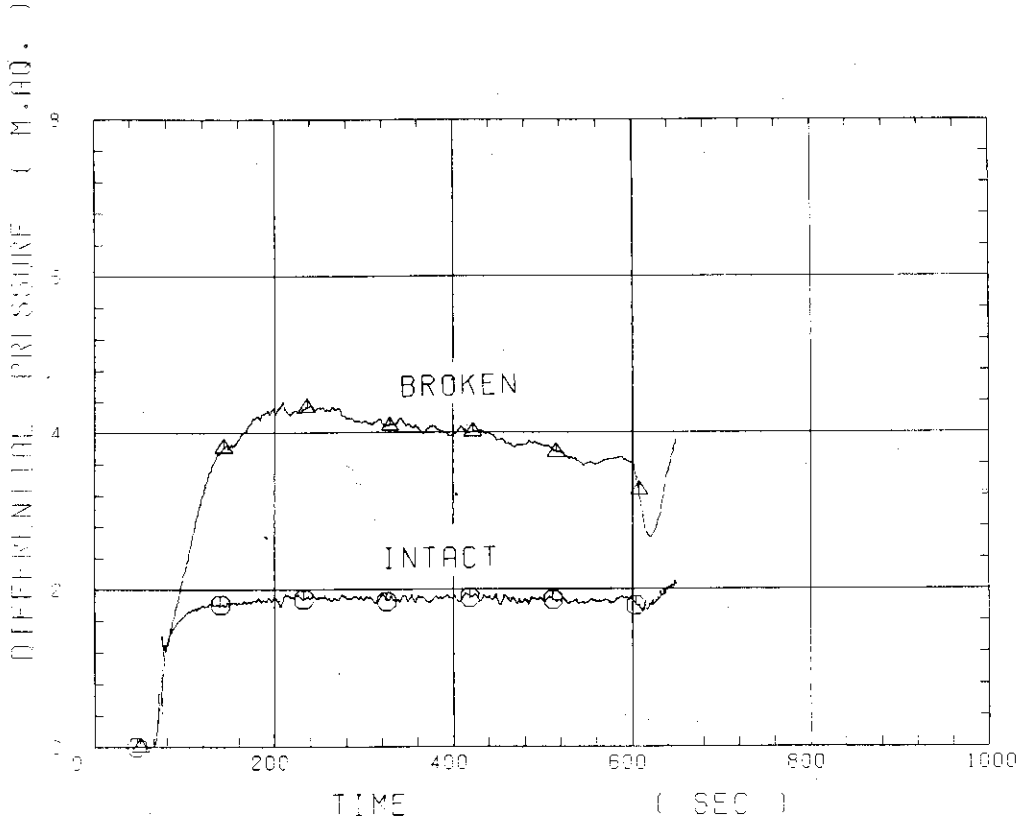

Fig. C-29 Differential pressure through intact and broken loops

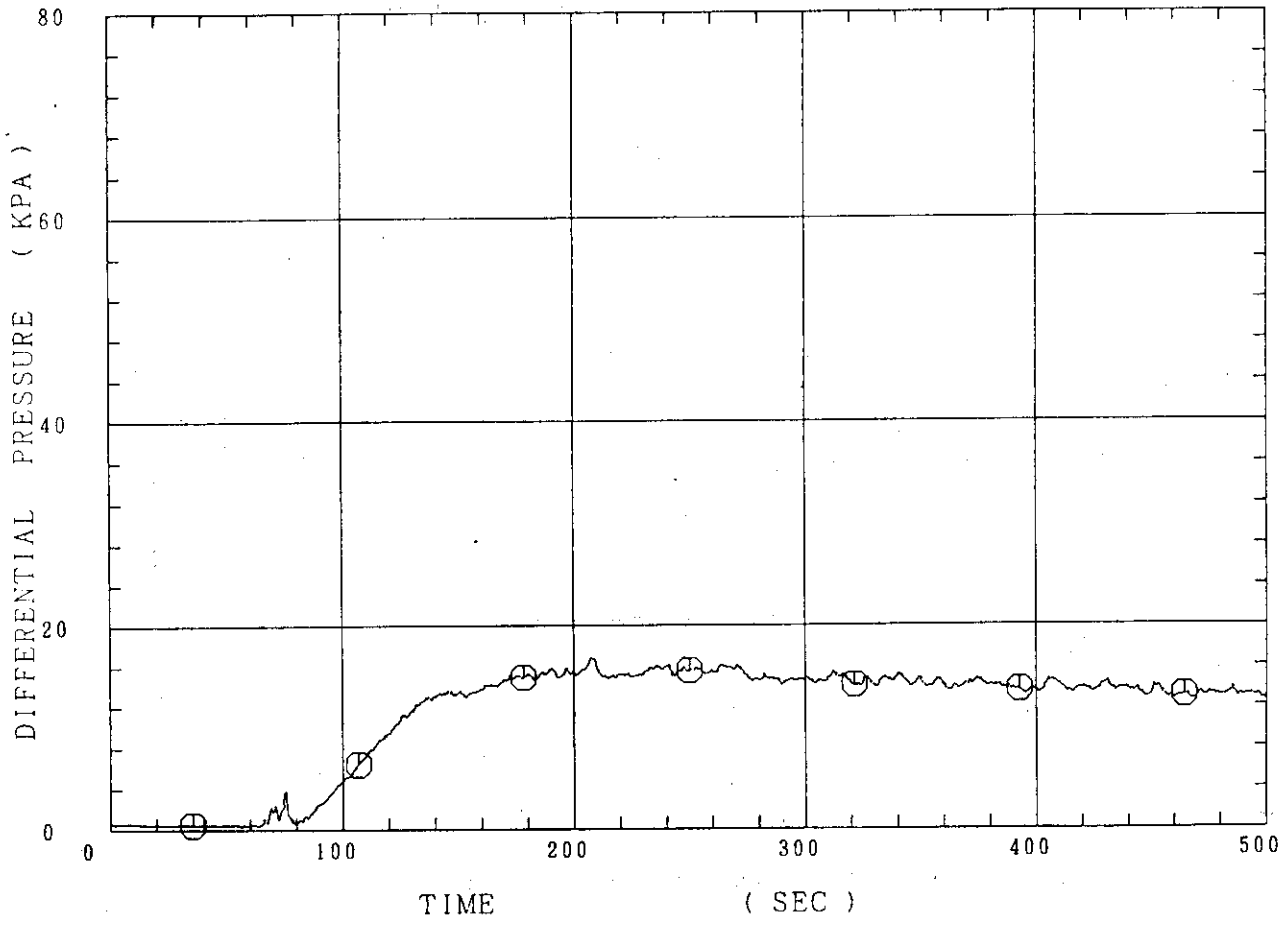

Fig. C-30 Differential pressure through broken cold leg nozzle

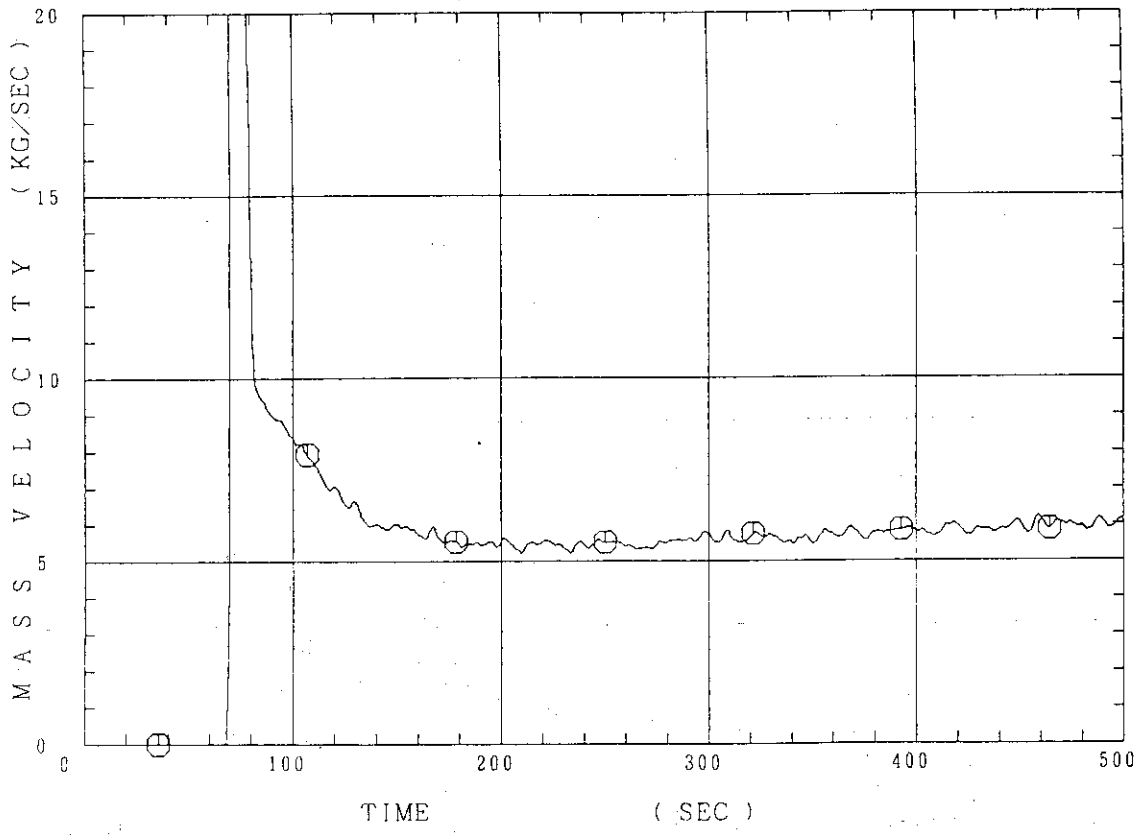

Fig. C-31 Total water mass flow rate from intact loops to downcomer

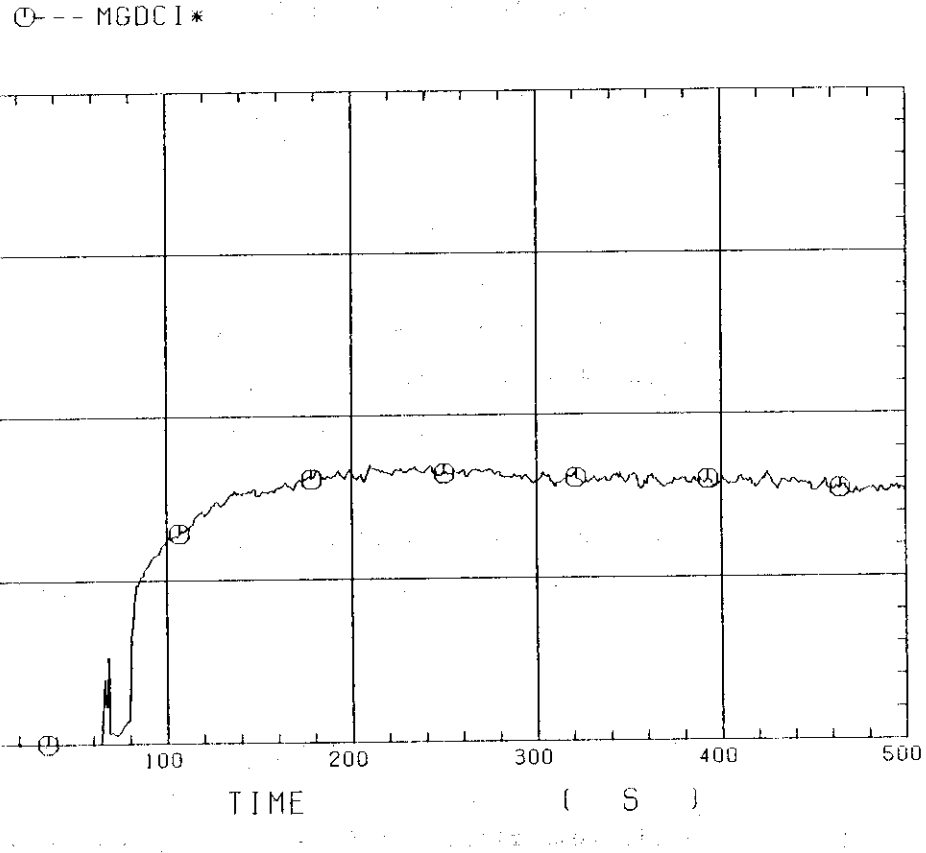

Fig. C-32 Total steam mass flow rate from intact loops to downcomer

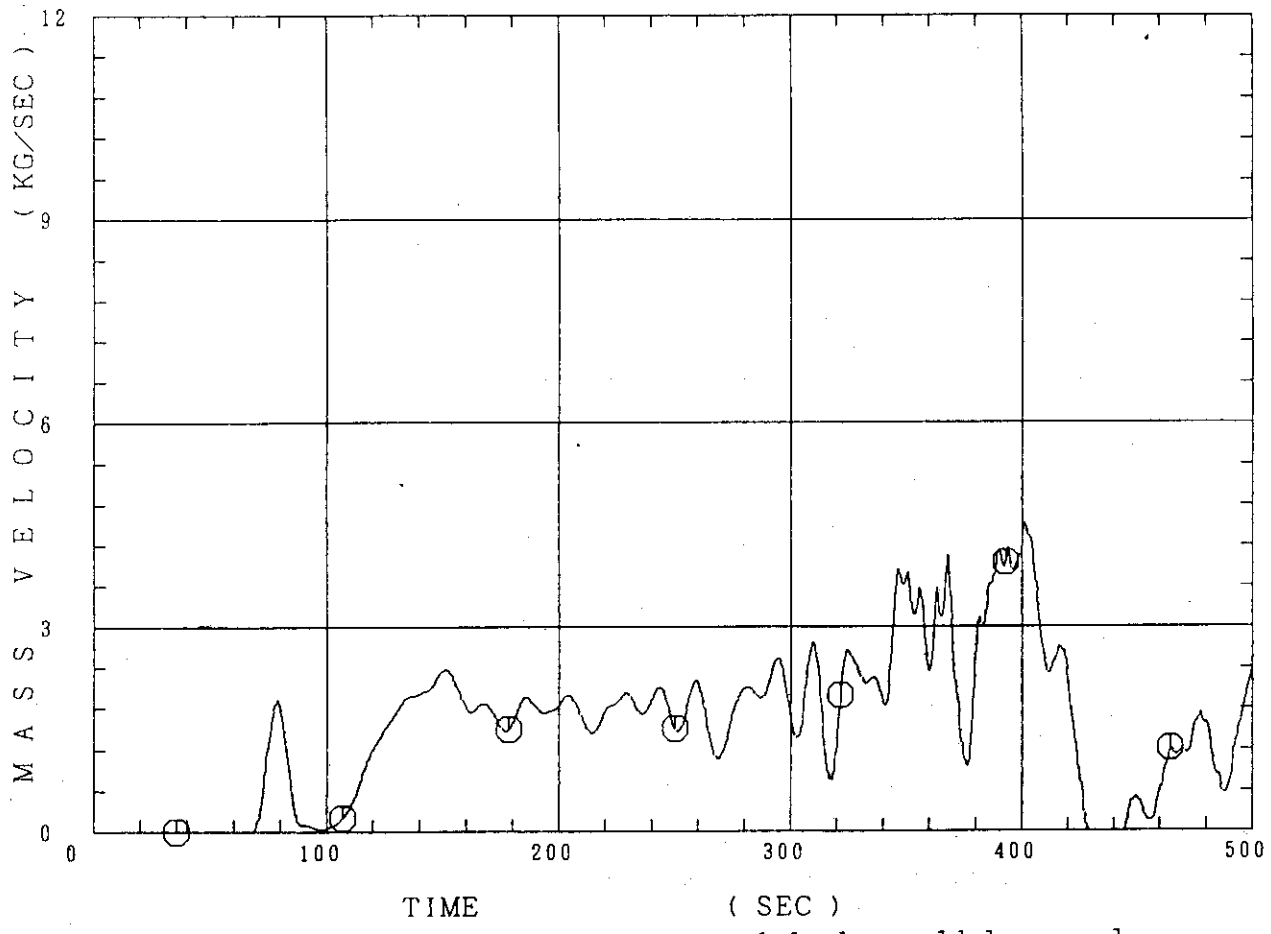

Fig. C-33 Water mass flow rate through broken cold leg nozzle

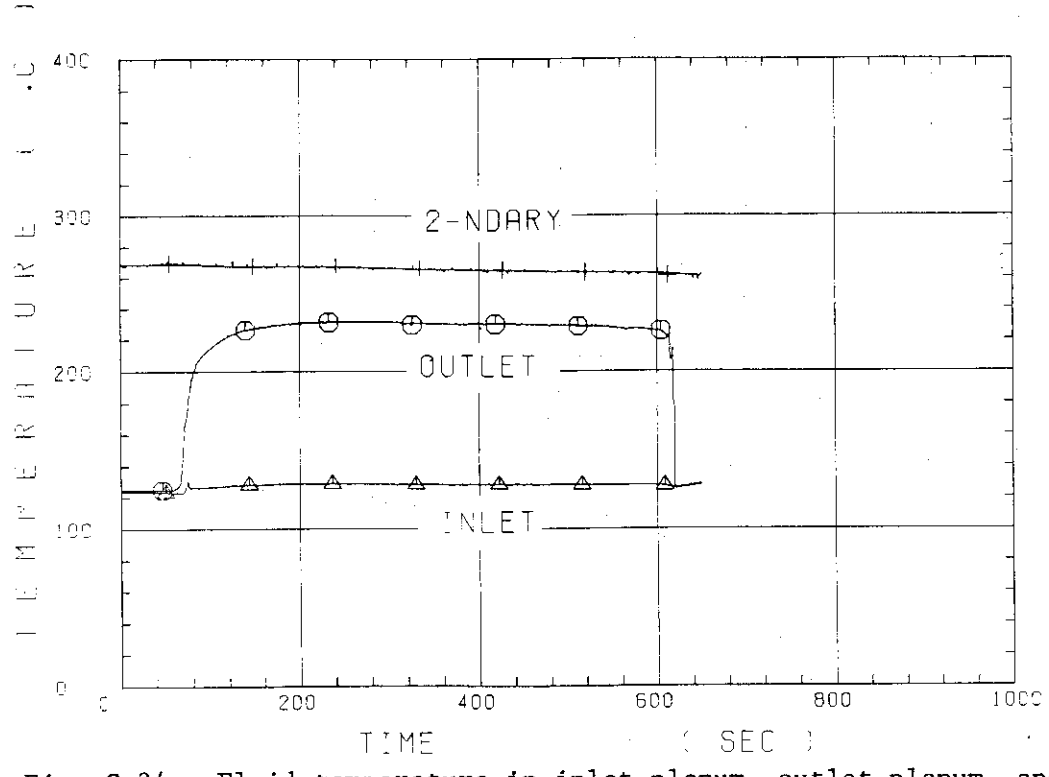

Fig. C-34 Fluid temperature in inlet plenum, outlet plenum, and secondary of steam generator 1

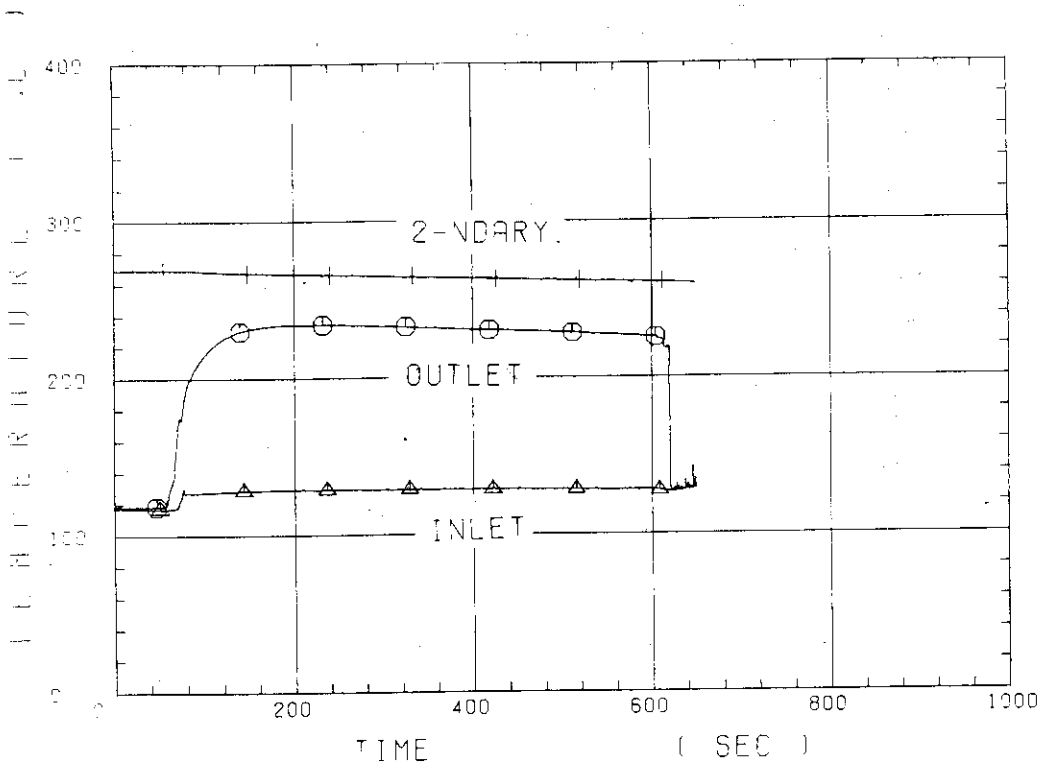

Fig. C-35 Fluid temperature in inlet plenum, outlet plenum, and secondary of steam generator 2

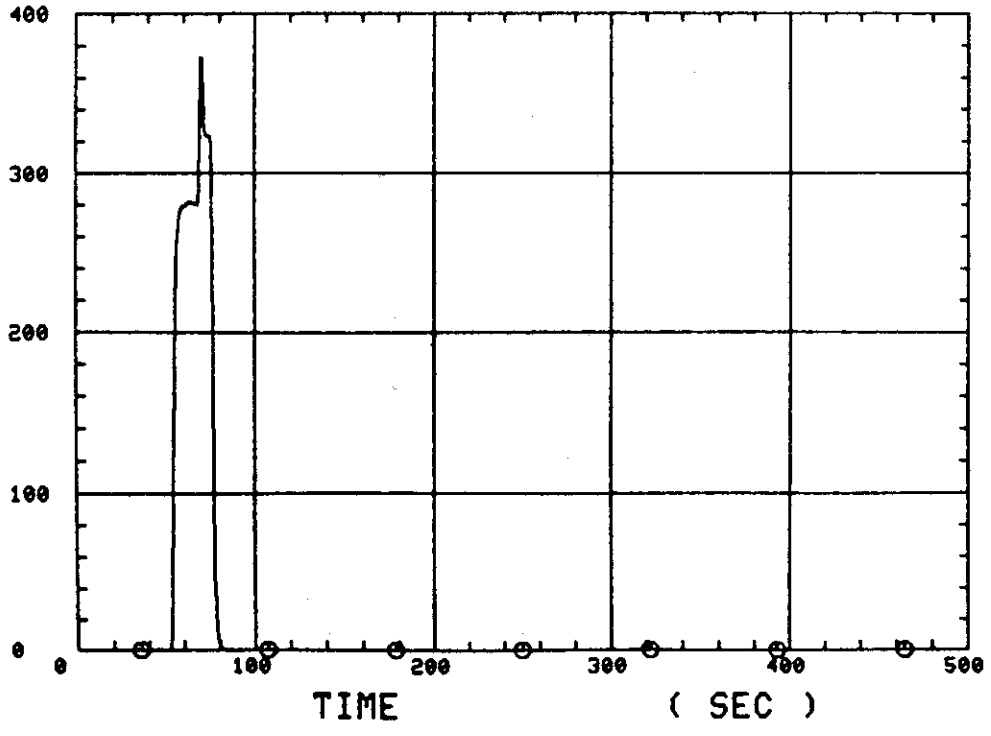

Fig. C-36 Total accumulator injection rate

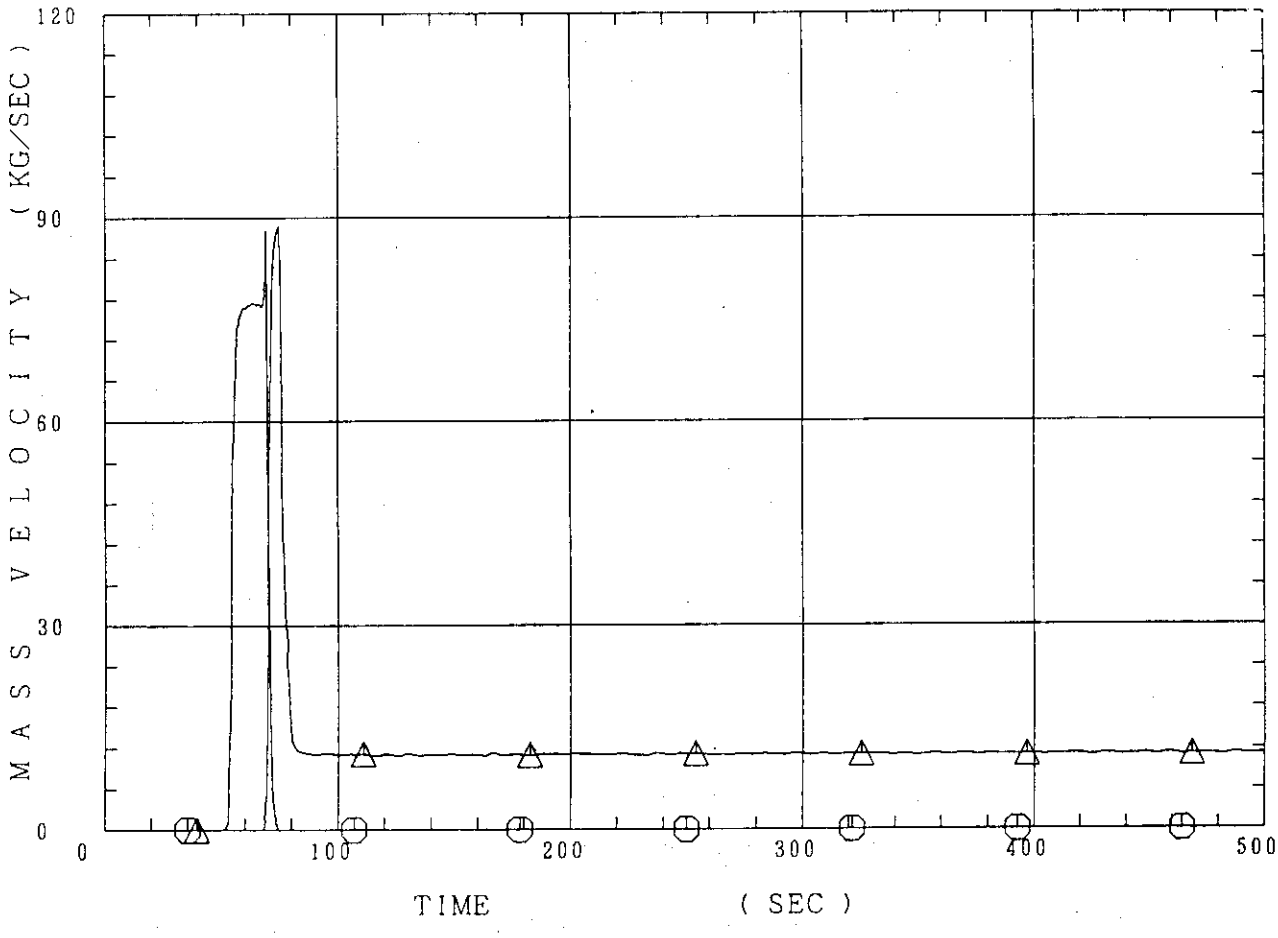

Fig. C-37 ECC water injection rates to lower plenum and to cold legs

Appendix D

Selected data of CCTF Test C1-11 (Run20)

Table and Figure List

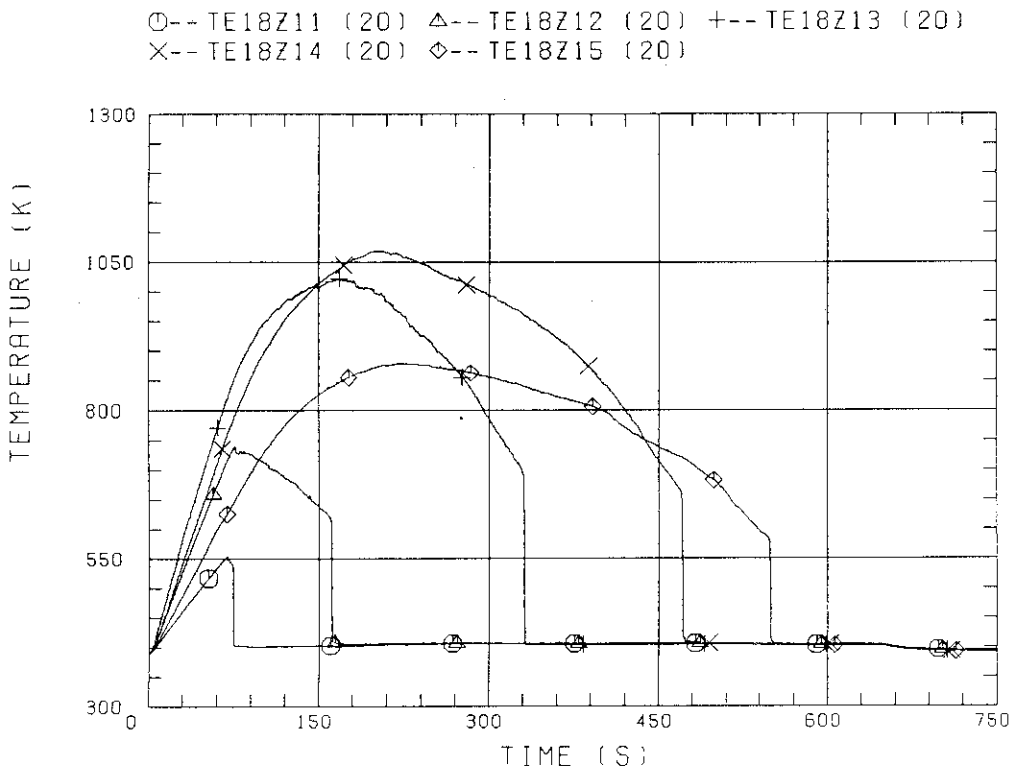

Fig. D-1 Surface temperature on low power rod (Z-rod) in medium power region (B region) (average power rod)

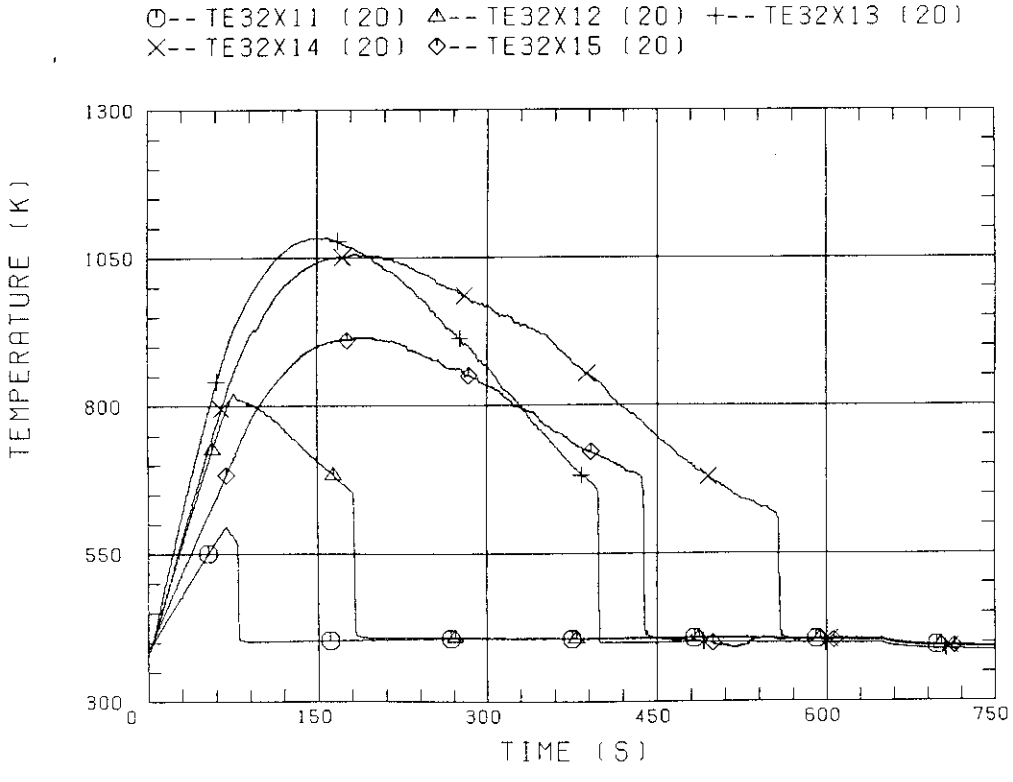

Fig. D-2 Surface temperature on high power rod (X-rod) in high power region (A region) (peak power rod)

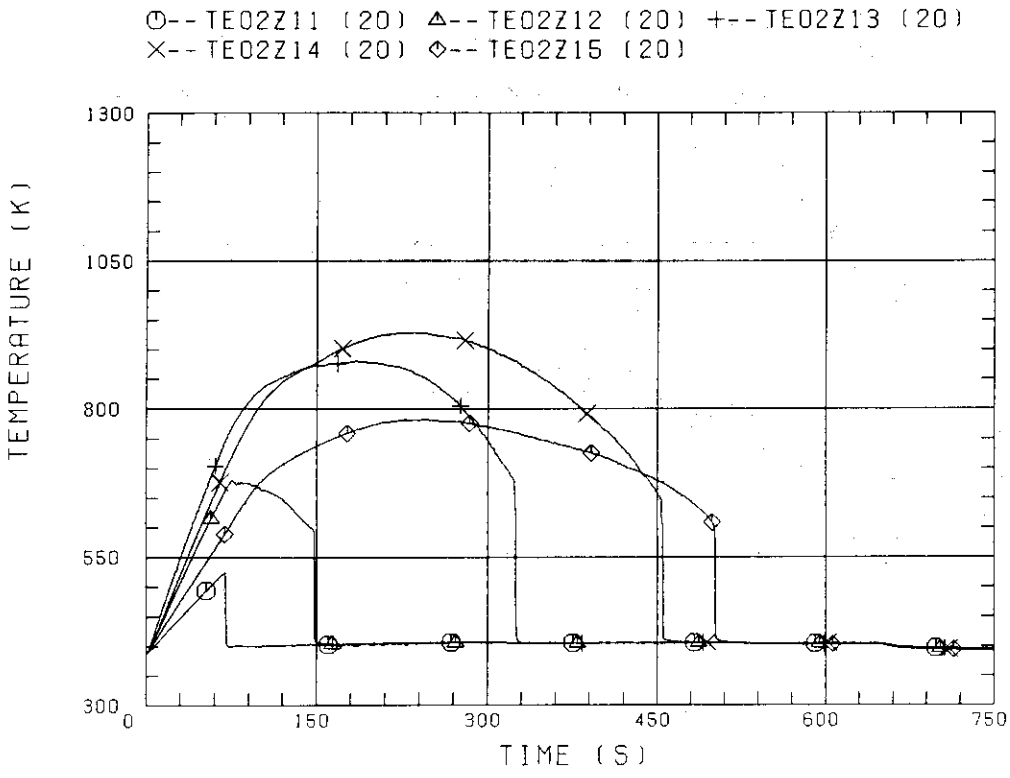

Fig. D-3 Surface temperature on low power rod (Z-rod) in low power region (C region) (lowest power rod)

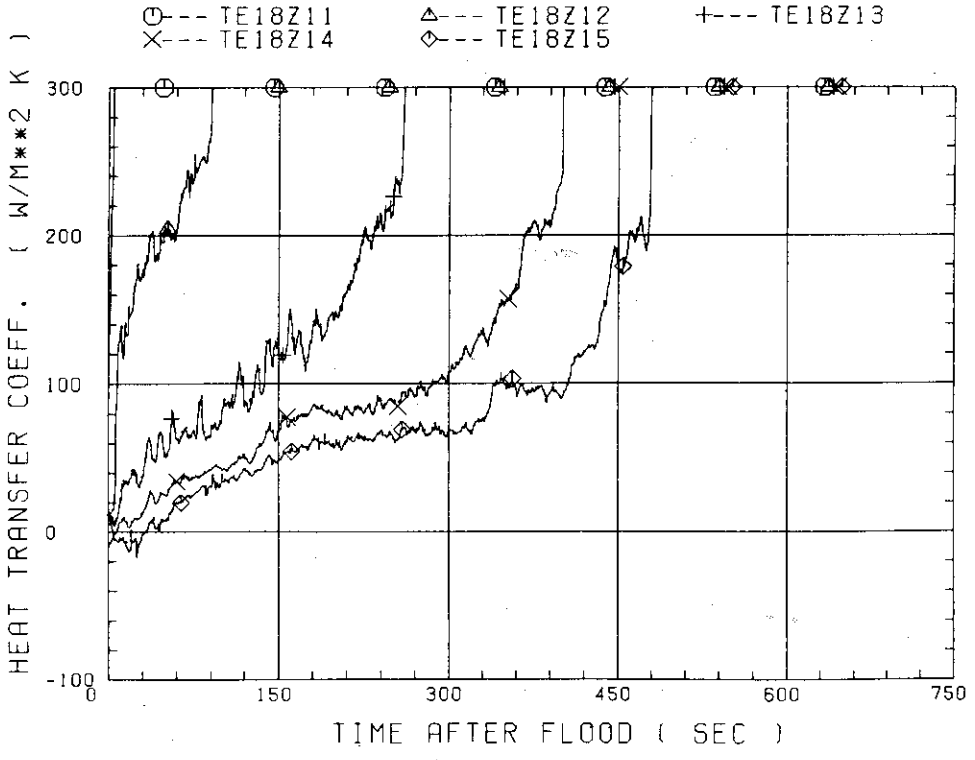

Fig. D-4 Heat transfer coefficient of low power rod (Z-rod) in medium power region (B region) (average power rod)

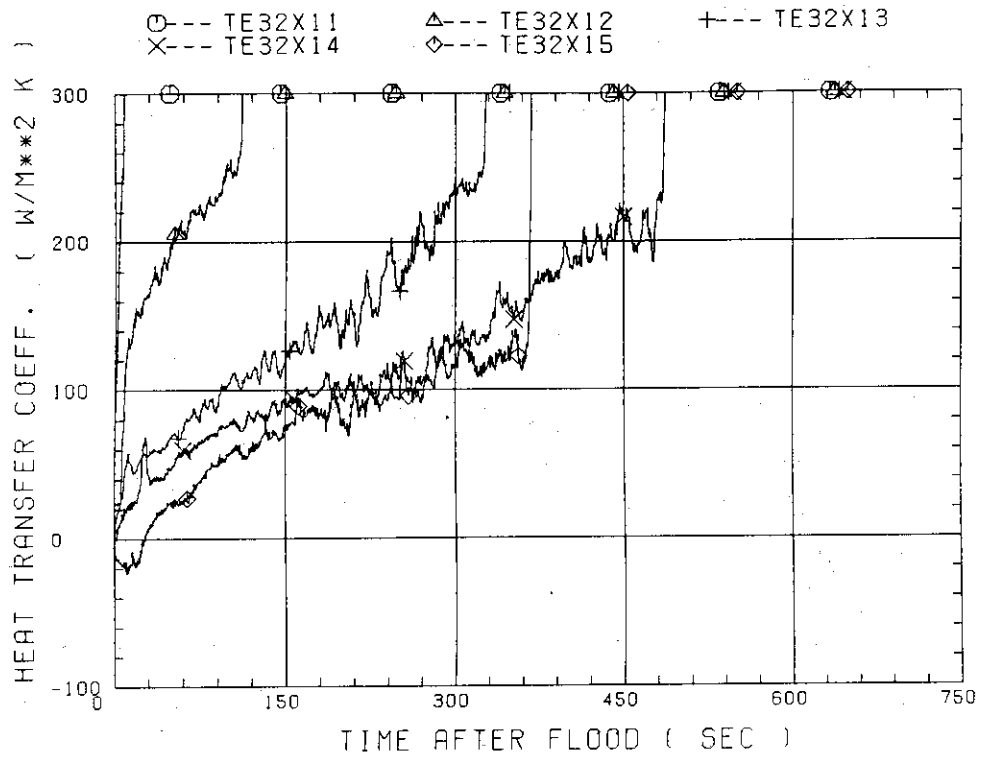

Fig. D-5 Heat transfer coefficient of high power rod (X-rod) in high power region (A region) (peak power rod)

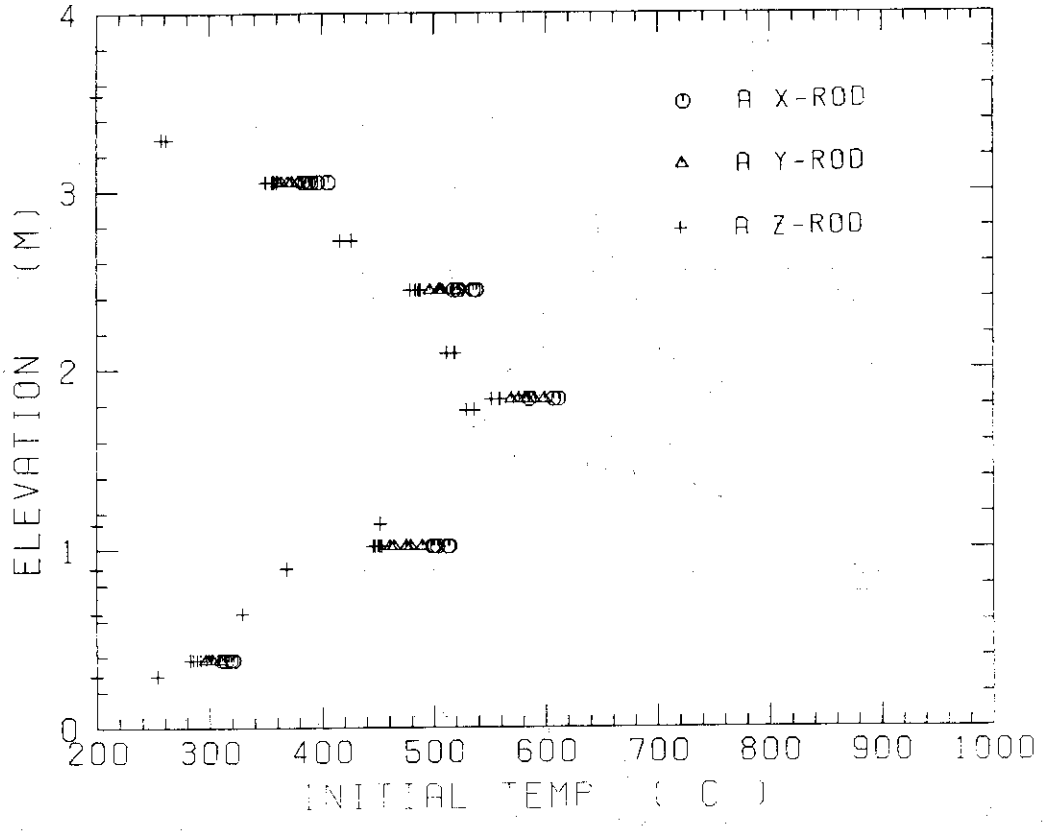

Fig. D-6 Initial rod surface temperature in high power region (A region)

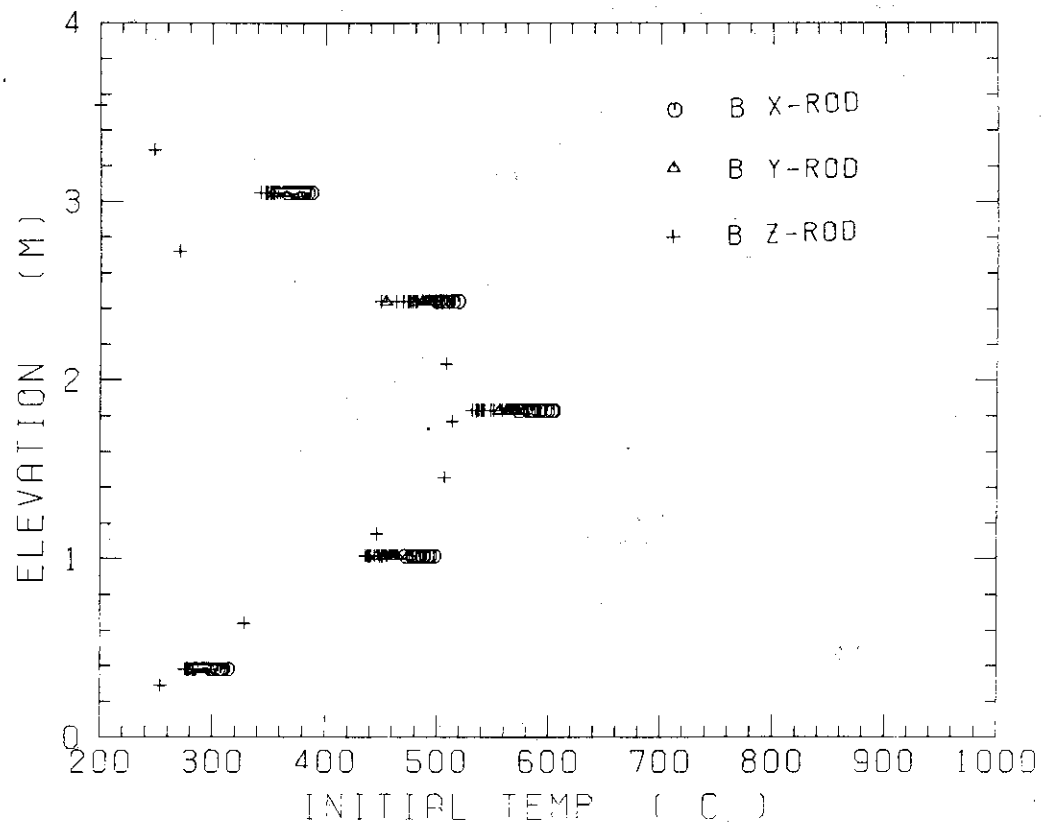

Fig. D-7 Initial rod surface temperature in medium power region (B region)

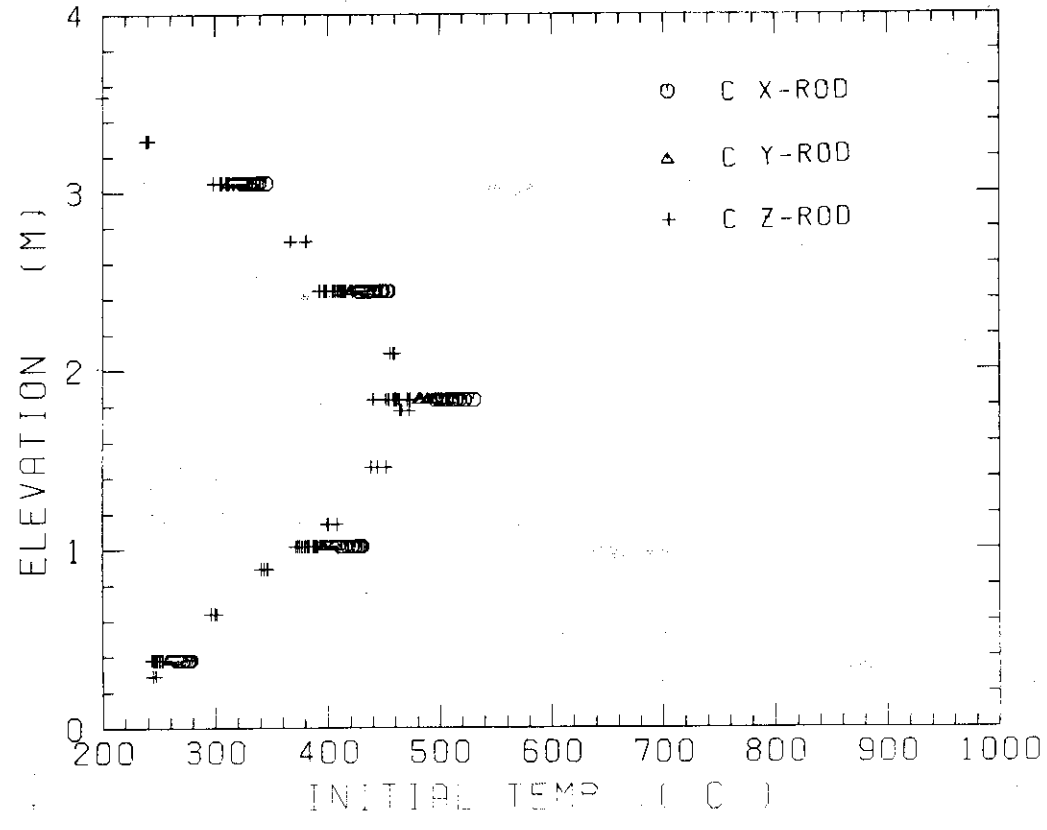

Fig. D-8 Initial rod surface temperature in low power region (C region)

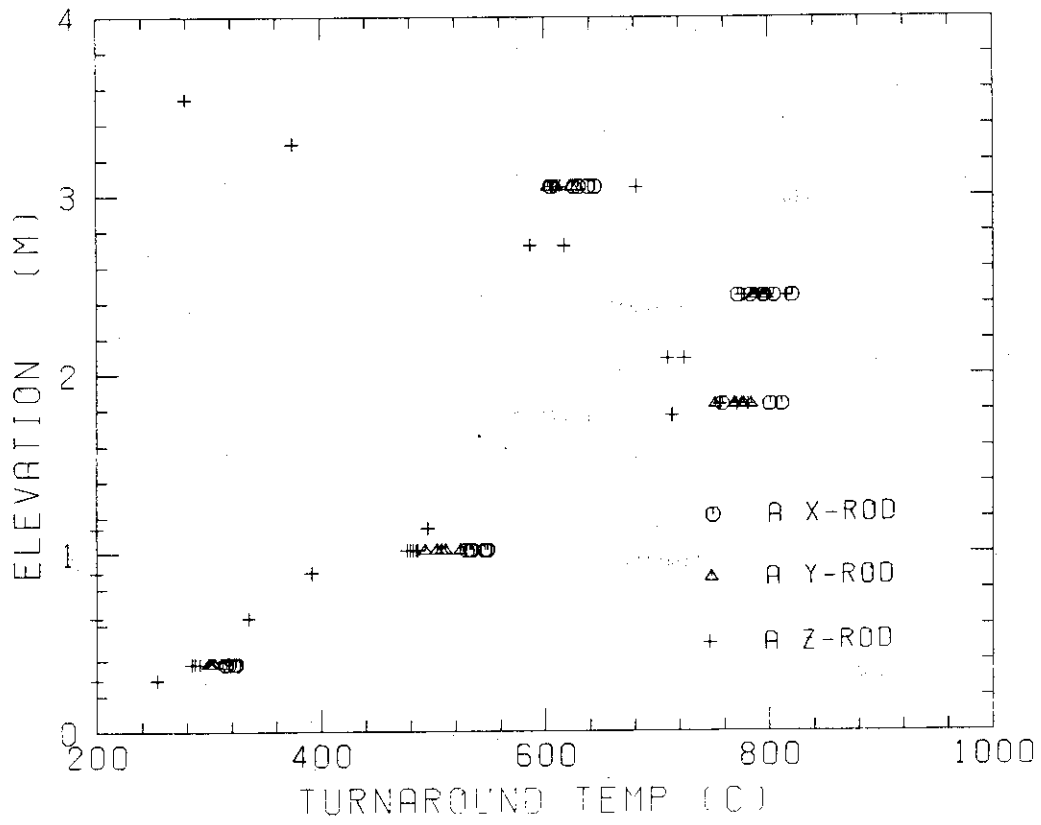

Fig. D-9 Turnaround temperature in high power region (A region)

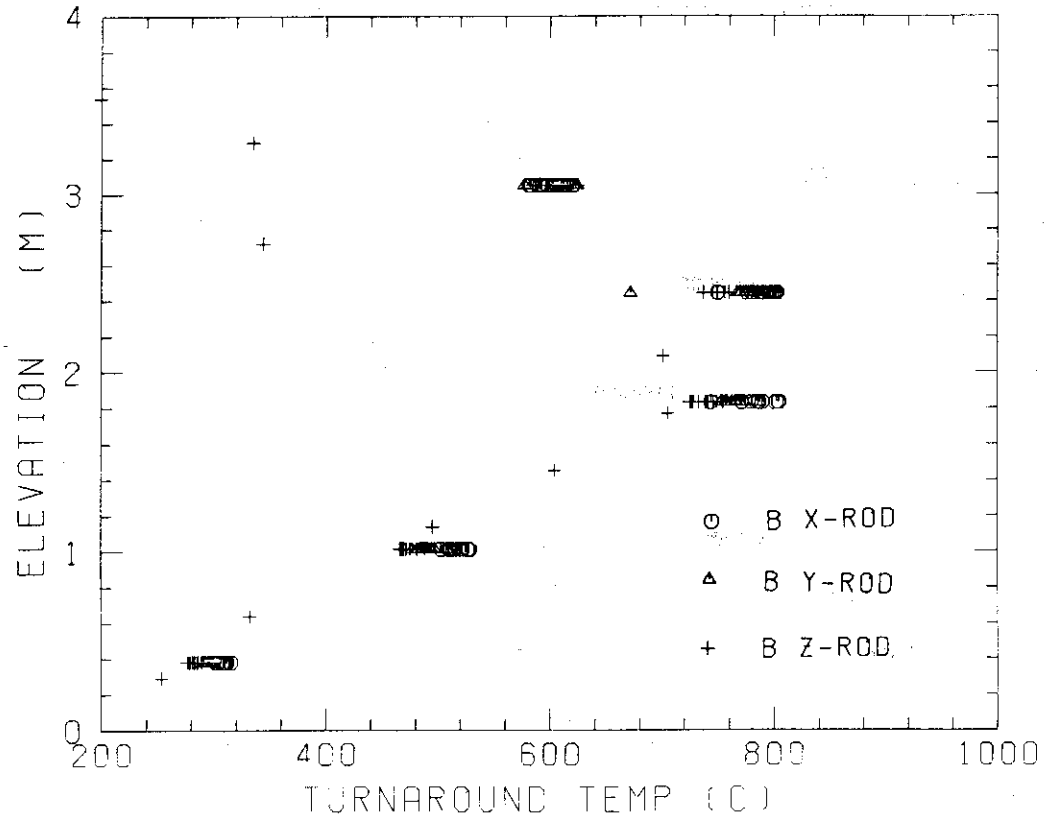

Fig. D-10 Turnaround temperature in medium power region (B region)

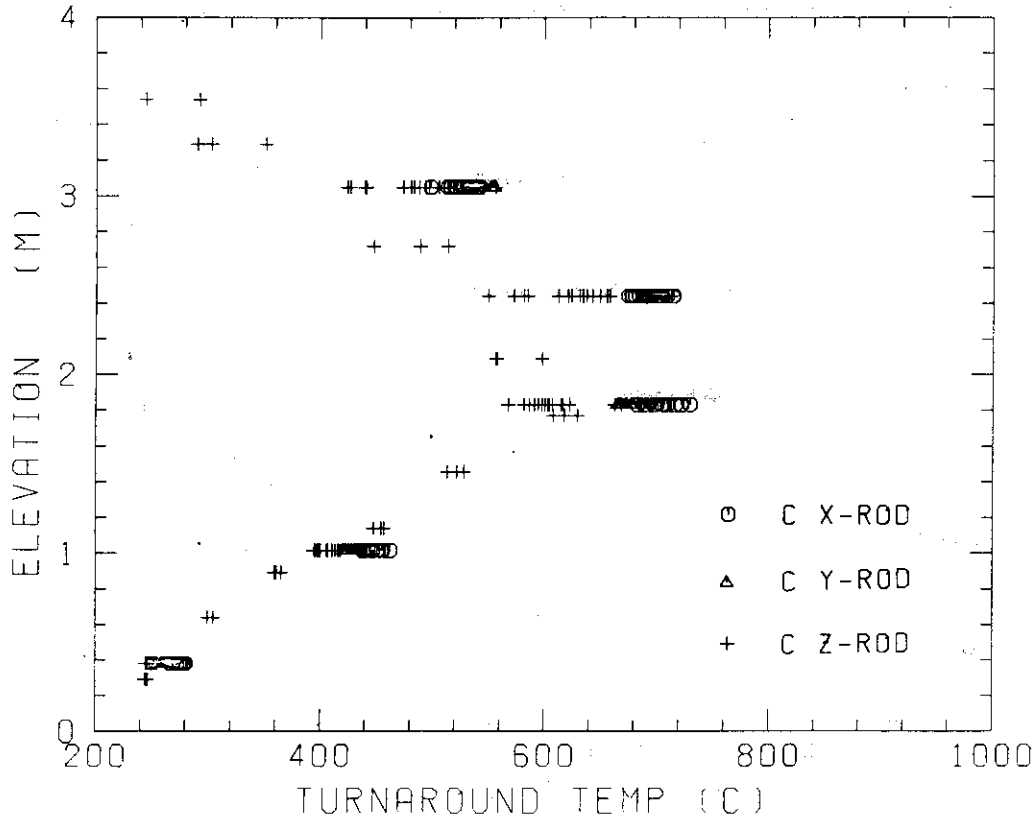

Fig. D-11 Turnaround temperature in low power region (C region)

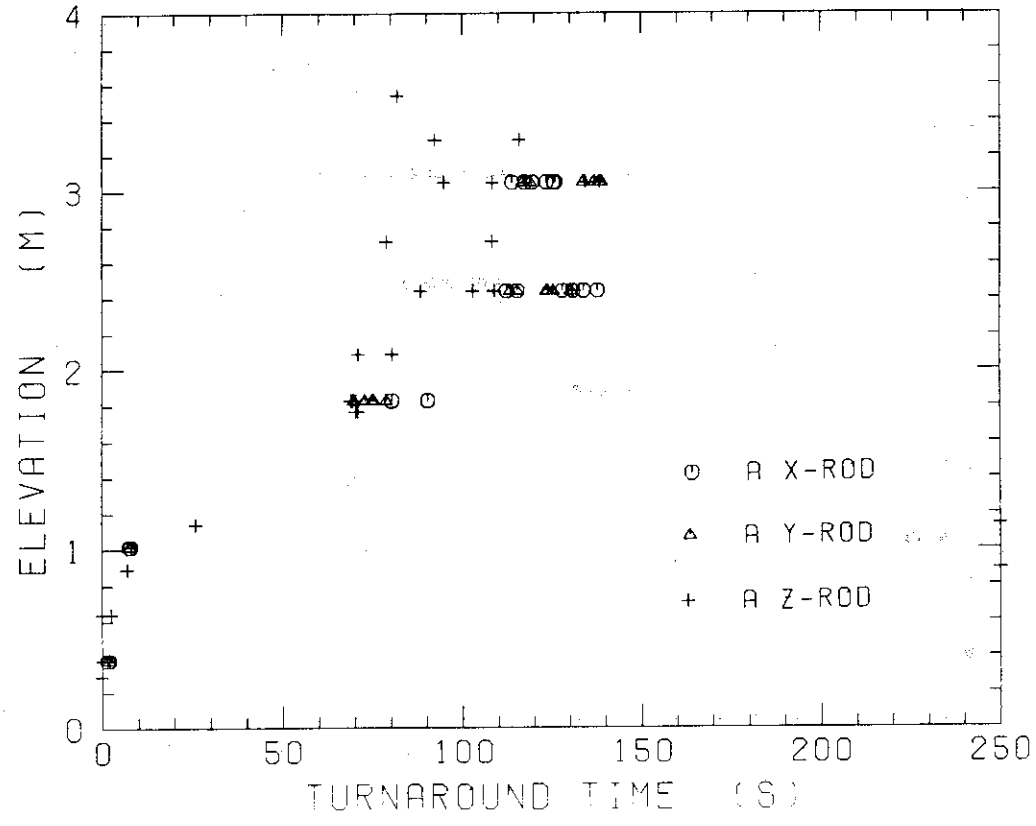

Fig. D-12 Turnaround time in high power region (A region)

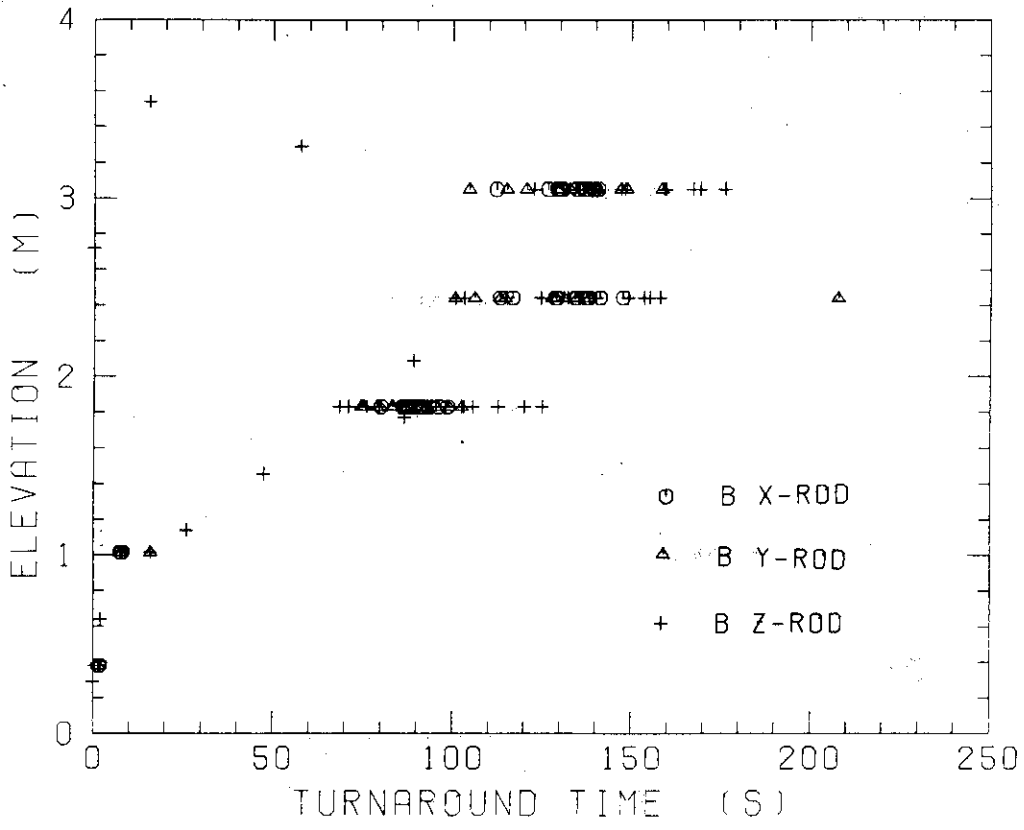

Fig. D-13 Turnaround time in medium power region (B region)

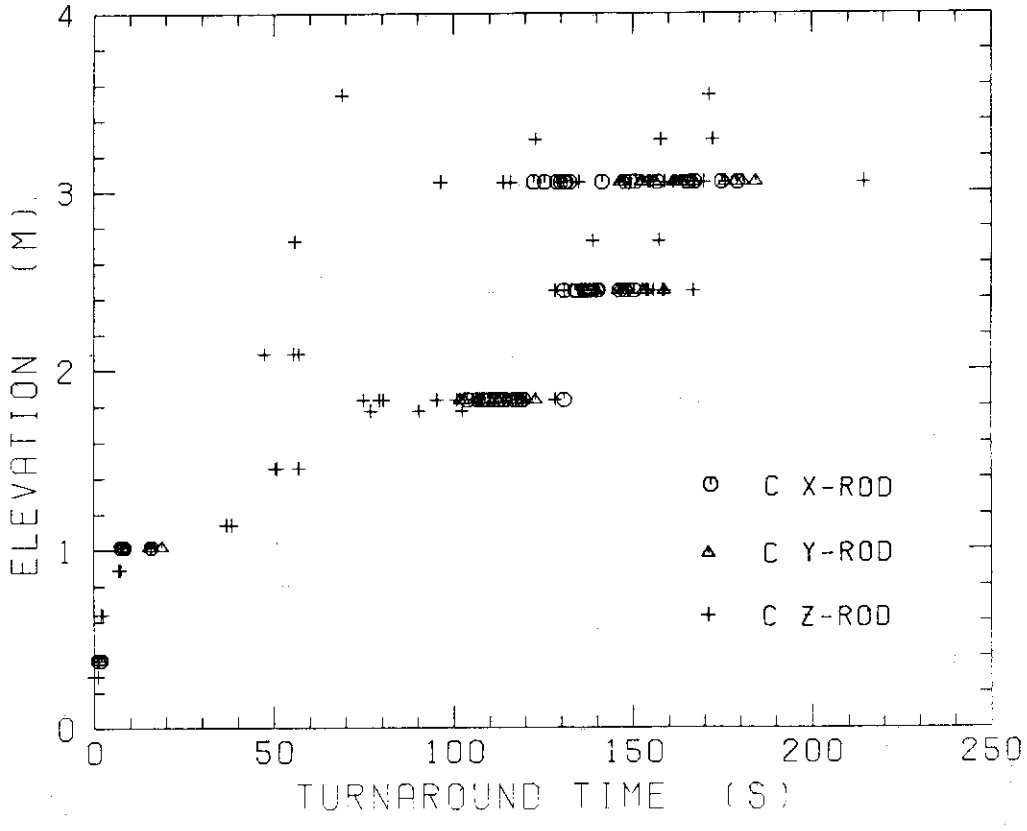

Fig. D-14 Turnaround time in low power region (C region)

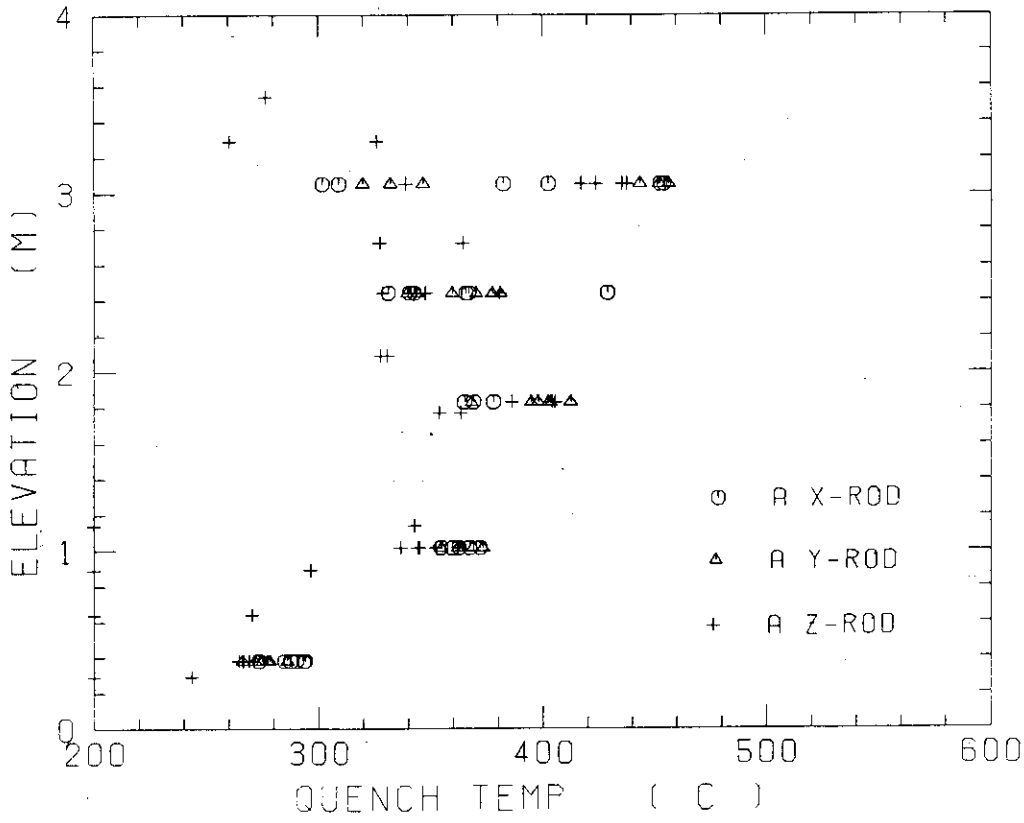

Fig. D-15 Quench temperature in high power region (A region)

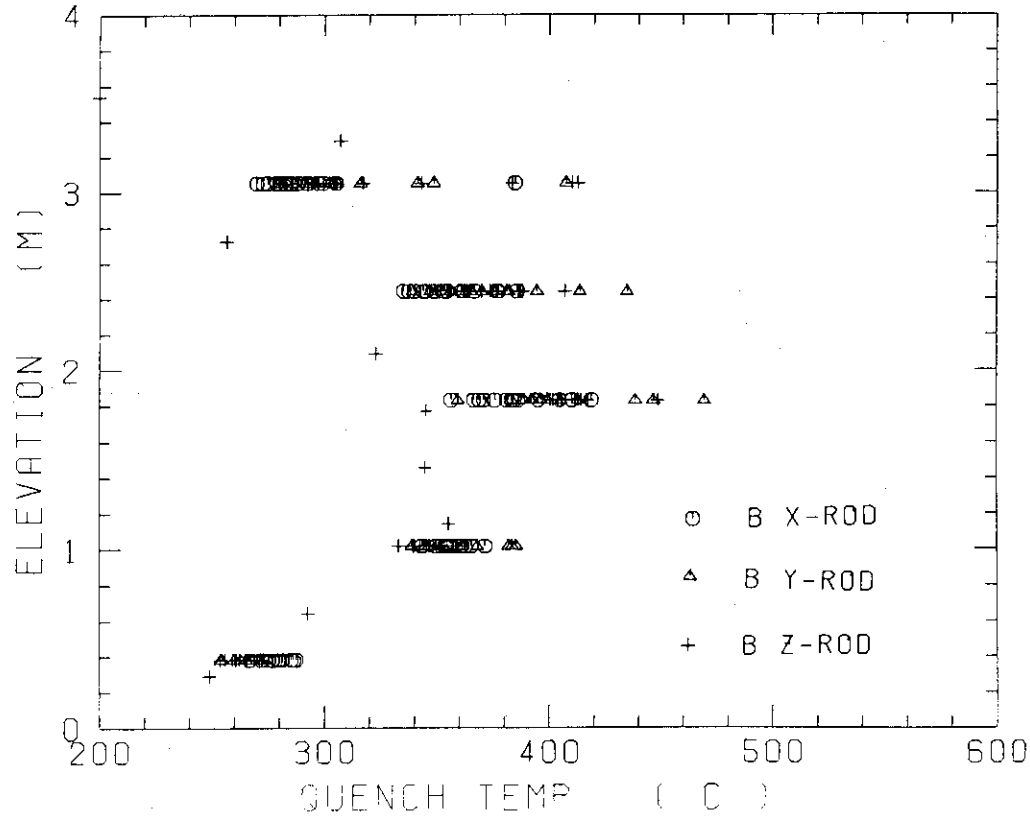

Fig. D-16 Quench temperature in medium power region (B region)

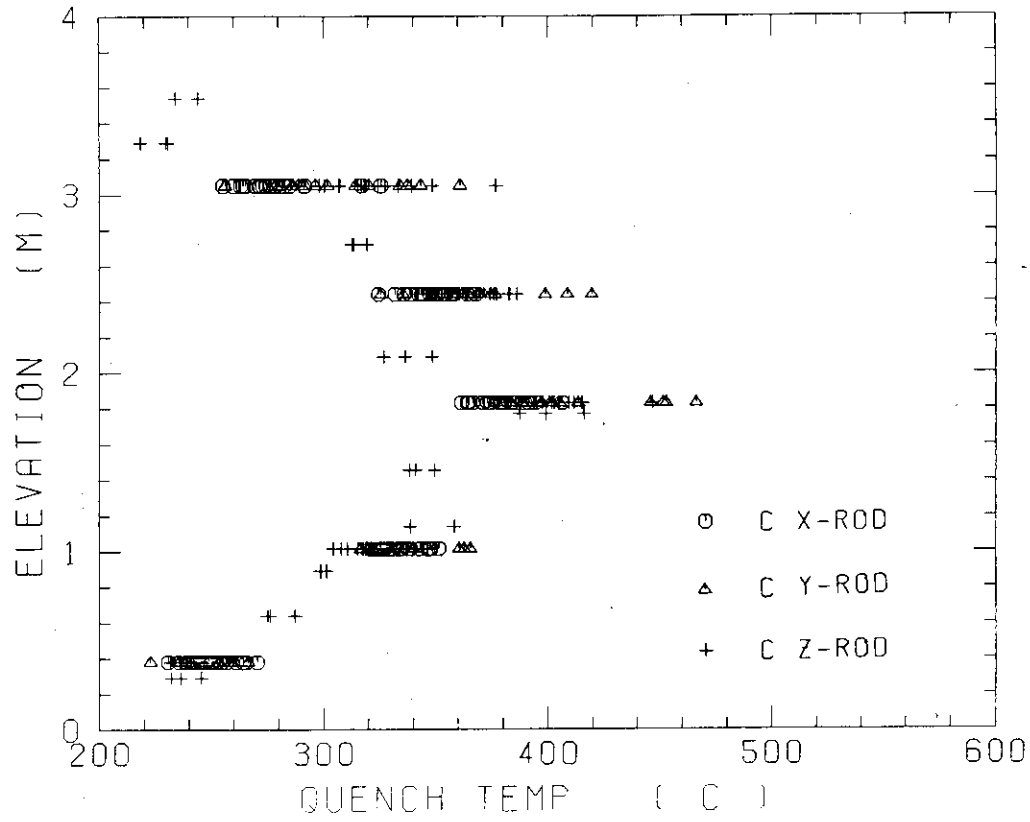

Fig. D-17 Quench temperature in low power region (C region)

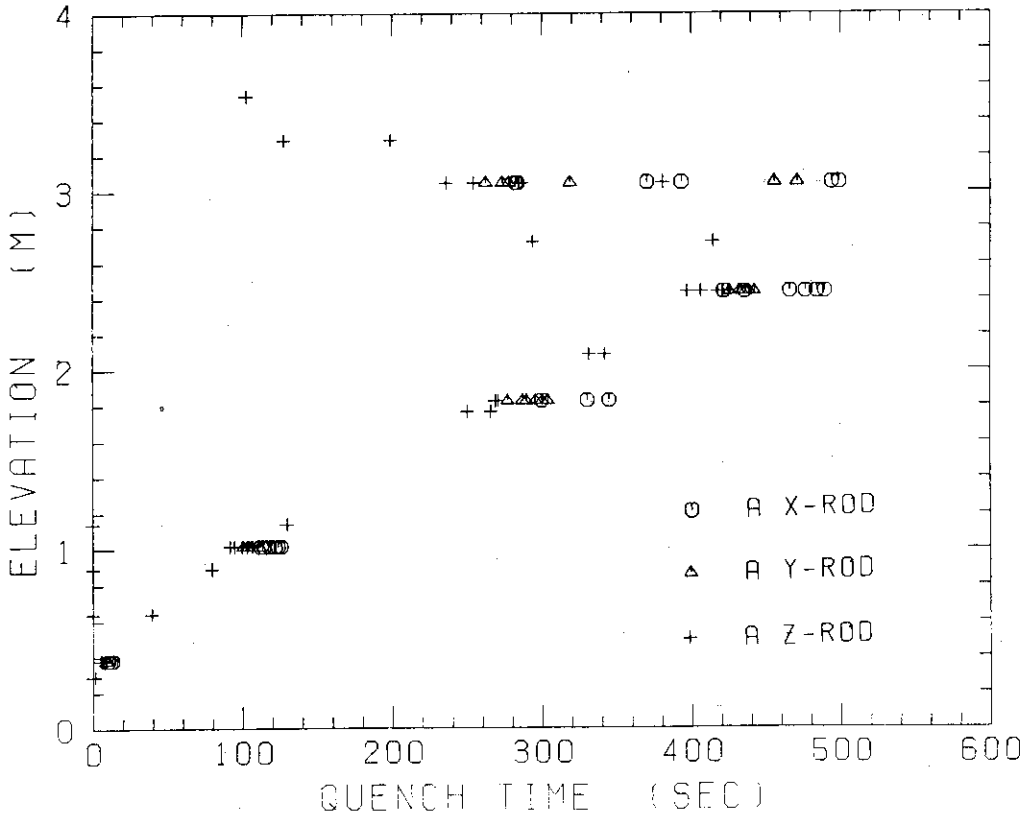

Fig. D-18 Quench time in high power region (A region)

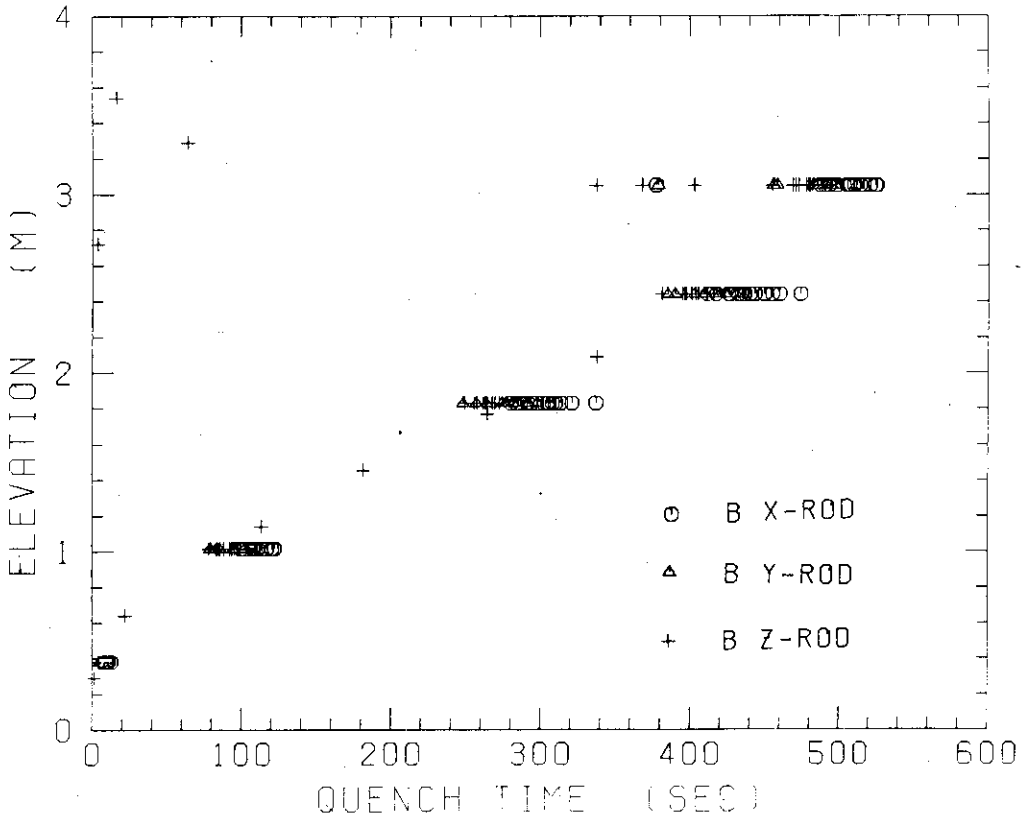

Fig. D-19 Quench time in medium power region (B region)

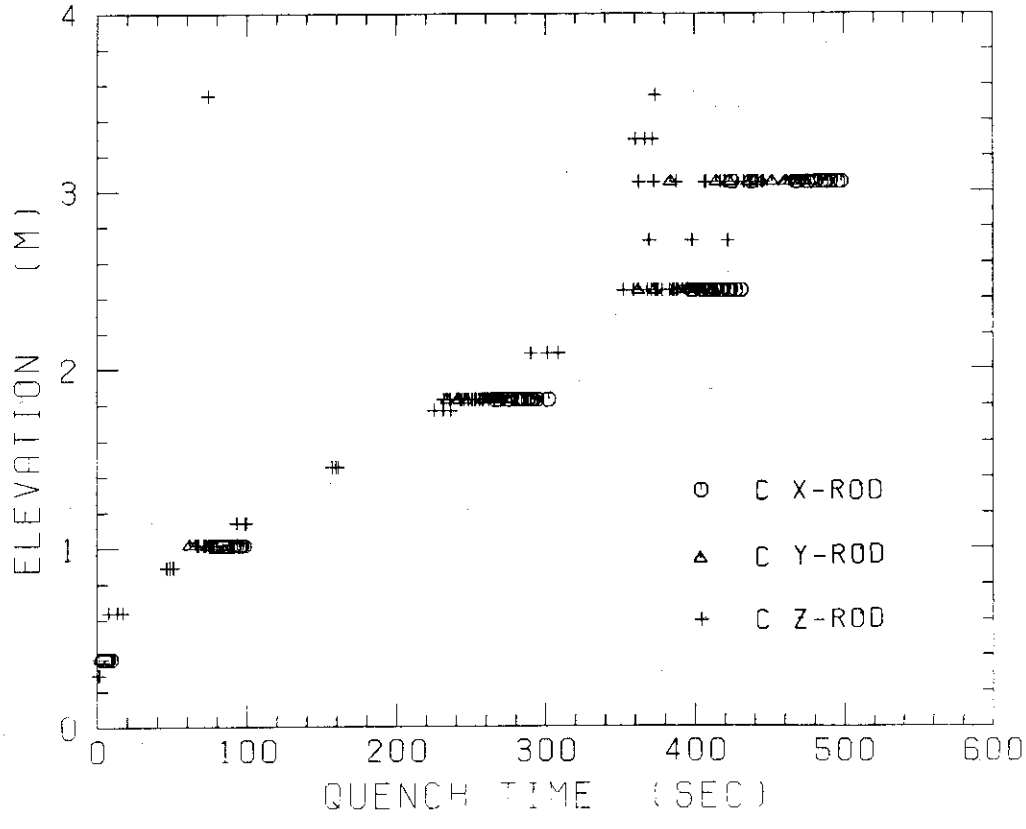

Fig. D-20 Quench time in low power region (C region)

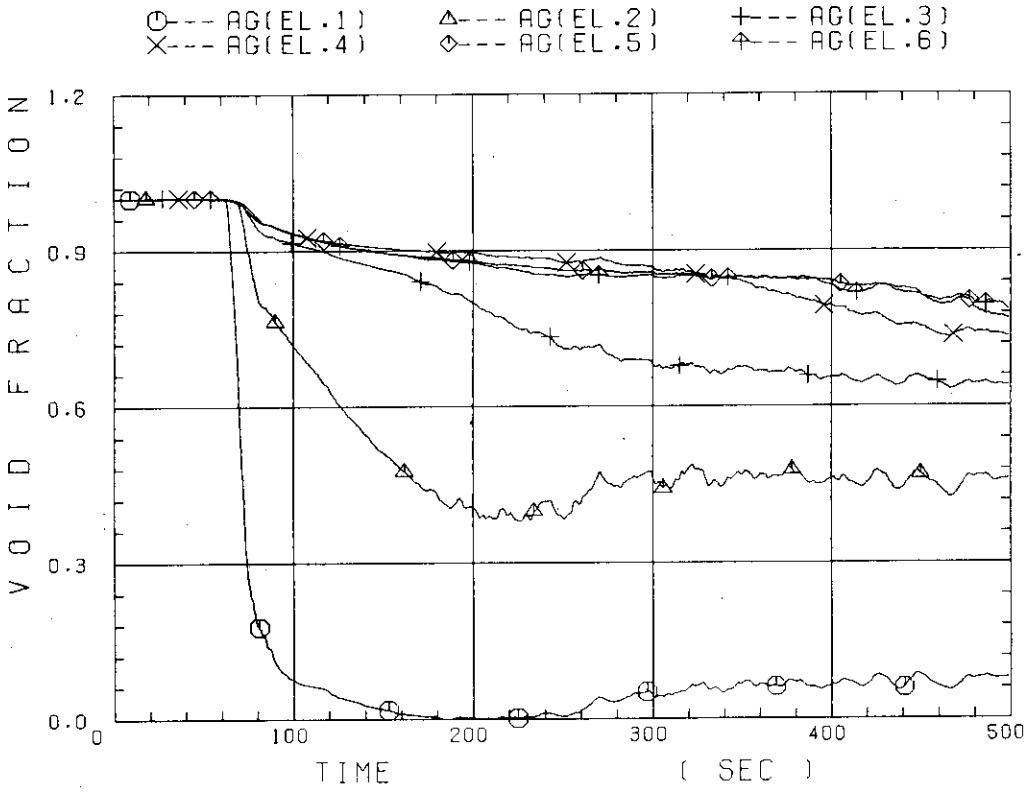

Fig. D-21 Void fraction in core

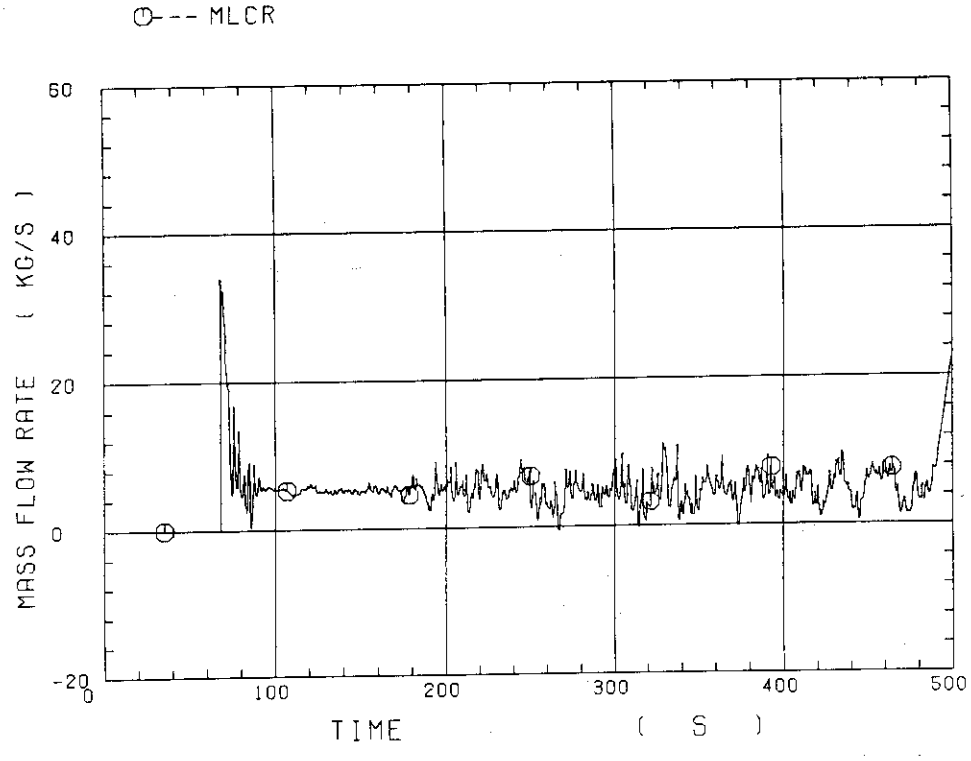

Fig. D-22 Core inlet mass flow rate (recommended value)

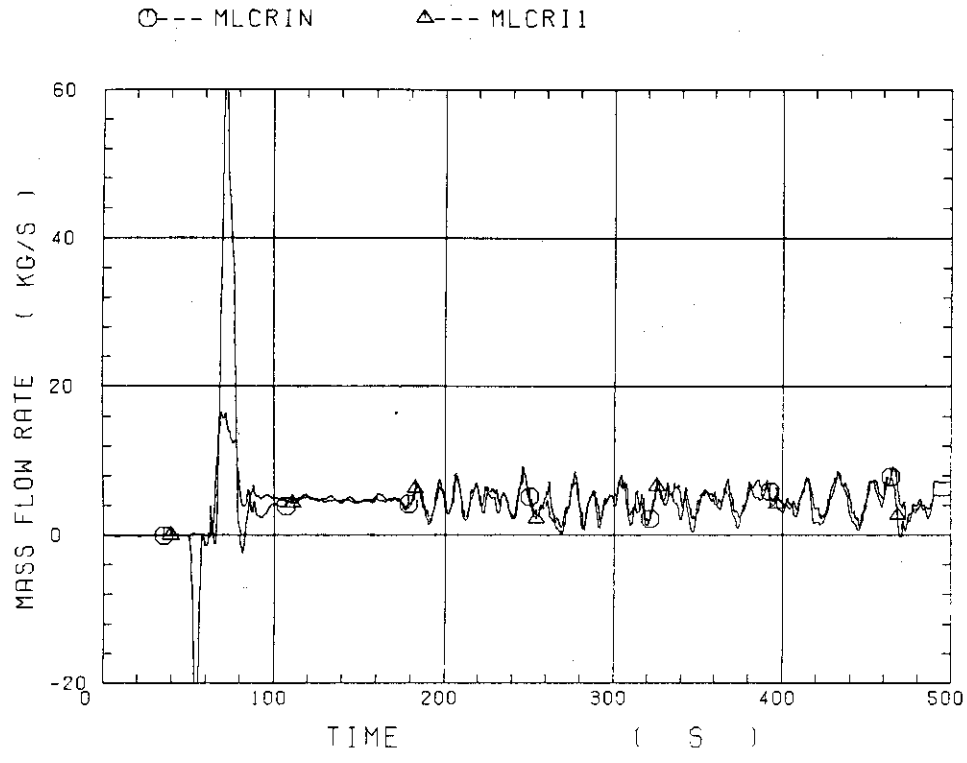

Fig. D-23 Core inlet mass flow rate

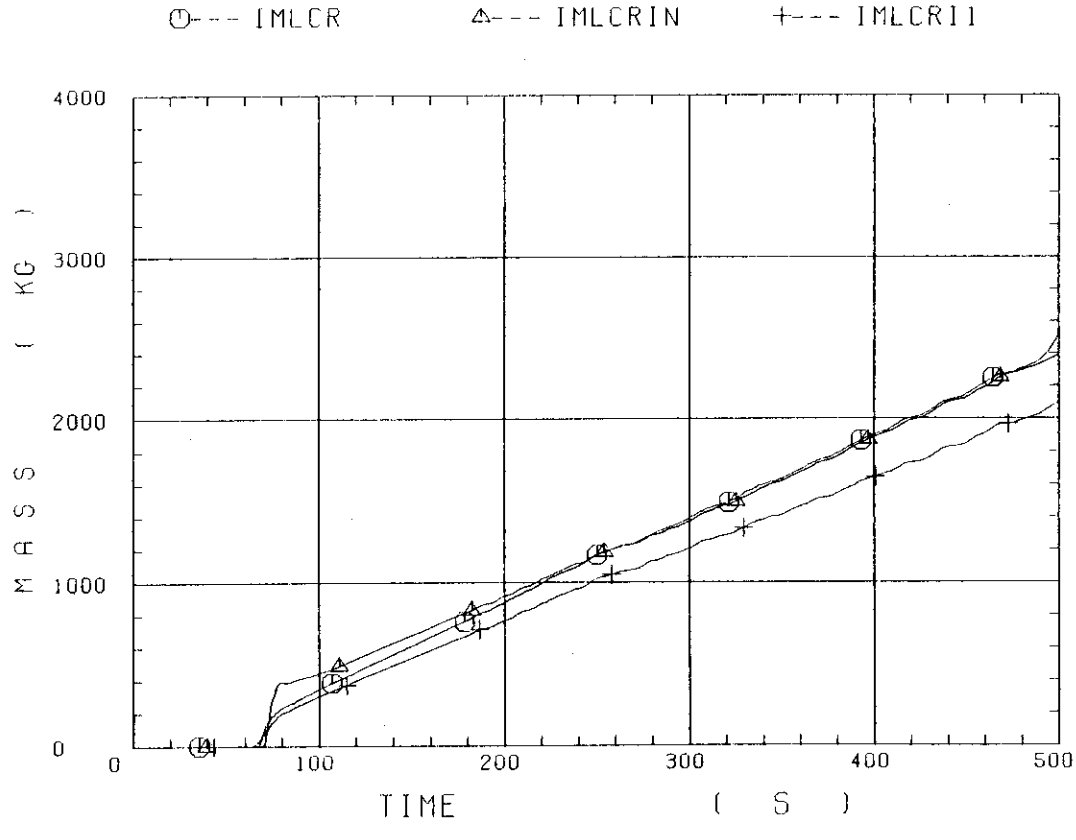

Fig. D-24 Time-integration of core inlet mass flow rate

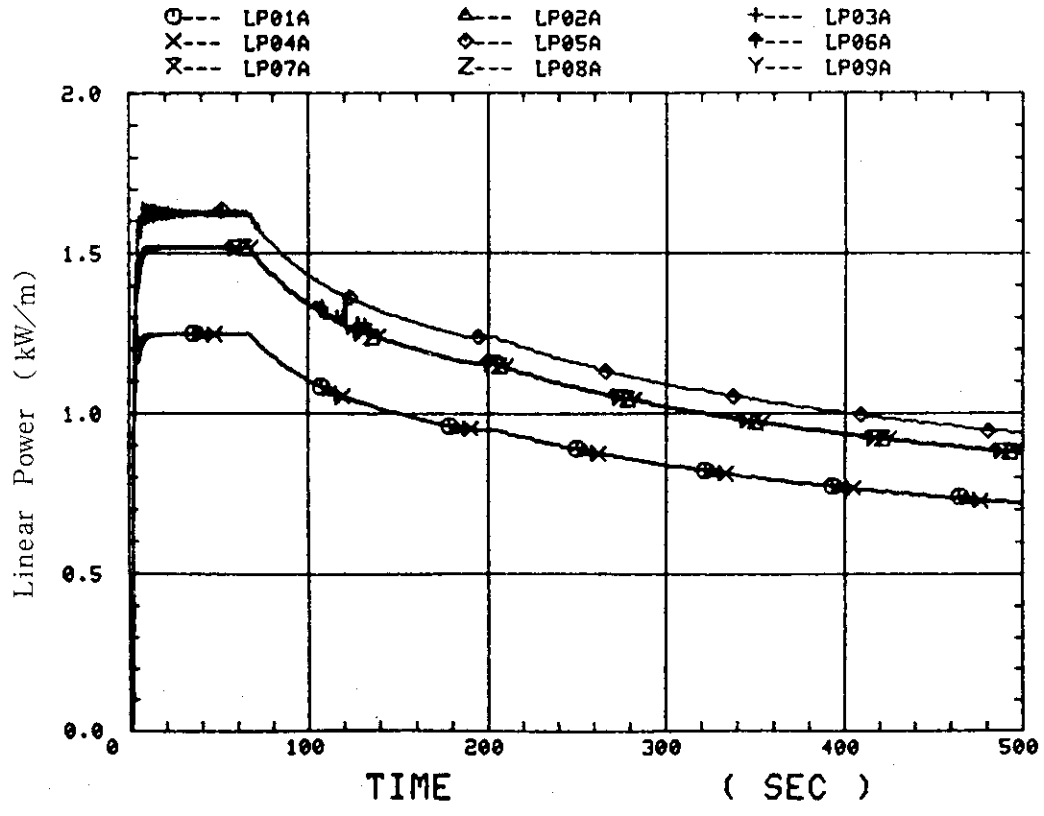

Fig. D-25 Average linear power of heater rod in each power unit zone

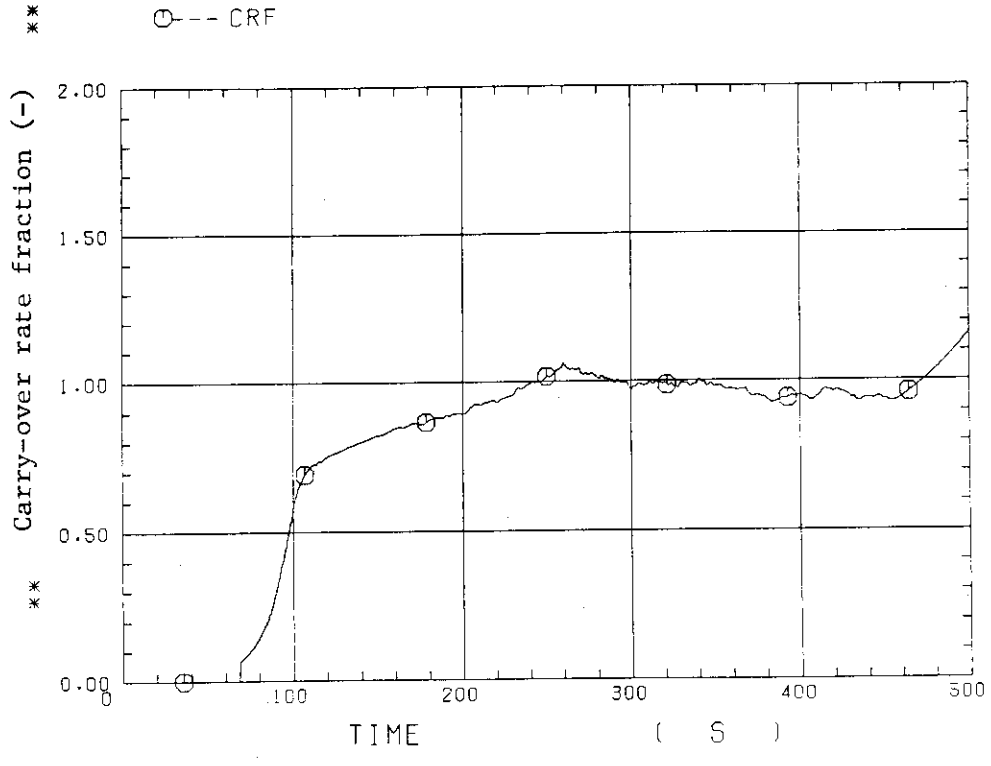

Fig. D-26 Carry-over rate fraction

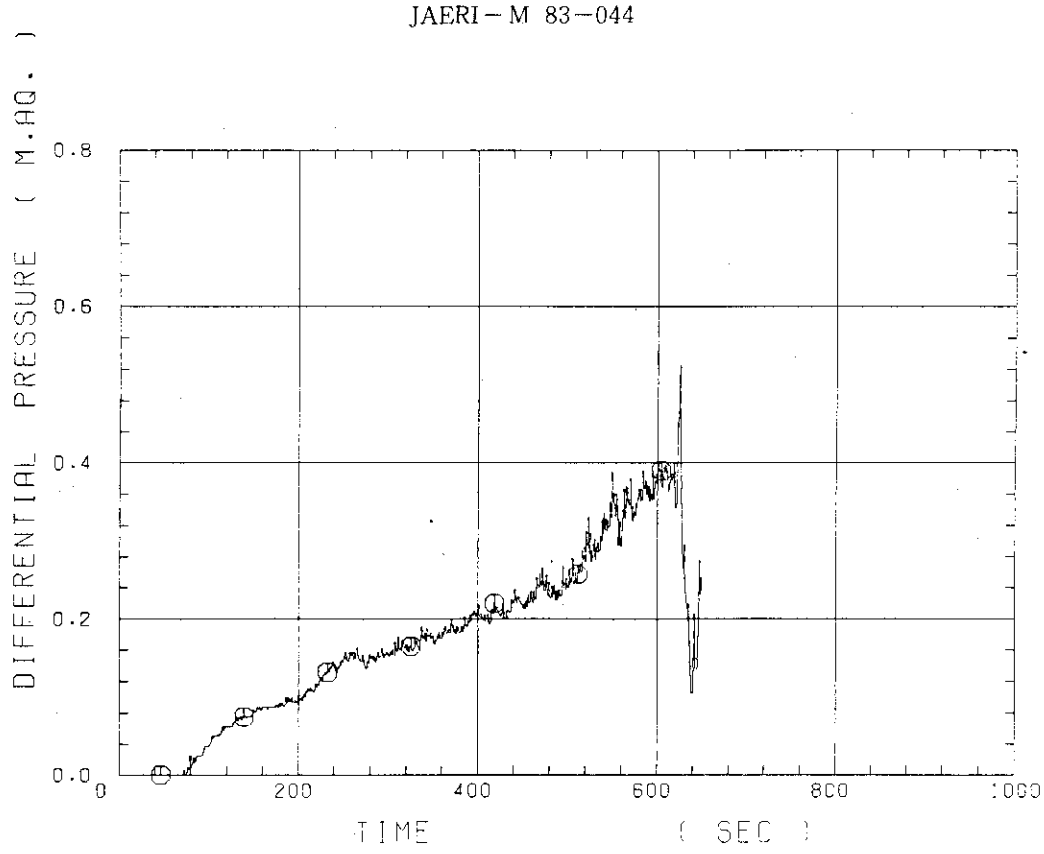

Fig. D-27 Differential pressure through upper plenum

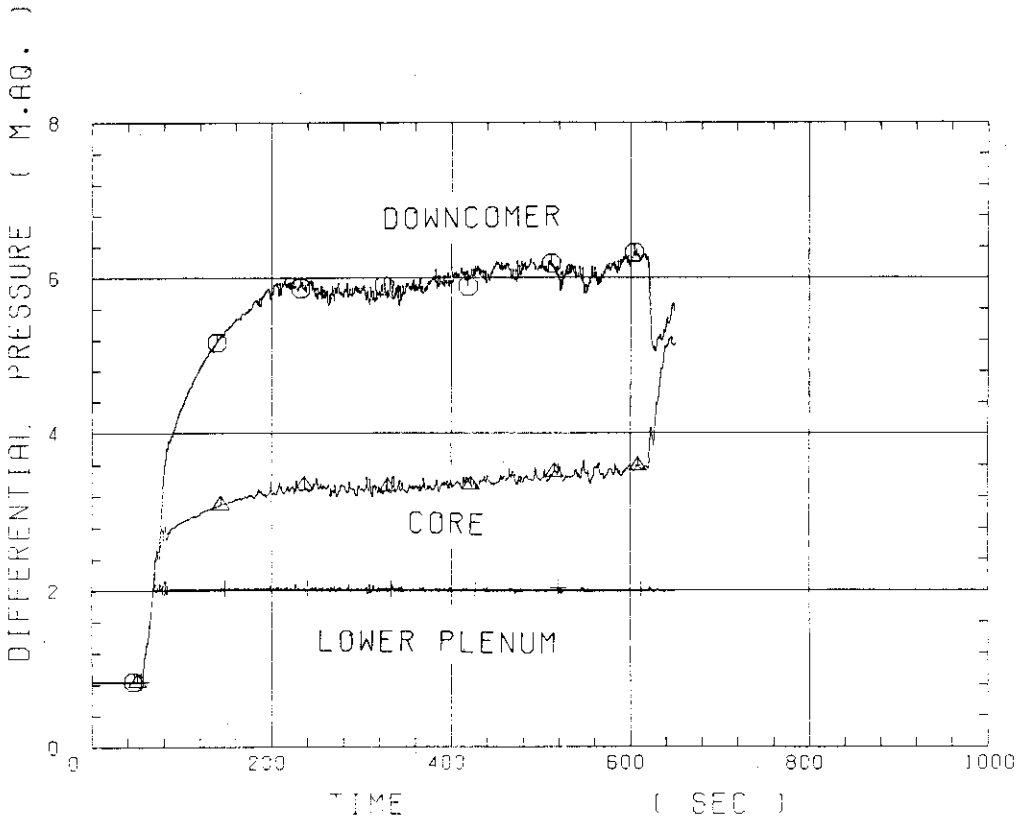

Fig. D-28 Differential pressure through downcomer, core, and lower plenum

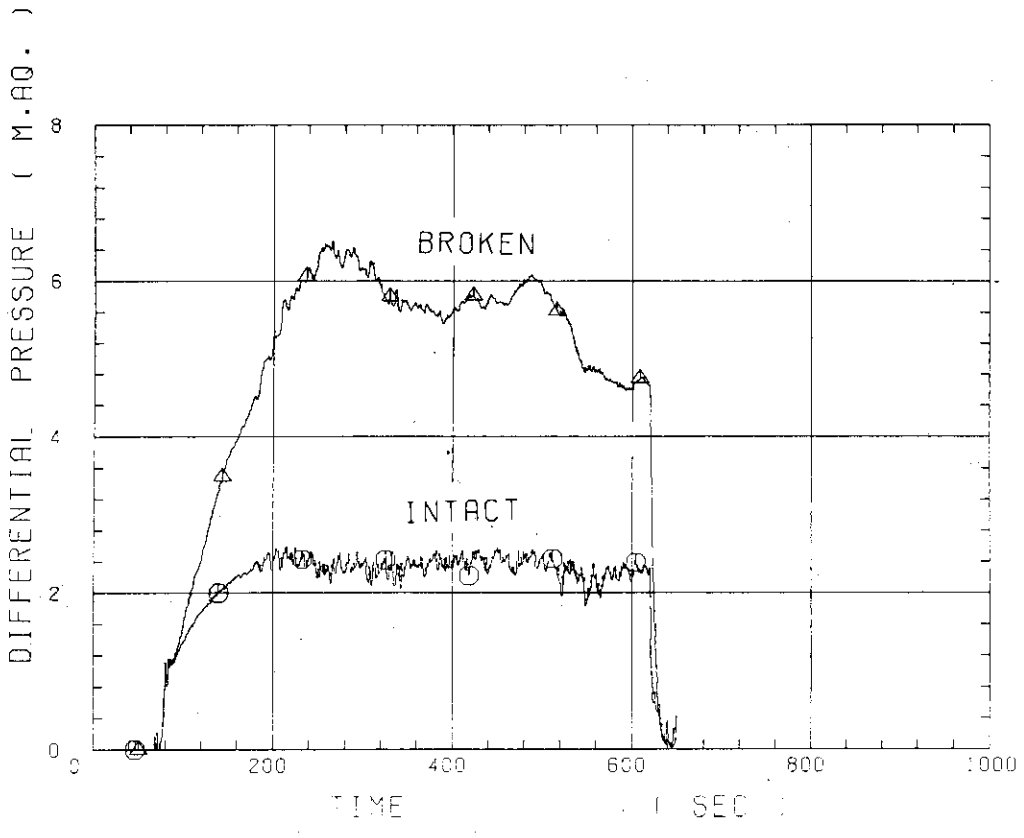

Fig. D-29 Differential pressure through intact and broken loops

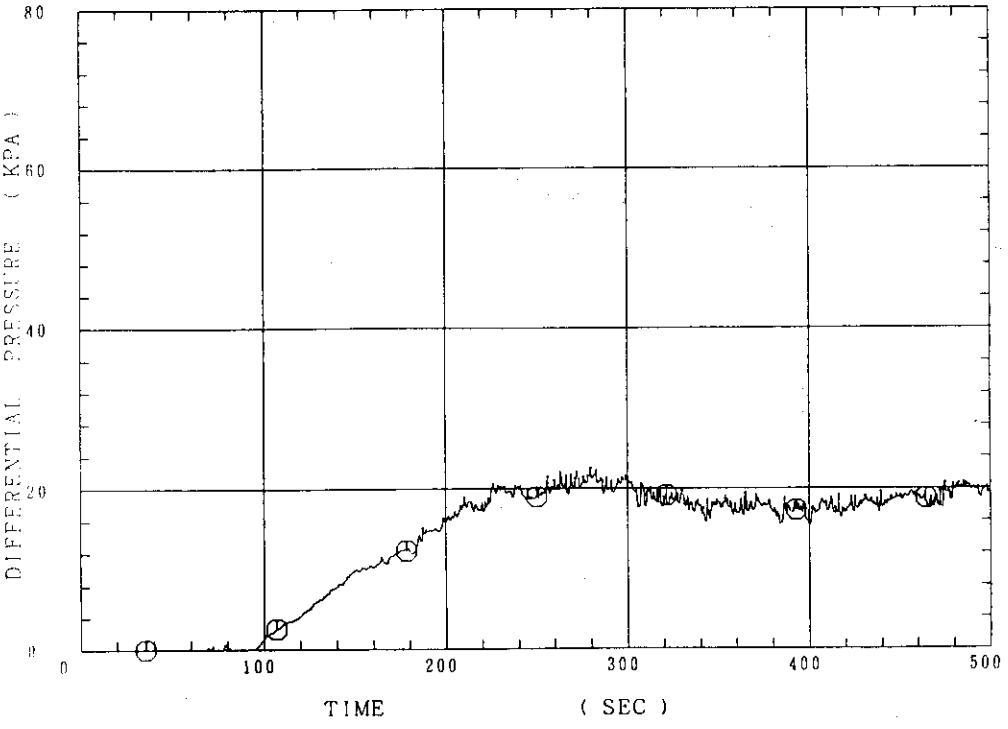

Fig. D-30 Differential pressure through broken cold leg nozzle

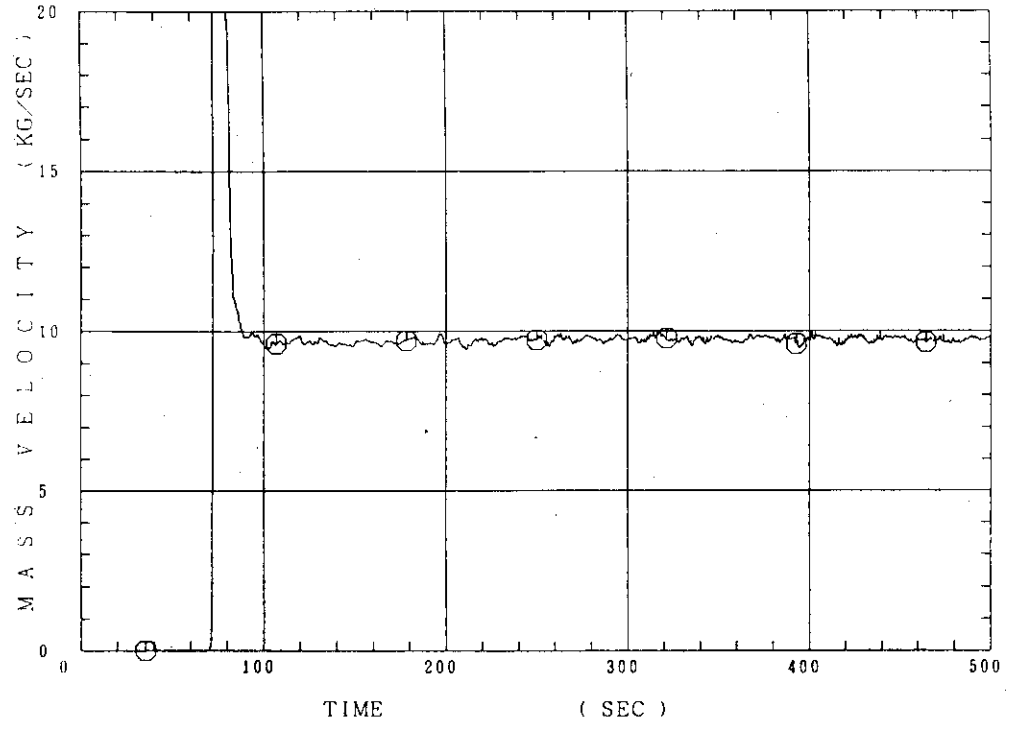

Fig. D-31 Total water mass flow rate from intact loops to downcomer

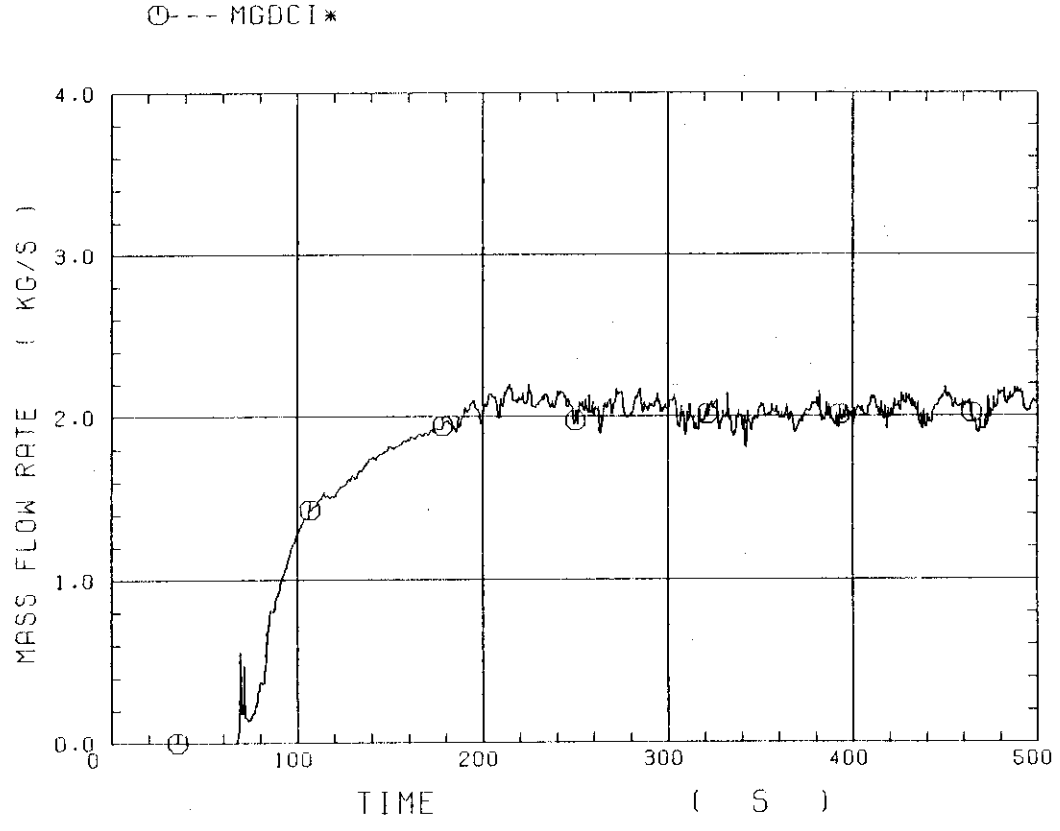

Fig. D-32 Total steam mass flow rate from intact loops to downcomer

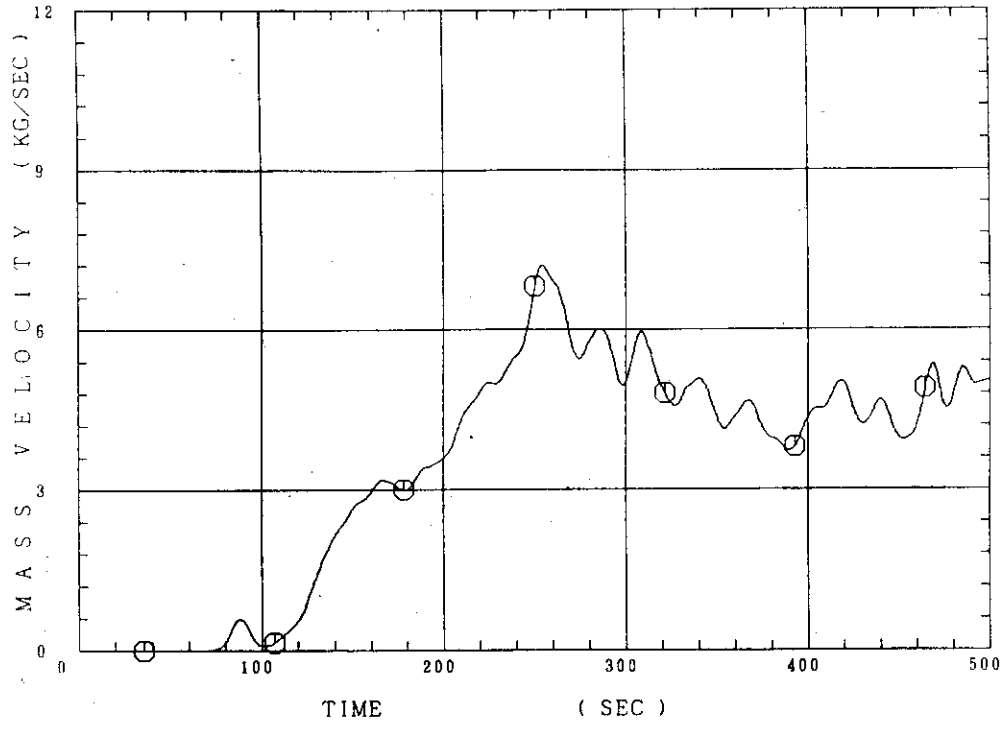

Fig. D-33 Water mass flow rate through broken cold leg nozzle

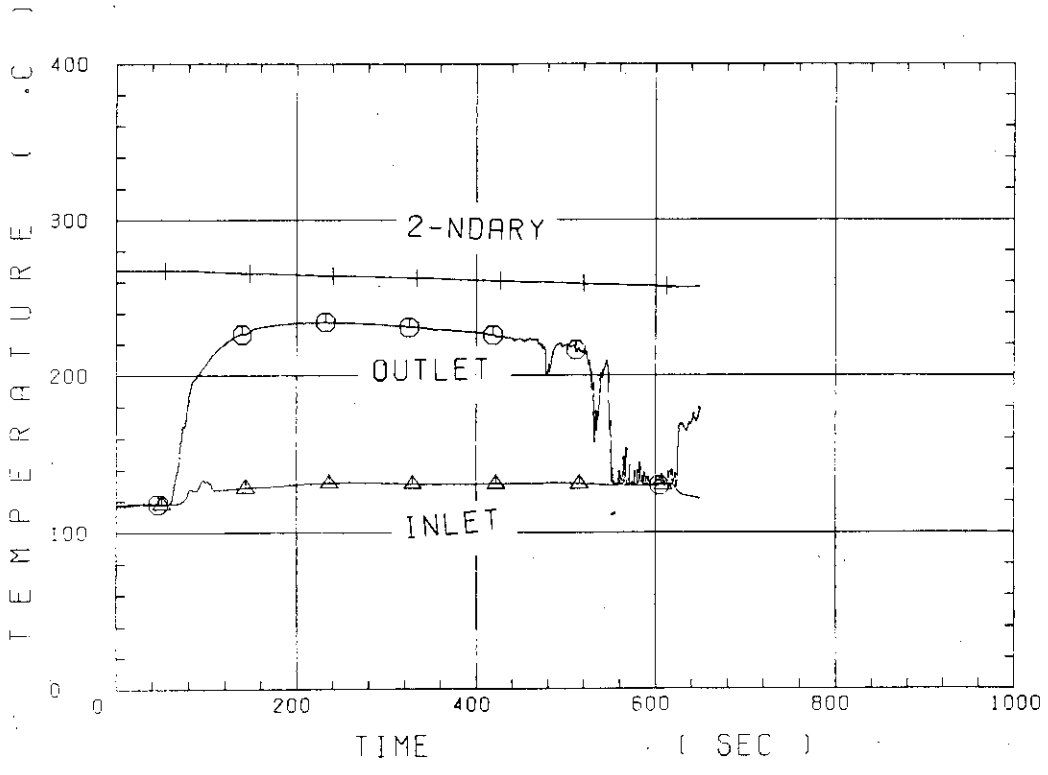

Fig. D-34 Fluid temperature in inlet plenum, outlet plenum, and secondary of steam generator 1

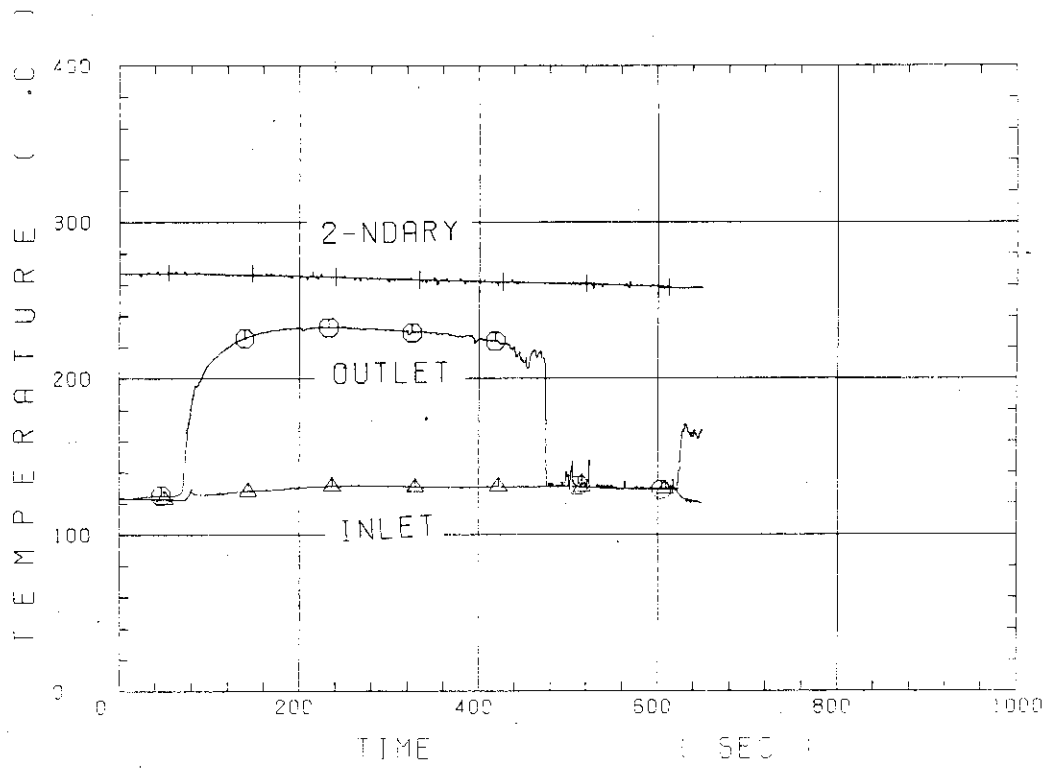

Fig. D-35 Fluid temperature in inlet plenum, outlet plenum, and secondary of steam generator 2

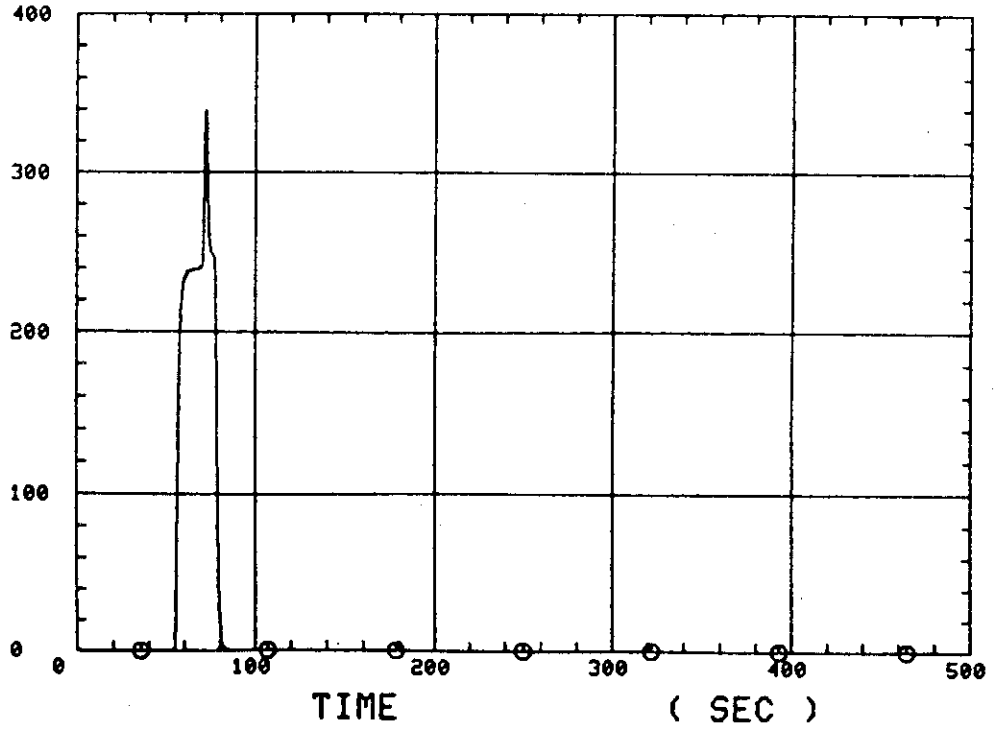

Fig. D-36 Total accumulator injection rate

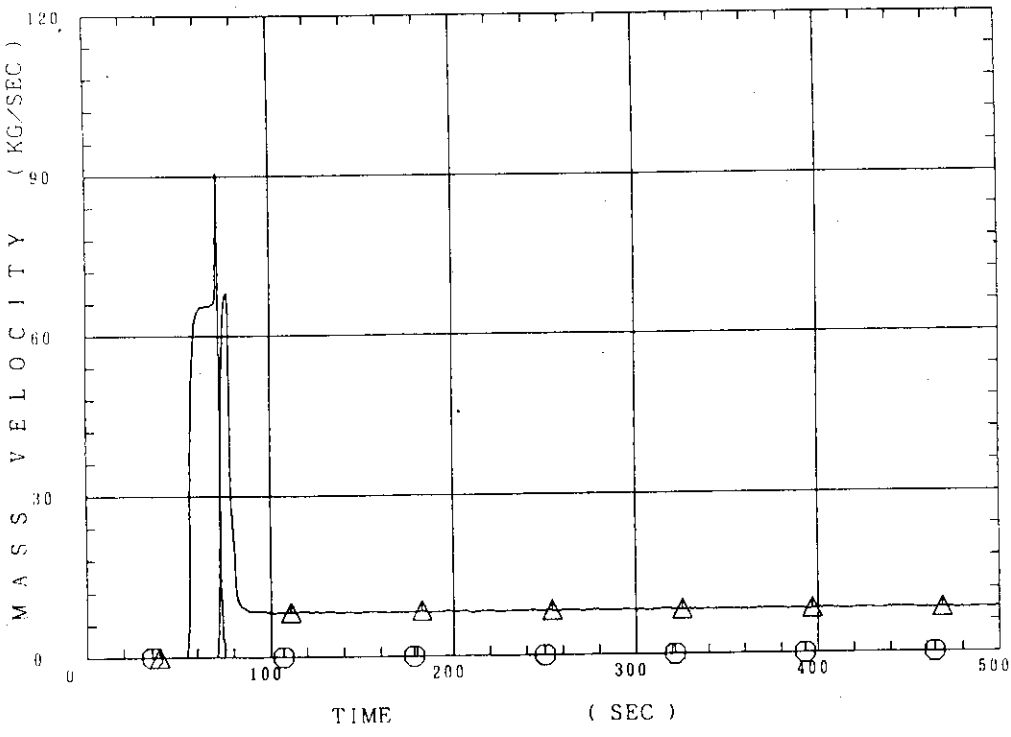

Fig. D-37 ECC water injection rates to lower plenum and to cold legs

Appendix E

Selected data of CCTF Test C1-13 (Run22)

Table and Figure List

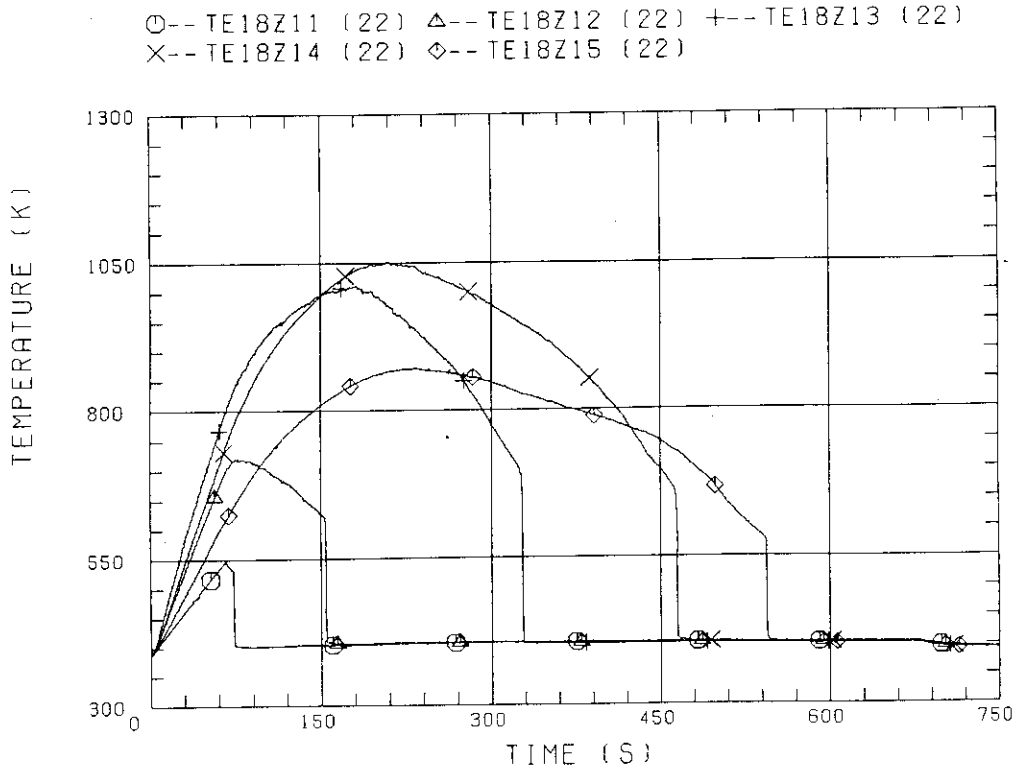

Fig. E-1 Surface temperature on low power rod (Z-rod) in medium power region (B region) (average power rod)

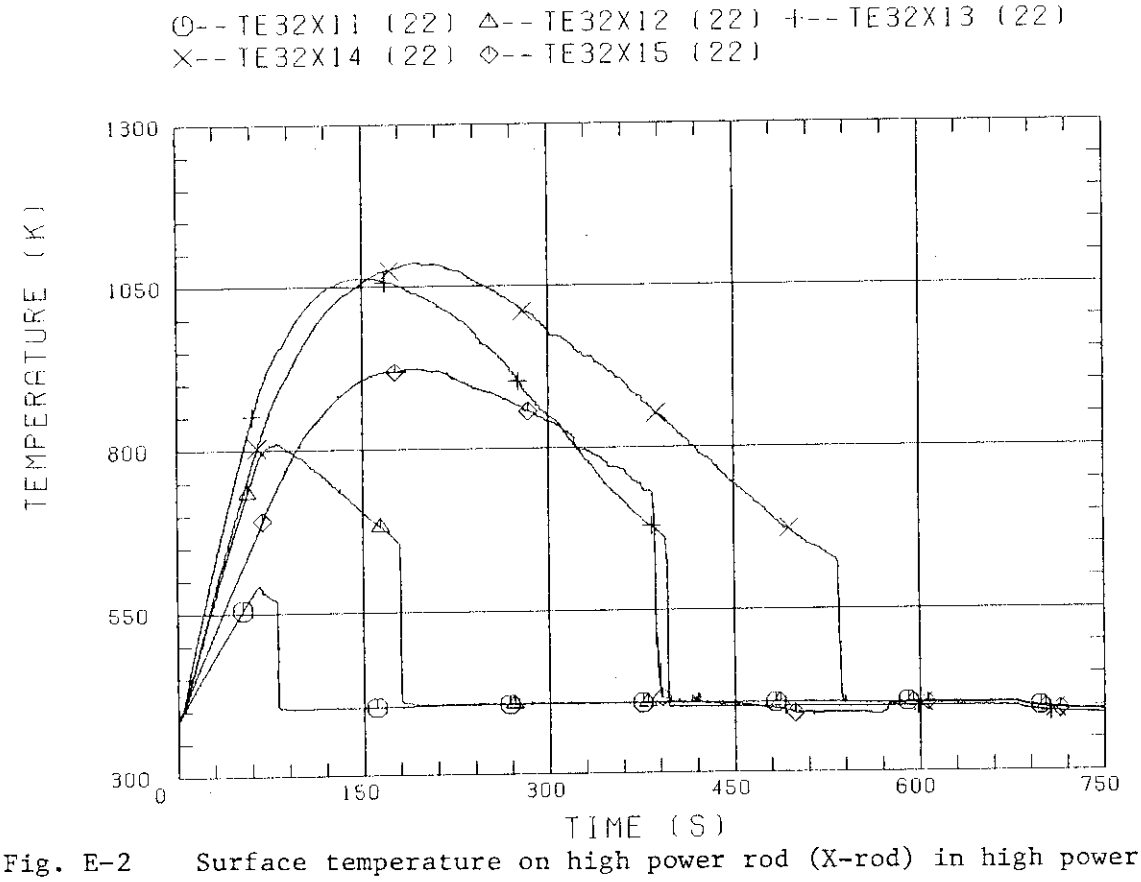

Fig. E-2 Surface temperature on high power rod (X-rod) in high power region (A region) (peak power rod)

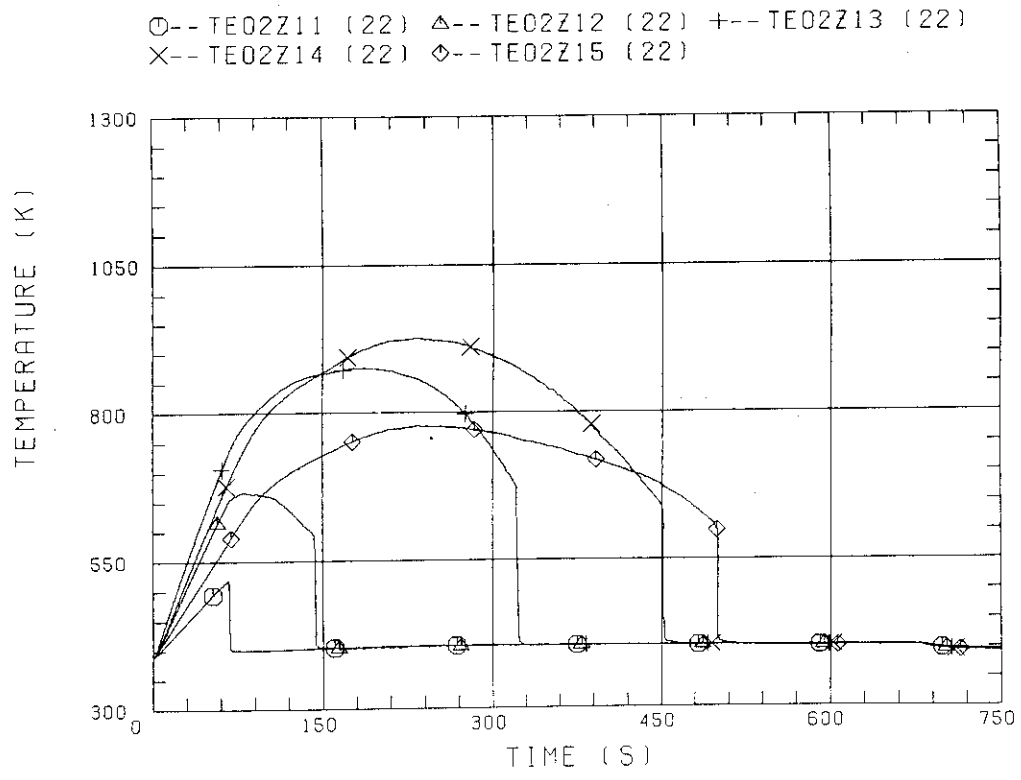

Fig. E-3 Surface temperature on low power rod (Z-rod) in low power region (C region) (lowest power rod)

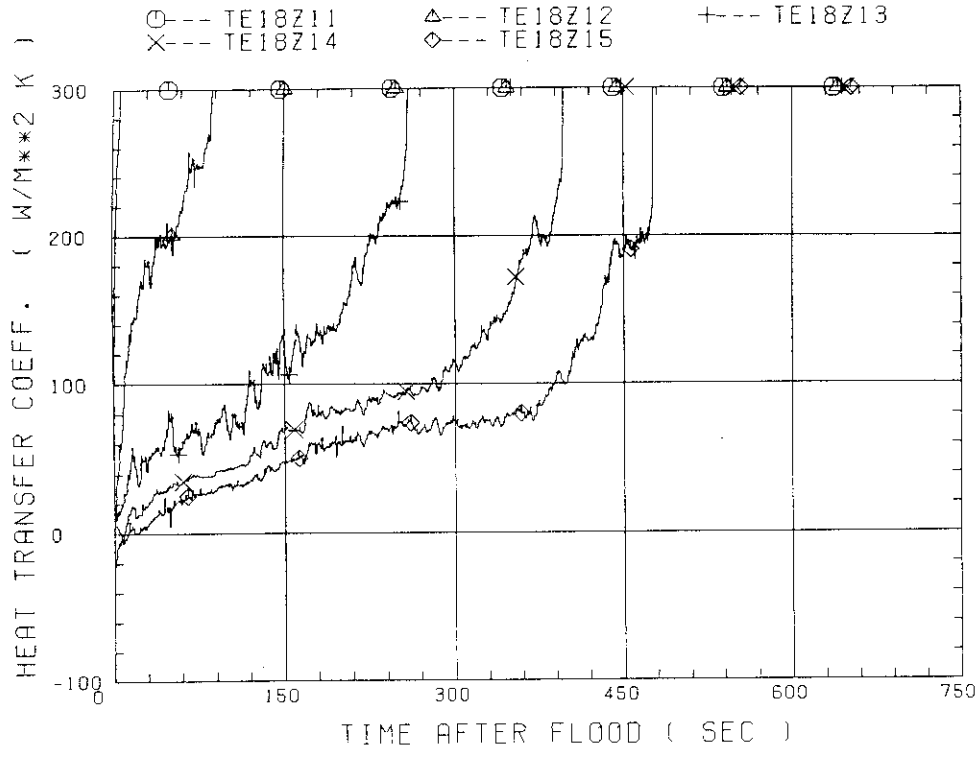

Fig. E-4 Heat transfer coefficient of low power rod (Z-rod) in medium power region (B region) (average power rod)

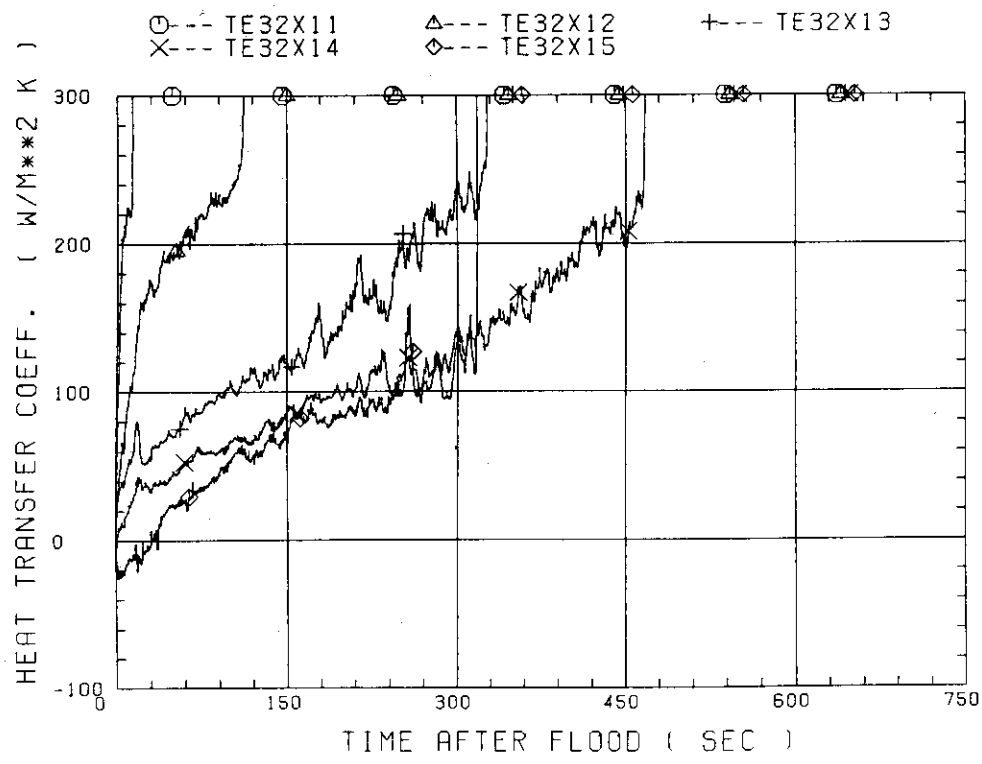

Fig. E-5 Heat transfer coefficient of high power rod (X-rod) in high power region (A region) (peak power rod)

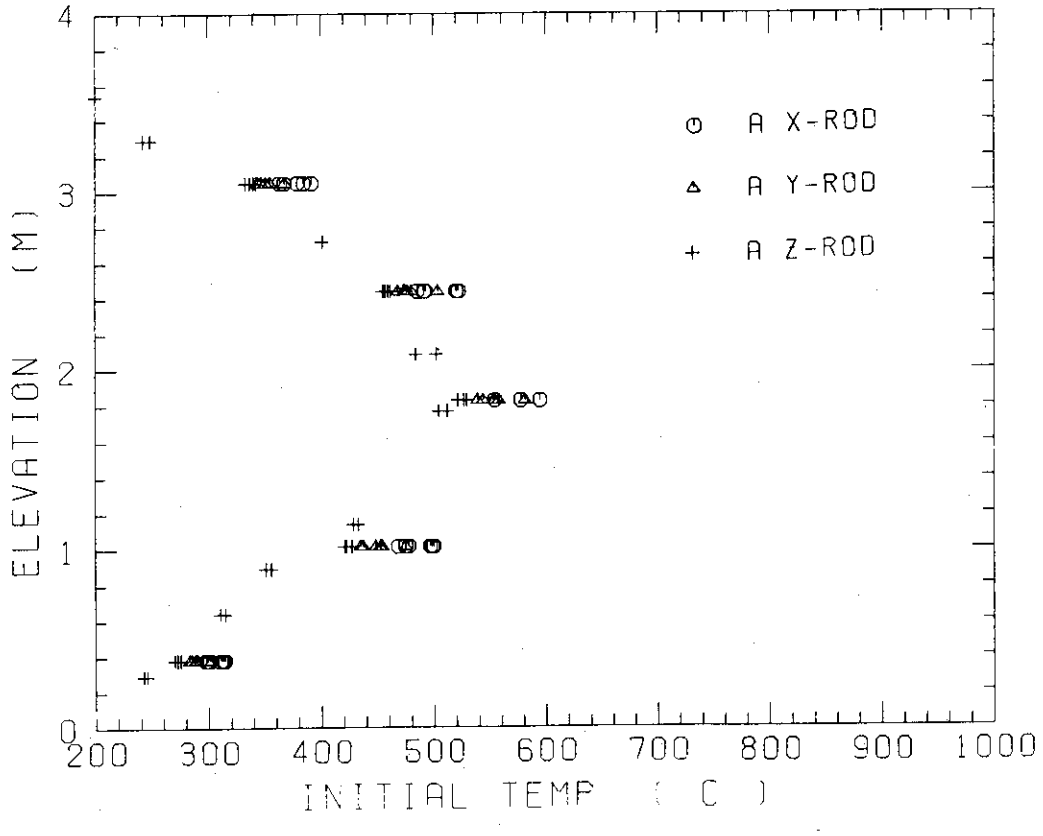

Fig. E-6 Initial rod surface temperature in high power region (A region)

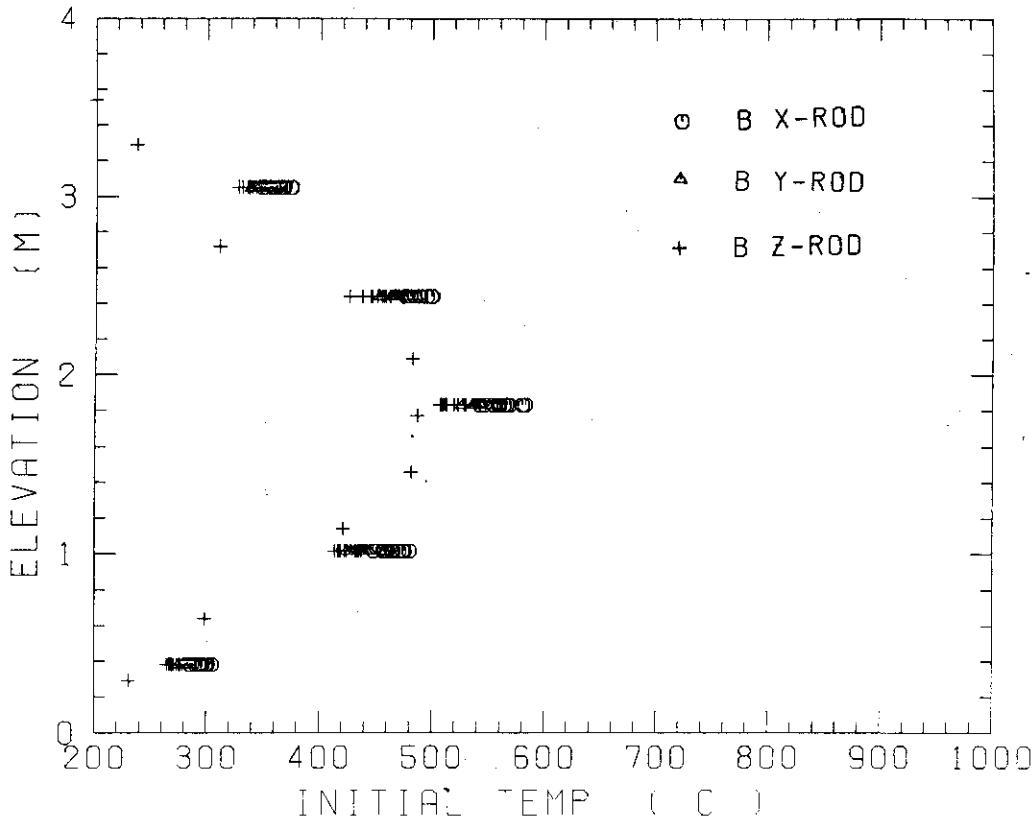

Fig. E-7 Initial rod surface temperature in medium power region (B region)

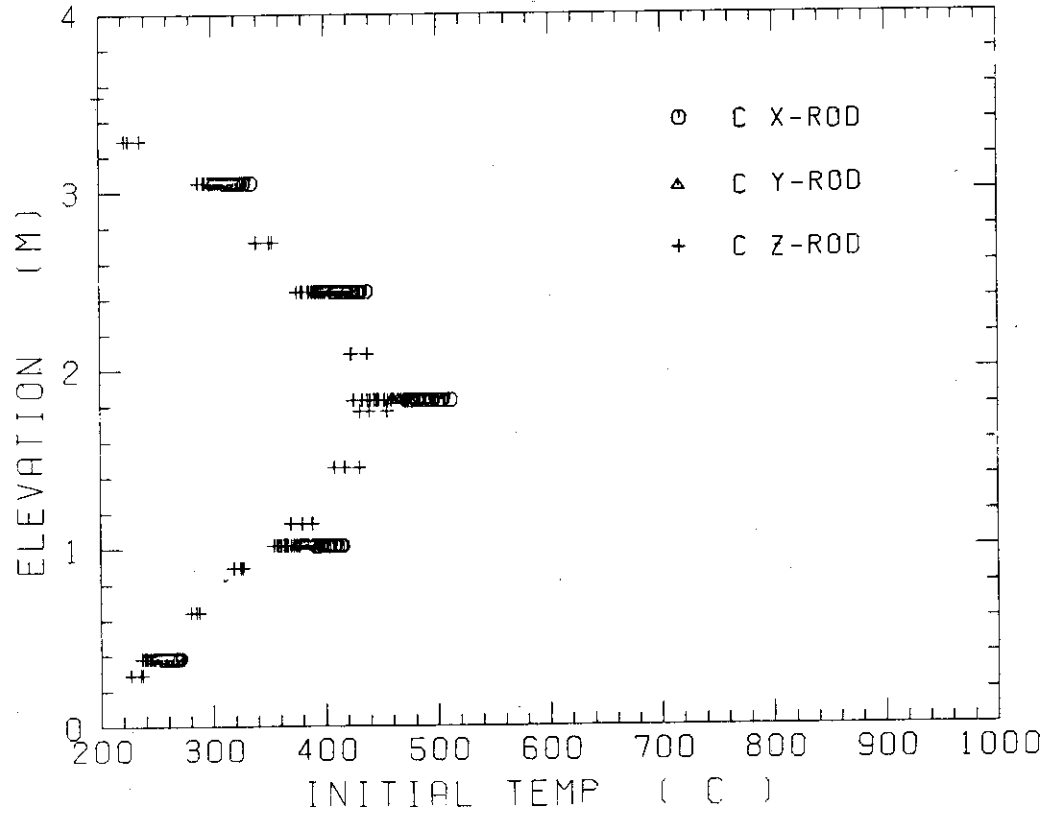

Fig. E-8 Initial rod surface temperature in low power region (C region)

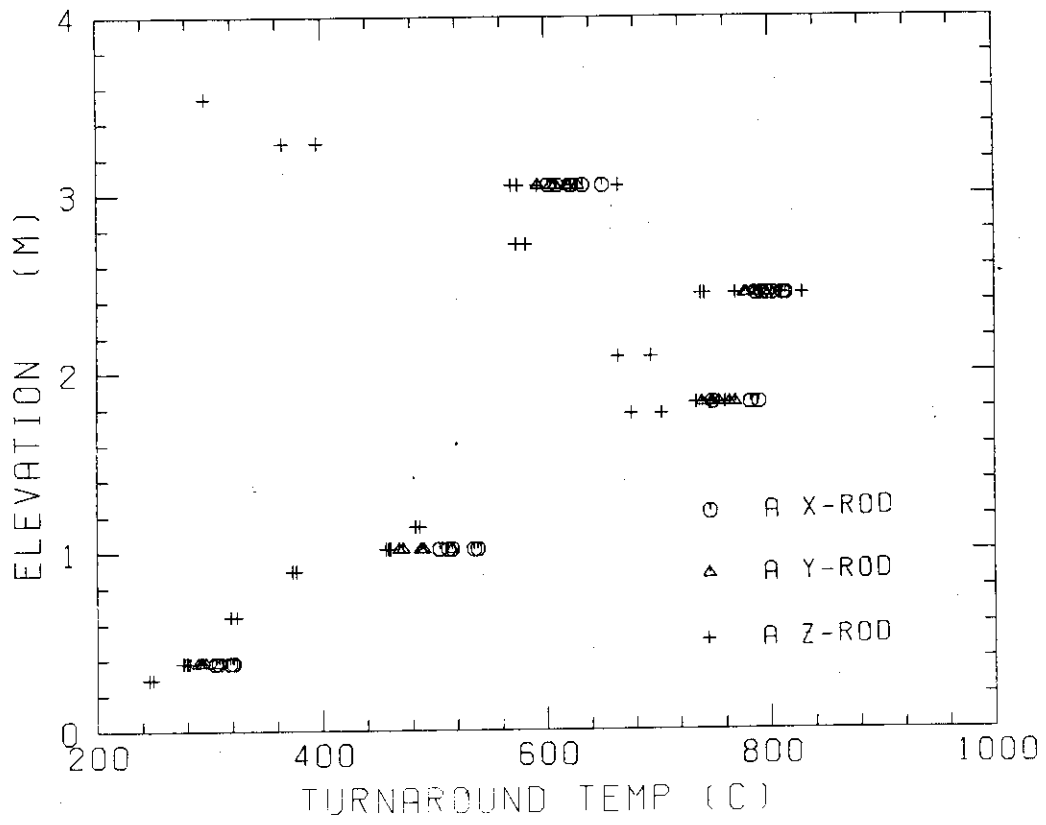

Fig. E-9 Turnaround temperature in high power region (A region)

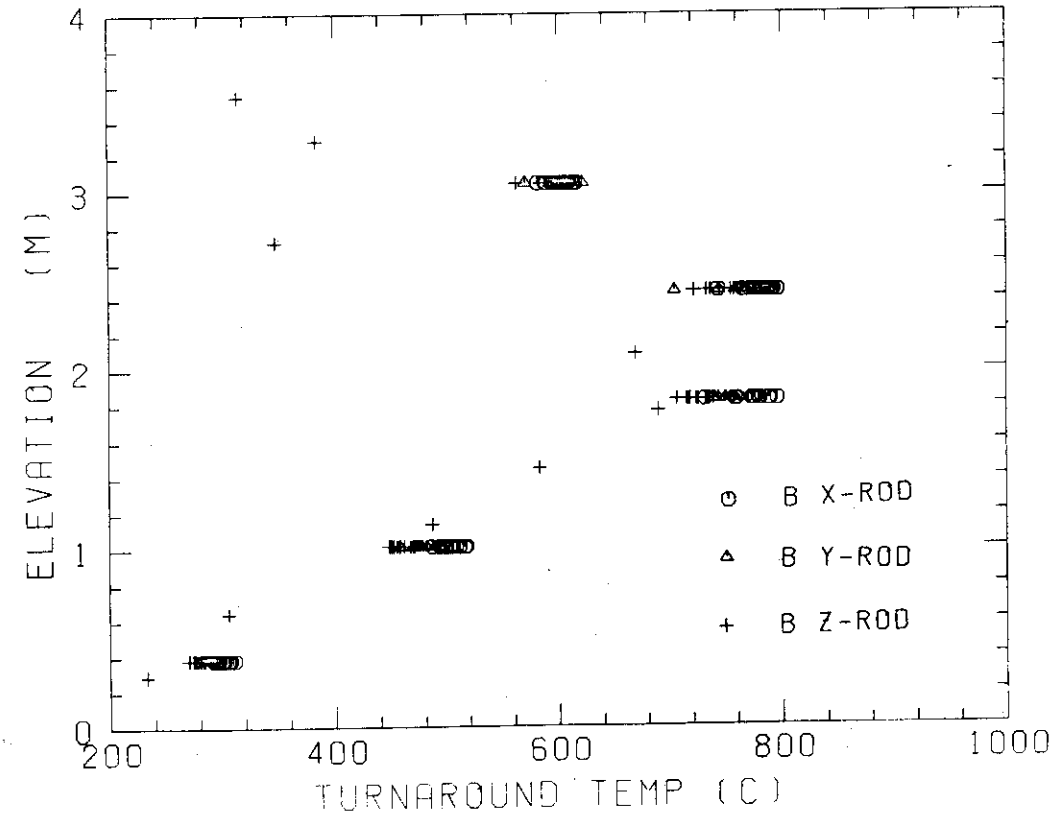

Fig. E-10 Turnaround temperature in medium power region (B region)

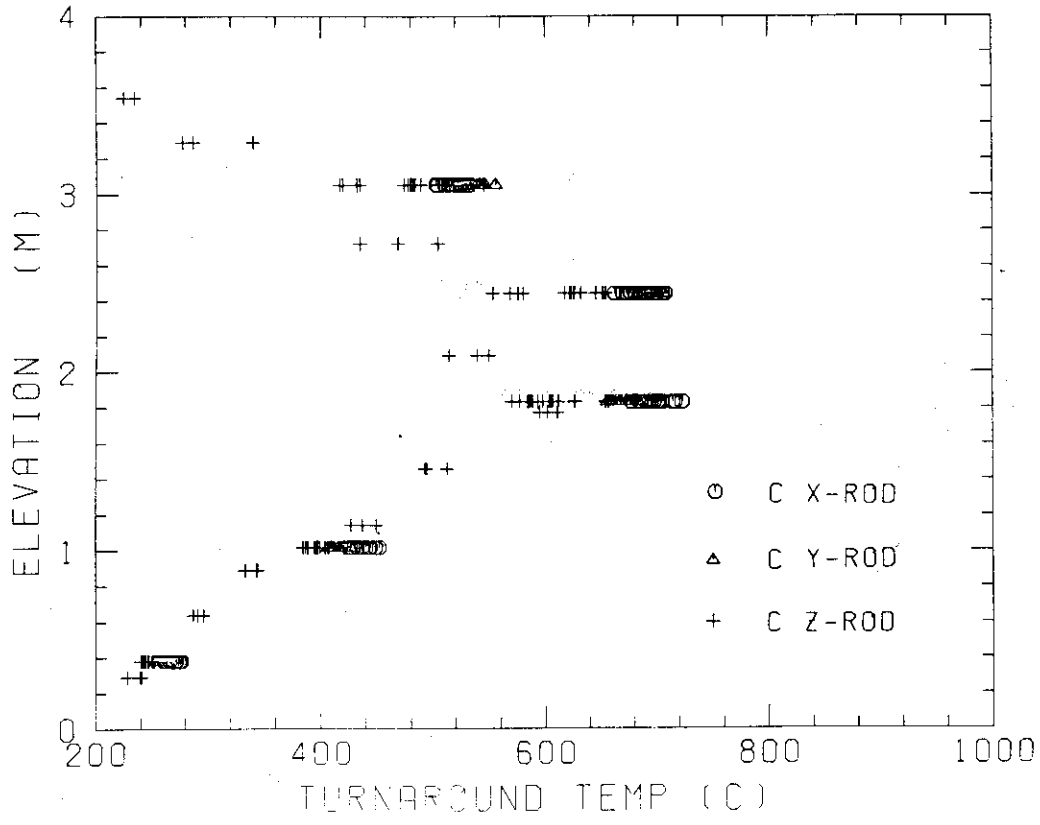

Fig. E-11 Turnaround temperature in low power region (C region)

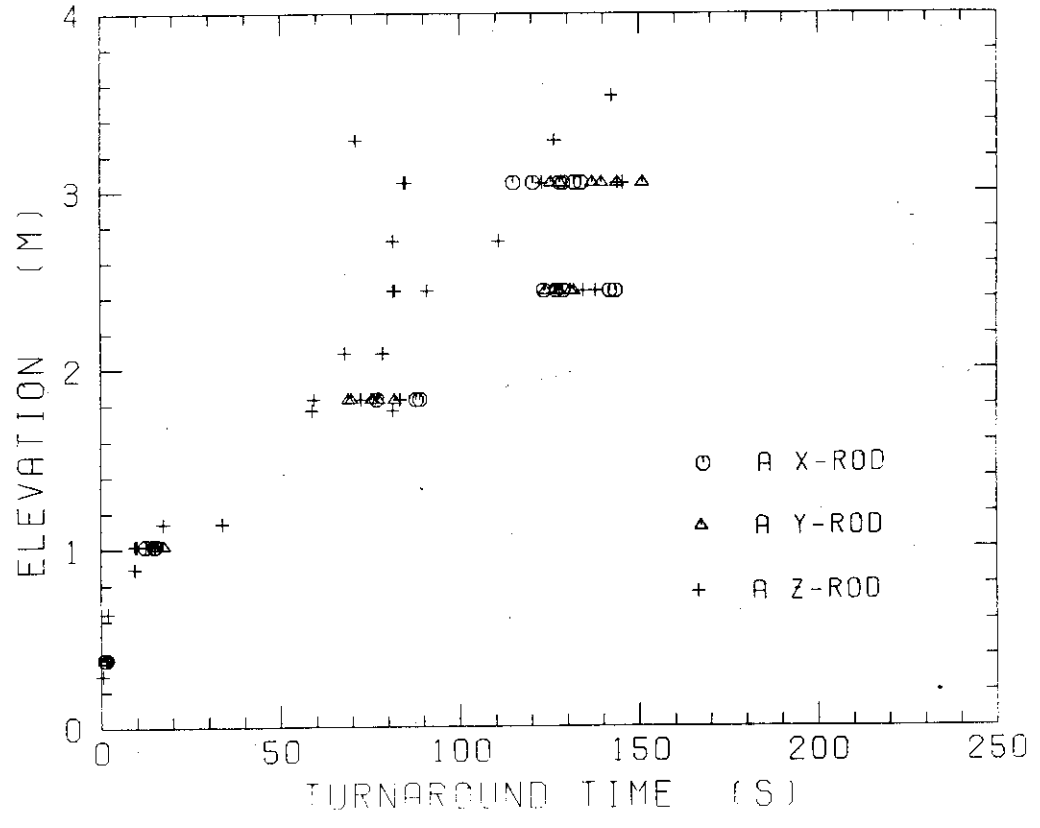

Fig. E-12 Turnaround time in high power region (A region)

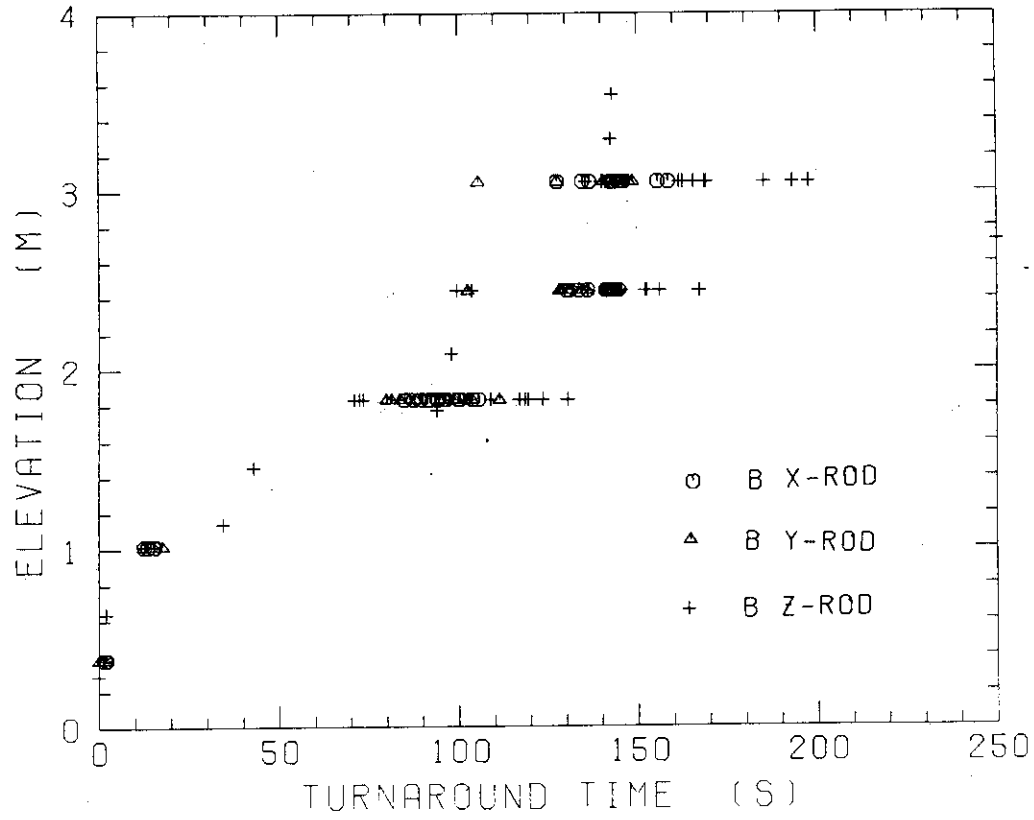

Fig. E-13 Turnaround time in medium power region (B region)

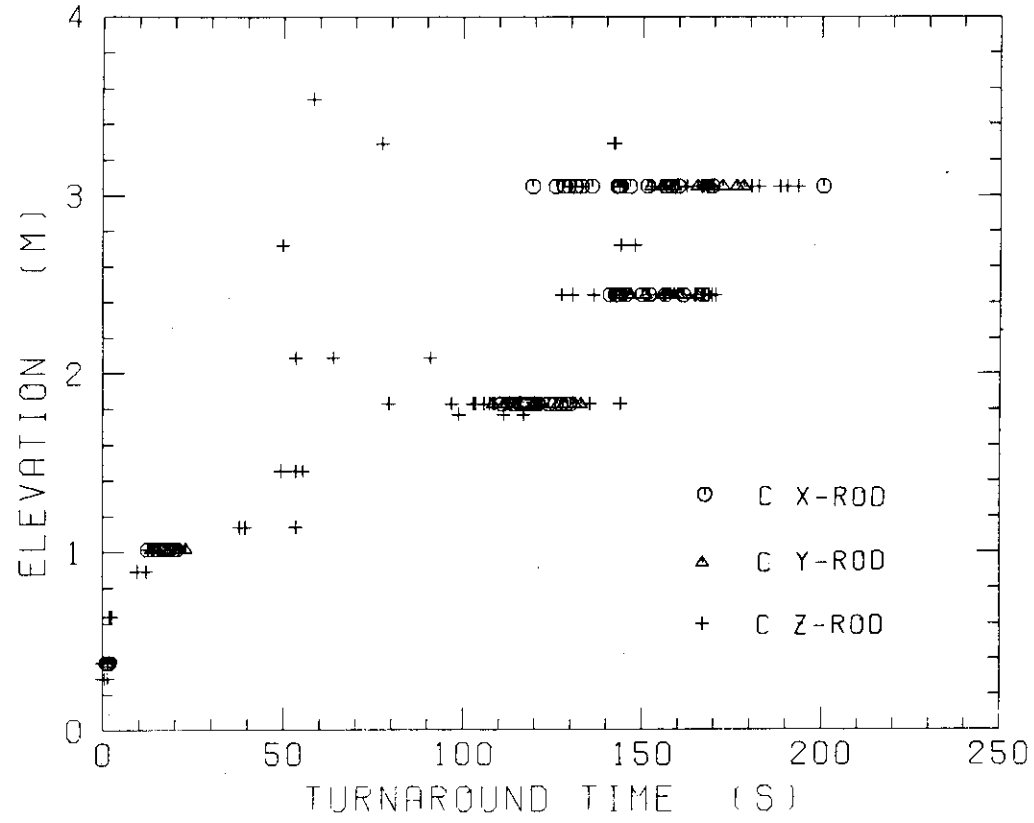

Fig. E-14 Turnaround time in low power region (C region)

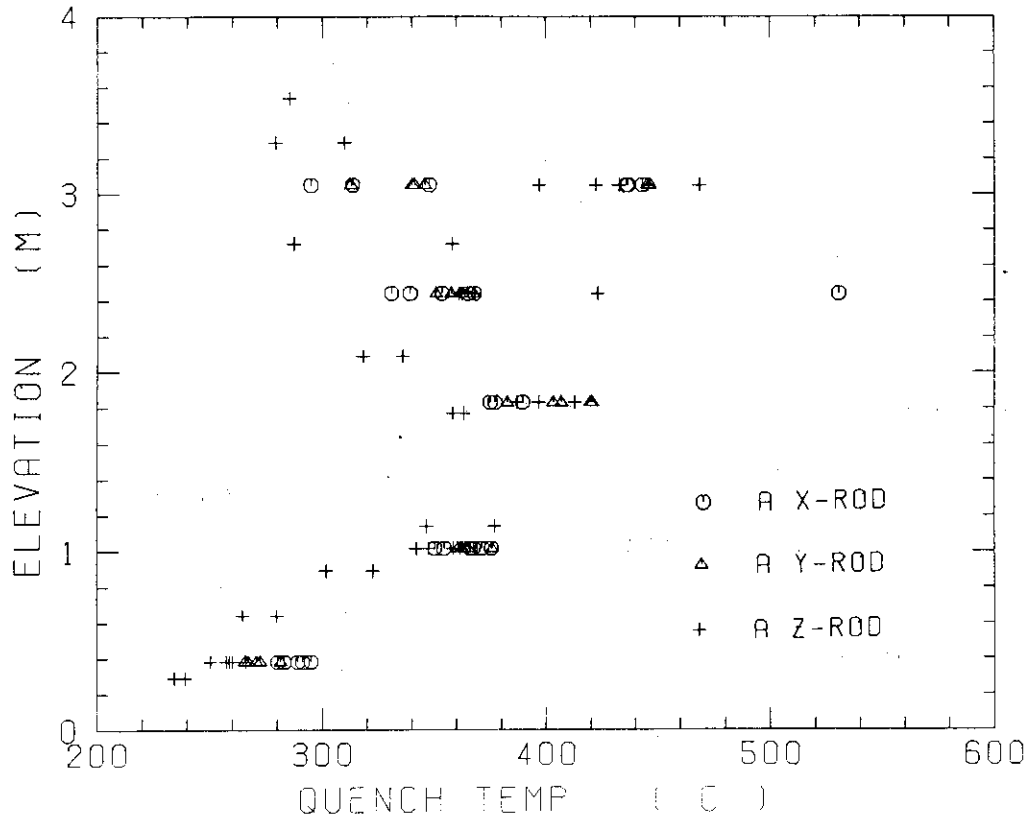

Fig. E-15 Quench temperature in high power region (A region)

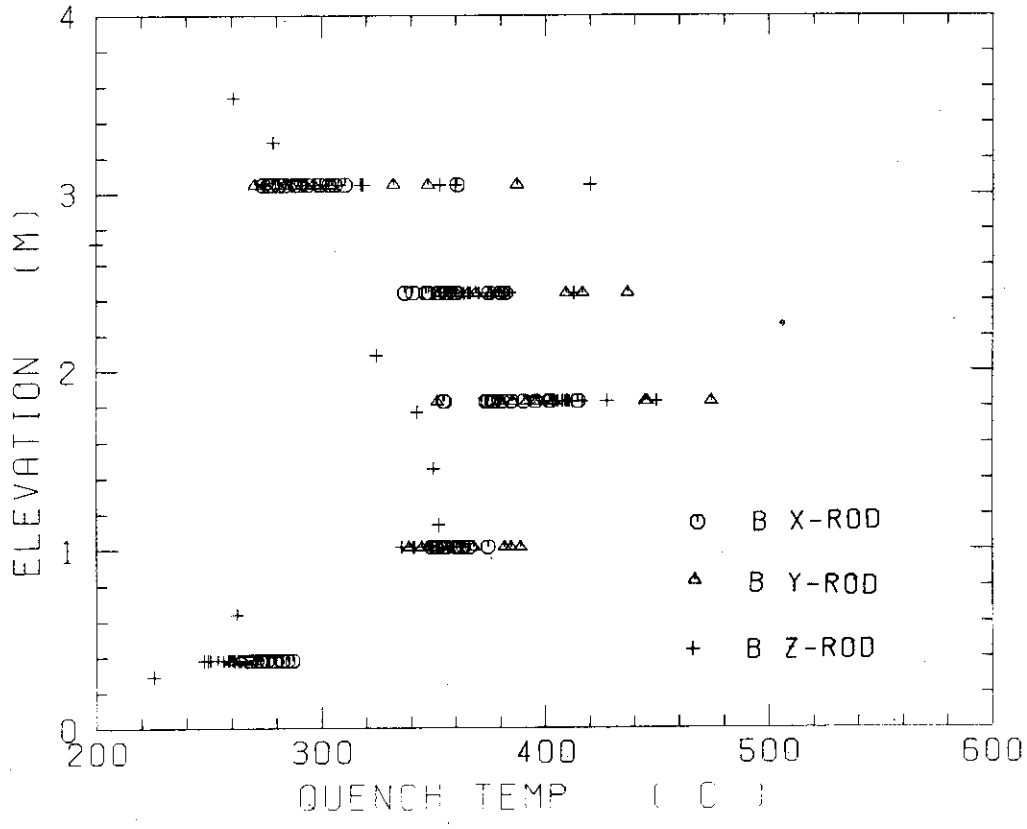

Fig. E-16 Quench temperature in medium power region (B region)

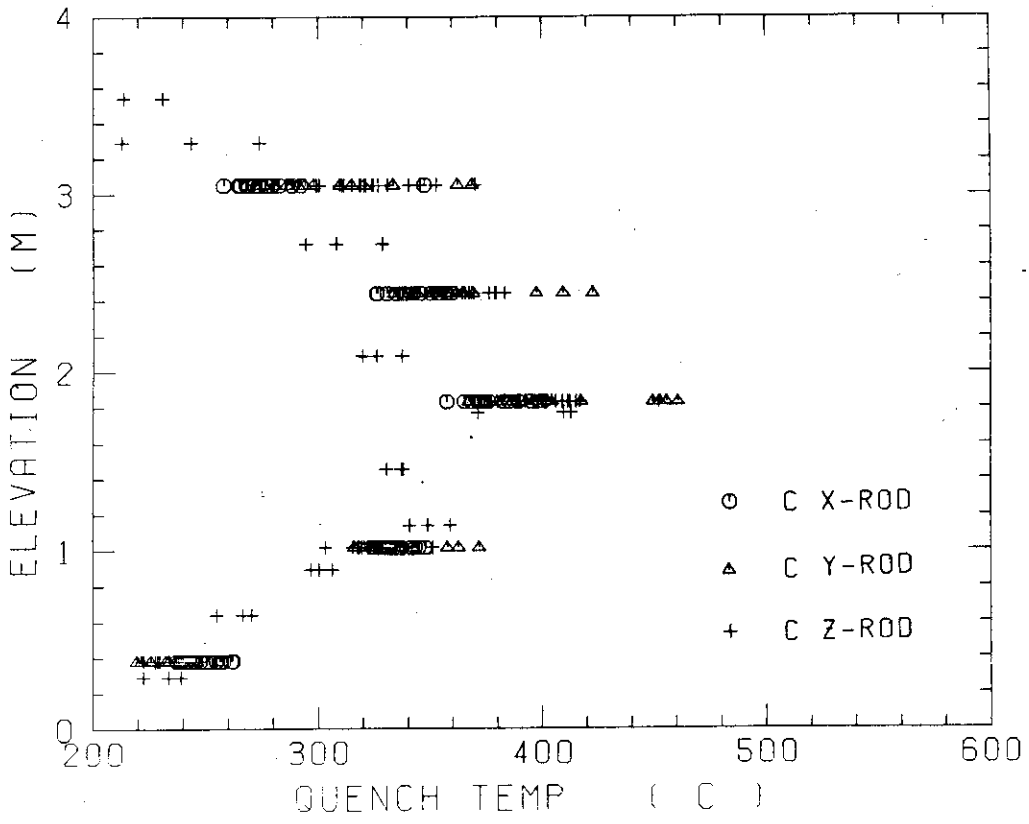

Fig. E-17 Quench temperature in low power region (C region)

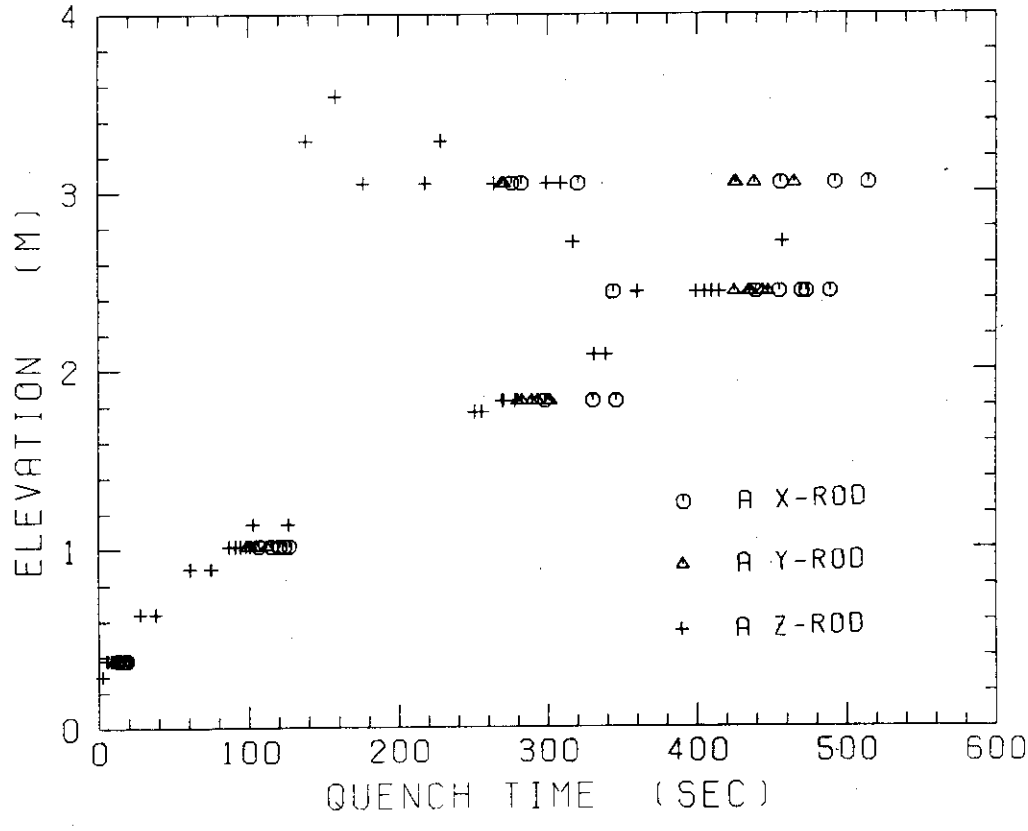

Fig. E-18 Quench time in high power region (A region)

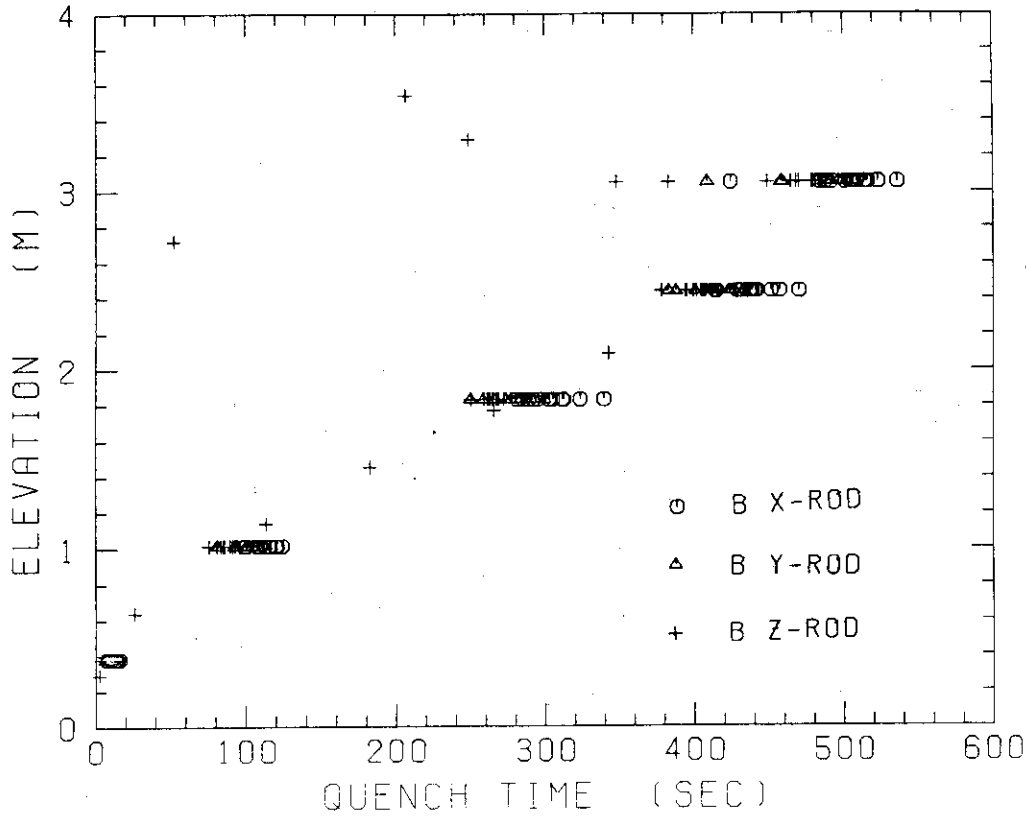

Fig. E-19 Quench time in medium power region (B region)

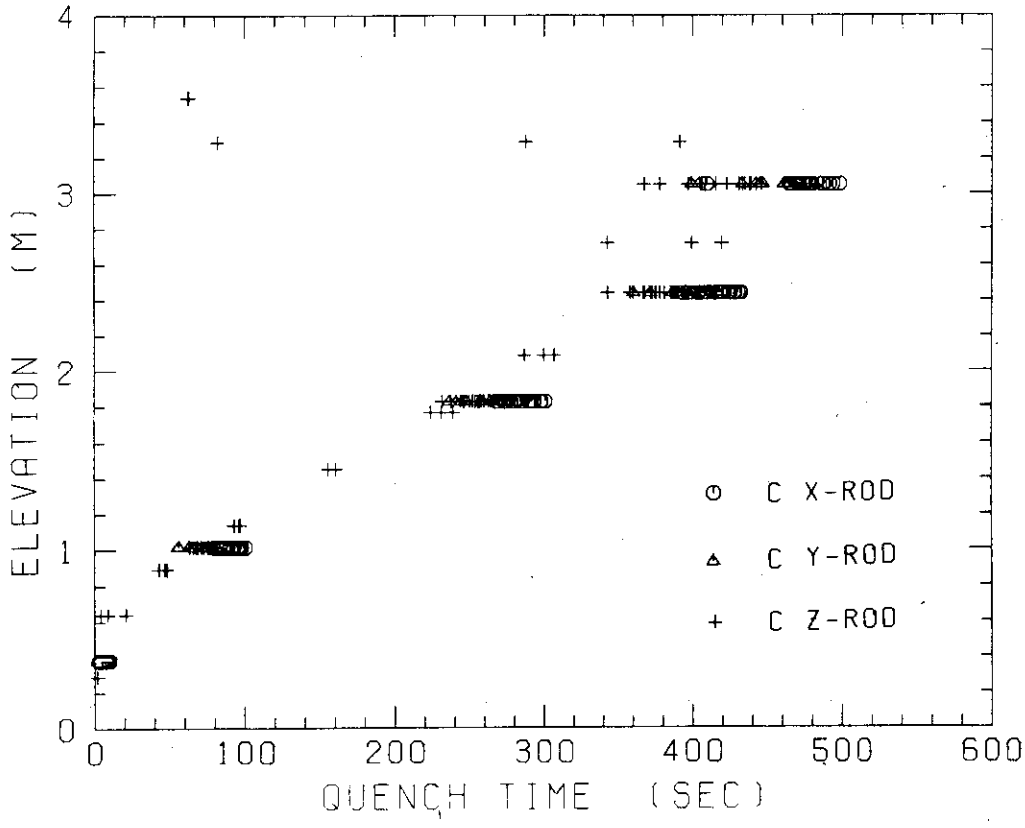

Fig. E-20 Quench time in low power region (C region)

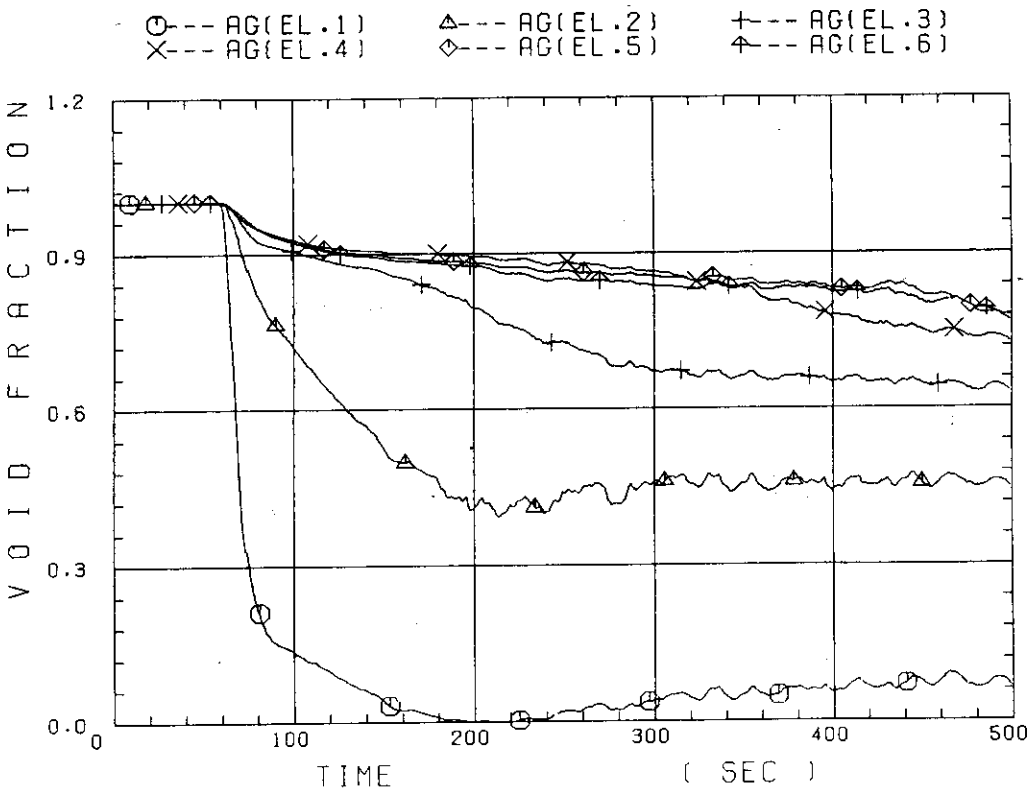

Fig. E-21 Void fraction in core

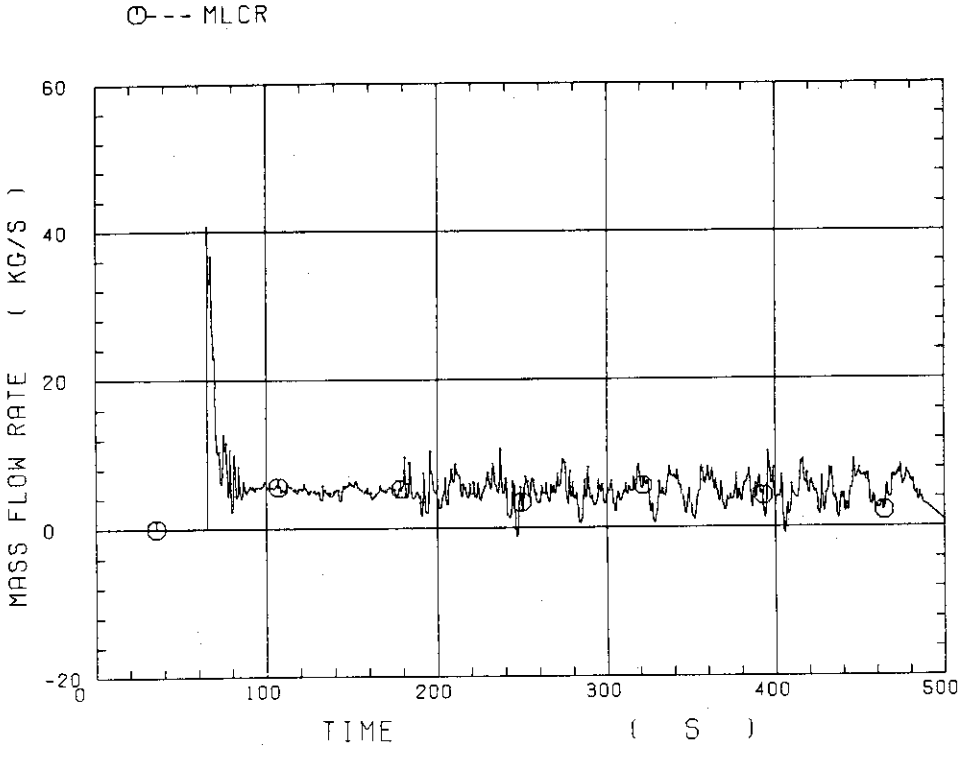

Fig. E-22 Core inlet mass flow rate (recommended value)

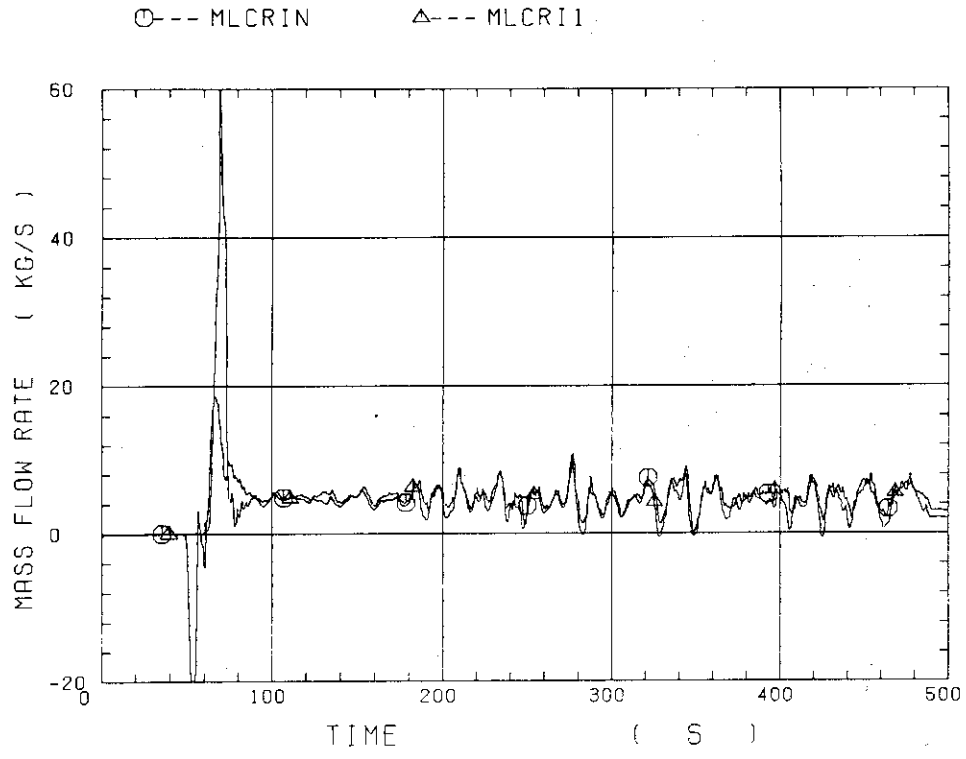

Fig. E-23 Core inlet mass flow rate

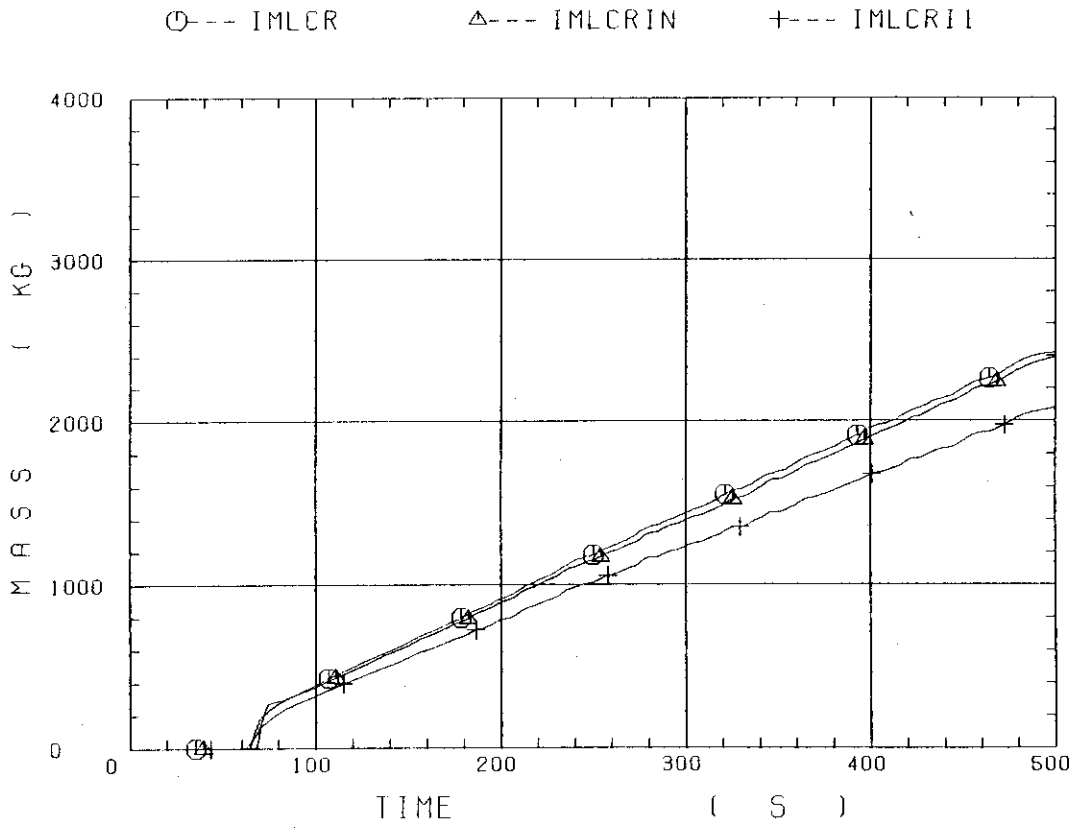

Fig. E-24 Time-integration of core inlet mass flow rate

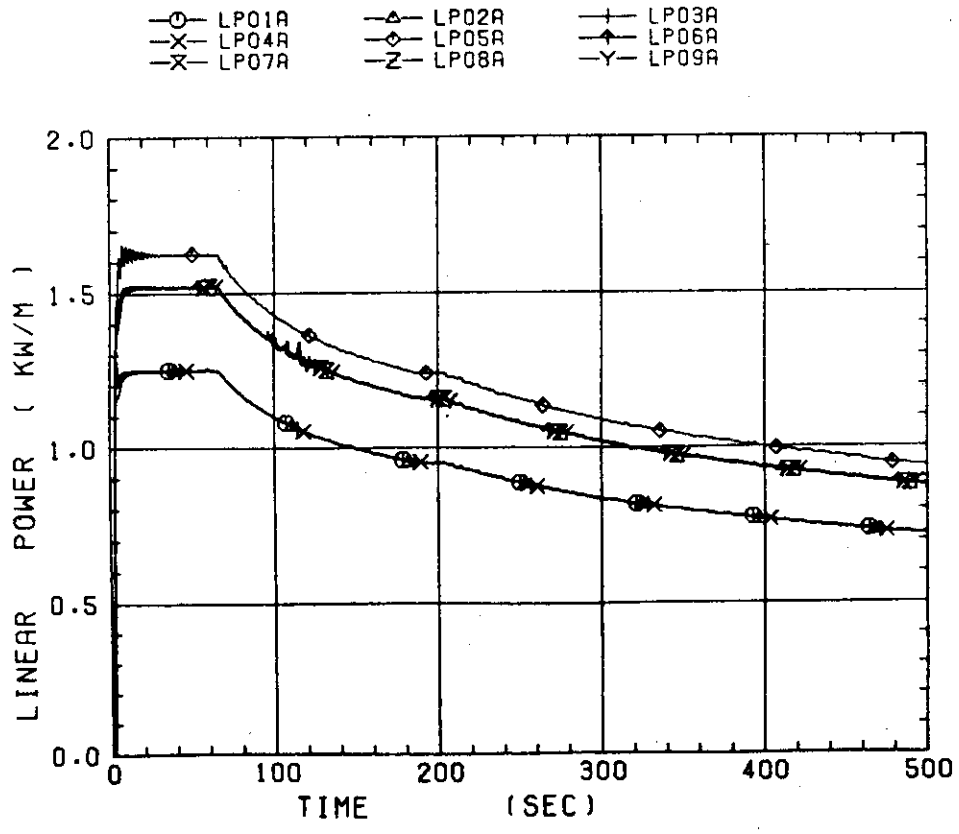

Fig. E-25 Average linear power of heater rod in each power unit zone

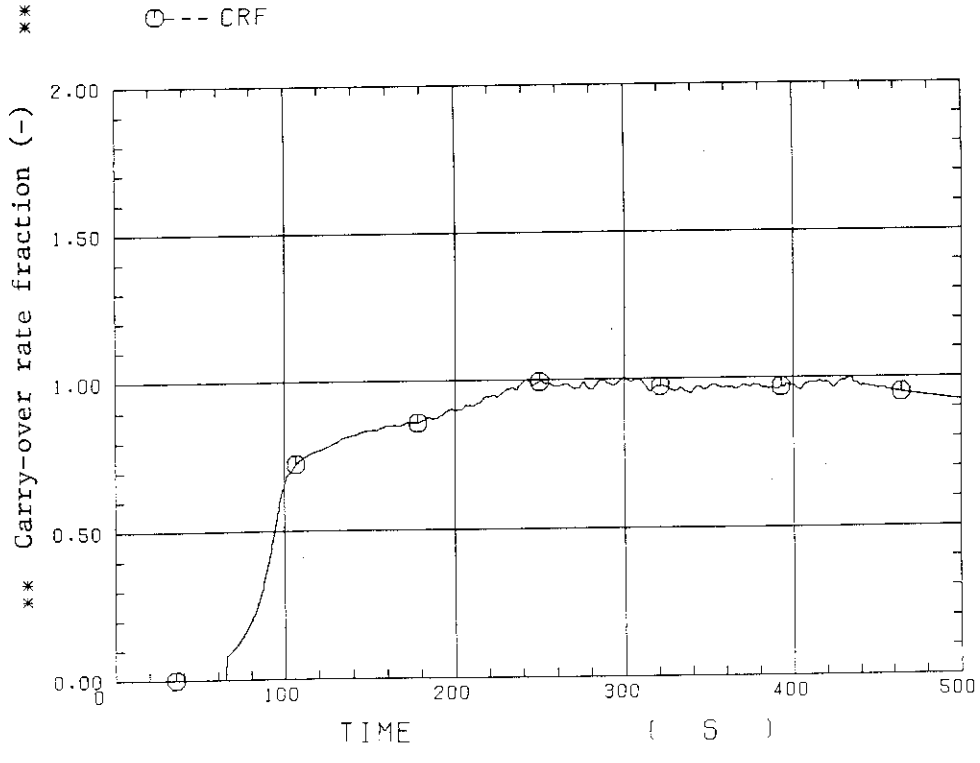

Fig. E-26 Carry-over rate fraction

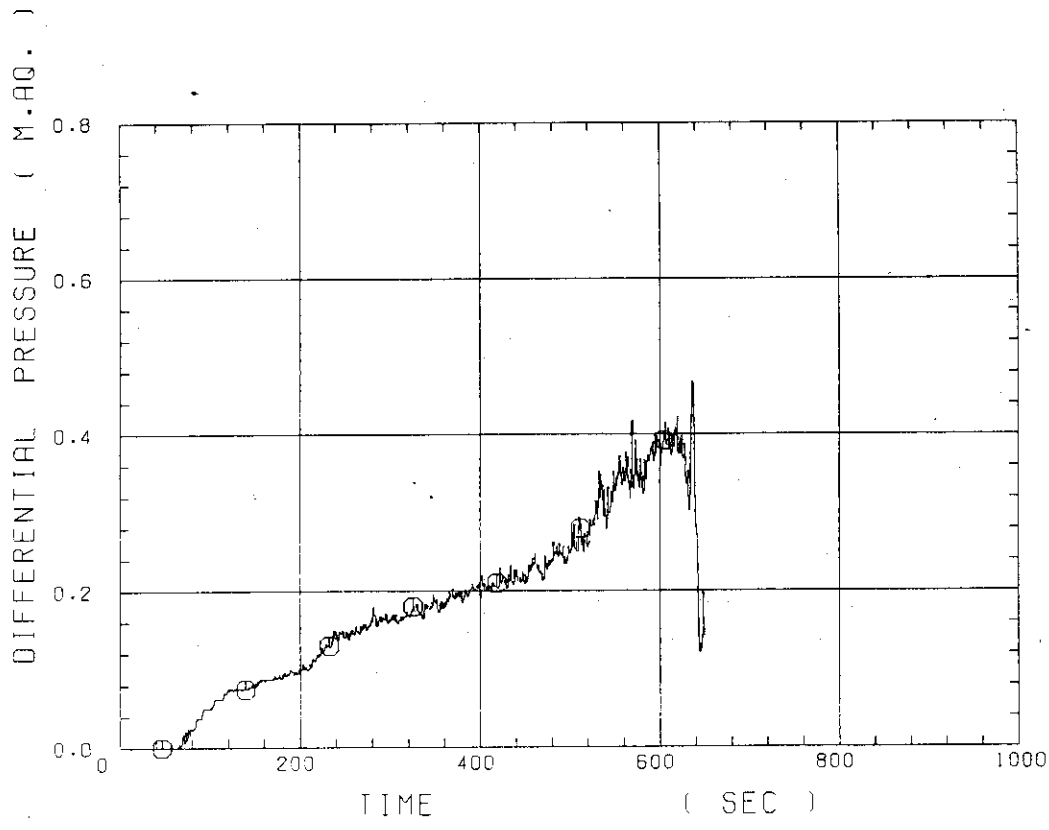

Fig. E-27 Differential pressure through upper plenum

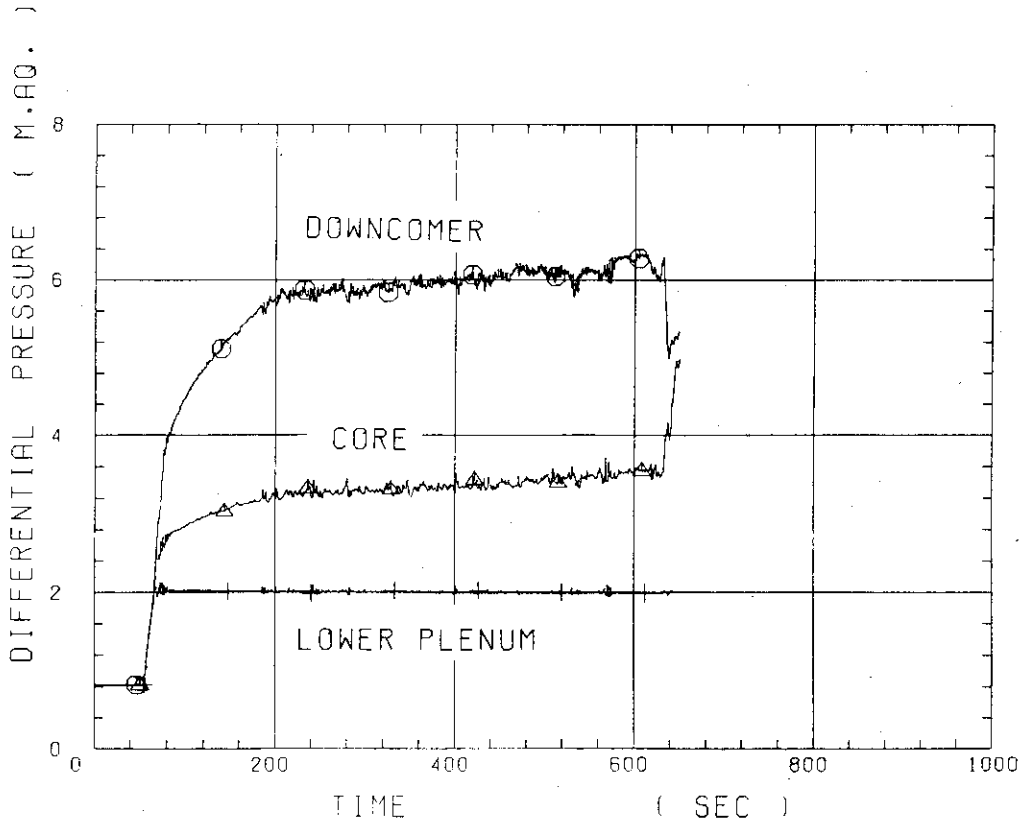

Fig. E-28 Differential pressure through downcomer, core, and lower plenum

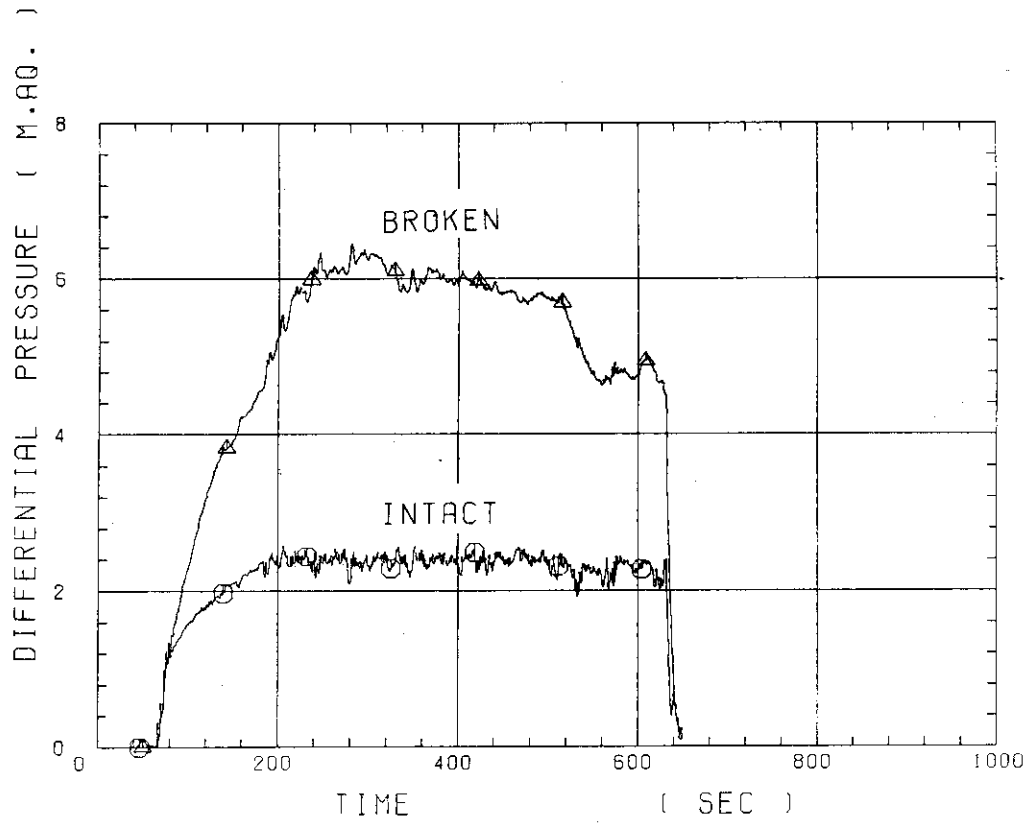

Fig. E-29 Differential pressure through intact and broken loops

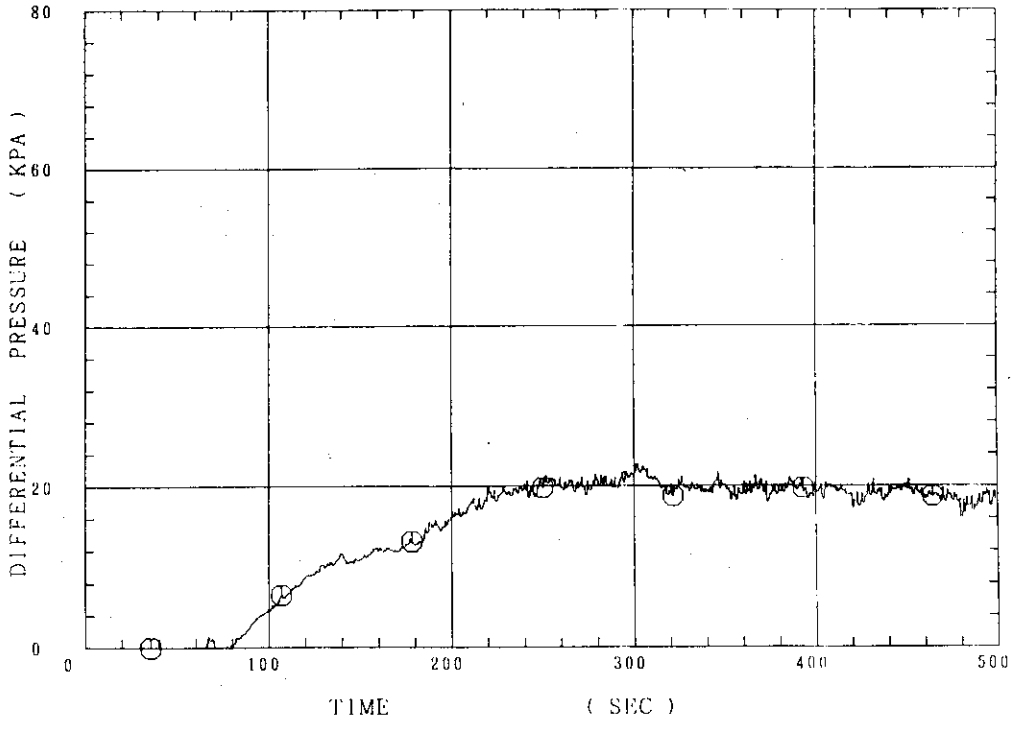

Fig. E-30 Differential pressure through broken cold leg nozzle

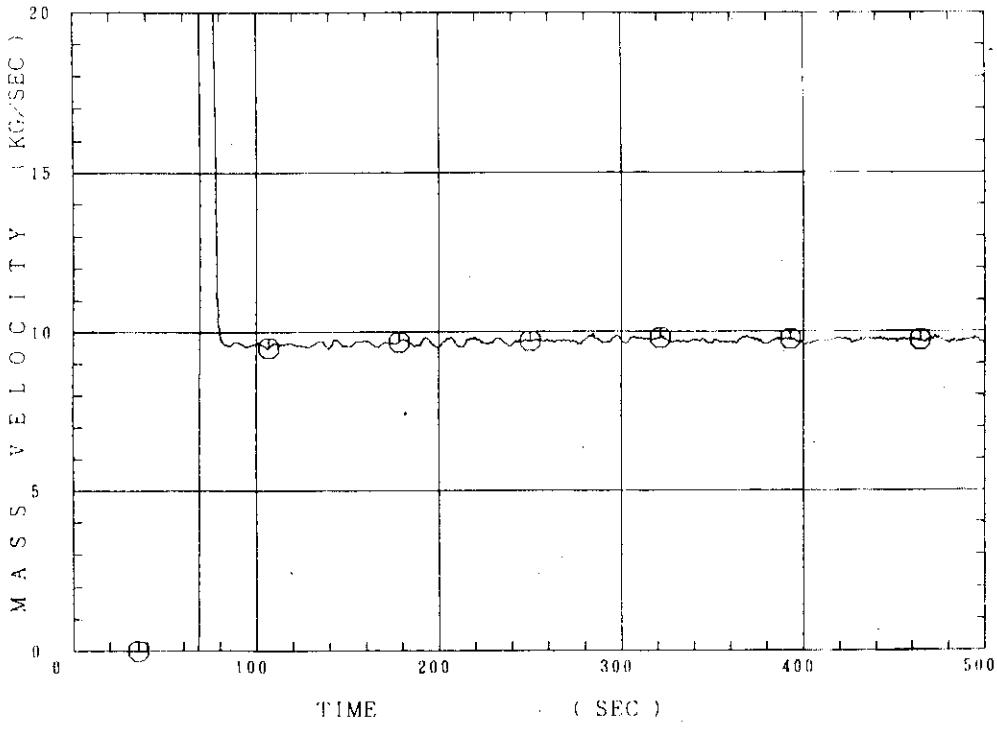

Fig. E-31 Total water mass flow rate from intact loops to downcomer

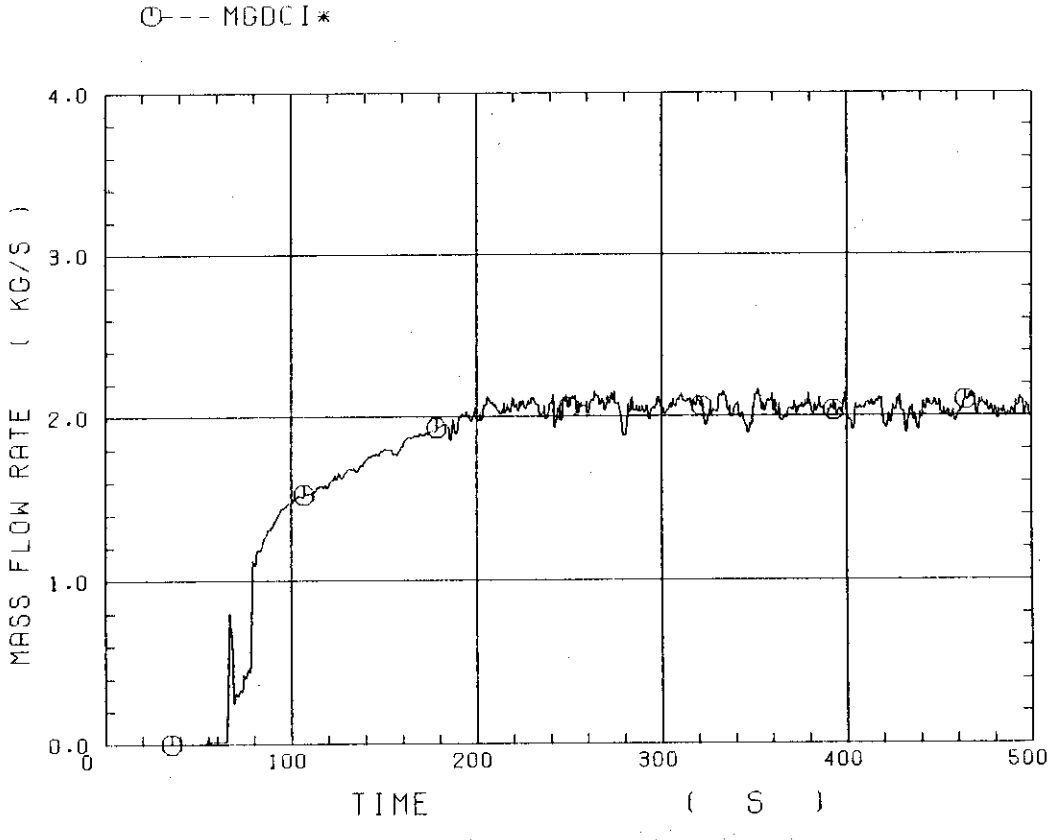

Fig. E-32 Total steam mass flow rate from intact loops to downcomer

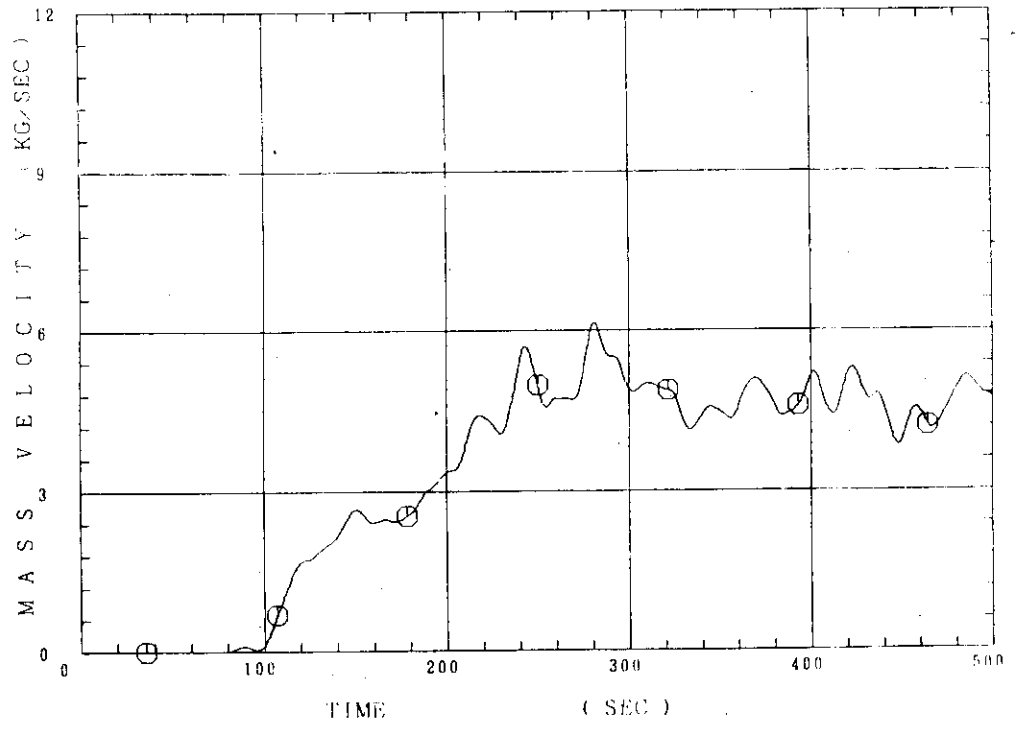

Fig. E-33 Water mass flow rate through broken cold leg nozzle

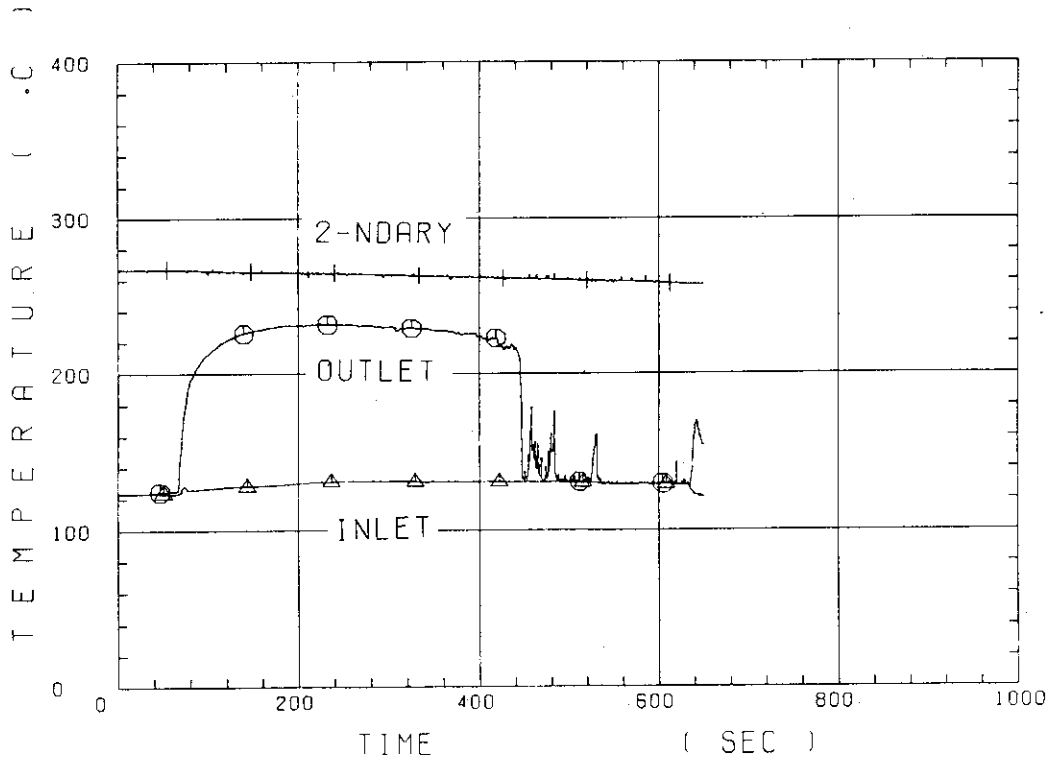

Fig. E-34 Fluid temperature in inlet plenum, outlet plenum, and secondary of steam generator 1

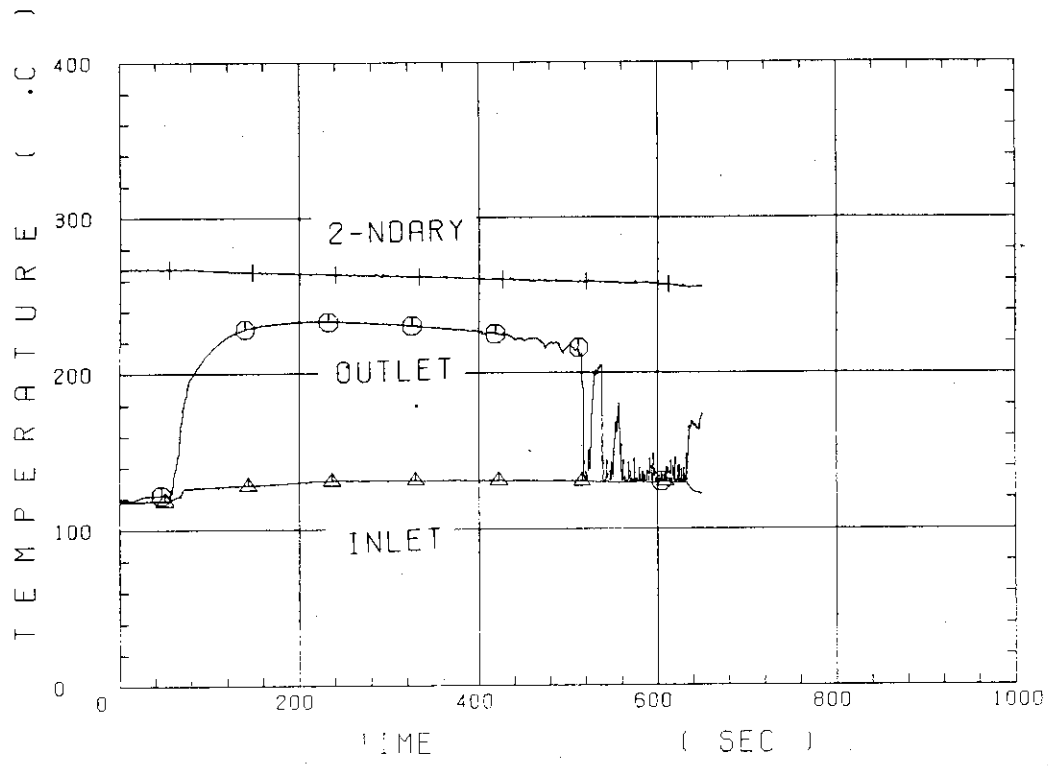

Fig. E-35 Fluid temperature in inlet plenum, outlet plenum, and secondary of steam generator 2

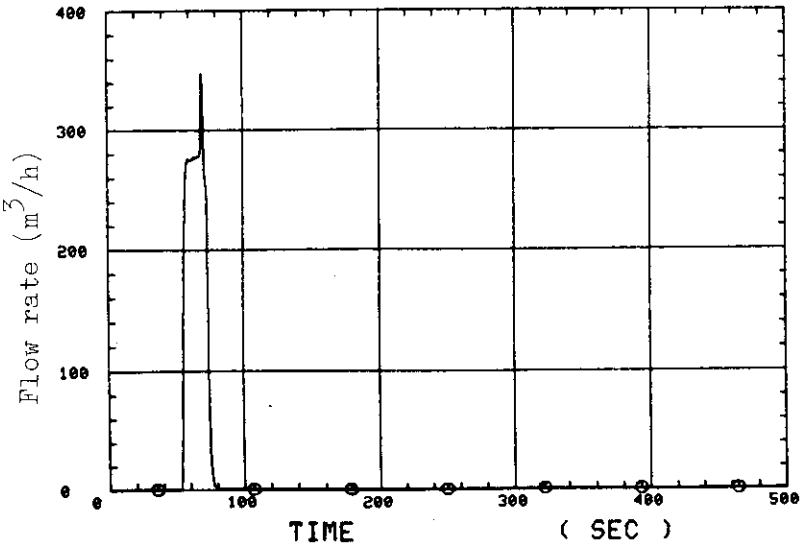

Fig. E-36 Total accumulator injection rate